University of Stavanger

FACULTY OF SCIENCE AND TECHNOLOGY

MASTER'S THESIS

Study programme/specialisation: Petroleum Geoscience Engineering	Spring semester, 2021 Open access
Author: Caroline Ruud	
Programme coordinator: Lisa Jean Watson Supervisor: Prof. Udo Zimmermann	
Title of master's thesis: First age constraints of the Marmora Terrane: the missing link for Neoproterozoic geology between South America and southern Africa	
Credits: 30	
Keywords: Marmora Terrane Gariep Belt Provenance U-Pb geochronology Whole-rock geochemistry Petrography	Number of pages: 72 + supplemental material/other: 84 Stavanger, 26.08.2021

First age constraints of the Marmora Terrane:

the missing link for Neoproterozoic geology between South America and southern Africa

by

Caroline Ruud

MSc thesis

Presented to the Faculty of Science and Technology

University of Stavanger, Norway

August 2021

Supervised by Prof. Udo Zimmermann

University of Stavanger

Acknowledgement

These past three years combining work and studies have been busy, but also educational and rewarding in so many more ways than I could have imagined. I feel lucky to be surrounded by some many great people. To some of those I owe a special thank you for the role they've played regarding this thesis project.

First of all, thank you to my supervisor on this project, Dr. Udo Zimmermann. From elective courses that ending up changing (and possibly saving) a degree, to research projects that have let me travel the world and learn from the many amazing scientists I would never have met if not, and for always being ready to answer questions over and over again. And perhaps most of all, for believing more in my academic skills than I did myself for a while. I am lucky to have learned from you as a professor in various courses and as a mentor in research projects, and I look forward to continue learning. Your passion for research and geology is inspiring!

To the University of Oslo and especially Magnus Kristoffersen for helping me obtain the data needed for this thesis, and to Thomas M. Olsen for the Isoplot guidance.

To the University of Stavanger and colleagues, for encouragement and support. Especially to Mona Minde for help with the electron microscope as well as making all analytical (nerdy) discussions fun, and my boss Hilde C. Jonsbråten for all the support and facilitation the last three years as well as many much-appreciated conversations and pep-talks along the way.

To family and friends for endless support, belief and encouragement, and especially to my parents for always believing out loudly that I can do whatever I set my mind to. To Jon Runar for patience and support, and for much needed breaks in form of everyday adventures. To Charlotte, you've truly been my rock this summer. Being a part of team stubby and stalky has been amazing, and I am forever grateful!

Thank you!

Abstract

The Gariep Belt stretches from the southwest of Namibia into the northwest of South America, crossing the international boarder at the Orange River. The mountain belt originates from a continent-continent collision related to the break-up of Rodinia and following amalgamation of Gondwana. Although known that the Gariep Belt with its low-grade metamorphosed Neoproterozoic record of rock succession holds information that can allow the understanding of one of the most significant Era's with regards to understanding palaeotectonic evolution of previous supercontinents and extreme climate conditions with possibly global glaciations, few to non-existing datasets of provenance data exists.

U-Pb analysis of zircons within the Marmora Terrane yield information of new depositional ages and concludes that two subterranes Schakalsberge and Chameis are younger than previously assumed, with age ranges of 550 Ma and 570 Ma respectively. Some rock successions of the latter (Dernburg Formation) have been intruded by gabbroic rocks containing zircons at around 540 Ma. The assumed ages by previous work for the third and last Oranjemund Subterrane are supported by more data and have a maximum depositional age of Uppermost Cryogenian age (c. 630 Ma).

The presence of zircons in all mafic rocks sampled from for this work indicates that the successions are underlain by continental basement and do not represent an oceanic terrane. Hence, palaeotectonic models arguing with the Marmora Terrane being solely oceanic crust are outdated and must be abandoned. The data also argues that the correlation of the succession within the Chameis Subterrane of those within the Schakalsberge Subterrane cannot be anymore based on isotopic data.

Detrital zircon populations match the eastern South America Punta del Este Terrane and the western Kalahari craton, but contains age populations absent within the Rio de la Plata craton (Nico Perez Terrane), indicating that the Marmora Terrane is related to the former units. More speculation about palaeotectonic and -geographic processes would be adventurous.

The resulting dataset of this thesis also demonstrate that depending on U-Pb ages alone solving a paleogeographic puzzle is a far stretch due to overlapping events on both sides of the south Atlantic Ocean. Although obvious that the geological history of the Marmora Terrane is strongly related to the one of eastern South America around the Rio de la Plata area and southwestern Africa with the Kalahari Craton, further research such as isotopic provenance data and quantification of detrital material are paramount to improve our understanding of the source areas during deposition.

Nomenclature

U	Uranium
Pb	Lead
Lu	Lutetium
Hf	Hafnium
Th	Thorium
Ar	Argon
Sc	Scandium
Zr	Zircon
Nb	Niobium
Ti	Titanium
Ta	Tantalum
UiS	University of Stavanger
UiO	University of Oslo
SEM	Scanning Electron Microscope
CL	Cathodoluminescence
EDS	Energy-dispersive X-ray Spectroscopy
FE	Field gun
LA	Laser ablation
ICP-MS	Inductively Coupled Plasma Mass Spectrometry
XRD	X-Ray Diffraction
GC	Geochemistry
OLM	Optical Light Microscopy
σ	Sigma
Ma	Mega-annum (million years before present)
MORB	Mid Ocean Ridge Basalts
OIB	Oceanic Island Arc

Table of Contents

List of figures

List of tables

1 Introduction

The Gariep Belt of Neoproterozoic to Early Cambrian age, stretches from the southwest of Namibia into the north-western part of South Africa, crossing the Orange River that named the orogenic belt Gariep, meaning “great river” in the local language (Frimmel, 2018). Former studies have divided the Gariep Belt into two terranes, the Porth Nolloth Zone in the east and the Marmora Terrane in the west (Frimmel, 2018; Frimmel et al., 2010; Zimmermann, 2018). The latter is further differentiated into three subterranes: the Schakalsberge, Oranjemund and Chameis subterranes (Frimmel, 2018). The Gariep Belt is situated in an area known for its significant diamond bearing deposits (Frimmel, 2018), leading to difficulty in sampling of rocks, and hence provenance analysis of the belt. The restricted access to the Gariep Belt has limited the research and hindered our understanding of the provenance (Zimmermann, 2018). According to Frimmel et al. (2010) the exposed rocks demonstrate an entire super-continental cycle during the Neoproterozoic Era, recording extreme climate conditions and global glaciations. This implies that the Gariep Belt with its generally low-grade metamorphism (Frimmel, 2018) could possibly, with its rock record of Neoproterozoic age, offer answers regarding the so-called “snowball earth” hypothesis. Although known that the Gariep Belt is arguably the key region to understand the regional Neoproterozoic geological history, few studies have been carried out. These studies lack sufficient databases regarding provenance data, creating a weak basis for substantial interpretations (Zimmermann, 2018). The main hypothesis today is that the Porth Nolloth Zone is assigned to a Neoproterozoic rift cycle, while the rocks of the Marmora Terrane are related to oceanic crust or back-arc crust as a result of rifting off major continental blocks (hence flooded by oceanic crust) (Frimmel et al., 2010). Another hypothesis considers the possibility that the entire area belonged to eastern cratons of South America. This hypothesis proposes that the Gariep Belt is exotic to the African Kalahari Craton and places the source as blocks of South American cratons (Basei et al., 2005).

The geological history of the Marmora Terrane is strongly related to the one of eastern South America around the Rio de la Plata area and south-western Africa, which includes the so-called Gariep Belt as a margin of the Kalahari craton (e.g., compilation in Oriolo and Becker, 2018). Due to the complexity of the rock succession and the data material this thesis has been limited to age determination of rock successions of the Marmora Terrane. In depth data regarding the petrography, igneous petrogenesis or the geochemical interpretation plus possible correlation has not been developed or reviewed here as this would be outside the scope of the thesis.

1.1 Aim of the study

This study will focus on key successions sampled from the Marmora Terrane. It will be the first study that attempts to reveal isotopic ages for all major rock successions representing the Marmora Terrane, and it will establish an opportunity for correlation with adjacent geological strata. Studies of the metasedimentary successions allow the interpretation of the first ever generated provenance data to commence with the identification, or not, of exotic detrital or magmatic rock material. This would enable identifying key source regions on either of the two continental blocks (eastern South America and southern Africa) involved in proposed collisional and extensional tectonic processes during the Meso- and Neoproterozoic (Frimmel et al., 2010). Moreover, the presented dataset will enable proposing the correct methodological techniques, moving forward with resolving the origin of the Marmora Terrane. Within this thesis, state-of-the-art methodology is used to gain uranium lead (U-Pb) crystallisation ages of zircons as a first step of determining emplacement ages for igneous rocks and for the estimation of maximum sedimentation ages of clastic and/or epiclastic formations, which is complemented with first petrographic and geochemical data of the studied rocks to understand the sampled successions to the extent possible.

1.2 Objective

The objective of the thesis is to provide a novel dataset of geochronology, with regards to U-Pb isotope crystallisation ages, of the up until now underexplored and still very much inaccessible area of the Gariep Belt which represents the major rock successions of the Marmora Terrane. This shall lead to the first isotopic age determination ever and shed light on the provenance of the detritus within the metasedimentary successions.

1.3 Covid 19 and implication for the thesis

The analytical work of this thesis was unfortunately strongly affected and delayed due to the Covid-19 situation. Most high precision laboratory equipment depends on specialists for service and maintenance, and often requires service visits from specialists abroad. Consequently, both the scanning electron microscope at the University of Stavanger (UiS) and the Nu Plasma HR instrument at the University of Oslo (UiO) suffered significant downtime due to international and national travel restrictions. First choice laboratories in Germany and the USA were and are still unavailable. The author of the thesis was also affected by travel restrictions and limitations in guest visits to laboratories according to international and national rules and regulations. As a result, this thesis could not add lutetium hafnium (Lu-Hf) isotopic data, so-called model ages of the magmas wherefrom zircons have been formed. This would have yielded important insights with regards to the regional provenance and the time of which the magma separated from the mantle source. In-depth interpretation of geochemical isotope data or petrography were also abandoned. All this was replaced with more U-Pb isotopic data covering the entire major successions of the Marmora Terrane, rather than concentrating on one subterrane as formerly planned.

2 Theoretical background

2.1 Zircon

Zircon is a common accessory mineral in nature with the chemical composition $ZrSiO_4$. It forms tetragonal crystals, often tabular to prismatic in crystal habit, with a relationship ratio between length and width ranging from 1 to 5. The relationship between length and width often reflects the velocity of which the zircon crystallized (Corfu et al., 2003). Zircons with a needle-shaped form are for example commonly observed in gabbros and rapidly crystallized rocks, while a stubbier and more equant form of the zircon indicates that it crystallized in more deep-seated intrusions where the cooling process happened slowly (Corfu et al., 2003). Zircons are often colourless, but could also be yellow to golden, reddish, brownish, bluish, or greenish. They have a hardness (Mohs scale) of 7,5 and a specific gravity of 4,6-4,7g/cm^3 (Anthony et al., 1995).

Zircon is one of the most stable minerals, resistant to both chemical and physical weathering. While other common minerals would be destroyed by magmatic, metamorphic and erosional processes, zircons have a unique way of storing these events in their internal structure as a record of events (Corfu et al., 2003). It is not without reason that zircons are popular to refer to as tiny time capsules.

The resistance of the zircon and its ability to record geological history it has been a part of, causes large variations when it comes to external morphology as well as internal textures of the mineral. Magmatic or metamorphic crystallisation and recrystallisation, chemical alteration and strain caused from both external and internal (metamictisation) forces gives distinct features to each zircon grain (Corfu et al., 2003). The external morphology such as shape and form are briefly described above and can relatively easily be observed in a binocular microscope with other macroscopic properties.

The internal texture such as zoning and internal fractures of a zircon on the other hand, requires imaging of the zircon in a scanning electron microscope (SEM) with a back scattered electron (BSE) or a cathodoluminescence (CL) detector. To identify growth patterns or different growth events CL is superior to BSE (Corfu et al., 2003). By CL-imaging one can observe different zoning patterns such as oscillatory zoning and discontinuities, identify cores that are xenocryst or metamict and distinguish a rim from the zircons core.

Zircon has become one of the most important minerals in geochronology not only due to its stable nature but also because it is one of the most abundant minerals in most rock types (Schoene, 2014). In igneous rocks, where fossils are lacking, zircons are even more valuable for dating purposes. Combined with CL-imaging one can date the crystallisation age as well as geologically significant zircon-forming events at later stages.

2.2 Uranium-lead (U-Pb) geochronology

Zircon has a high concentration of uranium (U), as well as thorium (Th). Zircon also discriminates against the daughter element lead (Pb) during crystallisation (Davies et al., 2003). This U-Th-Pb system forms the foundation for one of the most important isotopic dating methods; U-Pb geochronology. An initially very high U/Pb ratio means that Pb found in zircons originates from radioactive decay of U and Th after the mineral crystallized. As U easily substitutes for zirconium, while Pb is strongly excluded, the U-Pb relationship at the formation of the zircon grain can be used to set the time to zero. Lead atoms originating from the decay of uranium are then trapped in the crystal, and over time the concentration builds up. Assuming no outside factors have contributed to Pb gain or loss, the age of the zircon can thus be calculated by using the equations for exponential decay of a radioactive isotope:

$$N_t = N_i e^{-\lambda t} \qquad (1)$$

where N_t is the number of radioactive isotopes measured at time of analysis, N_i the number of radioactive isotopes initially, λ is the decay rate, e is Eulers' number and t the time passed (the age one wants to measure). N_i can further be substituted; $N_i = N_p + N_D$ where N_p is the present number of radioactive parent isotopes and N_D is the stable daughter isotope. The amount of parent isotopes after a given t, N_t, can also be substituted with N_P while the decay constant for the parent isotope is λ_p. The equation becomes:

$$N_P = (N_P + N_D)e^{-\lambda_P t} \qquad (2)$$

$$\frac{N_D}{N_P} = e^{-\lambda_P t} - 1 \qquad (3)$$

For the U-Th- Pb system the equations become:

$$\frac{^{206}Pb^*}{^{238}U} = (e^{-\lambda 238 t} - 1) \qquad (4)$$

$$\frac{^{207}Pb^*}{^{235}U} = (e^{-\lambda 235 t} - 1) \qquad (5)$$

$$\frac{^{207}Pb^*}{^{232}Th} = (e^{-\lambda 232 t} - 1) \qquad (6)$$

Where Pb* is radiogenic Pb. The method of dating zircons uses two decay chains as illustrated in figure X, the decay of the natural isotope ^{238}U to ^{206}Pb and the decay of the natural isotope ^{235}U to ^{207}Pb (Schoene 2014). The decay of thorium, more precisely ^{232}Th to ^{208}U, is also illustrated in Figure 2-1. The latter decay chain will not be discussed further in detail in this thesis as it is not part of the decay chains that are used for dating of zircons.

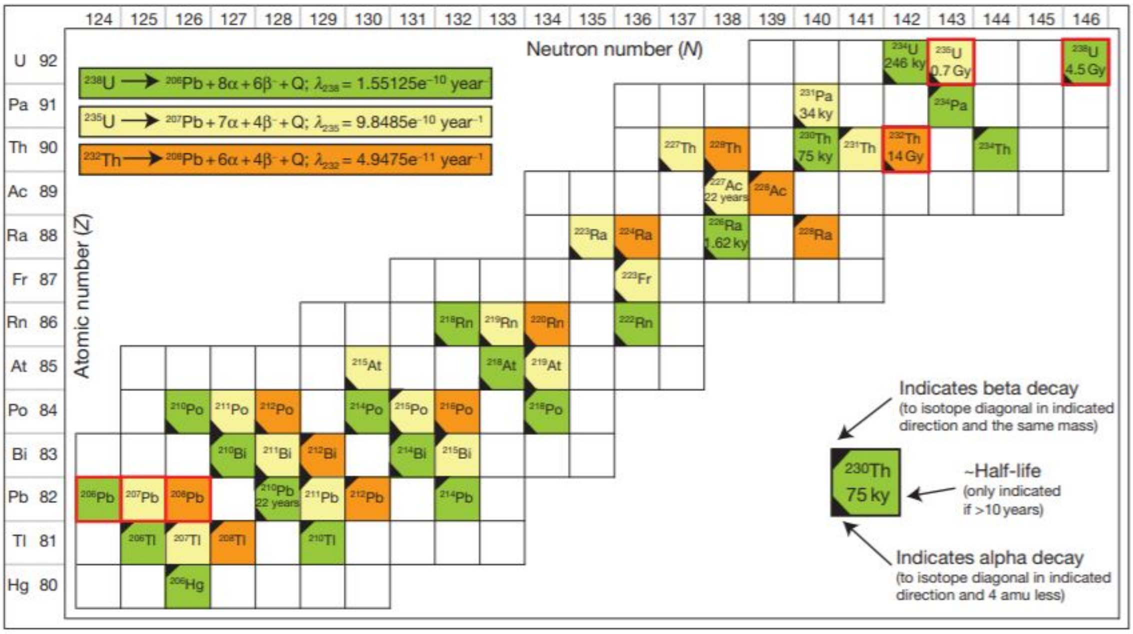

Figure 2-1 Illustration of the U-Th-Pb decay chains. The parent isotopes and their stable daughter isotopes are outlines in red, one colour for each chain (Schoene, 2014).

The length of the half-lives of both U-isotopes are important factors for the method to work; long enough that they can cover the entire timescale of the Earth, but short enough that both parent and daughter elements can be measured in the sampled zircons (Davies et al., 2003; Schoene, 2014). Half-life of a radioactive isotope is the time it takes for 50% of the amount to decay, and the half-life of a specific radioactive isotope is constant. The relationship between the decay constant (λ) and the half-life ($t_{1/2}$) is given by the following equation:

$$t_{\frac{1}{2}} = \frac{ln2}{\lambda} \qquad (7)$$

As the U decay system includes two systems that exists at the same time, based on the same parent (U) and daughter (Pb) pair, with different half-life (equation 2.2 and 2.3), two age determinations can be made using the same two elements.

$$^{238}U \rightarrow {}^{206}Pb + 8\alpha + 6\beta^- \; (t_{1/2} = 4468\,\mathrm{Myr}) \qquad (8)$$

$$^{235}U \rightarrow {}^{207}Pb + 7\alpha + 4\beta^- \; (t_{1/2} = 704\,\mathrm{Myr}) \qquad (9)$$

These two ages are compared, working as a test or quality check for the accuracy of the age (Corfu et al., 2003). If the ages for the two systems are the same within the given error, it is a so-called concordant age. Concordance is often interpreted to be the result of a closed system, hampering the mobility of the parent or daughter isotope (Corfu et al., 2003). The concordia diagram was introduced by Wetherill in 1956, plotting for each analysis the $^{206}Pb/^{238}U$ versus the $^{207}Pb/^{235}U$ ratios (Schoene, 2014). Analysis that plots on the non-linear concordia curve has remained closed system since the time of crystallisation. The ones that plot off the curve, also called the discordant ones, are interpreted to have experienced some sort of open-system behaviour (Schoene, 2014). There are numerous causes to why the results of an analysis are discordant. Loss or gain of Pb or U as well as analysing different age domains in the zircon grain (e.g., old core and younger overgrowth in a rim analysed together) can all cause discordant results (Schoene, 2014). The mixing of age domains and Pb-loss are the most common reasons for discordia. While the mixing of growth domains can be avoided by studies of the internal structure of a zircon prior to the analysis, Pb-loss is more difficult to correct for. One can avoid metamict grains, however the event that caused the Pb-loss could often point to a geological event of significance. If a series of grains have experienced a single Pb-loss, these will plot in a linear manner under the concordia curve. The upper and lower interception of the concordia curve with the linear regression of the discordant data points can be calculated, of which the lower intercept will represent the Pb-loss event and the upper intercept will represent the true crystallisation age. However, if several Pb-loss events have occurred, these intercepts will only represent an average time of the Pb-loss event and crystallization age. Pb gain in a zircon is called common Pb and originates from external sources of Pb and not the decay of uranium. However, most data reduction tools have the ability of correcting the analysis with regards to the so-called common Pb.

In addition to the two systems of the U-Pb method discussed above, the Pb-Pb method is also used to derive an age. This method is usually combined with the U-Pb method and is obtained only by Pb isotopic ratios. By dividing equation (5) by equation (4) we get:

$$\frac{^{207}Pb^*}{^{206}Pb^*} = \frac{^{235}U}{^{238}U}\left(\frac{e-\lambda 235t-1}{e-\lambda 238t-1}\right) \qquad (10)$$

This means that by measuring U and Pb isotopes, one can calculate three isotopic dates. In a closed system, all three ages would agree (Schoene, 2014).

2.3 Previous research on the Gariep Belt

Previous research on the Marmora Terrane, especially with regards to U-Pb geochronology, is scarce to absent. This is largely due to the restricted access of the area, and hence the limitations in sampling rocks of the terrane for analytical purposes. Most of the stratigraphic interpretation of the formations within the Marmora Terrane is based on chemo- and lithostratigraphic correlation with the Port Nolloth Zone done by amongst other Frimmel (compilations in 2018).

Metasandstones (sample name JM-001) of the Oranjemund Subterrane were dated by Basei et al. (2005). Their dataset included only 24 zircon grains and interpreted a maximum depositional age for the rocks around 610 Ma. Basei et al. (2005) also imply a trend for the Oranjemund Group based on few geochemical data, from island arc setting to a continental margin setting.

Based on the dataset from Basei et al. (2005), together with results from argon-argon (Ar-Ar) age spectra of amphiboles in the Chameis Subterrane and correlation with the Port Nolloth Zone (Frimmel and Frank, 1998), an age for the Marmora Terrane was proposed to be 610-550 Ma (Figure 2-2) as representing an oceanic entity, either an ocean or back-arc rifted oceanic area (Frimmel, 2018).

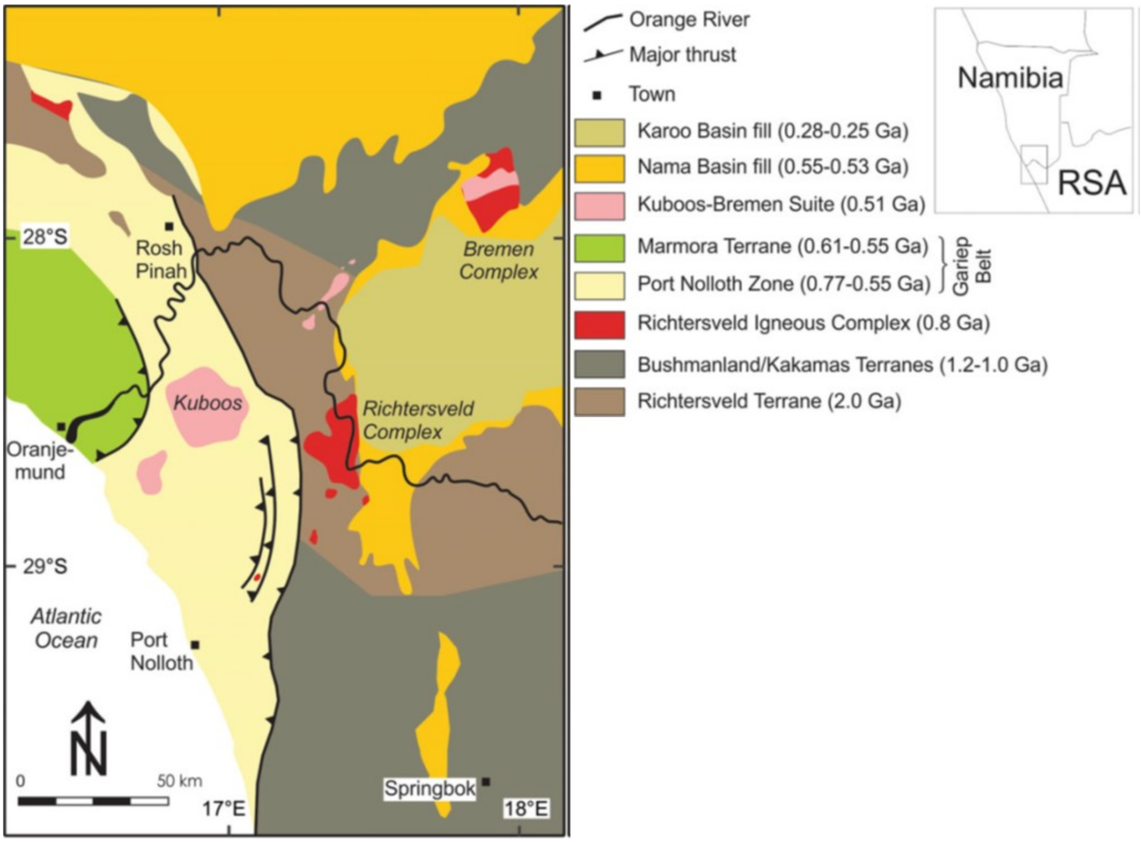

Figure 2-2 Proposed ages of the main tectonic units of southernmost Namibia and South Africa (modified from Frimmel, 2018)..

Andersen et al. (2018) dated another sandstone from the Oranjemund Group (sample name SA14-211), with a dataset including 42 concordant zircons. They found a Neoproterozoic age fraction as well, around 600-700 Ma, which did not help in improving the age determination.

A master thesis submitted at the Department of Geosciences in Tromsø (Norway) in May 2020 also studied two samples from the Oranjemund Group (Gilberg, 2020), where the youngest age fraction found was around 650-750 Ma (sample name NS 44, 122 concordant zircons). However, as no published and hence reviewed articles on these analyses are found, this thesis will not use the results as basis for comparison.

For the other two subterranes, the Chameis and the Schakalsberge Subterrane, the knowledge gap is even larger. There are no known age constraints besides two metamorphic ages based on Ar-Ar dating of hornblende and micas in the Chameis Subterrane (Frimmel and Frank, 1998), and pure lithostratigraphic correlation “dates” the succession. One metamorphic event interprets the accretion of some of the mafic successions of the Dernburg Formation and the Bakers Bay Suite around 580 to 570 Ma and a second metamorphic event represent the final closure of the oceanic basin at 545 Ma (Frimmel and Frank, 1998). This predates the gabbros and mafic rocks as well as the carbonates of the Sholtzberg Member to rocks deposited and/ or formed prior to 580-570 Ma. The mafic rocks of the Dernburg Formation are interpreted to be oceanic island basalt. Together with the Sholtzberg Member the depositional setting is believed to have been an atoll setting (Frimmel, 2000).

The diamictite in the Chameis Gate Member of the Dernburg Formation (Figure 2-3) is assumed to be a reflection of the Marinoan glaciation, based on the correlation of the cap carbonates on top of the Dernburg Formation with the cap carbonates above the diamictite in the Numees Formation (Figure 2.3-2) of the Porth Nolloth Zone (Frimmel, 2000). This correlation gives the diamictite of the Dernburg Formation an assumed Ediacaran age (635-543 Ma). However, the Numees Formation has later on been interpreted be of Gaskian age, around 580 Ma, based on biostratigraphic and lithostratigraphic interpretation (Gaucher et al., 2005). Besides lithostratigraphic interpretations, general interpretation of the diamictites as *not* being of glacial origin are abundant (Martin et al., 1985; Zimmermann et al., 2011) and challenge any correlations based on this interpretation.

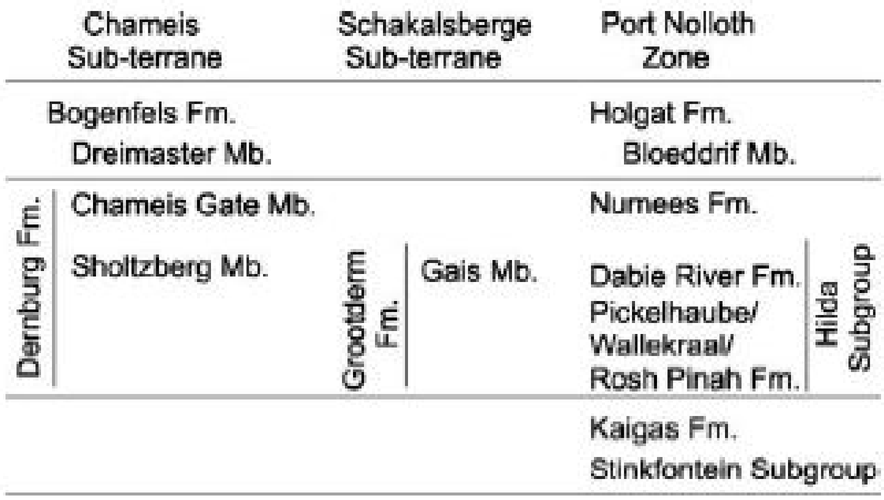

Figure 2-3 Correlation of the stratigraphic units within the Chameis Subterrane with those of the Schakalsberge Subterrane, as well as correlation with the Porth Nolloth Zone (Frimmel, 2018).

The overlying carbonates of the Dreimaster Member (lower Bogenfels Formation) and siliciclastic rocks (upper Bogenfels Formation) might or might not be younger. It has been argued that continental (clastic) input took place only during the deposition of the upper part of the Dernburg Formation and the overlying Bogenfels Formation (Figure 2.3-2), when closing of the ocean led to an oceanic basin narrow enough to receive clastic material from either the east or the west (Frimmel, 2000). The correlation of the Bogenfels Formation to the Holgat Formation of the Porth Nolloth Zone implies that the Marmora Terrane had already docked onto the Port Nolloth Zone prior to the deposition of the Bogenfels Formation. The depositional environment would in that case be a foredeep on top and east of an orogenic wedge advancing from the west during closure of the Gariep Basin (Frimmel and Foelling, 2014).

The Schakalsberge Subterrane has a similar succession of mafic rocks (the Grootderm Formation) and overlying carbonates (the Gais Member) as the Chameis Subterrane. Frimmel and Jiang (2001) correlate the Gais Member with the Sholtzberg Member and implies a correlation between the mafic units of both subterranes as well (Figure 2.3-2). Frimmel (2000) also points out the strong lithological similarities between the igneous rocks of the Dernburg Formation and the Grootderm Formation. This would constrain any age for the mafic rocks of the Grootderm Formation and the carbonates of the Gais Member prior to 580 to 570 Ma.

Geochemically the rocks in both subterranes are interpreted as alkaline tholeiitic mainly within-plate basaltic rocks where parts of the mafic successions of the Chameis Subterrane have signatures comparable with mid-ocean ridge basalt (MORB). This implies, and is as such interpreted within various tectonic models, that the rocks of the Schakalsberge Subterrane and those prior to the Bogenfels Formation in the Chameis Subterrane have been formed in an oceanic basin as seamounts or aseismic ridge basalts (Frimmel et al., 1996) or an oceanic back-arc basin without the influence of continental crust (Frimmel and Jiang, 2001; Frimmel et al., 2010 Fig 12c).

3 Geological setting

The former amalgamation of southwest Gondwana and the relationship between South America and Africa has led geologists in the pursuit of linking the two continents together for nearly a century (compilation in Basei et al., 2005). Remnants of sediment deposited while both continents were merged can be found on either side of the present South Atlantic Ocean (Basei et al., 2018). The search for tectonic and stratigraphic evidence that correlates the eastern part of South America with the western part of Africa has led to numerous palaeographic models and scientific contributions, however the theories remain highly speculative (Basei et al., 2005; Frimmel et al., 2010; Zimmermann, 2018).

The break-up of the Proterozoic supercontinent Rodinia and the following formation of the large continent Gondwana both took place during the Neoproterozoic Era (1000-542 Ma). Not only did the Neoproterozoic Era host a complete super-continental cycle, but it is also known for intense orogenic events and extreme climate conditions that is believed to not only have led to global or near-global glaciations but also other extreme climate conditions that amongst other modified the abundance of oxygen in the atmosphere, eventually leading up to the Earth becoming our habitable planet (Frimmel et al., 2010). The main glaciations that have been interpreted as possibly global, although still highly debated, are the Marinoan Snowball-Earth glaciation at around 635-630 Ma, the Sturtian glacial event around 716 Ma, the Kaigas glaciation at around 750-720 Ma, the Gaskiers glaciation at around 547 Ma and the post-Gaskiers Vingerbreek glaciation at around 547 Ma (Hofmann et al., 2014). The interpretations of a glacial origin are highly controversial and thus also the correlation, not mentioning the interpretation of a possible global or possibly only regional event (e.g., Martin et al., 1985; Zimmermann et al., 2011 and many others).

An interest in the Neoproterozoic Era is significant not only for the palaeotectonic reconstruction and paleogeographic evolution of Neoproterozoic continents such as southwest Gondwana, but even for nowadays climate changes, as the climate changes and the response to those has taken place over a few hundreds of thousands of years (Hoffman and Schrag, 2002). A better understanding of this geodynamic evolution will also help us to better understand the way supercontinents form, evolve, and eventually break up, and at what speed (Frimmel et al., 2001). In the reconstruction of the geodynamic evolution of the southwest Gondwana some of our knowledge gaps hinder our understanding of amongst other the global glaciations of the Neoproterozoic (Frimmel, 2010).

The break-up of Rodinia led to the South American Rio de la Plata Craton rifting away from the Kalahari and Congo Cratons in southern Africa during the Early Neoproterozoic. This rift is suggested to have evolved into a Neoproterozoic Ocean, the so-called Adamastor Ocean (Hartnady et al., 1985). The width of the ocean is still debated. The closure of the ocean started around 600 Ma with the amalgamation of oceanic crustal blocks (Frimmel and Foelling, 2004). A subsequent continental collision is indicated, interpreted by a second metamorphic event on the Kalahari side at around 550 Ma and several magmatic units incorporated into the Pan-African (southwestern Africa) and Pan-African/Brasiliano (eastern margin of Rio de la Plata) orogenic belts (Figure 3-1), containing arguably subduction and collision-related igneous suites. The Kaoko, Gariep and Saldania belts on the African side are interpreted to be the counterparts to the Dom Feliciano Belt in south-eastern Brazil and Uruguay (Basei et al., 2018).

It has been speculated if the eastern part of South America, represented by a terrane located mainly in Uruguay and southern Brazil, the Punta del Este Terrane (Basei et al., 2005) later renamed as Arachania (Frimmel et al., 2010) may be of “African” origin or representing a continental volcanic arc as the overriding plate during subduction and closure of the Brazilides Ocean (comparable to the Adamaster Ocean earlier defined). Between 650-600 Ma a smaller ocean opened between Arachania and the eastern Kalahari craton, producing the Marmora Terrane as an oceanic back-arc block. The Marmora Terrane was so thrusted onto the continental blocks during final collision and metamorphism of the Late Ediacaran and the Early Cambrian, at the same time as the Brazilides Ocean closed (Frimmel et al., 2010). This model implies a variety of tectono-magmatic conditions and processes which shall not be discussed here. An argument to avoid such speculations is the scarce data sets that exists (Zimmermann, 2018), and therefore more substantial data needs to be added to the discussion.

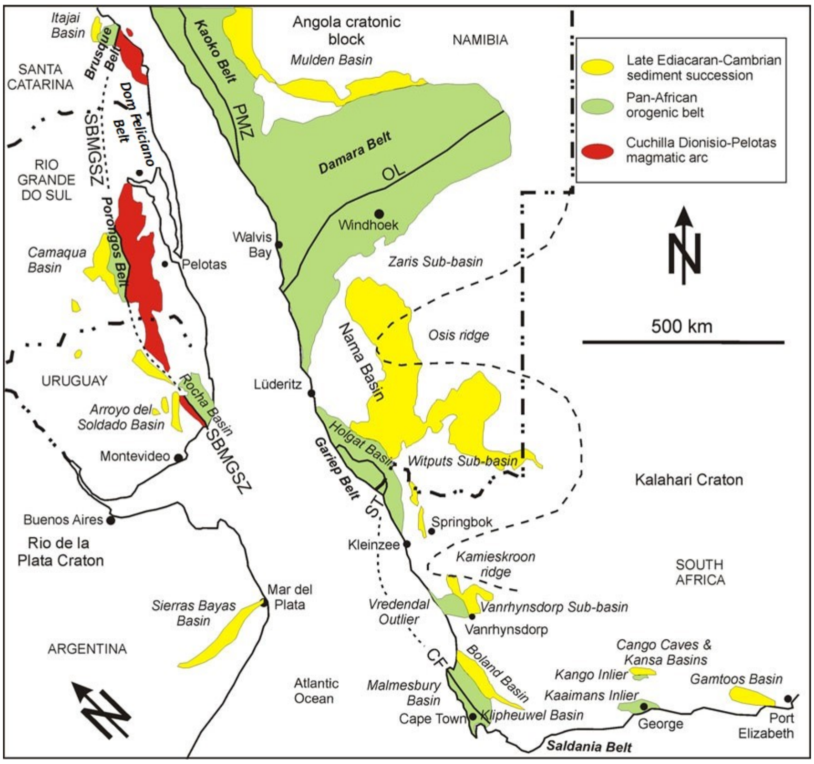

Figure 3-1 Position of Pan-African/Brasiliano orogenic belts on both sides of the south Atlantic Ocean. Abbreviations: CF Colenso Fault, OL Okajandja Lineament, PMZ Purros Mylonite Zone, SBMGSZ Sierra Ballena-Canguc¸u´-Major Gercino Shear Zone, SCT Schakalsberge Thrust (modified from Frimmel et al., 2010).

3.1 Gariep Belt

The Gariep Belt is one of the orogenic belts in the Pan-African/Brasiliano network that formed as a result of the Neoproterozoic Ocean basin, the so-called Adamastor Ocean, that separated the Kalahari craton of southern Africa from the Rio de la Plata craton in South America (Frimmel and Jiang, 2001). The continent-continent collision due to the closing of the ocean is believed to have peaked in the Gariepian orogeny. The belt stretches parallel to the Namibian coastline, from Lüderitz in the north to Kleinzee (South Africa) in the south (Figure 3-1) and has a width of up to 80 km. If the geodynamic model that includes the existence of the Neoproterozoic Adamastor Ocean is true, the Gariep Belt should reflect a passive continental margin, associated with an active continental margin in the Dom Feliciano Belt. The fact that the Gariep Belt has a generally low metamorphic grade, makes this belt important in the quest of understanding the Earth history of the Neoproterozoic. The rocks of the belt should give an exceptional insight into the crustal thinning and eventually break-up of Rodinia, the possibly global glaciations, the opening of an oceanic basin and continent-continent collision, with all it entails (Frimmel, 2018).

Although the metamorphism and syn-orogenic magmatism is considered to be low-grade, the Gariep Belt has undergone intense folding, thrusting and faulting making it difficult to interpret the extent and structure of former depositional basins (Frimmel, 2010). In addition, restricted access to parts of the belt due to diamond mining and the fact that other large parts are covered by sand of the Namib Desert, has led to significantly less research on this belt compared to other (Frimmel, 2018).

The belt is subdivided into two main tectonostratigraphic zones: the Porth Nolloth Zone and the Marmora Terrane (Figure 3-2). The Porth Nolloth Zone in the east and external parts is considered continental and para-autochthonous as it still sits on its basement. The Marmora Terrane in the west is considered to be largely oceanic deposits, and allochthonous, without any basement. A thrust fault called the Schakalsberge Thrust separates the two, and the Marmora Terrane is assumed to have been thrusted on top of the Port Nolloth Zone along the thrust in a south-eastern direction (Frimmel et al., 2010).

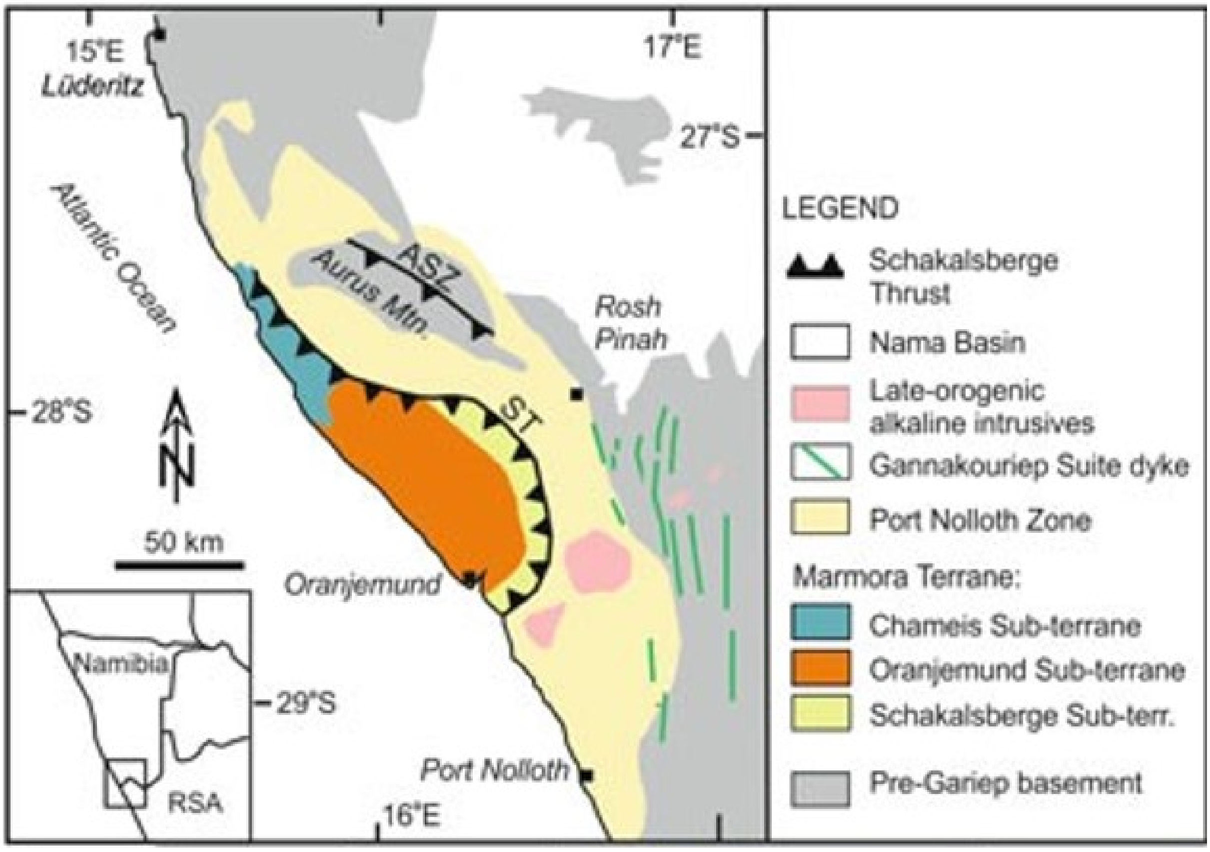

Figure 3-2 The main tectonostratigraphic units of the Gariep Belt (modified from Frimmel, 2018).

3.2 The Porth Nolloth Zone

The Port Nolloth Zone with its deposits is interpreted to reflect an entire rift-drift and collisional process and its sedimentary record should yield information of most of the Neoproterozoic Era from about 770-550 Ma (Basei et al., 2005). Two diamictites are exposed and correlated with the snowball earth hypothesis (Frimmel et al., 2010). The basement of which the Porth Nolloth Zone rest upon is Paleo- to Mesoproterozoic in age (Frimmel and Foelling, 2004). The age constraints for the Porth Nolloth Zone are constrained by a granite of the Lekkersing Formation providing a maximum age for the onset of the Neoproterozoic sedimentation of around 770 Ma and the Nama Group, which lies conformably on top of the youngest Porth Nolloth Zone sediments, estimated to be around 550 Ma and younger (Frimmel et al., 2010). The Porth Nolloth Zone is interpreted to represent three major stages of basin development (Figure 3.2-1) with the Stinkfontein Subgroup representing the continental rift-related sedimentation, the Hilda Subgroup (Pickelhaube, Rosh Pinah, Wallekraal and

Dabie formations in Figure 3.2-1) representing deposition along a passive margin and the Holgat Formation representing the syn-orogenic foredeep deposits (Basei et al., 2005).

Covering the different successions would go beyond the scope of this thesis. However, as the Porth Nolloth Zone has been used as basis for the age assumptions of the Marmora Terrane, the lithostratigraphic correlation of the two units (Figure 3-3) is of relevance (Frimmel, 2018).

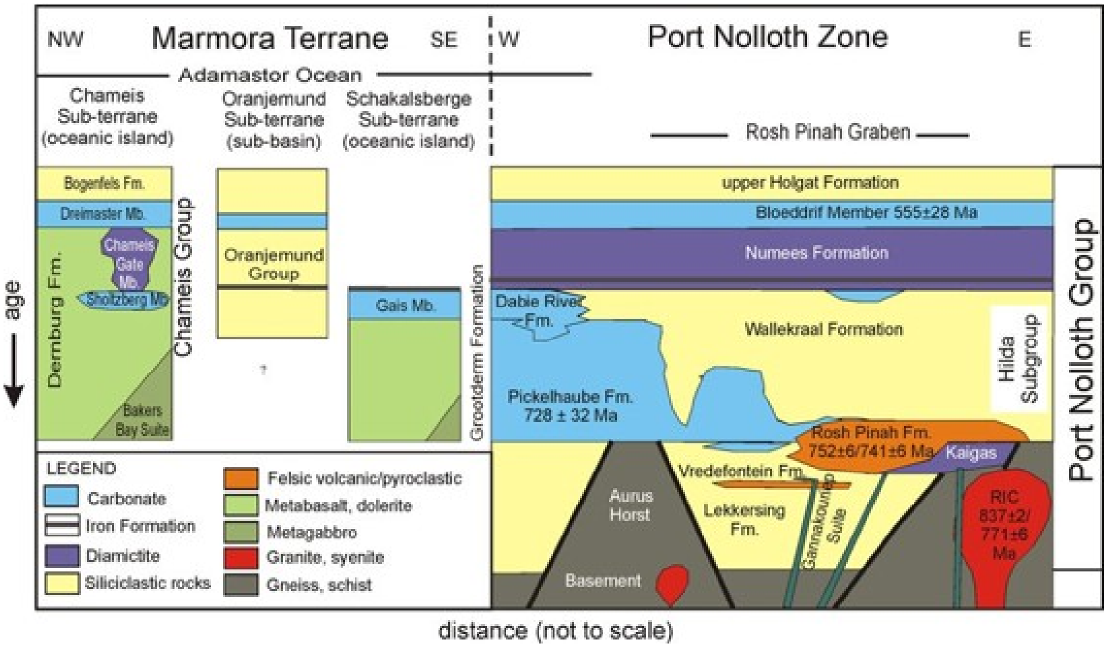

Figure 3-3 Lithostratigraphic correlation of the Porth Nolloth Zone and the Marmora Terrane (Frimmel et al. 2010).

3.3 The Marmora Terrane

In contrast to the Porth Nolloth Zone, the Marmora Terrane lacks a basement and is interpreted to be entirely allochthonous, thrust-bounded by the Schakalsberge Thrust (Frimmel, 2018). Few provenance data exist from the Marmora Terrane, and the detrital zircon ages that do are not enough to exclude any possible sources (Zimmermann, 2018). No significant input of continental siliciclastic rocks has been observed in the lower part of the stratigraphy. Oceanic crustal rock types are interpreted to dominate the lower part and the terrane is thus proposed to be made up of largely oceanic crust (Frimmel et al., 2010).

The Marmora Terrane is further divided into three different subterranes, all of which have their own characteristic distribution of rocks and differs in stratigraphy (Figure 3.2-1). The tectonically lowest subterrane (Schakalsberge Subterrane) is, together with the tectonically highest one (Chameis Subterrane), mostly made up of mafic volcanic rocks such as metabasalts and metagabbros. They both have carbonates over the mafic succession, and the Chameis Subterrane has a minor siliciclastic deposit on top of that. The middle unit is the Oranjemund Group, which differs from the other two. Not only is it lacking further subdivision into formations, it also consists mainly of siliciclastic rocks and is a sedimentary succession (Frimmel, 2018). While the mafic rocks of the Porth Nolloth Zone are subalkaline, those of the Marmora Terrane are alkali-basaltic.

3.3.1 The Schakalsberge Subterrane

The Schakalsberge Subterrane is further divided into the Grootderm Formation, which is a thick succession of metabasaltic rocks of alkaline composition capped by the silicified dolomitic Gais Member. At the base it was intruded by metagabbros (Frimmel et al., 1996). The depositional environment of the Grootderm Formation has been interpreted to represent a guyot (an underwater volcanic mountain with a flat top built up of oceanic crust), with the Gais member representing reef growth on top of that oceanic volcanic island. The interpretation is based on geochemical data of the mafic unit, showing typical signature of oceanic within-plate basalts, and the missing continental input in the Gais Member carbonate deposits.

3.3.2 The Oranjemund Subterrane

Large parts of the exposed rocks within the Oranjemund Subterrane are along the coast of Namibia and hence also within the restricted diamond mining area (Figure 3.1-1). The stratigraphy comprises large amounts of mafic chlorite schists, sometimes overlain by thin chert and dolomite, followed by a thick succession of low-grade metamorphosed arenites with a fining upwards trend (Basei et al., 2005; Frimmel, 2018). Due to large parts of the Subterrane being covered in sand of the Namib desert, contacts are not exposed. In addition, intense folding further hampers the understanding of the stratigraphy. It is thus not further subdivided into formations but defined as the Oranjemund Group. The chlorite schist can be interpreted as a product of proximity to eroding oceanic seamounts, while the fining upwards successions of arenitic beds are interpreted as being the product of down-slope turbidity currents (Basei et al., 2005).

3.3.3 The Chameis Subterrane

At the northwest end of the Marmora Terrane, along the coast of Namibia, the Chameis Subterrane is located (Figure 3.1-1). It is stratigraphically subdivided into the Dernburg and Bogenfels formations. The Dernburg Formation resembles the Grootderm Formation with its volcanic stratigraphy and metabasaltic rocks intruded by bodies of metagabbros of the Bakers Bay Suite. It even has its own dolomitic Sholtzberg Member, missing continental clastic input, which consequently have been correlated with the Gais Member of the Grootderm Formation. The Dernburg Formation is largely composed of mafic rocks such as thinly laminated greenschists originating possibly from amongst other rocks, former tuff beds and metamorphosed alkali basaltic lava flows (Frimmel, 2018). Associated with the Dernburg Formation is also a locally developed diamictite, the Chameis Gate Member, assumed to be stratigraphically placed in the uppermost part of the Dernburg Formation and correlated with the Numees Formation of the Porth Nolloth Zone (Figure 3.2-1). The diamictite is interpreted to be of glacial origin, although this is still highly speculative. The assumption of the diamictite representing a glacial event could indicate that the evaporation of seawater in an atoll setting on top of an oceanic island could have been triggered by sea-level fall. This sea-level fall would in that case be due to global cooling, ahead of the glacial event that covered the Gariep Basin Sea with ice (Frimmel, 2018).

On top of the Dernburg Formation lies the Bogenfels Formation. The lower part of the formation consists of the Dreimaster Member, composed mostly of carbonates. It comprises a thinly laminated and to some extent dolomitized limestone at the bottom and a thickly bedded, micritic dolomite as well as chert and dolomite breccia at the top. The upper part of the formation, overlying the Dreimaster Member, comprises a siliciclastic succession of quartzites, meta-arkose, phyllites, chlorite schists and calcareous metapelite. The Bogenfels Formation is, together with the upper Oranjemund Group, correlated with the Holgat Formation of the Porth Nolloth Zone.

4 Methodology

4.1 Outcrop localities and sample material

A review of existing data published with regards to the Gariep Belt points to the issue of contributions added before today's knowledge of sampling techniques and potential problems when carrying out quantitative analysis (Zimmermann, 2018). With this in mind, the extensive collection of samples given access to for this thesis was carefully handled with a critical view on how samples were selected and prepared for each analysis. One part of the sample material was always kept for record.

4.1.1 Outcrop localities

All samples were collected in previous years by the supervisor for this thesis, Dr. Udo Zimmermann. The outcrops are located along the west coast of Namibia, between Lüderitz in the North and just south of the town Oranjemund at the border to South Africa. The Marmora Terrane is part of an area that is very restricted, as it includes the Diamond Area No. 1, also known as the Sperrgebiet (means "restricted area" in German) National Park. Although access to the area was granted prior to the collection of these samples, other limitations did prohibit documentation such as photos of outcrops and surroundings while sampling, because the area is still highly active for diamond mining (by Namdeb Diamond Corporation (PTY) LTD). However, at each outcrop where samples were taken, the GPS-location was noted. The GPS coordinates allows for correlation with geological maps for further description of sample localities in this chapter.

The outcrops sampled from include all three subterranes within the Marmora Terrane defined by Frimmel (2000; 2018); Schakalsberge, Oranjemund and Chameis Subterranes (Figure 4-1).

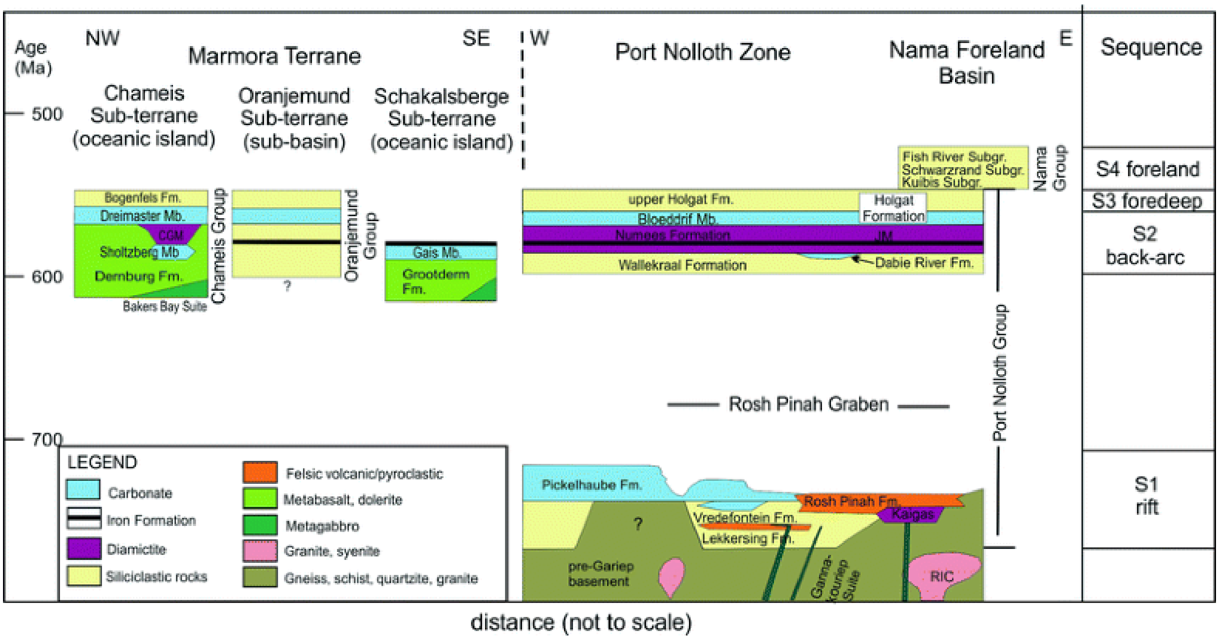

Figure 4-1 Lithostratigraphic subdivision of the Gariep Supergroup. To the left the Marmora Terrane and its subdivision, to the right the Porth Nolloth Zone (not sampled from for this thesis). Abbreviations: CGM = Chameis Gate Member; JM = Jakkalsberge Member; RIC = Richtersveld Igneous Complex; Fm= Formation; Mb = Member; Subgr. = Subgroup. (Frimmel, 2018)

The Schakalsberge Subterrane is the tectonically lowest of the three and consists of the mafic, predominantly volcanic Grootderm Formation with the dolomitic Gais Member as a cap carbonate on top (Frimmel, 2000; 2018). In this thesis only the Grootderm Formation from the Schakalsberge

Subterrane is analysed. The location of the two outcrops situated in this subterrane is marked by squares in Figure 4.1.1-2.

Within this tectonically sandwiched packet of rocks, the middle unit is represented by the sedimentary and then predominantly siliciclastic Oranjemund Subterrane. The Oranjemund Subterrane is, unlike the two others, not further subdivided into formations. This is largely due to the difficulty in understanding the regional extent and distribution of the subterrane as it is often covered by the Namib Desert (Frimmel, 2018). In this subterrane the extent of mafic volcanic and intrusive rocks is significantly lesser than for the other two. The location of the Oranjemund Subterrane outcrop is marked by a star in Figure 4-2.

At the tectonically highest position is the Chameis Subterrane, mainly consisting of mafic volcanic rocks overlain by carbonates and minor siliciclastic rocks (Frimmel, 2018). Within the Chameis Subterrane two formations are defined: the Dernburg and Bogenfels formations. The Dernburg Formation has a volcanic stratigraphy similar to that of the Grootderm Formation, containing a dolomitic succession, called the Sholtzberg Member. It also comprises few evaporites (Frimmel and Jiang, 2001). Gabbros and serpentinized ultramafic rocks compose the Bakers Bay Suite within the Dernburg Formation and are interpreted as intrusive metamorphosed bodies (Frimmel, 2011). The Chameis Gate Member (CMG) at the top of the Dernburg Formation shows an association of diamictites and mafic metatuff beds (Frimmel, 2018) together with metamorphic rocks of sedimentary origin. The overlying, and youngest succession, the Bogenfels Formation comprises at the bottom the carbonate-dominated Dreimaster Member overlain by siliciclastic strata of quartzite, meta-arkose, phyllite, chlorite schist and calcareous pelite (Frimmel, 2018). Circles in Figure 4.1.1-2. mark the exact location of the two outcrops within the Chameis Subterrane.

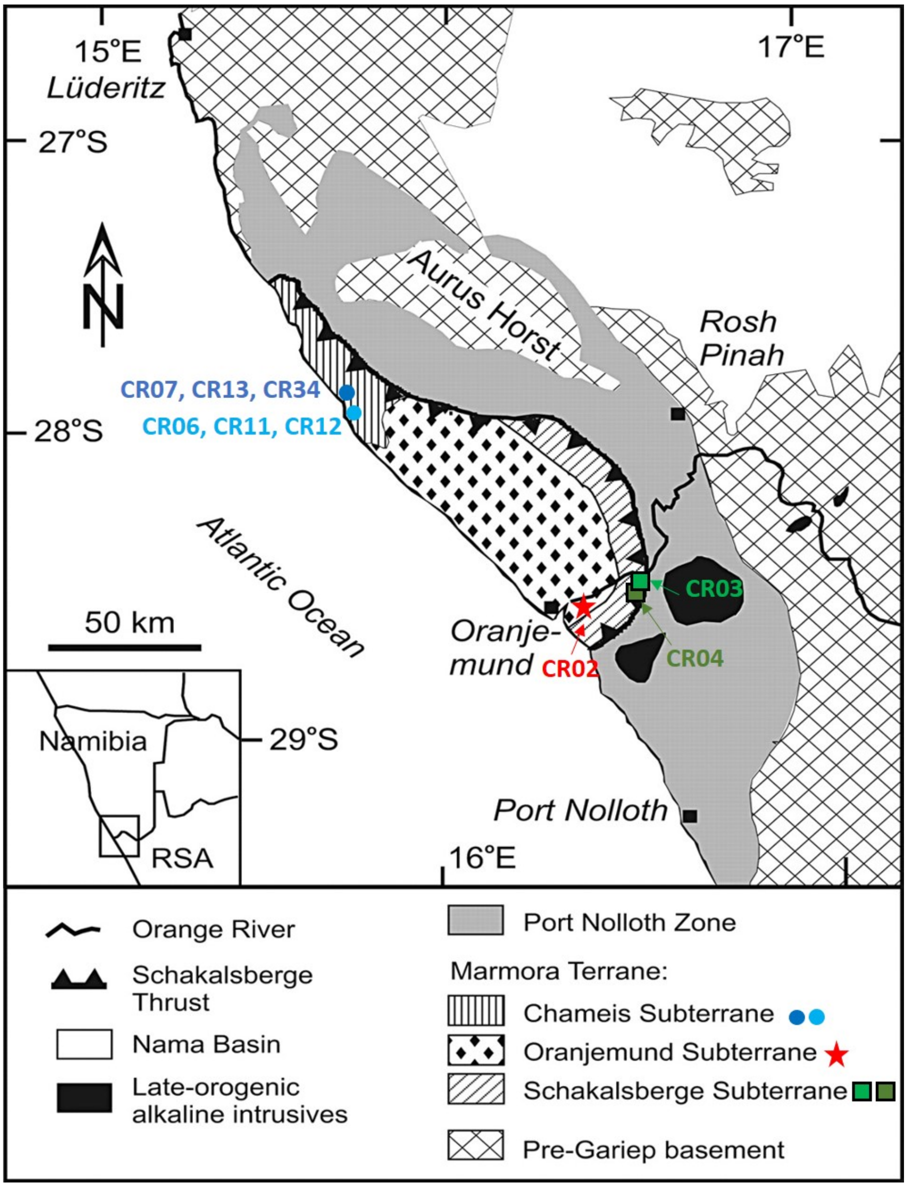

Figure 4-2 Map showing the units within the Gariep Belt on both sides of the Orange River, the international boundary between the Republic of South Africa (RSA) and Namibia. Modified from Frimmel (2011).

4.1.2 Sample overview

The samples used for further analytical work within this thesis originate from five unique outcrops within the Marmora Terrane. From each outcrop a variety of material within the exposed formation, or within each exposed formation if multiple exposed, were meticulously sampled to ensure that there was no bias in the sampling method due to sorting effects and grain size distribution.

Up to 1 kg of sample material for each rock type, within each formation, was combined into one zircon sample. Combining a variety of samples was done to avoid any bias due to sorting, and to cover all grain sizes. A case study from northern Spain (Zimmermann et al., 2015) revealed that the impact the sampling technique within a single sedimentary succession has on the results when it comes to interpreted maximum depositional ages, understanding of geological evolution of cratonic blocks or correlation purposes should not be ignored.

9 zircon samples were given a name with CR as prefix followed by a unique number, making the sample ID CRXX. The zircon samples have a zircon yield ranging from few only to excellent. Additionally, 3-4

samples within each zircon sample combination were also studied separately with respect to their mineralogical and geochemical content, to ensure that the samples originate from the same deposit. This was carried out with x-ray diffraction (XRD) and preliminary geochemical analysis on whole rock samples. Petrography of selected thin sections were used as a complementary resource to support the findings from other analysis. However, this study will only go in depth and concentrate on the isotopic data, as the complexity of petrography and geochemistry combined with the presented isotopic data would go beyond the scope of a master thesis. All analytical work was conducted by the author of the thesis, unless stated otherwise.

The entire overview of sample material used for this thesis, including GPS coordinates for sample location, zircon sample names and number of samples used for XRD analysis, petrography and geochemical analysis can be found in Table 4-1.

Table 4-1 Overview of the sampled material and number of samples used for analysis. Abbreviations: XRD: x-ray diffraction, TS=thin section, GC= geochemistry, Fm: Formation, BBS: Bakers Bay Suite, CMG: Chameis Gate Member, n/a=not applicable.

Outcrop location	Subterrane Name	Formation or Group name	Rock type	Zircon sample name	Samples analysed		
					XRD	TS	GC
28° 30' 26.8'' S, 16° 42' 39.9'' E	Schakalsberge	Grootderm Fm	Basalt	CR04	4	2	n/a
28° 30' 9.5'' S, 16° 43' 51.3''E	Schakalsberge	Grootderm Fm	Epiclastic	CR03	3	1	5
28° 35' 36.7'' S, 16° 30' 16.4'' E	Oranjemund	Oranjemund Group	Metaclastic	CR02	3	1	8
27° 54' 55.7'' S, 15° 41' 6.2'' E	Chameis	Bogenfels Fm	Metaclastic (micaschist)	CR11	3	1	5
		Dernburg Fm	Metaclastic (greenschist)	CR12	3	1	13
		Dernburg Fm/ BBS	Gabbro	CR06	3	1	n/a
27° 52' 41.3'' S, 15° 40' 32.8'' E	Chameis	Dernburg Fm/ BBS	Gabbro	CR07	3	3	n/a
		Dernburg Fm/ CMG	Metaclastic	CR13	3	3	11
		Dernburg Fm/ CMG	Diamictite	CR34	2	2	5

4.2 Zircon sample preparation

The preparation of zircon samples includes separating the zircons from other minerals of the host rock and mounting them in epoxy so that each zircon grain has an exposed polished surface, with known internal structure, to examine and analyse. For the sake of comparison, it was considered important that all samples were processed in the same way and with the same techniques. Laboratory work was always conducted with a high focus on avoiding risk of contamination or introduction of bias influence. For that reason, good laboratory routines with regards to cleaning and sample handling, experienced laboratory personnel and understanding of the potential risks remained essential throughout sample preparation.

4.2.1 Separation

The selected samples for zircon analysis were sent to Geotrack Mineral Services in Melbourne, Australia, for mineral separation. The following explanation of the procedure is provided by Geotrack Mineral Services as a courtesy. The applied method is a routine method for zircon separation. As three samples were already separated by Geotrack, all other samples analysed were separated there as well for the sake of comparison. Following the procedure of jaw crushing to reduce the size, disc pulverisation to disaggregate the rock, hand washing for small sample amounts and separating table for larger sample amounts, the resulting fine sand sample was dried before separation. The separation of heavy and light minerals was done with the use of a Frantz magnetic separator as well as two different heavy liquids; tetrabromoethane with a specific gravity of 2,95 g/cm^3 and methylene iodide with a specific gravity of 3,3 g/cm^3. Only the non-magnetic fraction at 25° slope, 10° angle and full scale on the Frantz magnetic separator was put into methylene iodide. The magnetic fraction was put aside. From the separation in methylene iodide the light fraction was stored in a separate vial, containing apatite, andalusite, fluorite and other composites. The heavy fraction was again processed at 25° slope, 2° angle and full scale on the Frantz magnetic separator. The resulting two fractions were the ones used for further analysis, zircon concentrate (non-magnetic) and zircon fraction (magnetic). Along with the resulting fractions Geotrack Mineral Services also provided an overview of the zircon yields and heavy mineral percentages.

4.2.2 Mounting

The zircon concentration, and/ or zircon fraction in the cases where the zircon yield was too low, was carefully transferred onto the lower part of a glass plate and placed under a binocular microscope. The tip of a thin needle placed on a shaft (micro pick from Ted Pella Inc) was used to handpick the zircon grains one by one and transfer them to double sided tape placed on the upper part of the glass plate. The zircon grains were carefully placed on an exposed line of the tape (200-300 zircons per line), at the centre of a circle measuring 25mm in diameter. Protective plastic film was used to cover the tape elsewhere but the thin line exposed. The picking was done randomly to avoid any bias. After initial picking the sample was studied to confirm that all grainsizes and shapes were represented. Further picking was conducted if the picked grains were not representative. When in doubt if a grain type was a zircon or not, it was picked to avoid possible exclusion of age populations based on ignorance. Only one sample was processed at a time, with careful cleaning of the equipment and working area between samples. After one sample was picked, the exposed area of the tape was changed. A mount map created while picking the zircons made sure all lines where meticulously noted down with sample names to avoid any risk of contamination. At the end, 5-6 samples were placed in thin lines on one piece of tape.

A plastic holder of 25mm diameter (Struers Fixiform) was placed upside down on the tape with the zircon lines centred and put in a vacuum chamber with a pressure of 0,12 bar (Struers CitoVac). Epoxy (mixture of Struers epofix hardener and resin) was then poured from the top until the form was half-filled. The epoxy was left to harden for 12 hours, before it was lifted off the tape. A visual check under the microscope was performed to check that the lines were all intact and as originally placed on the tape.

The epoxy mounts where then carefully grinded on a glass plate with 1000 grit silicon carbide powder to make sure the zircon grains were not covered by epoxy, and to expose their internal structure. After grinding they were polished with two different diamond suspensions; first with 3 µm (micrometre) diamond suspension on a polishing cloth made of woven acetate and then with 1 µm diamond suspension on a short synthetic nap polishing cloth. Between each step the epoxy mounts were cleaned in an ultrasonic cleaner with distilled water. Figure 4-3 shows a closeup of one of the lines on one of the epoxy mounts made for this thesis.

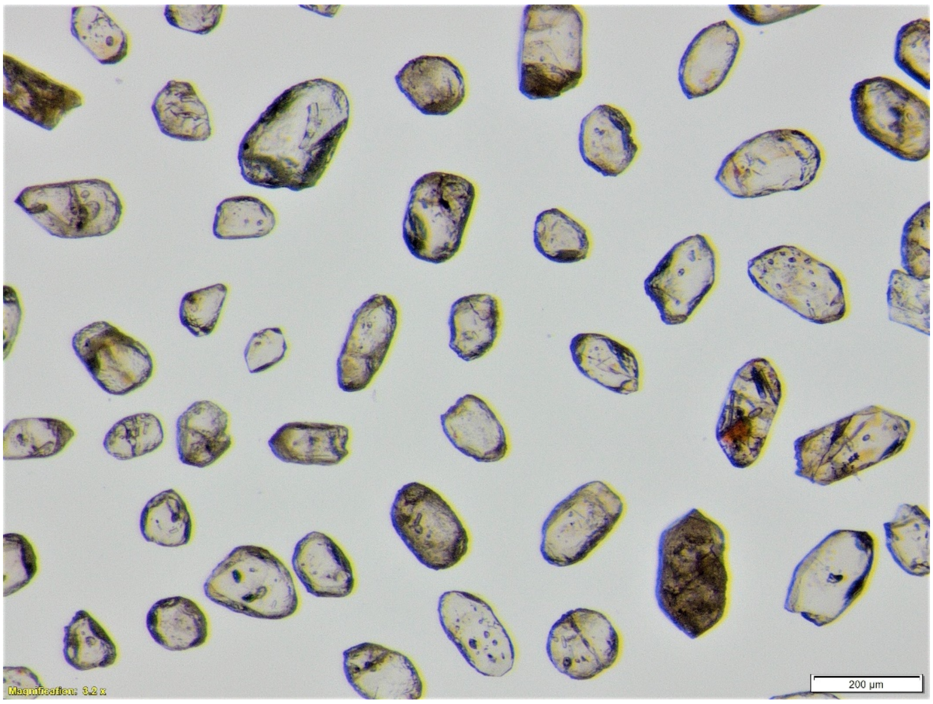

Figure 4-3 Polished surface of zircons mounted in 25mm diameter epoxy mounts, observed with an optical microscope.

4.3 Scanning electron microscopy

In the sample material, most zircons ranged from 30 to 150 µm in width, and from 50 to 250 µm in length. Although macroscopic properties such as colour, external morphology, presence of inclusions (to some degree), fractures and alterations could be observed while picking the zircons under a binocular microscope, information on the internal structure is also necessary before conducting U-Pb isotope analysis. The best resolution of a zircons internal structure is obtained with CL imaging in a SEM. The SEM used for imaging, and in some cases elemental composition analysis of unknown grains, was located at UiS. It was a Zeiss Supra 35VP FE-SEM equipped with a field emission (FE) gun, and the detectors used were a CL detector as well as an energy dispersive spectroscopy (EDS) detector of the type EDAX.

4.3.1 Carbon coating

Non-conductive material must be coated with a thin film of conductive material. If not, when scanned by a beam of high-energy electrons, electric charge will build up and distort the image (Goldstein et al., 2003). To ensure an electronically conductive surface, enabling imaging and inhibiting charging effects in the SEM, the epoxy mounts were coated with a 20-25 nm thick layer of carbon. This was done by evaporation of carbon thread. In addition, the epoxy mounts were fixed to the sample holder with carbon thread to ensure contact between the sample surface and the sample holder used to insert the sample into the SEM vacuum chamber. Carbon was chosen as coating material over gold or palladium firstly because it is the best choice for cathodoluminescence work and secondly because it also has a minimal effect on the x-ray spectrum (Goldstein et al., 2003).

4.3.2 Cathodoluminescence imaging

To obtain high resolution photos of each zircon sample, with the intergranular structure and zonation patterns revealed, the CL-detector of the SEM was used. The aperture size was set to 120 µm, and the acceleration voltage to 15kV. The working distance was around 9-11 mm for most samples, and the magnification of the obtained images ranged from 100 to 280 x in order to identify regions of interest and regions to avoid in the following U-Pb isotope analysis. After analysis the samples were again imaged with respect to their cathodoluminescence, this time to make sure the spot was correctly placed during ablation, as well as to discover any potential drifting while ablating the zircon (Figure 4-4). This was done to further improve the interpretation of the obtained ages, and to give the reader a better understanding of the data presented.

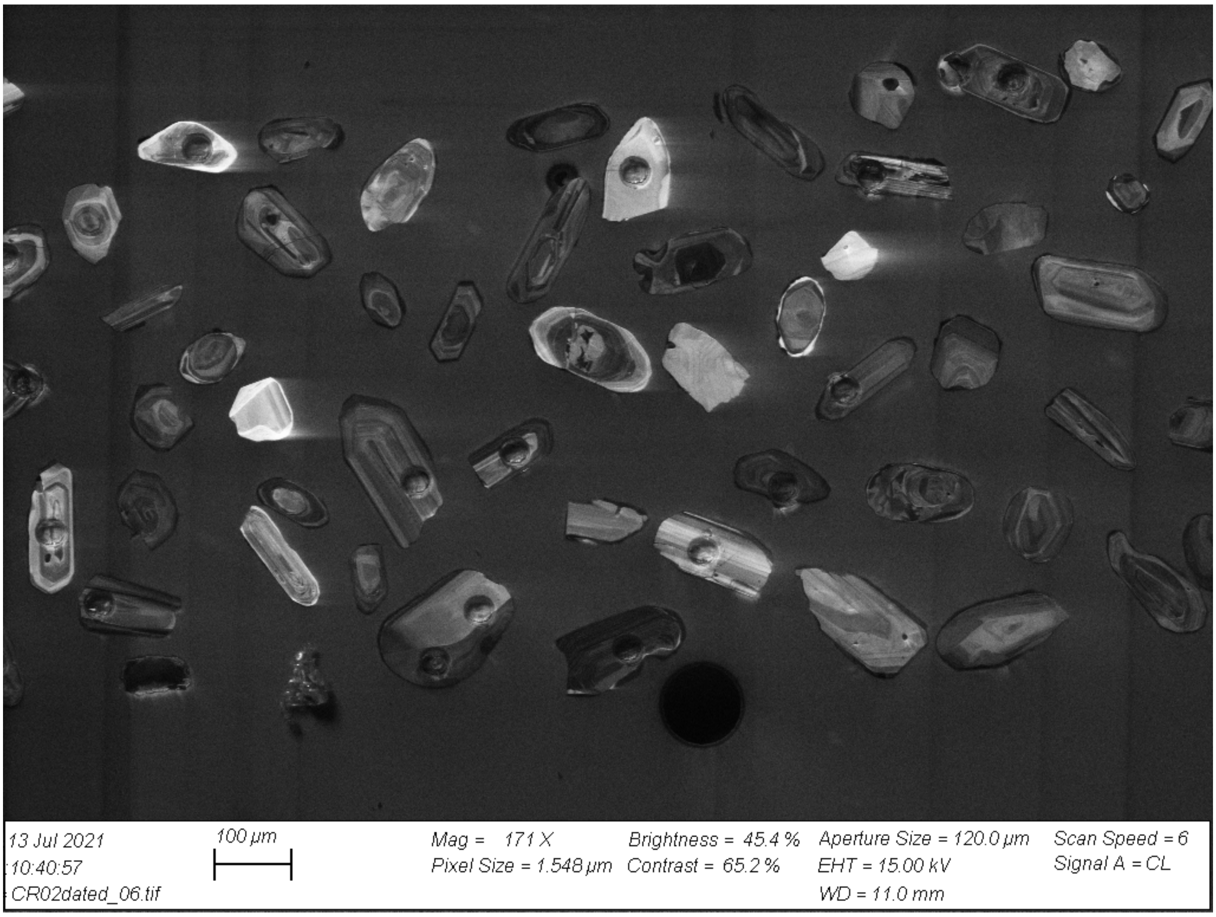

Figure 4-4 Zircons imaged in a scanning electron microscope with a cathodoluminescence detector. Imaging done after uranium lead isotope analysis. The circular spots on the zircon grains are the visible impact crater resulting from the ablation by laser.

4.3.3 Backscattered electron imaging and energy dispersive analysis

In samples with presence of unknown grains that did not show a clear zircon signature with CL-imaging, BSE images and EDS-analysis was performed to avoid any confusion and possible exclusion of zircon grains in the following U-Pb isotope analysis. The BSE-images and the interpretation of the EDS spectra for the relevant samples were actively used during the U-Pb isotope analysis, in order not to introduce any bias where in doubt. In most samples where other minerals than zircons were present, EDS analysis revealed that for most cases the mineral was apatite.

4.4 Uranium lead isotope analysis

The U-Pb isotope analysis was conducted by laser ablation, inductively coupled plasma mass spectrometry (LA-ICP-MS) at the ICP-MS laboratory at the Department of Geosciences at UiO.

4.4.1 Data acquisition

The specific instrument used was a Bruker Aurora Elite quadrupole mass spectrometer equipped with a Cetac LSX 213 G2 + laser microprobe. The ablations were made in helium, which was mixed with argon within the plumbing system of the ablation cell (Andersen et al., 2018). The commonly used spot size was 40 µm in diameter, with a laser shot frequency of 10Hz. A bug in the laser software inhibited accurate reading of the laser energy and this value is therefore not reported. The shutter delay was set to 10 seconds, and the burst count to 400. For some of the samples the zircon grain size did not allow for a 40 µm spot size. In these samples the spot size was set to 30 µm while the other parameters remained unchanged. Standards and references were ablated several times to take extra care that the drop in spot size did not affect these measurements. The standards used to calibrate isotope fractionations were zircon standards GJ-1 (600,5 $\pm$ 0.4 Ma; Belousova et al., 2006; Schaltegger et al., 2015), 91500 (1065 $\pm$ 1 Ma; Wiedenbeck et al., 1995) and A382 (1877 $\pm$ 2 Ma; Huhma et al., 2012). The standards were run at the start and end of each session. In addition, the standards GJ-1 and 91500 were run at regular intervals during the session (for every 20th ablation for GJ-1, together with 91500 for every 40th ablation). An in-house reference zircon STA (294,2 $\pm$ 0,3 Ma) from the Stavern syenite pegmatite in the Oslo Rift (Norway), was also run at the beginning of every session as an unknown. In samples displaying Archean ages, an older standard was added as an unknown; OG1 (3465,4 $\pm$ 0,6 Ma Stern et al., 2009).

The reduction of the raw data was done using an in-house, inter-active Microsoft Excel spreadsheet. A filter excluding analyses that were more than 10 % normally discordant was applied. Only zircon ages with discordance of 10 % or less, which had no other analytical concerns, were considered concordant ages and thus used for further discussion in this thesis. Zircon spots with high concentrations of lead were corrected for common lead, but those corrections are complicated (Andersen et al., 2020) and not all corrected zircons revealed an acceptable discordance (< 10 %) after correction. A total of 21 analyses were corrected for common lead, while only 6 of these are presented as acceptable discordant ages. If an age that is presented or discussed in the thesis has undergone common lead correction, it is noted for the convenience of the reader.

The number of single zircons ablated for each sample ranges from 10 to 124, largely depending on the zircon yield of each sample. The number of total ablations for each sample ranges, however, from 16 to 153. This difference in number of zircons ablated and total number of ablations is due to both several shots in larger grains and ablations for rims and cores in one single grain where a distinct rim was present. For larger grains several ablations were done to test the homogeneity of the age within the grain. For those grains with a distinct core and rim large enough to be analyzed, both were ablated to gain information about the growth evolution of the grain. If interpreted as a rim at the time of analysis, the sample name was given the letter “r” at the end (e.g., CR03_77 for the core and CR03_77r for the rim). If uncertain if the outer edge of a zircon was a rim, or if the grain was large enough to ablate several times, a number was added at the end of the sample name (e.g., CR04_35 and CR04_35-2). An overview of ablations, concordant analysis, rims and common lead corrections is given in Table 4-2. All data from ablated zircons are given in Appendix A.

Table 4-2 Overview of zircon yield, total number of ablations and number of analysed zircons per sample. Please see the chapter 4.4.1 for explanation of discordance.

Zircon sample name	**Zircon yield**	**Number of total ablations**	**Number of zircons analysed**	**Number of concordant zircons (<10% discordance)**	**Percentage of con-cordance (%)**	**Number of con-cordant rims**	**Number of concordant zircons corrected for common lead**
CR04	Low 40+	104	80	62	77,5	13	0
CR03	Excellent	127	124	84	67,7	4	0
CR02	Excellent	153	120	85	70,8	7	4
CR14	Very good	69	60	41	68,3	6	0
CR07	Few only	28	17	13	76,5	0	0
CR34	Low	83	76	48	63,2	0	0
CR13	Low 30+	57	49	29	59,2	1	0
CR12	Low – good 100+	75	61	54	88,5	3	1
CR11	Low 40+	47	31	30	96,8	3	1
CR06	Few only	16	10	6	60	0	0
CR01	Excellent	112	100	91	91	6	0

4.4.2 Data visualization

The U-Pb data obtained was plotted as Wetherill concordia diagrams ($^{206}Pb/^{238}U$ versus the $^{207}Pb/^{235}U$ ratios) and probability density histograms with Isoplot version 4.15 (Ludwig, 2012). The ages plotted in the probability density histograms represent the $^{207}Pb/^{206}Pb$ age for zircons older than 1000 Ma and the $^{206}Pb/^{238}U$ age for zircons younger than 1000 Ma. This cut-off age was used to compare the data within this thesis to former data from the Oranjemund Formation by Andersen et al. (2018). The correct cut-off age, if this can exist, is highly disputed (e.g., Puetz et al., 2021) and not a matter of importance for the scope of this thesis.

The youngest concordant ages are interpreted by four different methods, according to the study done by Dickinson and Gehrels (2009). (1) The youngest single grain age (YSG) with 1σ uncertainty. However, if the youngest single grain age has 1σ > 10 Ma and overlaps at 1σ with the next youngest single grain age, the latter grain age is used. (2) The youngest graphical DZ age peak on the age-probability plot (YPP), as controlled by multiple U-Pb grain ages (single-grain age peaks ignored). (3) The weighted mean age of the youngest cluster of two or more grains (YC1σ) whose uncertainties overlap at 1σ. (4) The weighted mean age of the youngest cluster of three or more grains (YC2σ) whose uncertainties overlap at 2σ.

4.5 Optical light microscopy on polished thin sections

The microscope used for optical light microscopy (OLM) is a standard Zeiss Axio Lab A1 microscope with objective lenses ranging from 2,5 to 20 x magnification, rotary stage and the possibility of transmitted light as well as crossed polarized light. OLM was used to get a better understanding of the host rock of which zircons were extracted. The rock type, main minerals and framework, grain sizes and degree of metamorphism are all characteristics where thin sections can offer a better insight. Thin sections were either provided by ACME Laboratories in Vancouver, Canada, or made at UiS. Microphotographs were taken to support the description of the rock types.

4.6 Xray diffraction analysis on whole-rock samples

XRD analysis was conducted as a qualitative analysis on powdered, whole-rock (bulk) samples, to identify the main mineralogic composition of the samples. This was done to provide supportive analysis for the rock characterisation performed in OLM. The analysis was carried out at UiS, with a Bruker D8 advance Eco diffractometer equipped with a Lynxeye detector (Cu-Kα radiation, 40 kV voltage, 25 mA current). Each sample was analysed as a bulk sample, hand milled to fine powder and prepared after standard XRD protocols for sample preparation of powdered materials. The measuring conditions were set to analyse from 5-90 degrees using a 0,6 mm divergence slit, with 1 degree per minute while rotating the sample continuously during measurement.

4.7 Geochemistry (GC) on whole-rock samples

Results of whole-rock geochemical analysis were made available for the thesis. The samples were analysed for total whole-rock characterisation (analytical code LF202) by ACME Laboratories in Vancouver, Canada, with standard ICP-MS protocols for trace elements and Inductively Coupled Plasma Emission Spectrometer (ICP-ES) for major and minor element determination. A further detailed description of the analytical specification can be found in e.g., Zimmermann et al. (2016) or at http://acmelab.com. For the igneous samples CR04, CR06 and CR07, the geochemical results did not differ significantly from the results published by Frimmel et al. (1996). For these samples the short comments on the composition and origin were based on the already published data by Frimmel et al. (1996).

5 Results

5.1 Mineralogical composition

The interpretation of the mineralogical composition is based on XRD-analysis of whole-rock samples and petrographic studies of polished thin sections. The results are presented with an interpreted XRD spectrum of 3-4 analysed samples for each zircon sample. Microphotographs of polished thin sections with 2,5 x magnification in plane polarized light (ppl) and cross polarized light (xpl) respectively at the top and bottom, are presented to the right of the spectrum. Under are two microphotographs with 10 x magnification, taken with (from left to right) ppl and xpl. Scale is included in all microphotographs of thin sections. The samples are presented under their respective subterranes and formations.

5.1.1 The Schakalsberge Subterrane

5.1.1.1 The Grootderm formation

Two samples, CR04 and CR03, were analysed from the Grootderm Formation of the Schakalsberge Subterrane. The samples show similarities in their mineral composition. The interpretation of the mineralogical composition for the Schakalsberge basalt (CR04) is based on XRD analysis of 4 whole-rock powdered samples, and petrographic studies of 2 polished thin sections under OLM. The Schakalsberge basalt has a mineralogical framework consisting of quartz (less than 5%), chlorite, feldspar (albite), epidote and calcite. Rutile, zircon and iron oxides are also observed in thin sections, while interpretation of the XRD results also reveals titanite and biotite (Figure 5-1). The rock is extremely chloritized and albitized. The heavy mineral percentage is calculated to be 3,16 %.

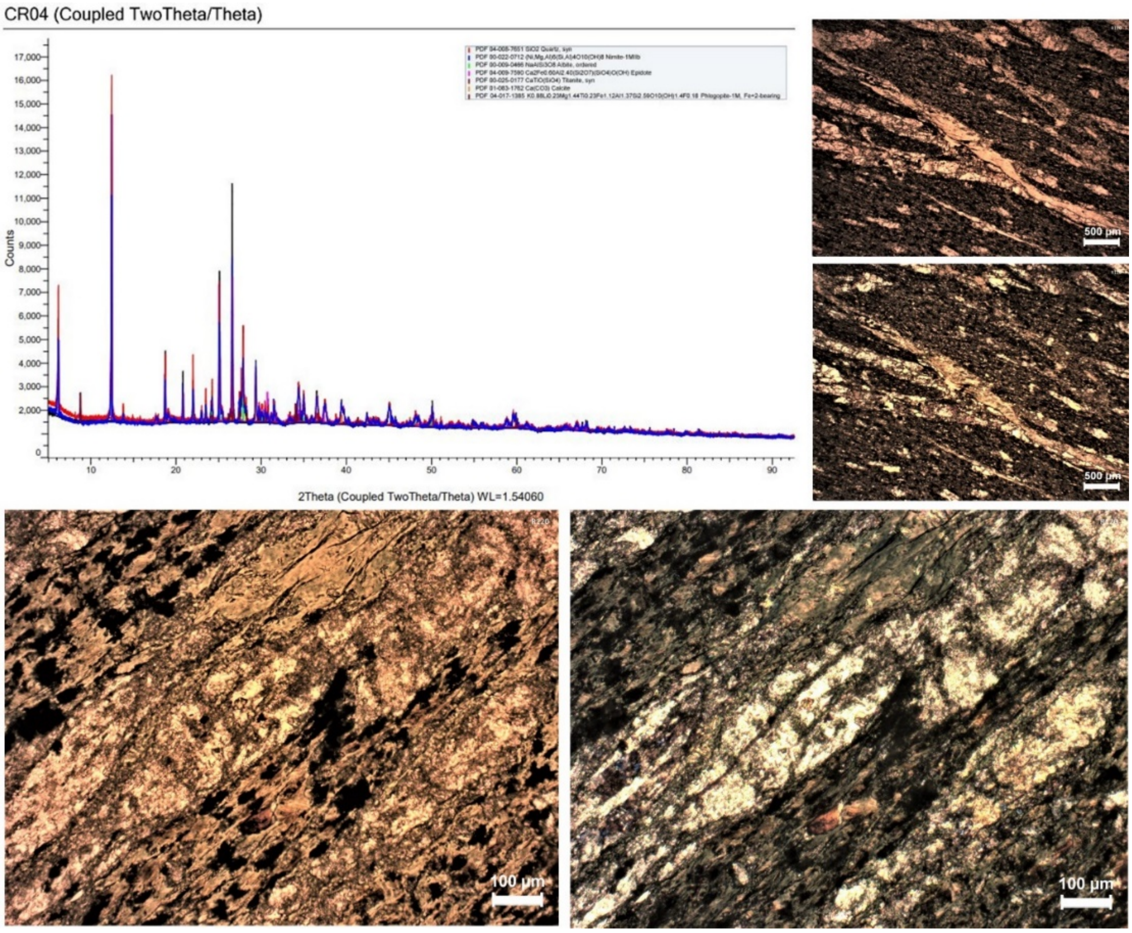

Figure 5-1 Interpreted XRD patterns and thin section microphotographs (ppl and xpl) of the extremely chloritized and metamorphic sample CR04.

A phyllite of the Schakalsberge Subterrane (CR03) was analysed by XRD with 3 whole-rock powdered samples. The XRD patterns within the samples gathered as zircon sample CR03 show no significant change in the mineralogy. The heavy mineral percentage of CR03 was calculated to be 0,08 %. A thin section was also studied under OLM, revealing squared calcite/dolomite, feldspar (mostly albite but with some plagioclase left) and opaque minerals like magnetite, hematite or pyrite (Figure 5-2). Rutile and zircon are also observed. The main mineralogical composition from the XRD diffraction patterns of the analysed samples was interpreted to consist of feldspar (albite), chlorite, quartz and calcite. The amount of carbonate was relatively high and could be secondary as in some areas the calcite was observed in thin veins. The higher amount of quartz and the grainy texture with the absence of ghost structures or any relicts of former glass, allows for interpretating that this rock also contains clastic material, and that the material has been reworked. The phyllite is therefore classified at this stage of knowledge as an epiclastic rock with unknown amount of non-volcanic material.

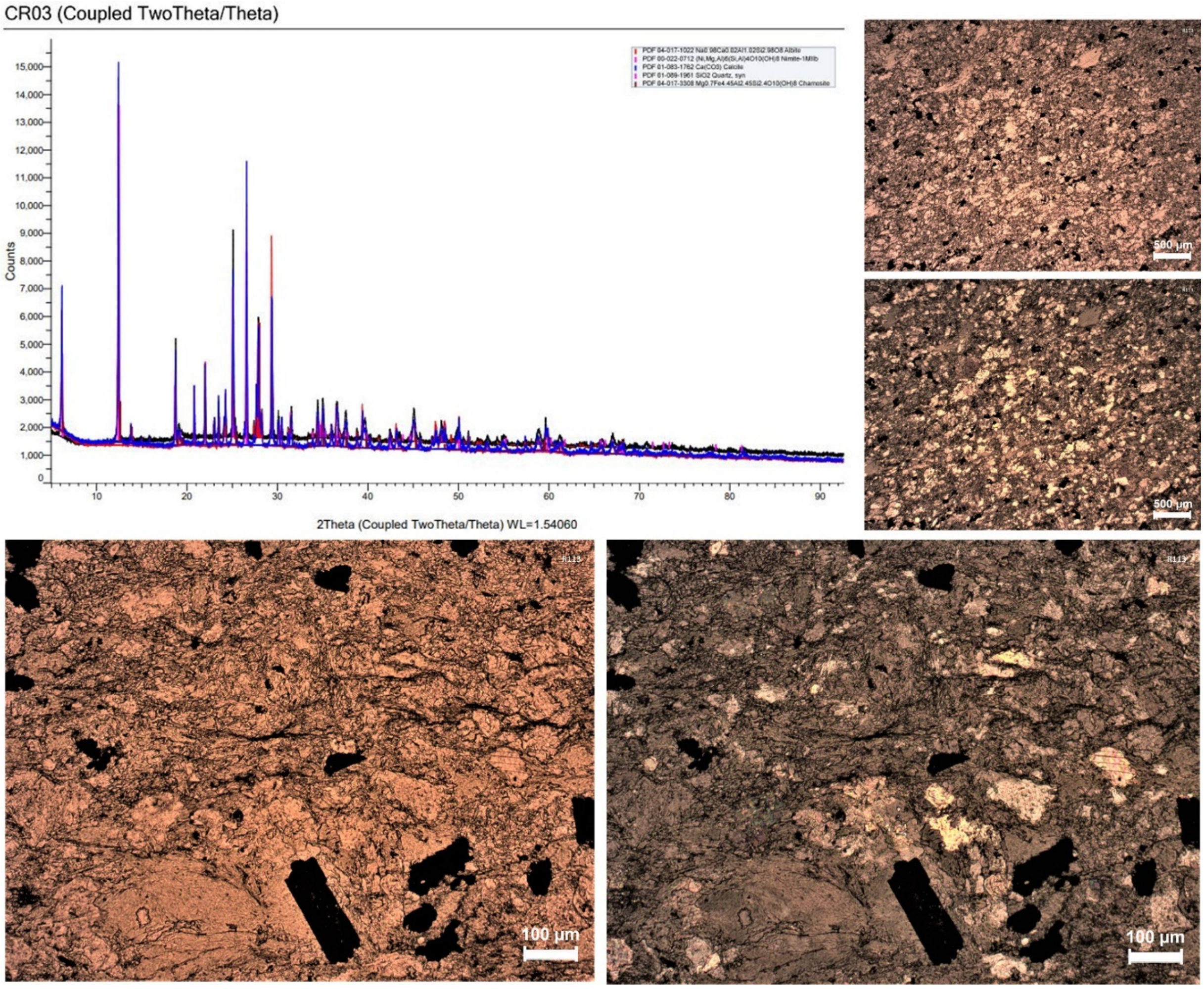

Figure 5-2 Interpreted XRD potterns and thin section microphotographs (ppl and xpl) of sample CR03.

5.1.2 The Oranjemund Subterrane

5.1.2.1 The Oranjemund Group

The metaclastic rocks sampled from the Oranjemund Group were classified as phyllites to slates (CR02). Interpretation of the mineralogical composition was based on XRD analysis of 3 whole-rock powdered samples and a thin section studied under OLM. The thin section revealed quartz veins with calcite and muscovite (Figure 5-3). The calculated heavy mineral percentage of CR02 was 0,09 %. The interpreted diffraction pattern from the XRD analysis supported the interpretation of quartz, calcite and muscovite. In addition, feldspar (albite) and chlorite were observed. The rock showed thin dismembered layers and clusters of quartz, mostly polycrystalline with different grain sizes within a matrix of very fine-grained material. The texture could be described as proto-mylonitic reflecting the mentioned strong deformation of the entire rock package of the Marmora Terrane. Former studies describe the rocks as turbidity currents (Basei et al., 2005) which is possible, but possibly more convincing in other outcrops than the one sampled from for this thesis.

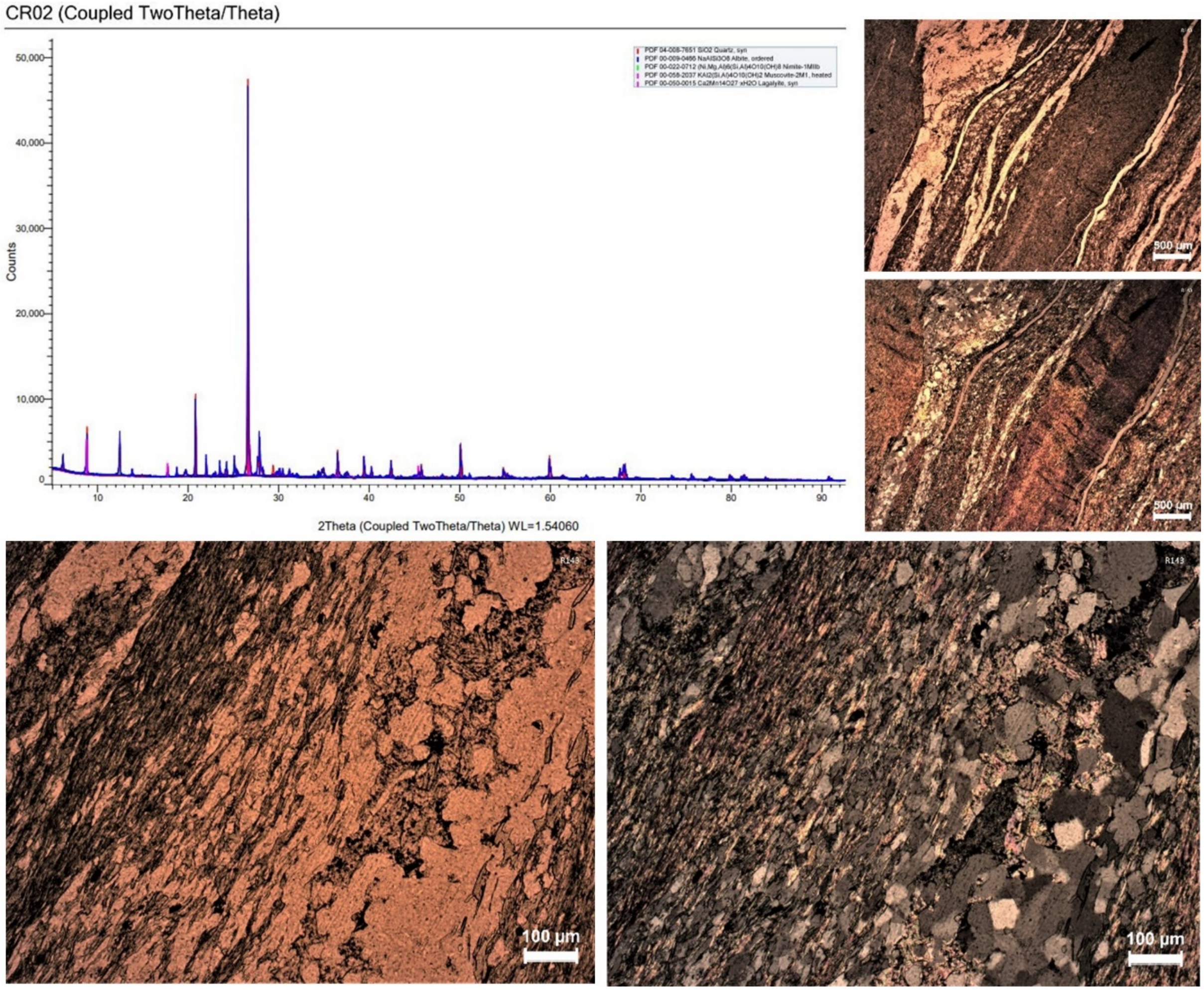

Figure 5-3 Interpreted XRD patterns and thin section microphotographs (ppl and xpl) of sample CR02.

5.1.3 The Chameis Subterrane

Within the Chameis Subterrane, samples were analysed from two formations, the Bogenfels and the Dernburg formations.

5.1.3.1 The Bogenfels Formation

From the Bogenfels Formation metaclastic rocks, classified as a micaschist, has been sampled (CR11). It had a calculated heavy mineral content of 2,41 %. Petrographic analysis of thin sections and XRD analysis of 3 powdered whole-rock samples provided basis for interpretation (Figure 5-4). The main mineralogical composition compiled quartz, feldspar (albite/microcline), chlorite and mica (muscovite). The thin section revealed a highly deformed rock, showing signs of beginning mylonitization and strong metamorphic overgrowth by phyllosilicates. Polycrystalline quartz and titanite were observed in the optical microscope.

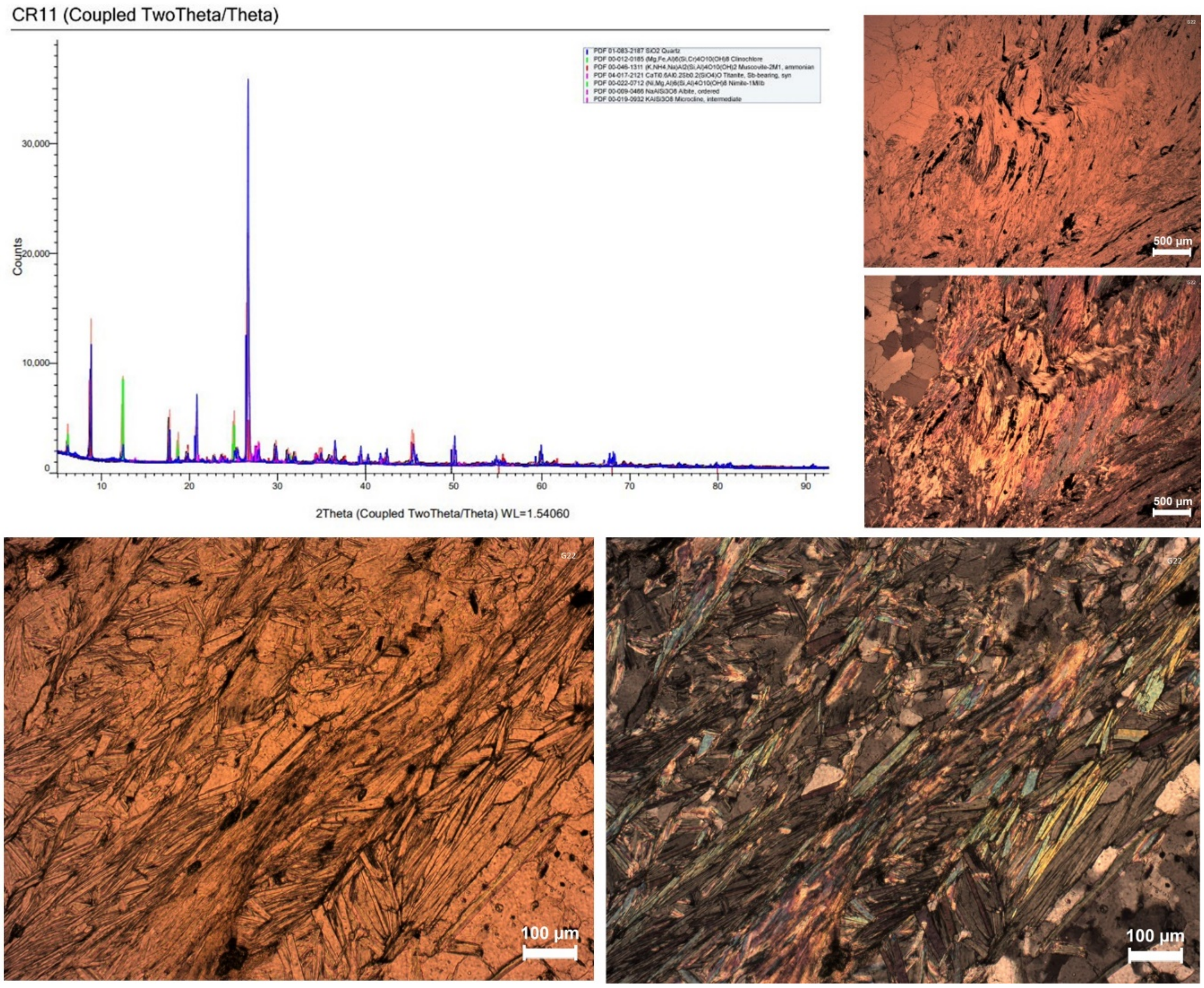

Figure 5-4 Interpreted XRD patterns and thin section microphotographs (ppl and xpl) of sample CR11. Note the polyphase deformation of the sample revealed in the optical microscope.

5.1.3.2 The Dernburg Formation

From the Dernburg Formation a metaclastic rock (CR12) as well as two gabbros (CR06, CR07) of the intrusive Bakers Bay Suite were analysed. Metaclastic rocks (CR13) and a diamictite (CR34) from the Chameis Gate Member (part of the Dernburg Formation, see Figure 3.2-1) were also studied.

The metaclastic rock (greenschist) of the Dernburg Formation, CR12, yielded a calculated heavy mineral percentage of 1,21 %. Petrographic analysis of a thin section and XRD analysis of 3 powdered samples provided insights to the main mineralogical composition. The mainly occurring minerals were feldspar (albite), chlorite, amphibole (hornblende/actinolite), calcite, epidote, mica and quartz (Figure 5-5). The thin section also reveals hematite and zircon grains. The mineral composition within the sampled material varies insignificantly. Actinolite and chlorite are very common minerals in low grade metamorphic overprints of mafic rocks, and the combination with metamorphic hornblende is typical for greenschist (Deer et al., 2013). Textural characteristic as in the optical microscope images of Figure 5-5 allow in interpreting clastic input in this rock, which may be partly also of volcanic origin, hence a meta-volcaniclastic rock.

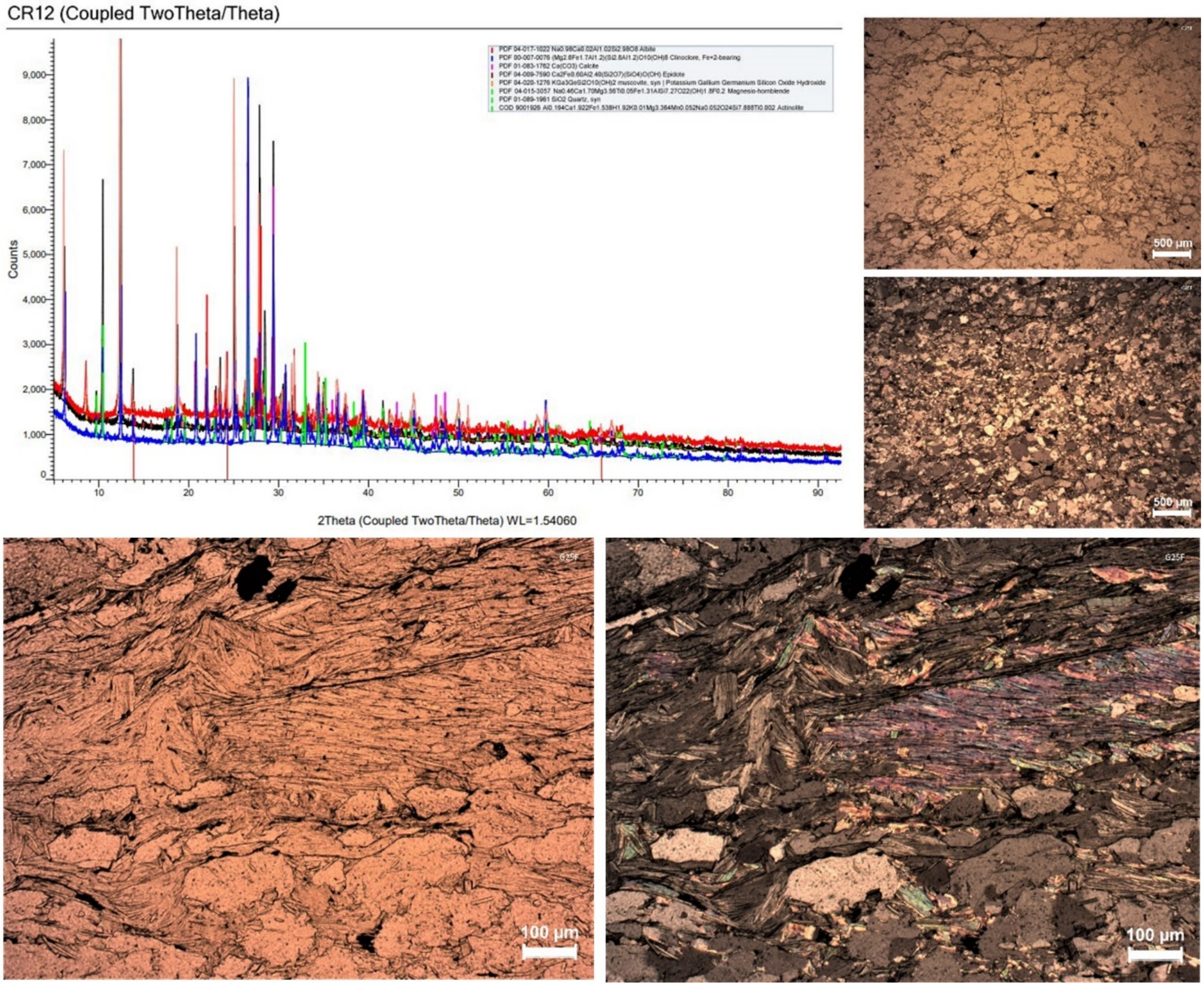

Figure 5-5 Interpreted XRD patterns and thin section microphotographs (ppl and xpl) of sample CR11

One gabbro of the Bakers Bay Suite within the Dernburg Formation (CR06), associated with the described CR12, had a calculated heavy mineral percentage of 4,44 %. Petrographic analysis of a thin section and XRD diffraction patterns of 3 powdered bulk samples provided basis for interpretation of the mineralogical content (Figure 5-6). The main minerals interpreted were feldspar (anorthite), mica (biotite), quartz, clinopyroxene (diopside) and chlorite. Orthopyroxene, a large amount of feldspar (weathered plagioclase) and magnetite as well as a few amphiboles were also observed in the thin section. The thin section revealed a matrix less weathered, a better crystallinity and more mafic rock type than the following gabbro (CR07) of the Bakers Bay Suite. The gabbro is strongly weathered but its texture is still recognizable.

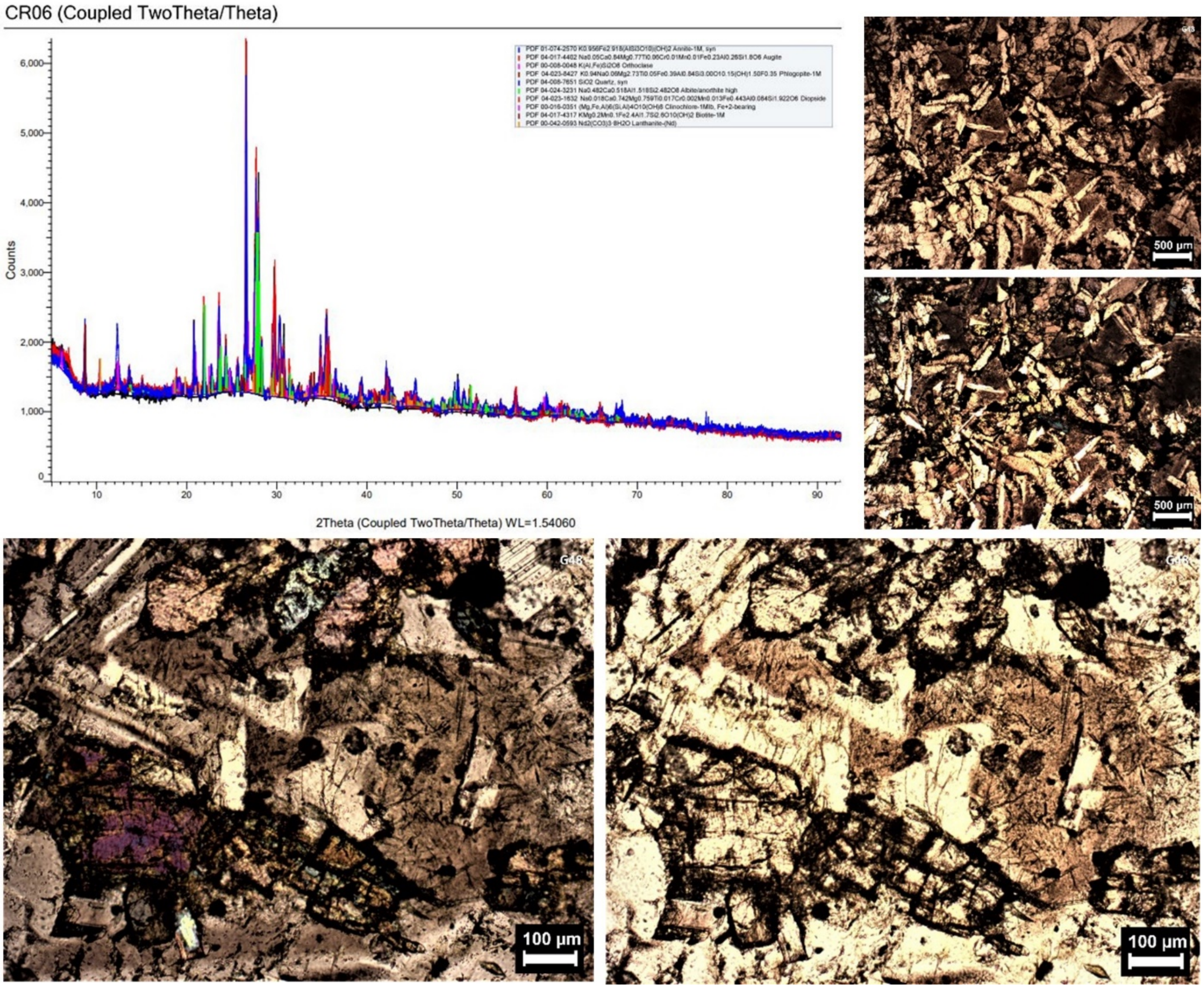

Figure 5-6 Interpreted XRD patterns and thin section microphotographs (ppl and xpl) of sample CR06

The other gabbro (CR07) of the Bakers Bay Suite had a calculated percentage of heavy minerals of 10,67 %. It is associated with the rocks of the Chameis Gate Member. Interpretation of the mineralogical composition was based on petrographic analysis of 3 polished thin sections and XRD analysis on 3 powdered whole rock samples (Figure 5-7). The main mineralogical composition was made up of epidote (clinozoisite), greenish and brownish amphibolite, feldspar (albite), chlorite and biotite. The sample revealed a higher amount of amphibole than the previous gabbro, and appeared in thin sections extremely weathered, abandoning nearly entirely a visible plutonic texture; the latter being easier to recognise in a hand sample of the rock. Nevertheless, quartz, clinopyroxene and purple to white plagioclase were observed. The presence of quartz might be a results of pyroxene weathering to amphibole, realising SiO_2 in the process that crystallized to quartz.

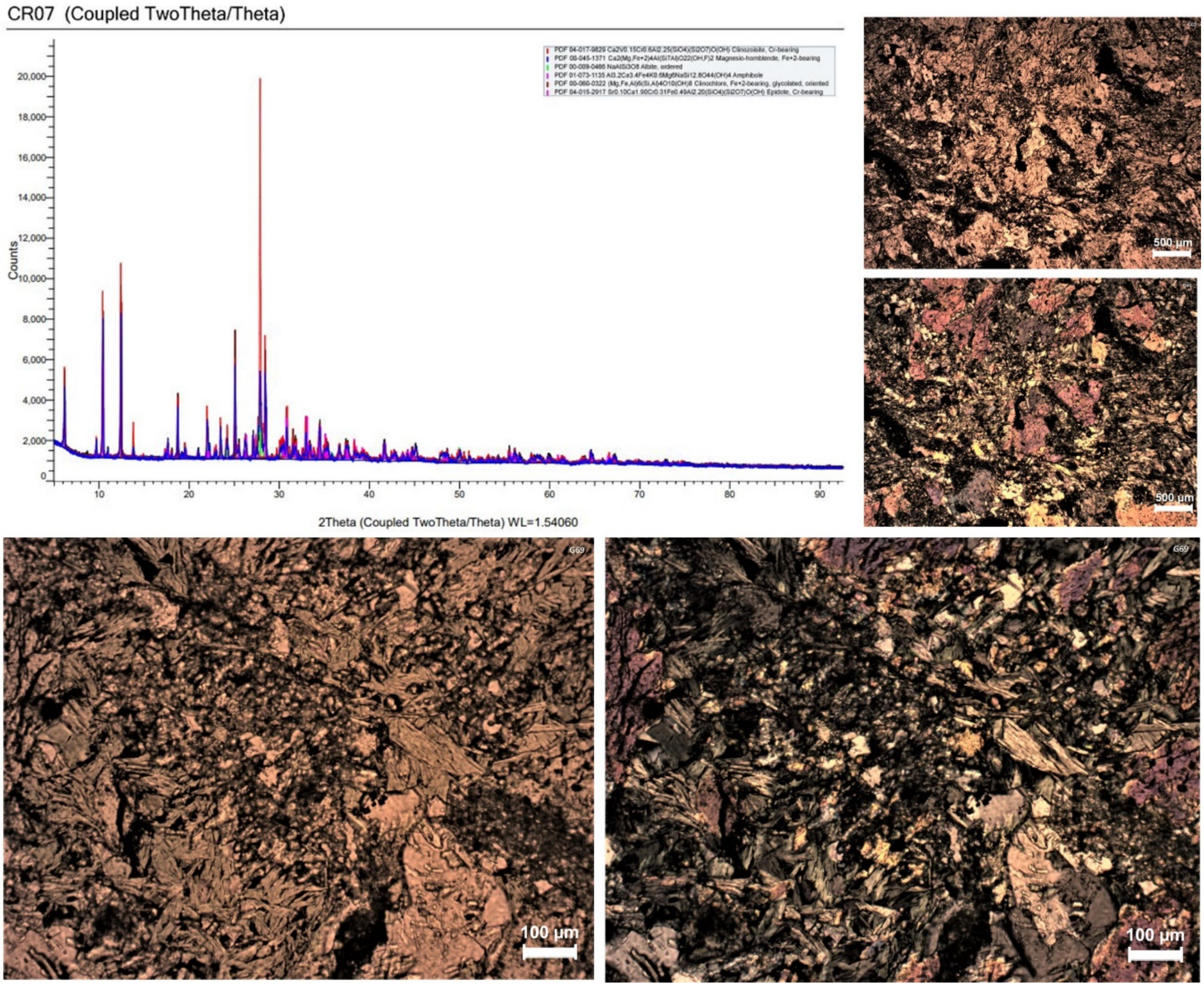

Figure 5-7 Interpreted XRD patterns and thin section microphotographs (ppl and xpl) of sample CR07 showing the extreme effect of weathering of the mafic igneous rock.

The Chameis Gate Member is represented by two samples, a diamictite or metadiamictite (CR34) and a metaclastic rock. This sample (CR13) may be interpreted as a metatuff. The high amount of quartz points to a felsic tuff or an epiclastic rock with an unknown amount of detrital material within a reworked tuff. This interpretation is preferred at this stage of knowledge. CR13 had a heavy mineral content of 28,46 %. Petrographic study of 3 polished thin section and XRD analysis of 3 powdered rock samples provided the basis for interpretation of mineralogical composition (Figure 5-8). The main minerals interpreted were quartz, feldspar (albite), mica (biotite), chlorite, epidote and amphibole (hornblende/actinolite). The thin section indicated, as mentioned, a metamorphosed reworked volcaniclastic rock, probably with high amount of tuff material, but the interpretation is not yet conclusive. Pyrite, phyllosilicates, quartz and amphiboles are also observed in the thin sections.

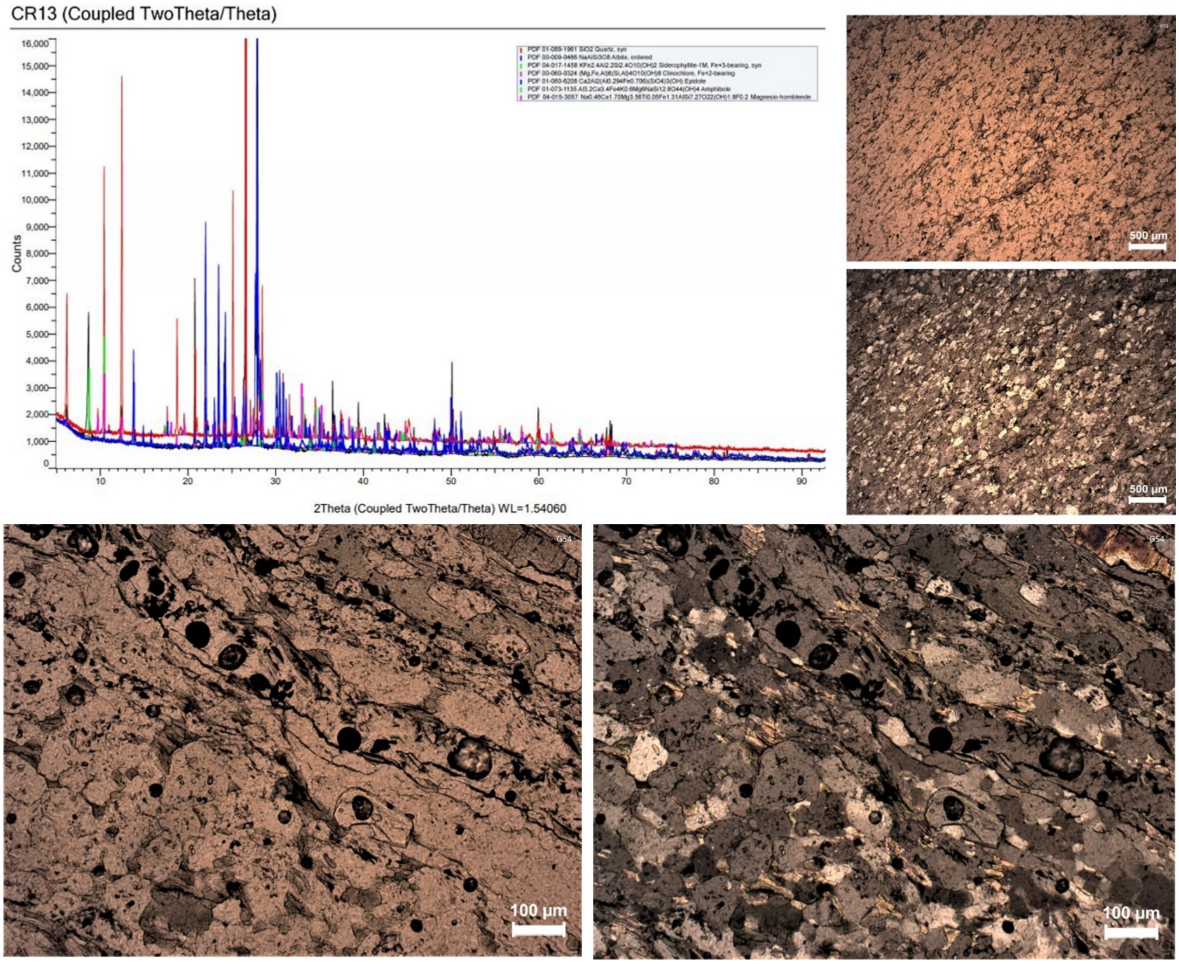

Figure 5-8 Interpreted XRD patterns and thin section microphotographs (ppl and xpl) of sample CR13, showing the felsic nature of the rock.

The last sample discussed here, CR34 from the Chameis Gate Member within the Dernburg Formation, has been interpreted to be a diamictite. In the literature this sample has been interpreted as being of glacial nature within the wake of the "snowball earth hypothesis" (Frimmel et al., 2010) and correlated with other diamictites proposed to be of glacial origin. Therefore, age constraints are of highest interest for this succession. The metamorphosed and strongly deformed diamictite has a heavy mineral content of 1,24 %. Petrographic analysis of 2 samples as well as XRD analysis on 2 samples (Figure 5-9) revealed the presence of feldspar (albite), calcite, quartz, chlorite, amphibole (hornblende/actinolite), pyrite, apatite, zircon and hematite. The amphiboles are definitely not detrital but metamorphic and the rocks are strongly deformed.

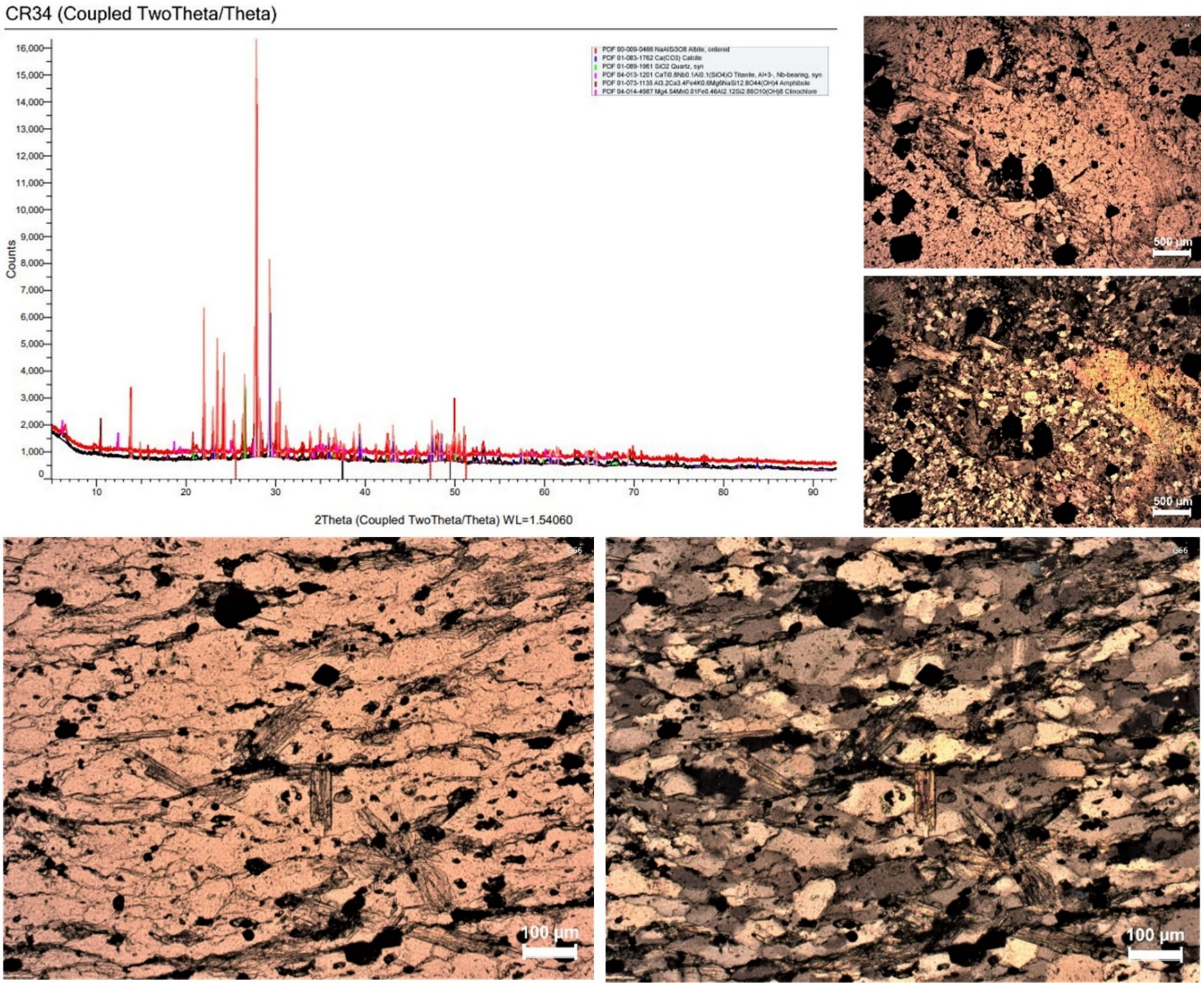

Figure 5-9 Interpreted XRD patterns and thin section microphotographs (ppl and xpl) of sample CR34, with small overgrowing amphiboles visible.

5.2 Geochemical composition

The results from whole-rock geochemistry analysis performed on a number of powdered bulk-samples from each zircon sample were interpreted. The analysis yields a highly complex geochemistry for the different rock successions and formations. For the igneous rocks the results do not differ significantly from data already published (Frimmel et al., 1996) and therefore the already published data were used for the basalt of the Grootderm Formation and the gabbros of the Bakers Bay suite in the Dernburg Formation. This thesis presents a brief overview of the general geochemical character of the different formations, based on the published data from Frimmel et al. (1996). Results from geochemical analysis conducted as part of the thesis on the non-igneous samples can be found in Appendix C.

5.2.1 The Schakalsberge Subterrane

5.2.1.1 The Grootderm formation

The basic rocks of the Schakalsberge Subterrane, both intrusive and extrusive of character, are mainly alkaline tholeiitic and related to an oceanic island basalt (OIB) origin. This points to an extensional setting with an enhanced mid ocean ridge basalt (E-MORB) signature. The phyllites (CR03) within the Grootderm Formation are more differentiated and contain a higher amount of incompatible trace elements. Non-igneous material may be reworked into these rocks, and they are for that reason classified as epiclastic rocks.

5.2.2 The Oranjemund Subterrane

5.2.2.1 The Oranjemund Group

The clastic rocks from the Oranjemund Group show partly low Th/Sc ratios, but Zr/Sc ratios between 20-80 clearly shows reworking within the sample, comparable to the results presented by Basei et al. (2005). Further interpretation of a tectonic setting recorded within the detrital material will not be attempted here as this can only be substantiated within a larger framework of data sets, which are not available at this stage. Any comments otherwise would be pure speculation.

5.2.3 The Chameis Subterrane

5.2.3.1 The Bogenfels Formation

The Bogenfels Formation (sample CR11) contains samples with Th/Sc ratios below 1, and Zr/Sc ratios between 10-40, pointing to a reduced reworking component. The sample undeniably contains mafic and intermediate material as the dominant source component. It may have a reworked detritus from sources rather close, and not have reworked strongly the detritus itself within its depositional environment.

5.2.3.2 The Dernburg Formation

The gabbros of the Bakers Bay Suite in the Dernburg Formation can be divided as proposed by Frimmel et al. (1996) into two suites. One suite (CR06) is related to typical E-MORB signatures with elevated Nb/Yb ratios and characteristics of alkaline tholeiitic rocks related to an extensional tectonic regime. They are partly similar to the mafic rocks of the Grootderm formation with regards to their incompatible element distribution, however the former contains less Nb, Ti and Ta (Frimmel et al., 1996). The other Gabbro suite (CR07), associated with the Chameis Gate Member, shows a geochemical signature more similar to normal mid ocean ridge basalt (N-MORB). This may indicate that the two gabbros of the Dernburg Formation are of different magmatic suites and hence perhaps not related. The different geochemical signatures and the giving association within the other samples may point to tectonic contact rather than intrusive. However, Frimmel (2000) conclude such a setting based on his data set.

Sample CR12 is geochemically similar to the strongly volcaniclastic part of CR13 (see below) as well as the phyllites (CR03) of the Grootderm Formation. All these "mafic" volcaniclastic successions show amounts of silica less than 50 weight percent. The amount of clastic input varies from minute to clearly visible, as shown in the petrography section, and quartz is always abundant. The fact that all rocks, including the gabbros, carried zircons, allows the interpretations in this thesis.

The sample CR13 (part of the Chameis Gate Member) can, based on its geochemistry, be divided into two lithologies: (i) a meta-volcaniclastic rock with enriched compatible elements and a pure mafic composition containing very little clastic material, if any, and (ii) a felsic variation, with Th/Sc ratios above 1 and Zr/Sc ratios between 20-80, definitely comprising a strong clastic input.

The meta-diamictites of the Chameis Gate Member show a typically geochemical fingerprint for well mixed diamictites, with a large variety of ratios for Th/Sc between 0,3-2, and rather low Zr/Sc ratios below 22 (Van Staden et al., 2006; 2010). This indicates that mostly rock successions have been reworked containing immature detritus or are of metamorphic origin. Reworking processes when forming the diamictite have been not able to implement recycled material. Compatible elements do, however, not dominate the detrital composition and are less abundant than in the definitely clastic rocks of the Chameis Gate Member (CR13).

5.3 Zircon Morphology and texture

The morphology and texture of the analysed zircon samples were studied under a normal binocular microscope, while CL-imaging gives insights into the internal characteristics of each grain. For best resolution CL-images, please see Appendix B.

5.3.1 The Schakalsberge Subterrane

5.3.1.1 The Grootderm formation

The zircons of sample CR04 varied in size from 70 to 210 µm in length and 50 to 130 µm in width. Most of the zircons had a stubby or stalky shape, some prismatic crystals were observed as well (Figure 5-10). Quite a few zircons showed their original euhedral shape, the rest are more subrounded. Several of the zircons were fragments of larger crystals. Many grains showed zoning, mostly oscillatory and euhedral oscillatory zoning. Very few grains in CR04 showed no zoning at all. Grains with a xenocryst or complex core were observed frequently. Several grains had inclusions or fractures.

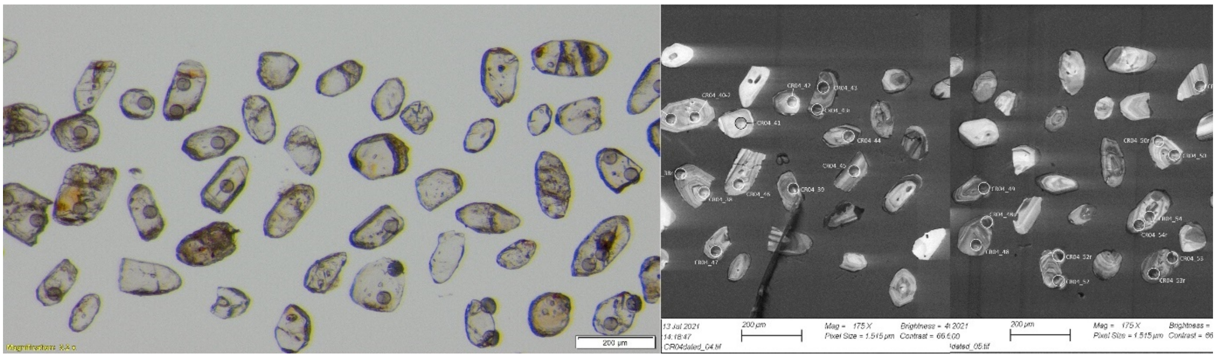

Figure 5-10 Zircon grains of CR04 observed under binocular microscope to the left, with CL-imaging to the right.

The zircons of sample CR03 varied in size from 60 to 350 µm in length and 40 to 150 µm in width. The zircons also varied in elongation (Figure 5-11). Most of the grains showed stubby and poorly rounded shape, however stalky and prismatic grain-shapes were also observed. The stalky and prismatic grains varied from being well rounded to having a more rectangular shape. Few needle-like grains were also observed. Several of the grains were fragments of larger crystals. A number of grains showed zoning, several of them oscillatory or euhedral oscillatory zoning. One grain showed sector zoning. Quite few zircons showed no inner zoning. Several grains showed a complex internal morphology. A few showed xenocryst cores. There were also observed numerous inclusions and some fractures.

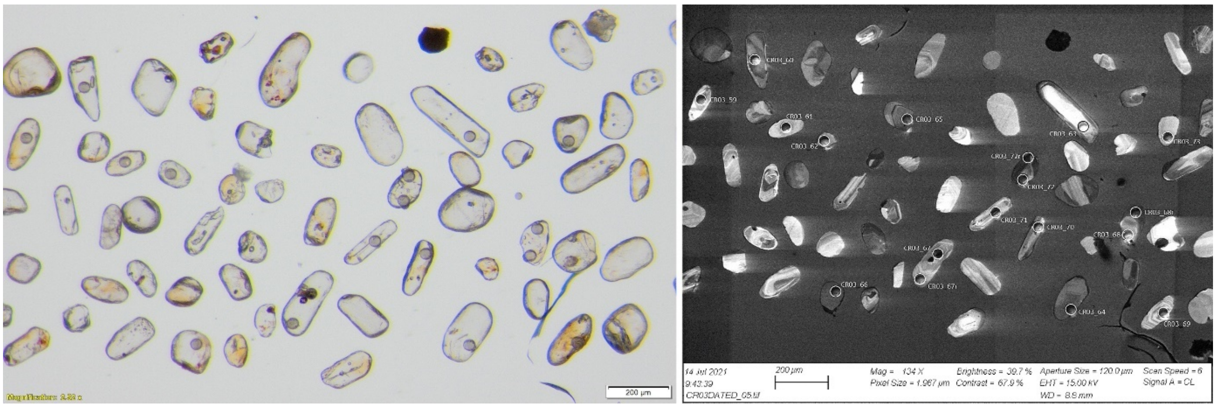

Figure 5-11 Zircon grains of CR03 observed under binocular microscope to the left, with CL-imaging to the right.

5.3.2 The Oranjemund Subterrane

5.3.2.1 The Oranjemund Group

The zircons of sample CR02 ranged in size from 50 to 300 µm in length and 30 to 190 µm in width. Most of the grains had an elongated shape that ranged from stalky to prismatic (Figure 5-12). While the majority were subrounded, some of the grains still showed euhedral form. Needle-like and stubby grains were also observed. Several of the stubby grains were poorly rounded. Quite a few of the grains were fragments of larger crystals. Most of the zircons were zoned, but some grains show no zoning at all. Several of the zircons showed euhedral oscillatory zoning. Numerous of the zircons had an xenocryst core. There were also few grains with a complex internal structure. Fractures and inclusions were observed.

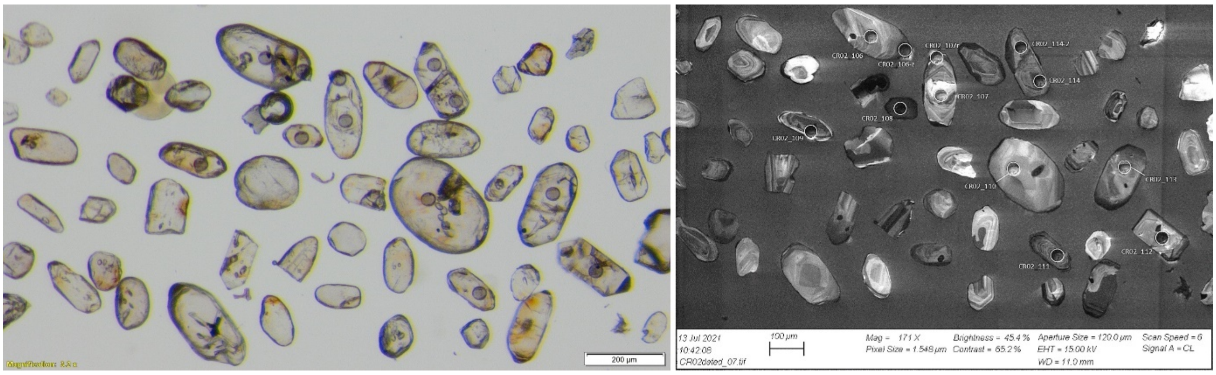

Figure 5-12 Zircon grains of CR02 observed under binocular microscope to the left, with CL-imaging to the right.

5.3.3 The Chameis Subterrane

5.3.3.1 The Bogenfels Formation

The zircons of sample CR11 varied in size from 50 to 210 µm in length and 30 to 150 µm in width. Stubby, stalky and prismatic shape were observed in the sample (Figure 5-13). Several of them were poorly rounded, but some were also well rounded. One grain had a needle-like elongation. Quite few of the grains were fragments of former grains. Few zircons show zoning patterns. Some xenocryst cores were observed, as well as some with complex internal morphology. Inclusions and fractures were also present.

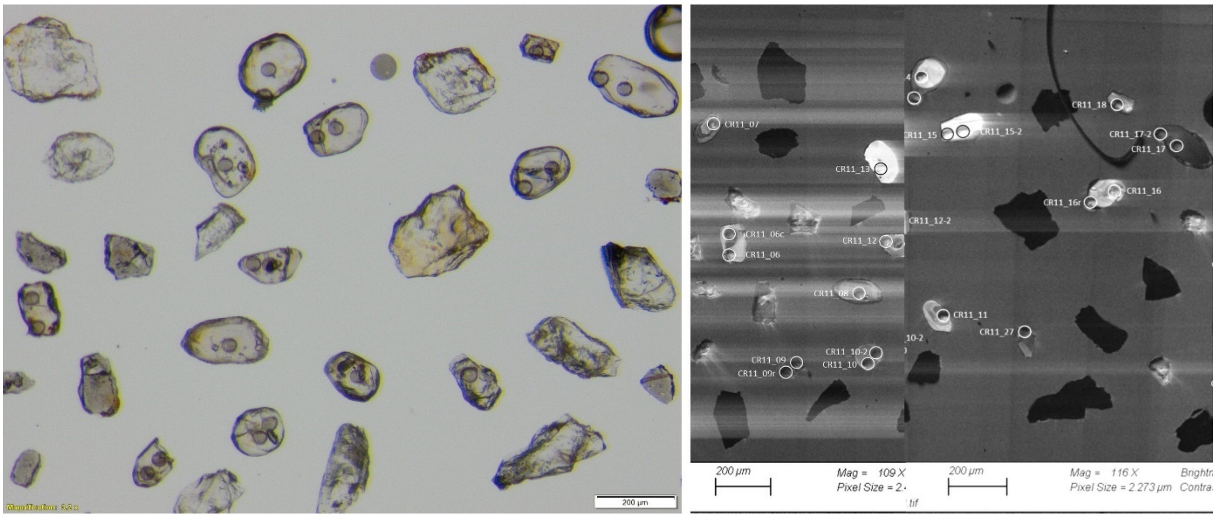

Figure 5-13 Zircon grains of CR11 observed under binocular microscope to the left, with CL-imaging to the right.

5.3.3.2 The Dernburg Formation

The zircons of sample CR12 ranged in size from 50 to 270 µm in length and 30 to 150 µm in width. Some grains showed a prismatic elongation, the rest had a stalky or stubby elongation (Figure 5-14 Most of the grains were subrounded, while some had kept most of their euhedral form. Several of the grains were fragments of former larger crystals. Quite few grains had a xenocryst core, while several other grains revealed complex cores. Many inclusions and some fractures were observed.

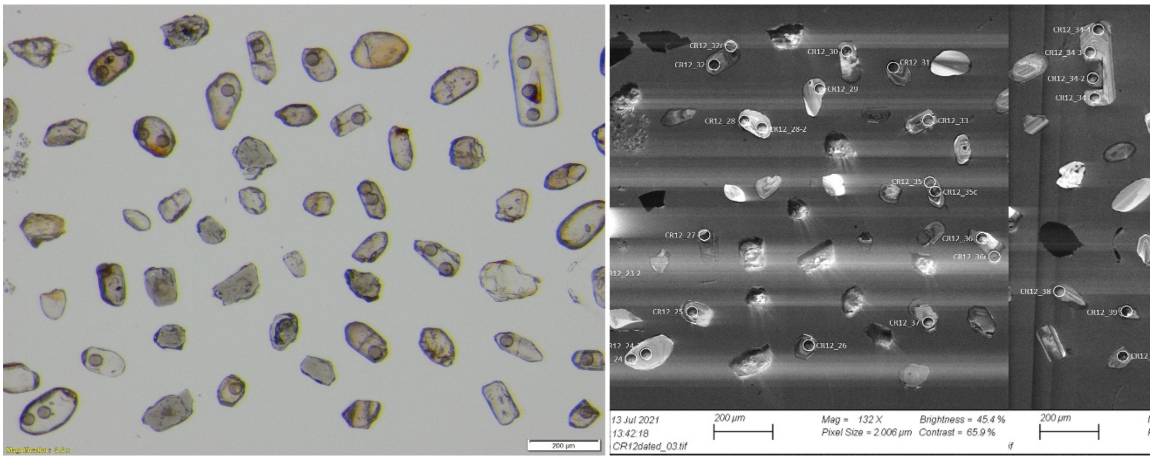

Figure 5-14 Zircon grains of CR12 observed under binocular microscope to the left, with CL-imaging to the right.

The few zircon grains of sample CR06 varied in size from 40 to 100 µm in length, except for one grain that had a length of 230 µm. The zircons ranged in width from 40 to 60 µm. Two grains showed stalky elongation, while one showed prismatic elongation (Figure 5-15). Two grains were more euhedral, while the rest were subrounded to rounded. Some of the grains were fragments of larger crystals. Most grains showed zoning. More complex inner morphology was observed in some of the grains. Few grains had inclusions.

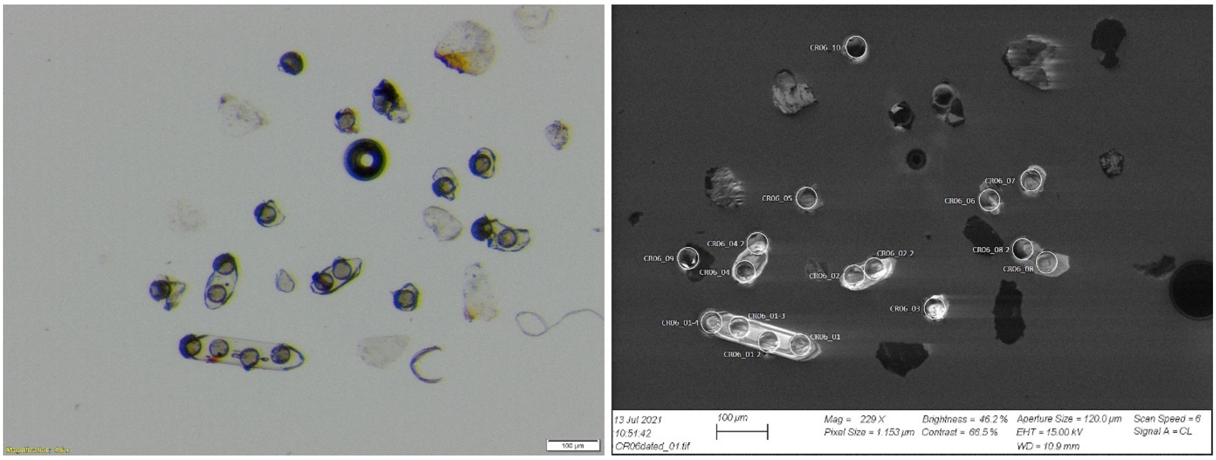

Figure 5-15 Zircon grains of CR06 observed under binocular microscope to the left, with CL-imaging to the right.

The zircons of CR07 varied in size from 60 to 190 µm in length and 40 to 140 µm in width. The shape of the zircons ranged from stubby to stalky, and from poor to well rounded (Figure 5-16). Several of the grains were fragments of former larger crystals. Few grains showed zoning patterns. Both complex and xenocryst cores were observed. Some inclusions and fractures were present in zircons of the sample as well.

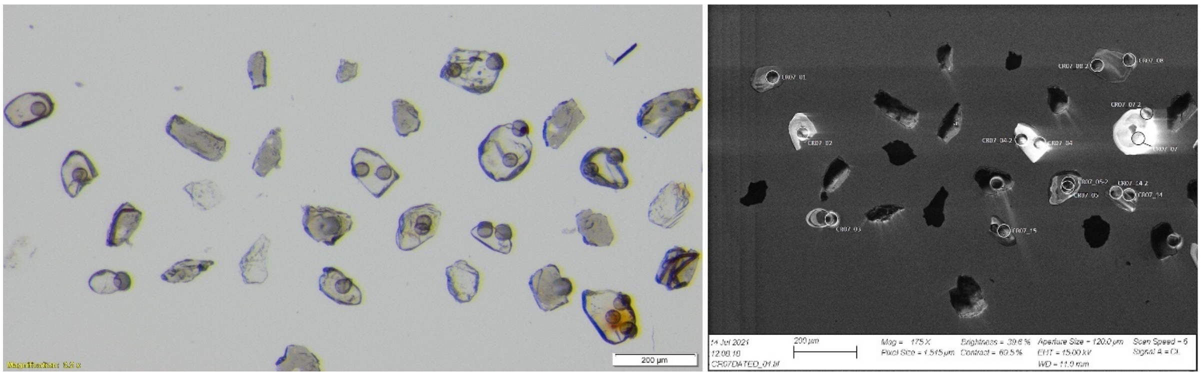

Figure 5-16 Zircon grains of CR07 observed under binocular microscope to the left, with CL-imaging to the right.

The zircon grains of CR13 varied in size from 50 to 200 µm in length and 30 to 90 µm in width. Few prismatic grains and one needle-like grain were observed (Figure 5-17). The rest of the zircons had either a stubby or stalky elongation. The grains ranged from poorly to well rounded. Some of the grains were fragments of former crystals. Several grains showed zoning patterns, and euhedral oscillatory zoning was present. Numerous grains showed complex internal structures. Inclusions and fractures were also frequently observed.

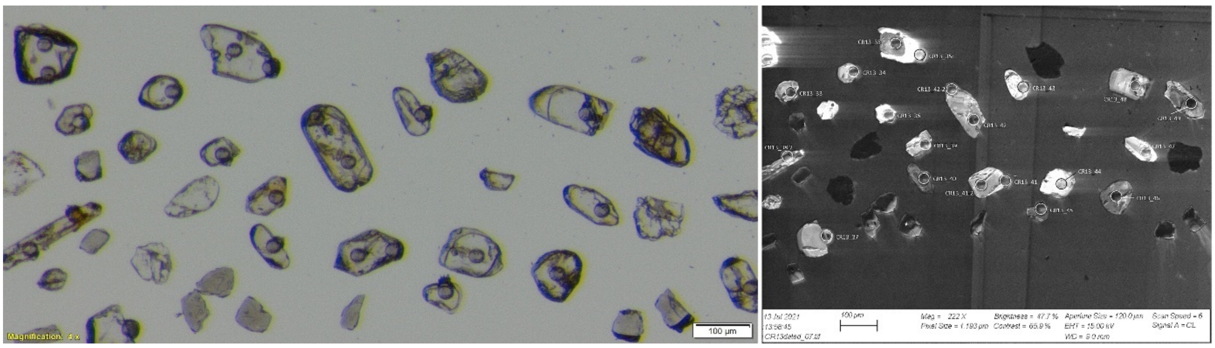

Figure 5-17 Zircon grains of CR13 observed under binocular microscope to the left, with CL-imaging to the right.

The zircon grains varied in size from 30 to 200 µm in length and 20 to 100 µm in width. The grains varied in shape between stubby, stalky, and prismatic (Figure 5-18). Several had more or less maintained their euhedral shape, the rest was subrounded to rounded. Some of the grains were fragments of former, larger crystals. Most of the grains showed zoning. Oscillatory and euhedral oscillatory zoning were most frequently observed. Few grains showed no zoning at all. Numerous zircons revealed complex cores, and few grains had xenocryst cores. Several grains with inclusions or fractures were observed.

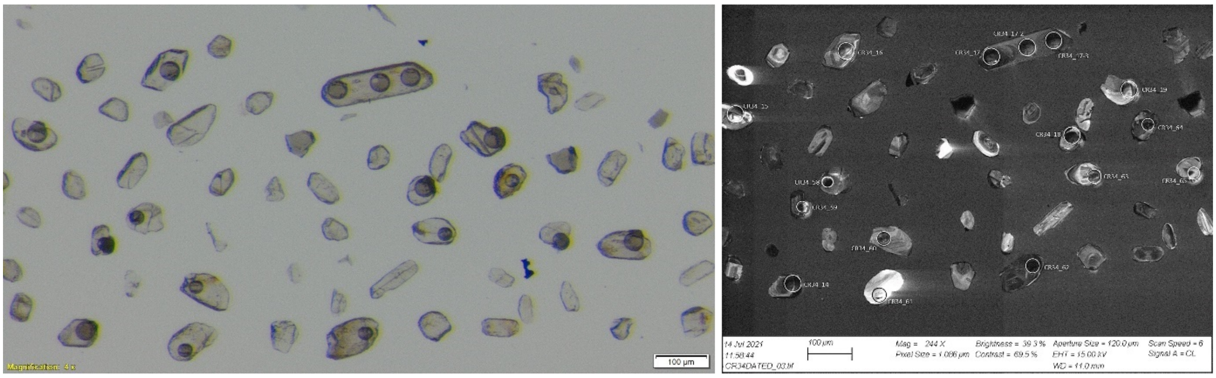

Figure 5-18 Zircon grains of CR34 observed under binocular microscope to the left, with CL-imaging to the right.

5.4 Uranium-lead geochronology

The ages are given with ± 1σ error. For ages older than 1000 Ma the Pb^{207}/Pb^{206} age was used, for ages younger than 1000 Ma the Pb^{206}/U^{238} was preferred. All data can be found in Appendix A. When an interpreted rim was ablated, the letter "r" was added to the end of the sample name. When a zircon grain was ablated multiple times without a rim probed, a number was added at the end of the sample name. If a zircon yielded several concordant ages (excluding rims), the most concordant age was picked as the main age. For a more detailed description of the methodology behind the data acquisition and data visualization, including the method and description of the youngest concordant age, see section 4.4 in Chapter 4 of this thesis. The youngest concordant ages are summarized for all samples in Table 5-1 below.

*Table 5-1 Summary of the youngest concordant ages (in Ma) obtained by four different methods as describes by Dickinson and Gehrels (2009) and in chapter 4, section 4.4.2 of this thesis. Number in brackets correspond to number of grain ages in the cluster. * = youngest single grain age was not the youngest concordant grain analyse. ** = means youngest graphical age was adjusted. See text for further description.*

Sample	**YSG**	**YPP**	**YC1σ (2+)**	**YC2σ (3+)**
CR04	1048 ± 30	1215	1192 ± 29 (3)	1204 ± 28 (5)
CR03	504 ± 11 *	580**	523 ± 22 (2)	516 ± 18 (3)
CR02	592 ± 15	630	625 ± 10 (3)	629 ± 10 (5)
CR11	523 ± 22 *	550	568 ± 14 (2)	573 ± 19 (4)
CR12	593 ± 12 *	600	673 ± 12 (2)	667 ± 13 (3)
CR06	628 ± 9 *	1940	n/a	n/a
CR07	543 ± 7	545	540 ± 9 (2)	544 ± 10 (3)
CR13	499 ± 10	500	557 ± 10 (2)	1076 ± 43 (6)
CR34	724 ± 10	1130	999±20 (4)	1004 ± 21 (6)

For some samples, the YSG age not yield any geological significant age. This could be due to contamination in the field or lab, lead loss or damage to the zircon grain (Dickinson and Gehrels, 2009; Andersen et al., 2019; Oyhantcabal et al., 2021). In order to avoid confusion when discussing depositional age, these samples were not included when further presenting and discussing the youngest concordant ages. For sample CR03, the ages in question influenced the youngest graphical peak as well, and the age given as YPP is hence also adjusted by removal of the geologically insignificant and uncertain ages. Otherwise, all ages are presented and included as other concordant ages, to not manipulate the dataset. For the youngest concordant ages, the analysis left out are:

- CR12 = 1 sample, CR12_58 (age 220 ± 5 Ma)
- CR06 = 1 sample, CR06_01-3 (age 247 ± 4 Ma)
- CR11 = 1 sample, CR11_03 (age 306 ± 10 Ma)
- CR03 = 4 samples, CR03_65 (age 254 ± 6 Ma), CR03_91 (age 312 ± 12 Ma), CR03_47 (age 460 ± 10 Ma), CR03_40 (age 472 ± 9 Ma).

5.4.1 The Schakalsberge Subterrane

5.4.1.1 The Grootderm formation

80 zircons of CR04 were analysed, resulting in a total of 77 concordant analysis for 62 zircons. 14 analysed rims (out of 21) had concordant ages. For 9 grains, both the analysed core and rim yielded concordant ages (Figure 5-19). One zircon was ablated twice without a distinct core and rim being identified.

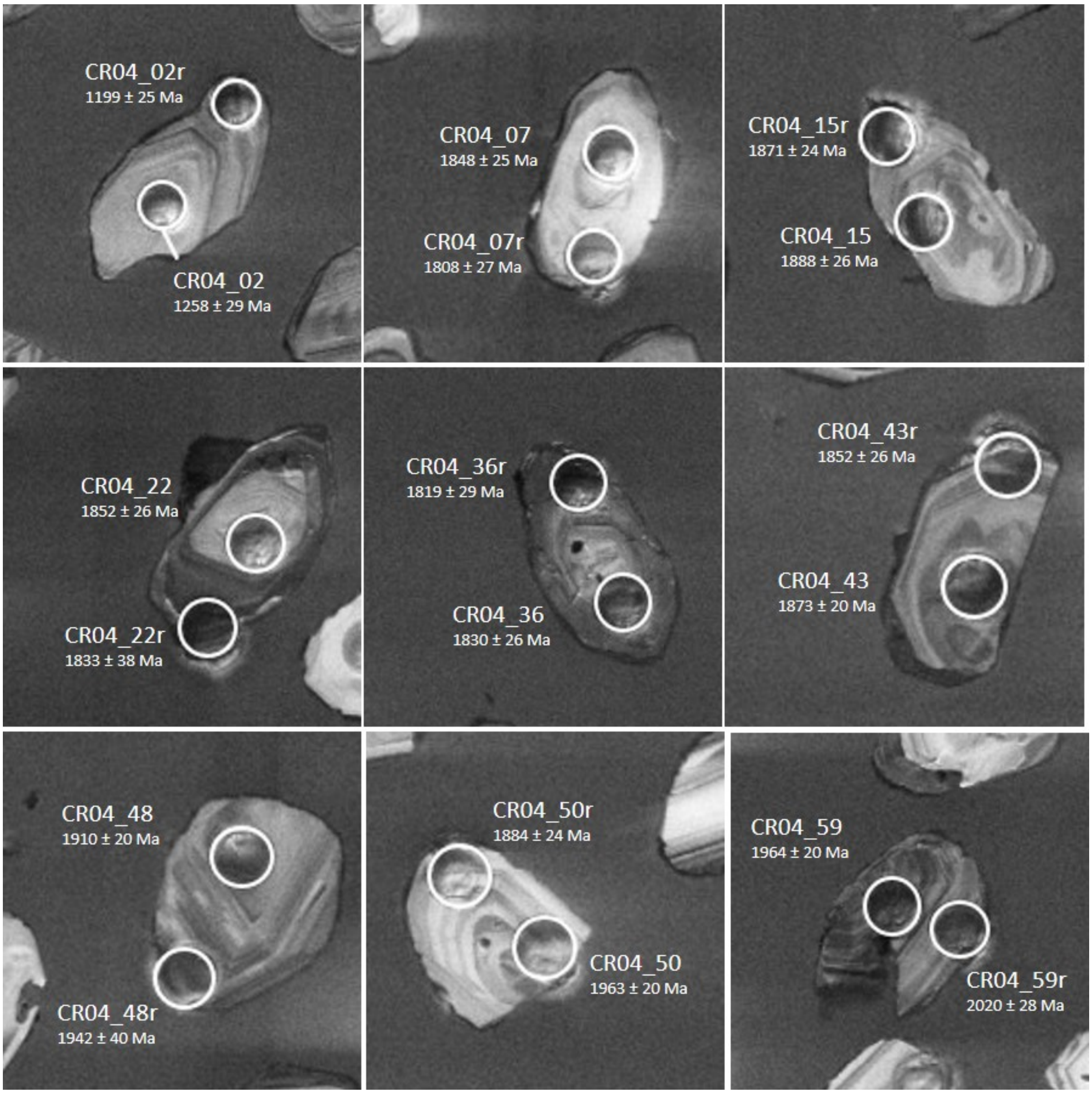

Figure 5-19 Zircons of CR04 where both rim and core yielded concordant ages. The diameter of the white circles marking the ablated spots are 40µm.

Excluding the rims, discordant analyses and double ablations, the concordant ages were plotted in a probability density plot and a concordia diagram (Figure 5-20). None of the concordant zircons needed to undergo common lead corrections. The main peak was at 1900 Ma. The youngest concordant zircon age was 1048 ± 30 Ma, while the oldest was 2020 ± 30 Ma. The main peak was observed at around 1870 Ma, the second largest peak at around 1215 Ma. The probability density plot show that the two main clusters in sample CR04 had ages from the Paleoproterozoic Era (where most plot within the Orosirian Period 2050-1800 Ma), and the Mesoproterozoic Era (where most plot within the Ectasian and Stenian Period, respectively 1400-1200Ma and 1200-1000 Ma).

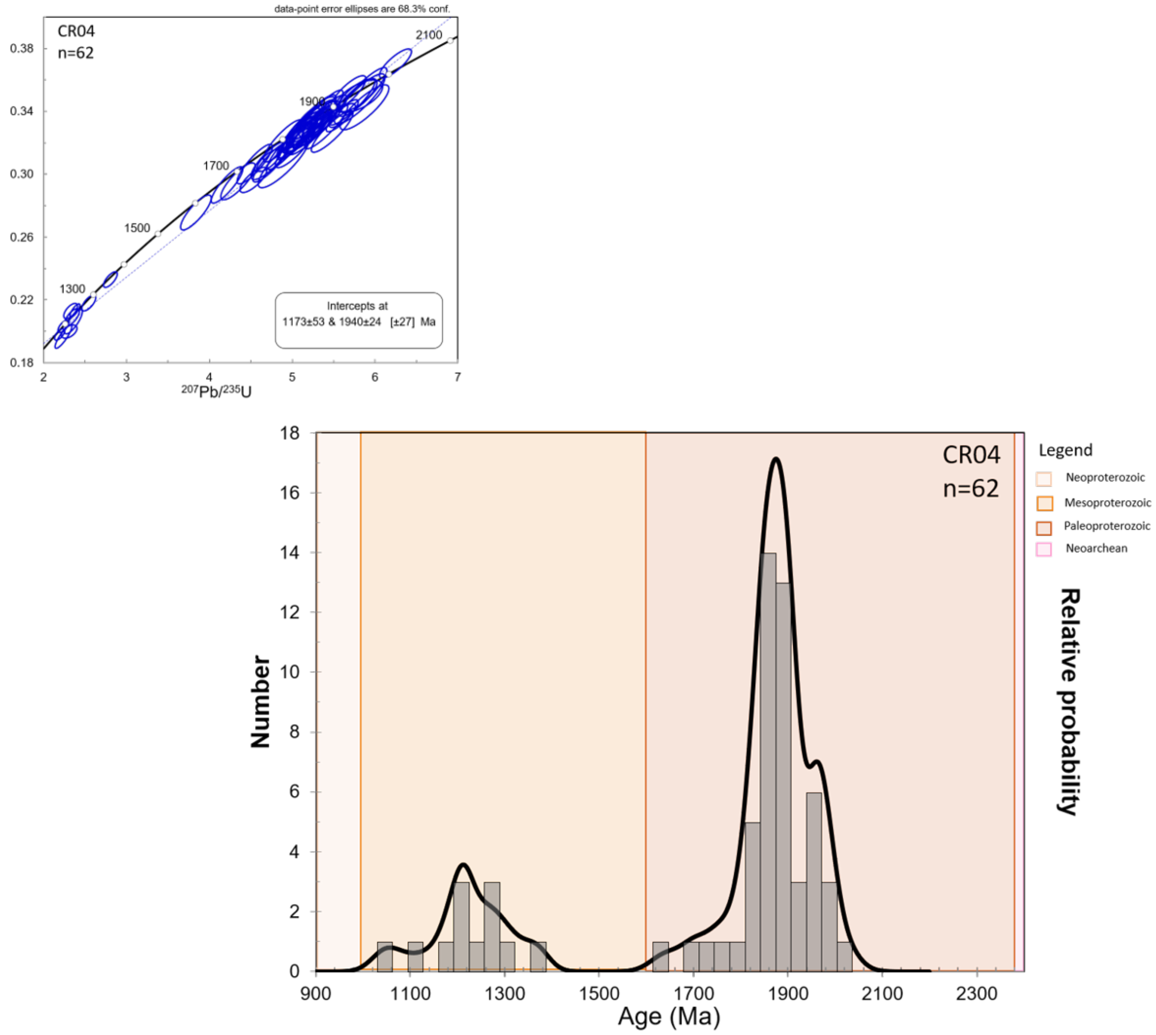

Figure 5-20 Concordia diagram (uppermost photo to the left) and probability density plot of sample CR04.

For CR03, the concordant zircons yielded a wider spectrum of ages, from Paleoarchean to Paleozoic. 124 zircon grains were analysed, resulting in 88 concordant ages. 4 of these were interpreted as rims. Only one grain gave concordant ages in both the analysed core and rim (Figure 5-21).

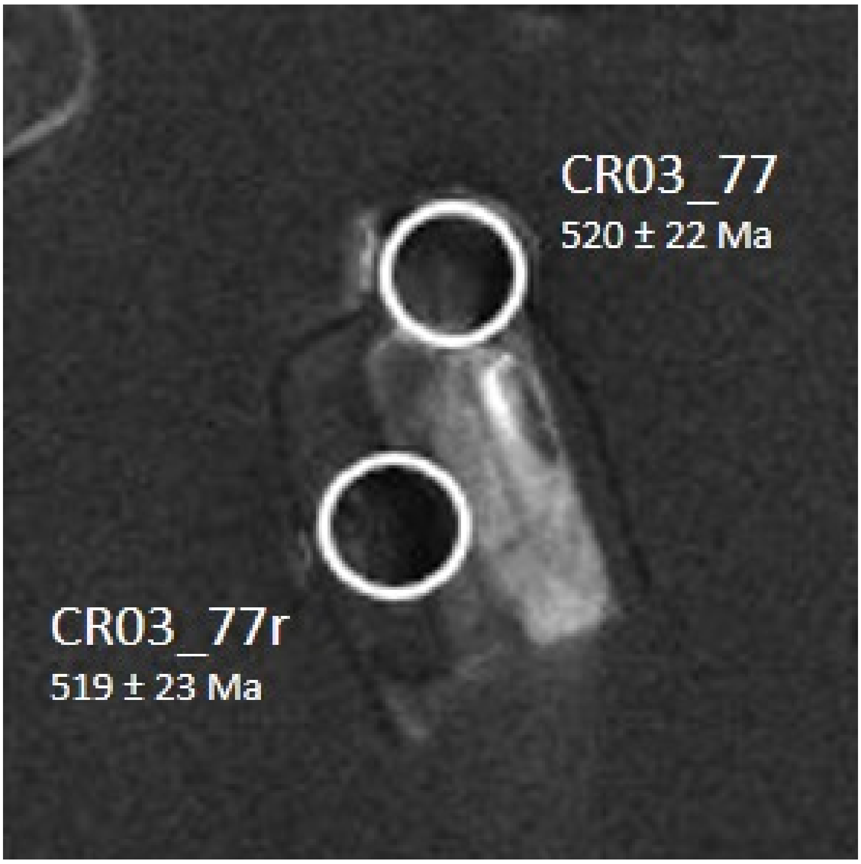

Figure 5-21 Zircon grain yielding concordant age for both rim and core.
The diameter of the white circles marking the ablated spots are 40µm.

84 concordant ages from unique zircons were plotted in a probability-density plot and a concordia diagram (Figure 5-22). None of the concordant ages were corrected for common lead. The youngest concordant zircon age was 254 ± 6 Ma, while the oldest was 2693 ± 36 Ma. Excluding geologically insignificant ages the youngest grain analysed had an age of 504 ± 11. Several peaks were observed in the probability density plot for CR03. The two major peaks were at around 1200 Ma and 600 Ma. The largest cluster of ages stretches from the Mesoproterozoic Era (with a main peak within the Ectasian and Stenian Period, 1400-1000 Ma) and into the Neoproterozoic Era (with a main peak within the Ediacaran Period, 635-542 Ma). Other significant age populations were (in descending significance) within the Orosirian Period (1800-2050Ma), the Rhyacian Period (2050-2300Ma) and the Neoarchean Era (2500-2800Ma).

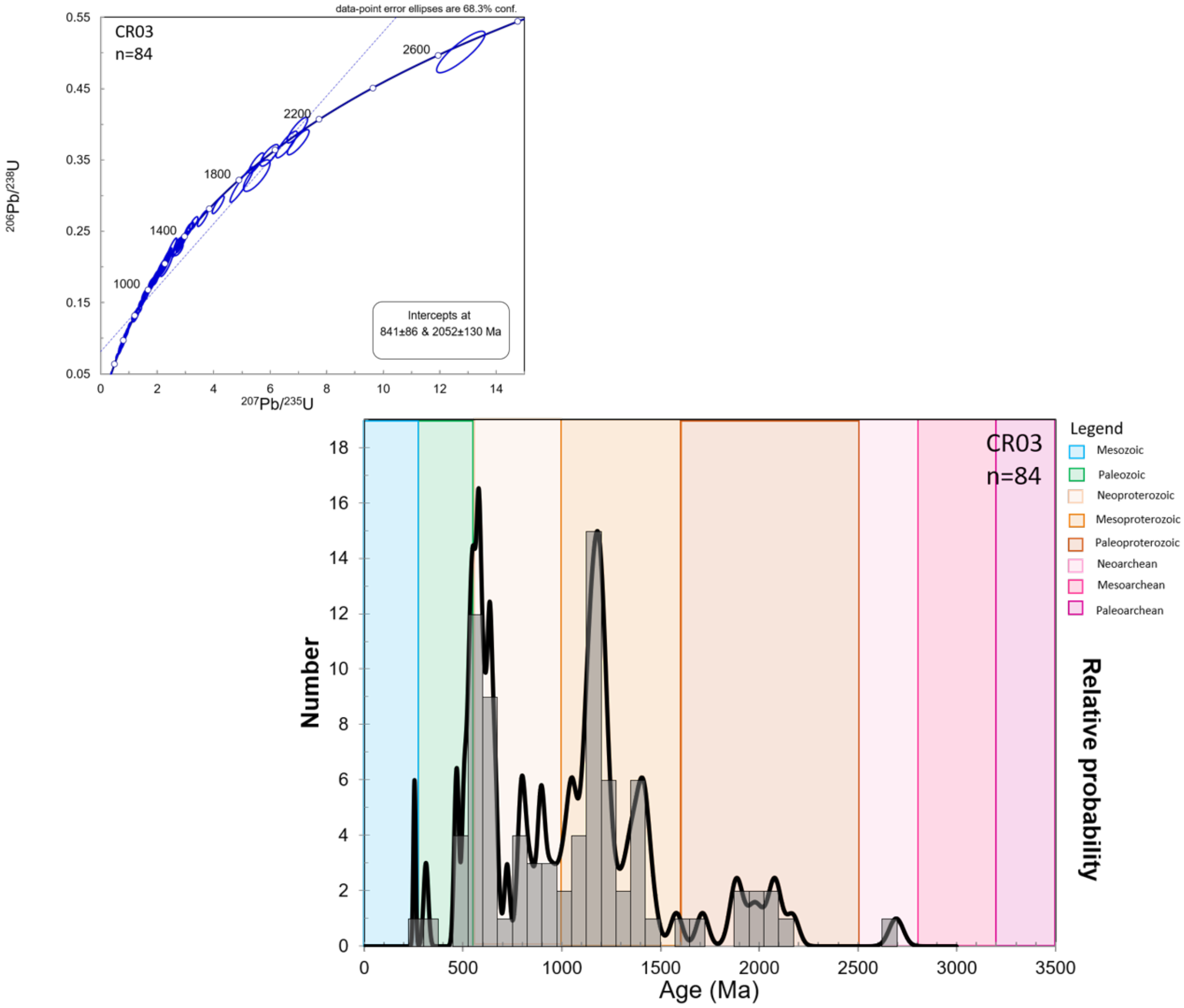

Figure 5-22 Concordia diagram (uppermost photo to the left) and probability density plot of sample CR03. Note that the Upper Paleozoic ages are not geologically meaningful.

5.4.2 The Oranjemund Subterrane

5.4.2.1 The Oranjemund Group

120 zircons of CR02 were analysed, resulting in 99 concordant ages for 85 zircons. 7 concordant analysis derived from interpreted rims, resulting in 6 grains with concordant ages for both core and rim (Figure 5-23).

Figure 5-23 Zircons of CR02 where both rim and core yielded concordant ages. The diameter of the white circles marking the ablated spots are 40µm.

3 concordant zircon ages were slightly corrected for common lead, as well as one concordant rim (please see Appendix B). 85 concordant ages for 85 different zircon grains were plotted in a probability-density plot and a concordia diagram (Figure 5-24), yielding major peaks in the late Mesoproterozoic Era, around 1050 Ma and in the Middle to Late Neoproterozoic Era, around 700-650 Ma. The youngest concordant age analysed was 636 ± 12 Ma, the oldest 2609 ± 40 Ma. All 4 zircon ages corrected for common lead yielded ages within the Cryogenian Period (850-635 Ma). The major age interval of which most concordant zircons plotted within were in the Stenian, Tonian and Cryogenian Periods, from 1200-635 Ma, of which the Tonian Period (1000-850 Ma) were the least represented age. Other peaks was observed around 1850 Ma (Orosirian Period) and 2600 Ma (Neoarchean Era).

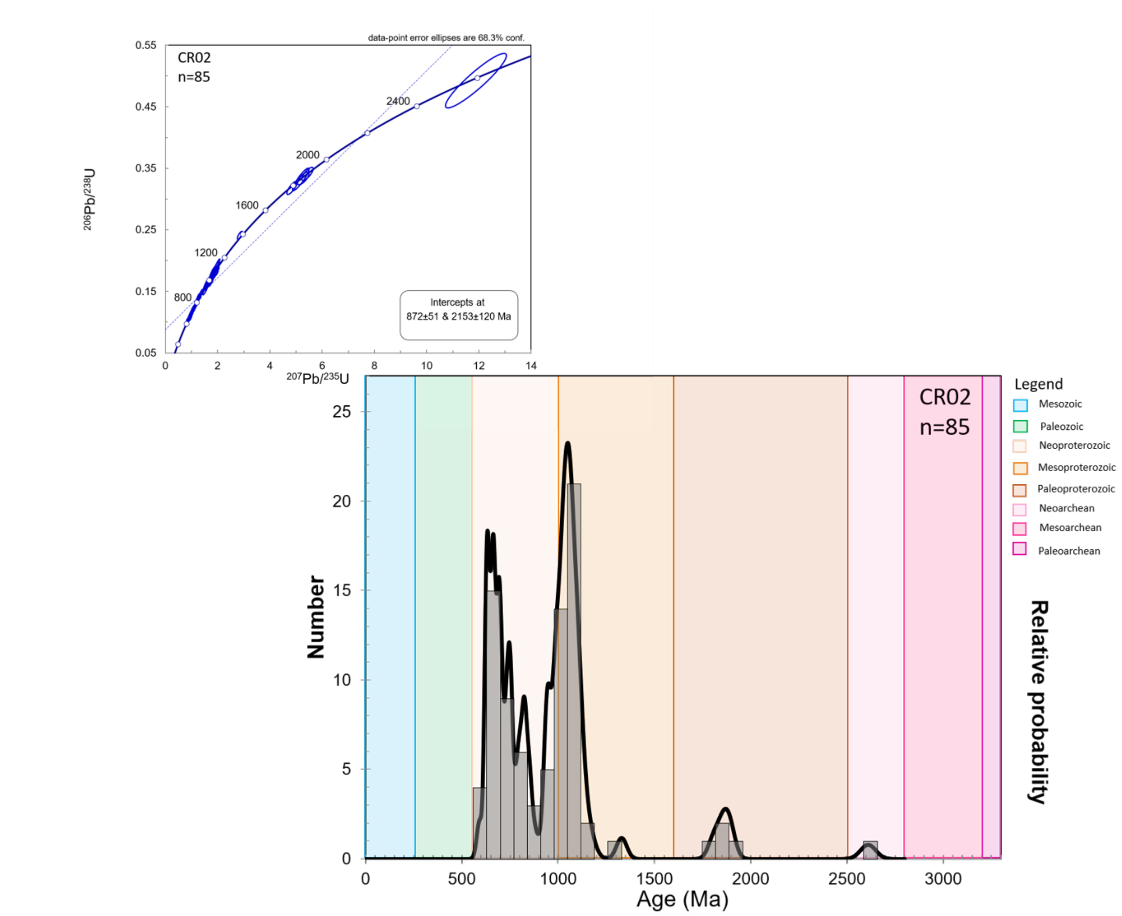

Figure 5-24 Concordia diagram (uppermost photo to the left) and probability density plot of sample CR02.

5.4.3 The Chameis Subterrane

5.4.3.1 The Bogenfels Formation

For sample CR11 from the Bogenfels Formation, 47 analyses were done on 31 zircons. This resulted in 41 concordant ages for 30 zircons, where 3 grains had concordant ages for both core and rim (Figure 5-25).

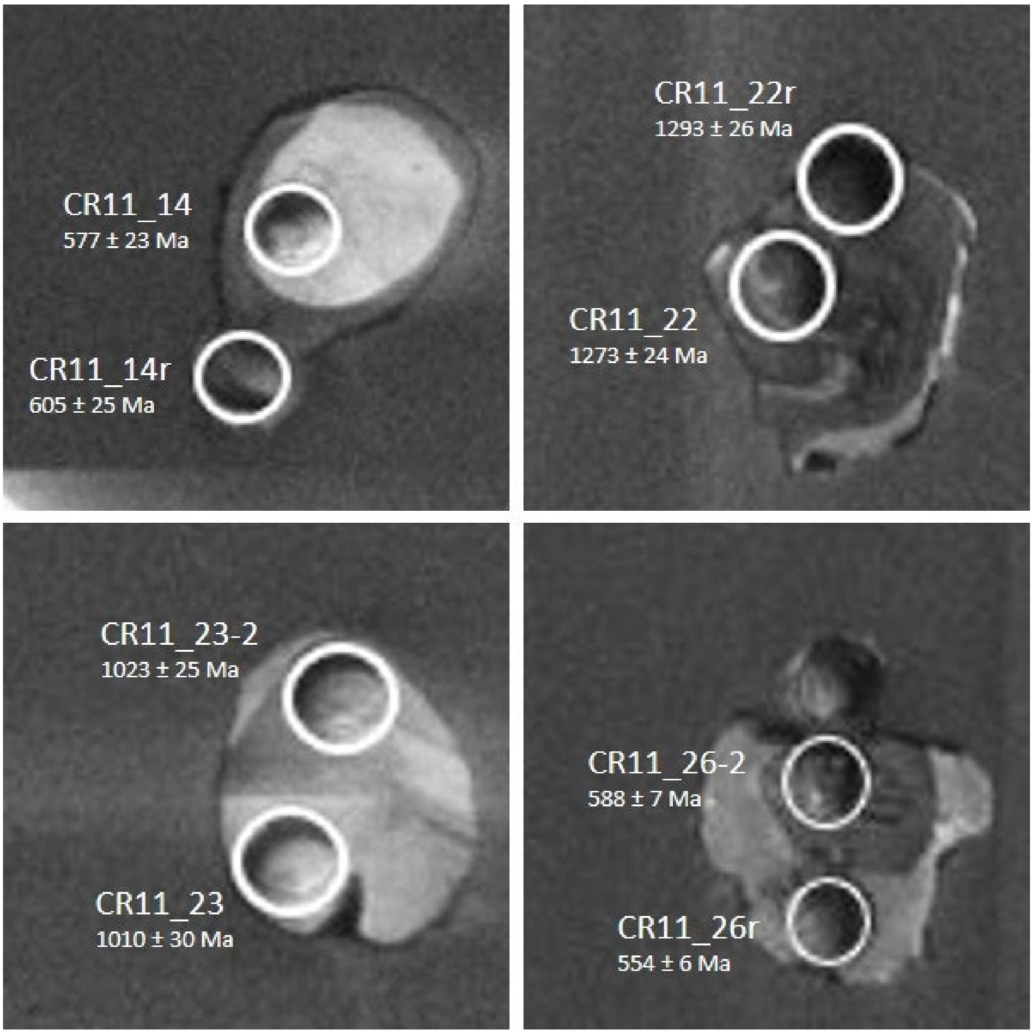

Figure 5-25 Zircons of CR11 where both rim and core yielded concordant ages. The diameter of the white circles marking the ablated spots are 40µm.

Excluding double ablations and rims, the 30 concordant ages left was plotted in a probability density plot and concordia diagram (Figure 5-26). One concordant age has undergone common lead correction. The youngest concordant age found was 235 ± 8 Ma, considered geologically insignificant. The next youngest grain analysed yielded an age of 523 ± 22. CR11 shows several peaks in the probability density plot, but the major peak is observed at the end of the Neoproterozoic Era, around 550 Ma. Other significant age clusters stretch over the Mesoproterozoic Era (with a main peak within the Ectasian period, around 1250 Ma) and the Paleoproterozoic Era (with main peaks around 1750 Ma, within the Statherian Period and 2150 Ma, within the Rhyacian Period). The oldest grain yielded an Archean age of 2834 ± 47 Ma.

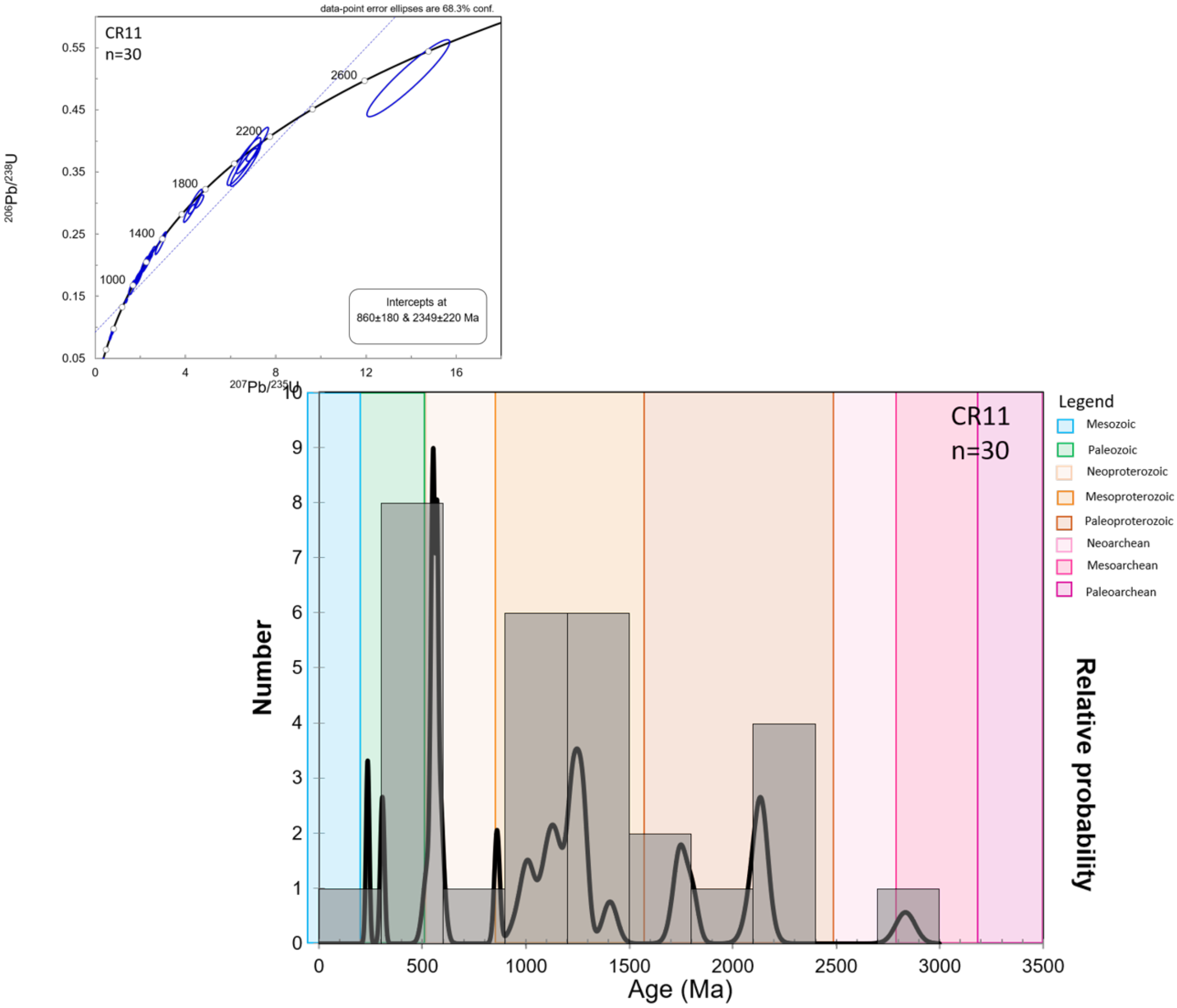

Figure 5-26 Concordia diagram (uppermost photo to the left) and probability density plot of sample CR11.

5.4.3.2 The Dernburg Formation

For the greenschist of the Dernburg Formation, CR12, 61 zircons were analysed with a total of 75 ablations. The analyses resulted in 64 concordant ages for 54 zircon grains, where 3 of these were rims and 7 were ablations in previously analysed grains (Figure 5-27).

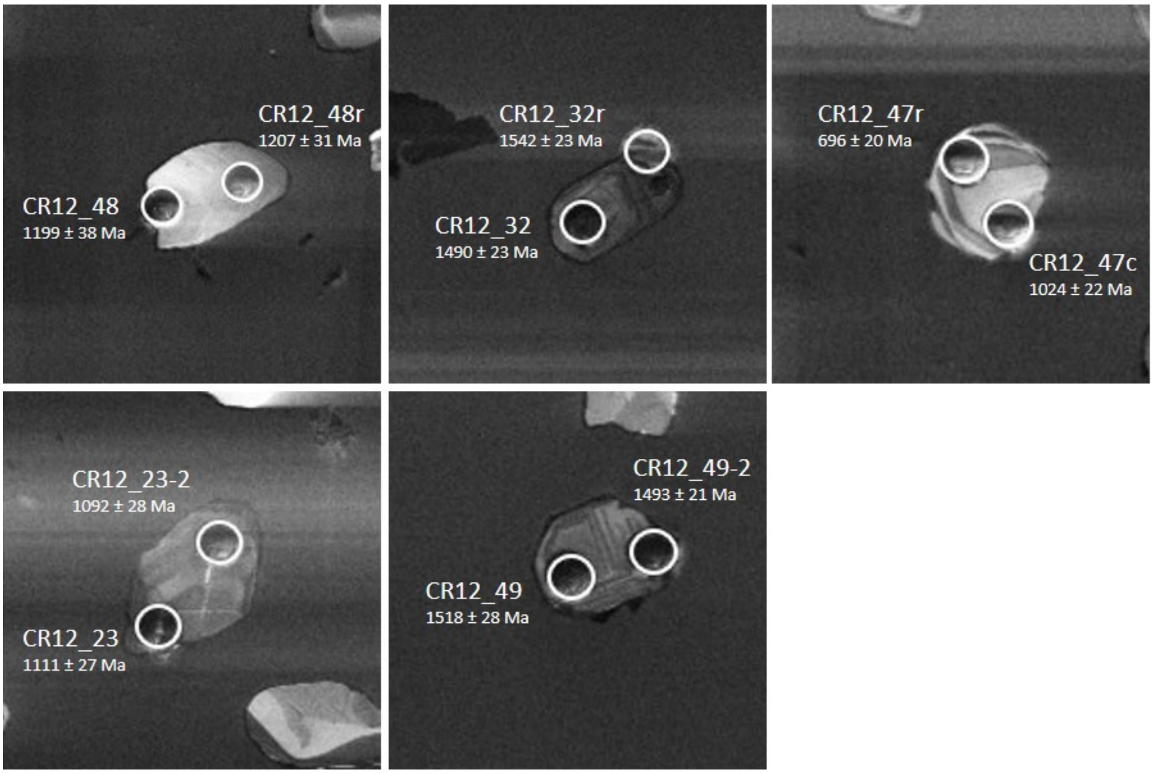

Figure 5-27 Zircons of CR11 where both rim and core yielded concordant ages, and 2 zircons ablated twice yielding concordant ages. The diameter of the white circles marking the ablated spots are 40µm.

Excluding extra ablations, rims and discordant analyses, 54 analysis of unique zircon grains were plotted in a probability-density plot and a concordia diagram (Figure 5-28). One concordant age was corrected for common lead. The youngest concordant age was 220 ± 5 Ma and geologically insignificant. The second gave an age of 593 ± 12, and the oldest 2099 ± 27 Ma. Two major peaks can be observed at around 1120 Ma and 1220 Ma. Other significant peaks are observed at approximately 1880 Ma, 1520 Ma, 920 Ma, 670 Ma and 220 Ma. The most significant cluster of ages is found in the late Mesoproterozoic Era, in the Ectasian (1400-1200 Ma) and Stenian (1200-1000 Ma) Period.

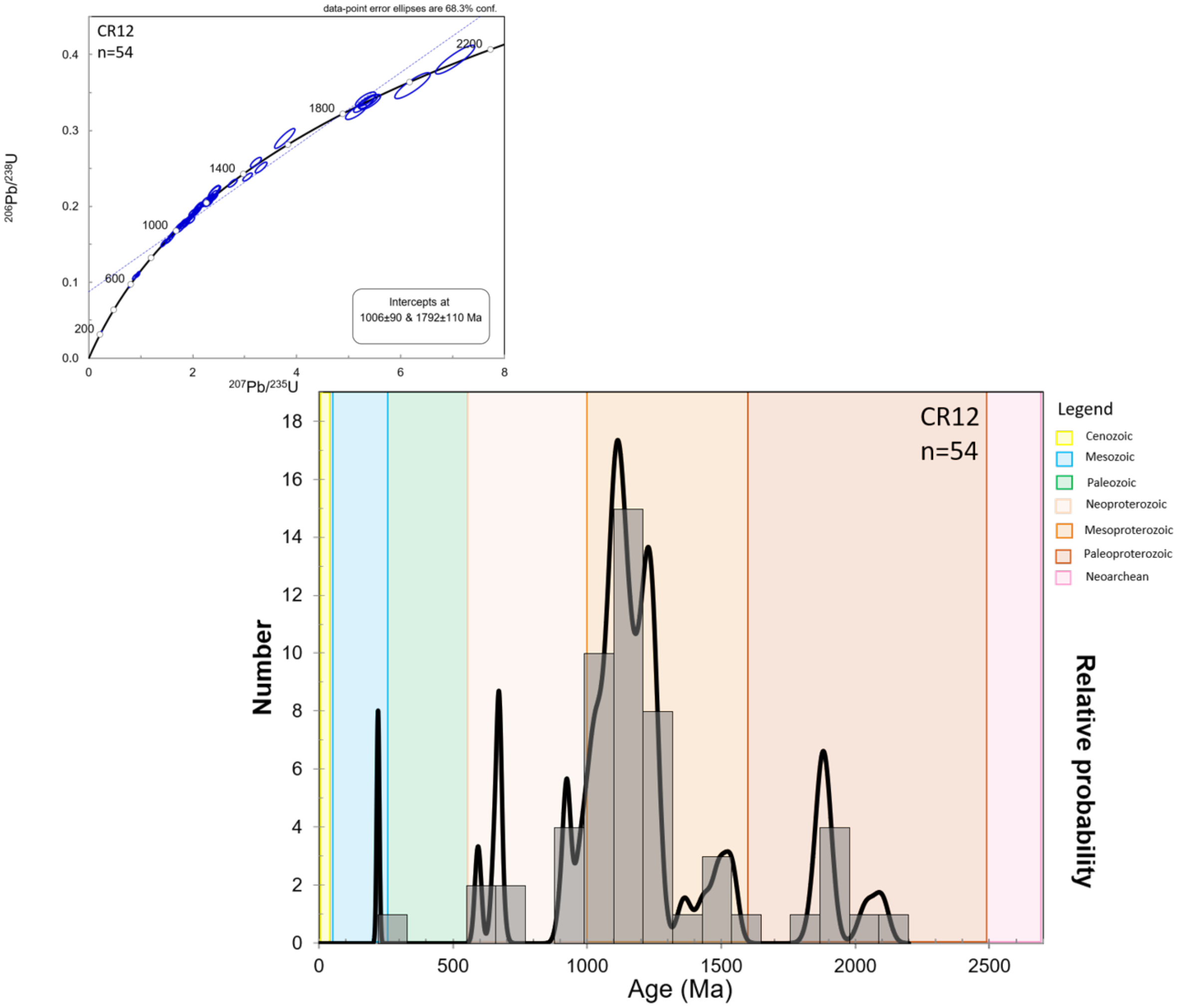

Figure 5-28 Concordia diagram (uppermost photo to the left) and probability density plot of sample CR12.

One of the two gabbros, CR06, had a very low zircon yield with only few grains. Nevertheless, the rock surprisingly did contain zircons. 16 analyses were performed on 10 zircon grains. This resulted in 8 concordant ages, for 6 zircons. No rims were identified. 6 concordant ages for 6 zircons were plotted as a probability-density plot and a concordia diagram (Figure 5-29). None of the concordant ages were corrected for common lead. The youngest concordant zircon age was 247 ± 4 Ma, an insignificant age geologically speaking. The second youngest gave an age of 628 ± 9 Ma. The oldest analysed grain was 1959 ± 29 Ma. Three grains were Paleoproterozoic of age, one Early Mesoproterozoic and one Late Neoproterozoic. Although this population cannot be interpreted due to few grains, it shows a contamination of the gabbroic magma by continental material during ascent of the magma.

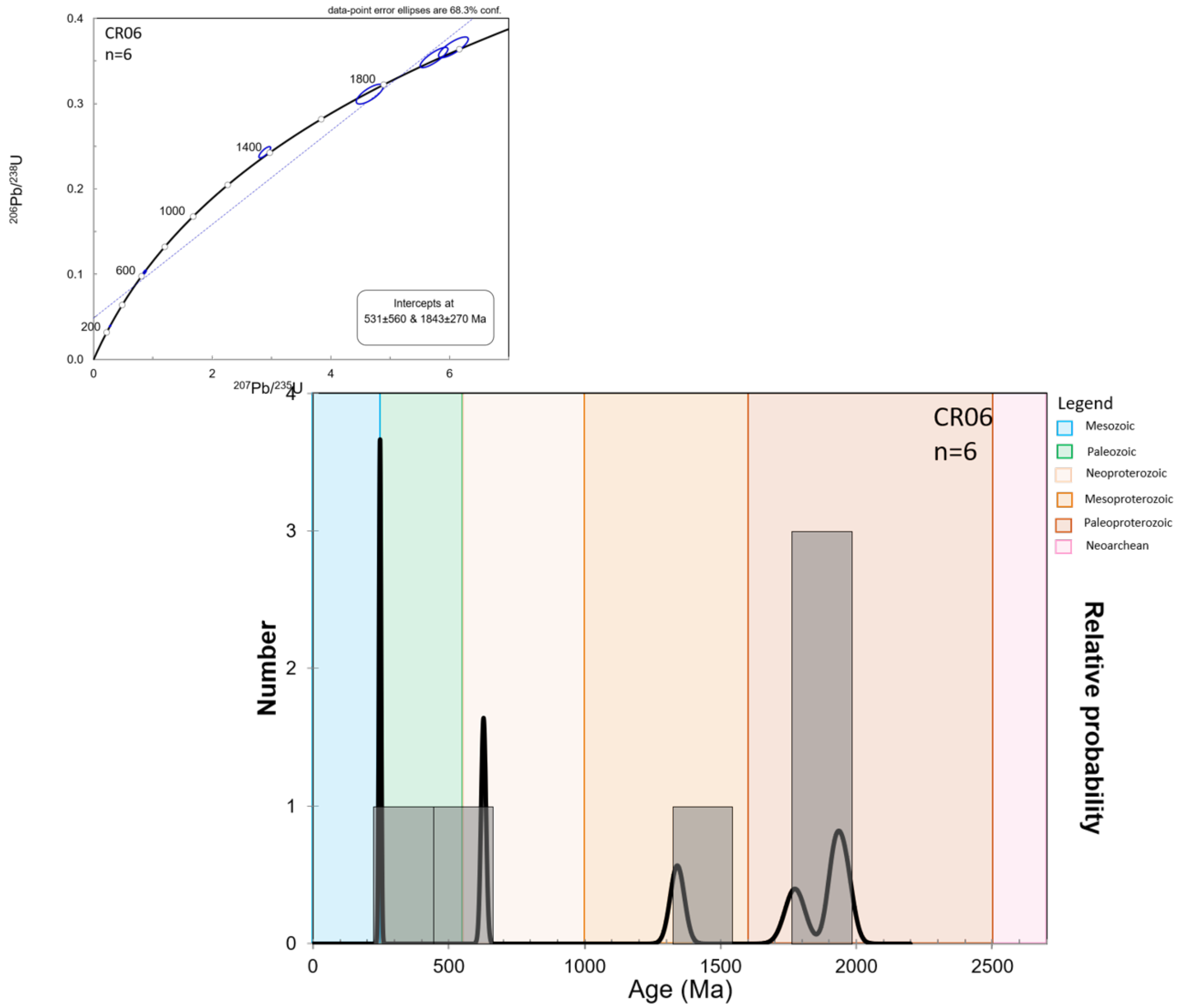

Figure 5-29 Concordia diagram (uppermost photo to the left) and probability density plot of sample CR06.

For the other gabbro of the Dernburg Formation, CR07, 28 analyses were conducted on 17 zircons. This resulted in 17 concordant ages for 13 zircon grains. No rims were identified or large enough to be analysed. One concordant age has been corrected for common lead. Concordant ages for 13 zircons were plotted in a concordia diagram and probability density plot (Figure 5-30). The youngest concordant age was 537 ± 11 Ma, the oldest 1966 ± 24 Ma. The main peak was observed around 550 Ma, the second largest peak is around 610 Ma. Other significant peaks are at 760 Ma and in the intervals 1050-900 Ma, 1400-1200 Ma, 2000-1750 Ma.

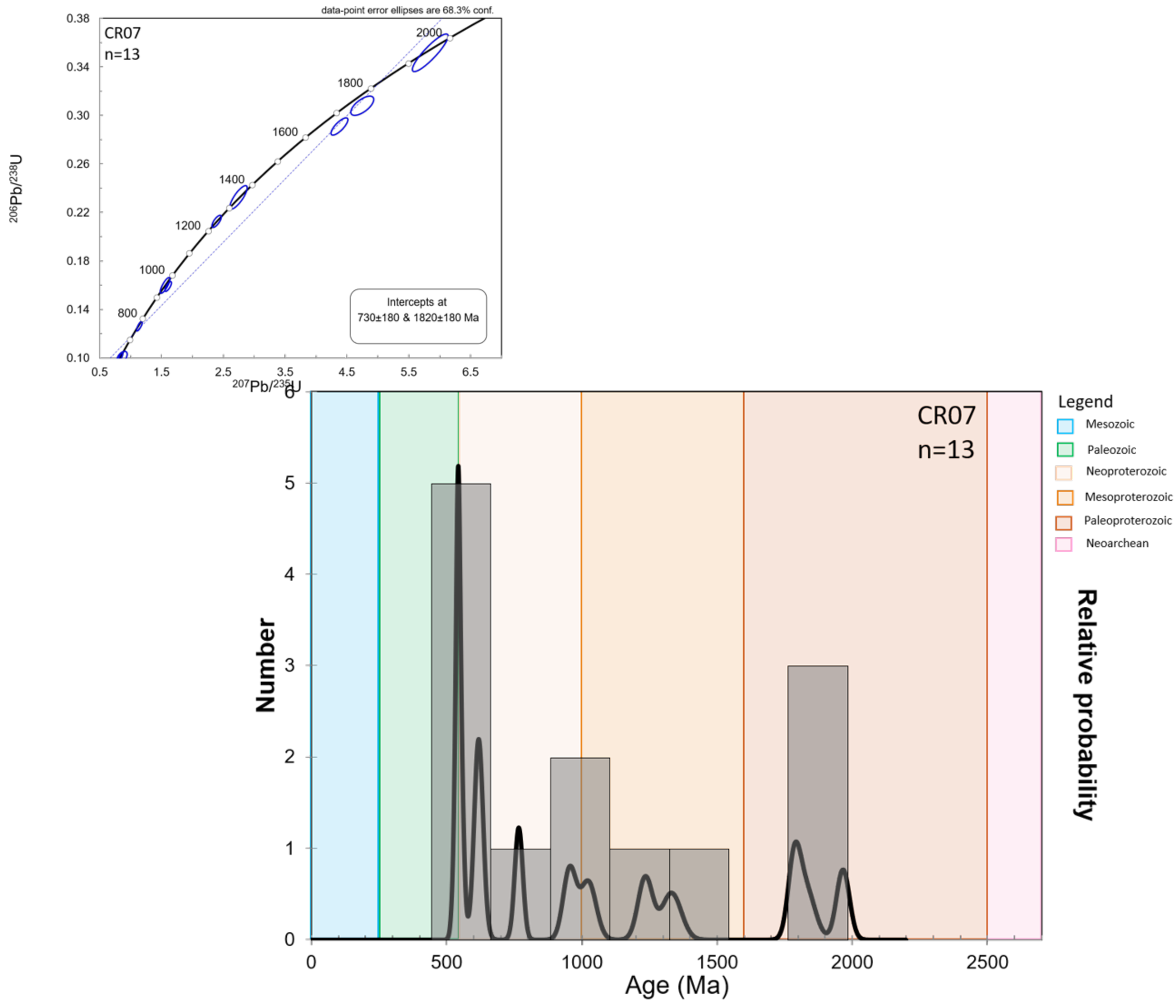

Figure 5-30 Concordia diagram (uppermost photo to the left) and probability density plot of sample CR07.

For CR13, 57 analyses were performed on a total of 49 zircons. This resulted in 32 concordant ages for 29 unique zircons. One grain had concordant ages in both core and rim (Figure 5-31). Two grains were ablated twice.

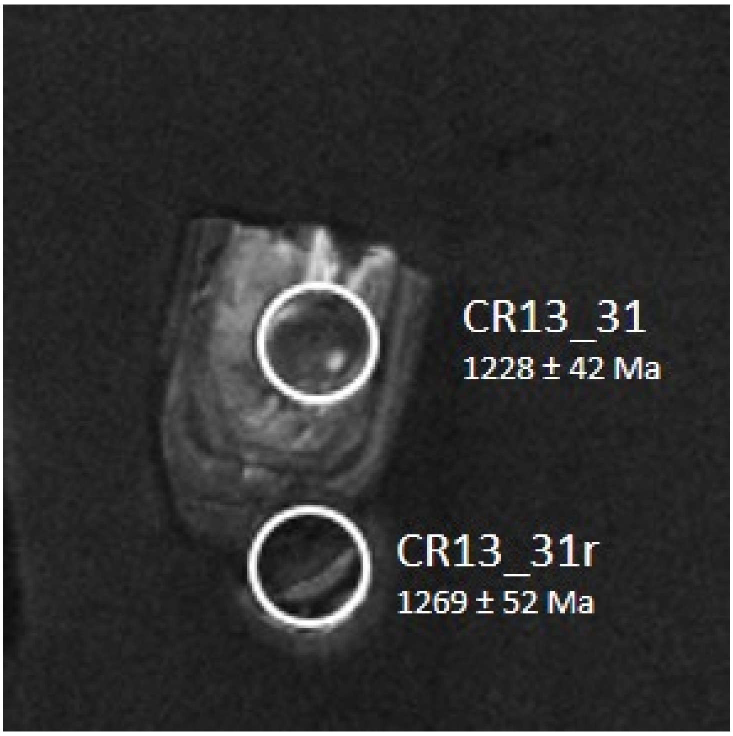

Figure 5-31 Zircon grain yielding concordant age for both rim and core. The diameter of the white circles marking the ablated spots are 30µm.

Excluding rim and double ablations, 29 concordant ages for 29 zircons were plotted in a probability-density plot and a concordia diagram (Figure 5-32). None of the concordant ages were corrected for common lead. The youngest concordant age analysed was 499 ± 10 Ma, the oldest 2173 ± 64 Ma. The sample show several peaks, and two major age clusters. The main age cluster was observed between 1250-500 Ma, the other age cluster between 2250-1750 Ma.

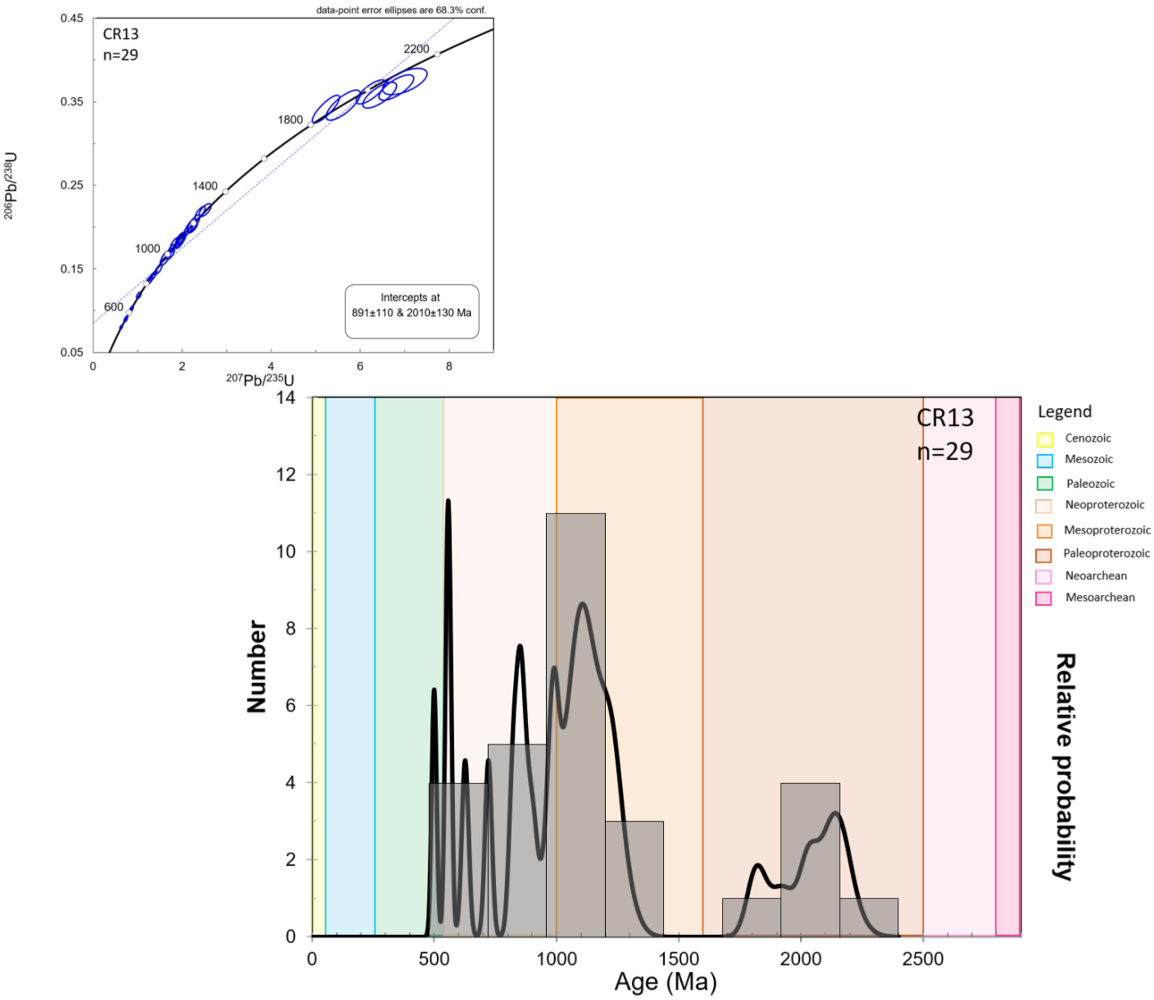

Figure 5-32 Concordia diagram (uppermost photo to the left) and probability density plot of sample CR13.

For the last sample from the Dernburg Formation, the diamictite CR34, 83 analyses were done on 76 zircons. The sample yielded 52 concordant ages for 48 unique zircons. Two grains yielded ages that after analysis were interpreted as possibly being core and rim, or at least show growth evolution (Figure 5-33).

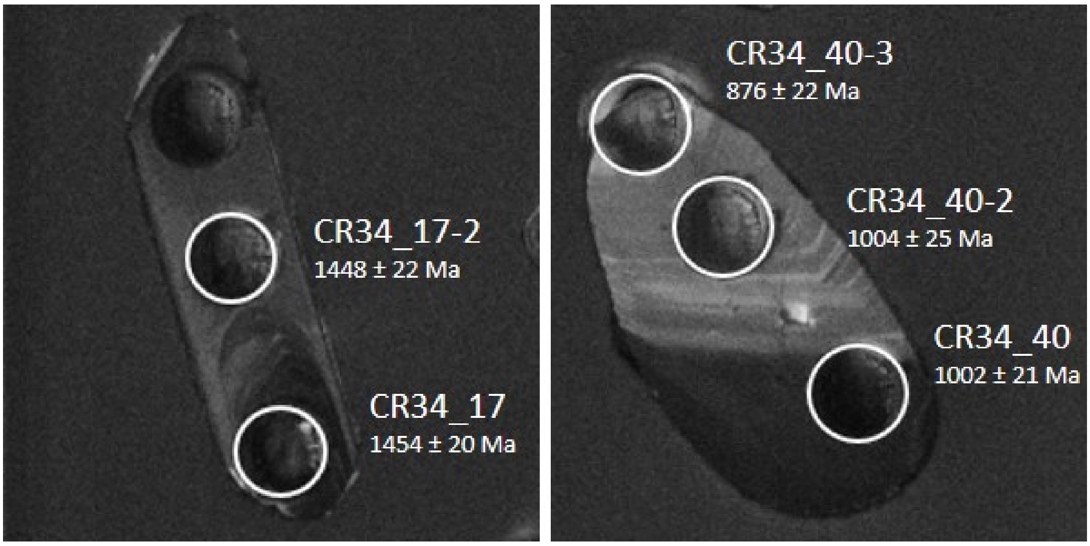

Figure 5-33 Two zircons of CR34 ablated twice, yielding concordant ages possibly interpreted as different growth events.

None of the concordant ages were corrected for common lead. Excluding rims and double ablations, the rest of the concordant ages (n=48) were plotted in a probability density plot and concordia diagram (Figure 5-34). The youngest concordant age analysed was 724 ± 10 Ma, the oldest 1977 ± 21 Ma. The two major peaks were both observed in the Mesoproterozoic Era, at around 1150 Ma and 1020 Ma. Smaller peaks were observed around 1880 Ma and 1560 Ma, and in the interval between 1450-1300.

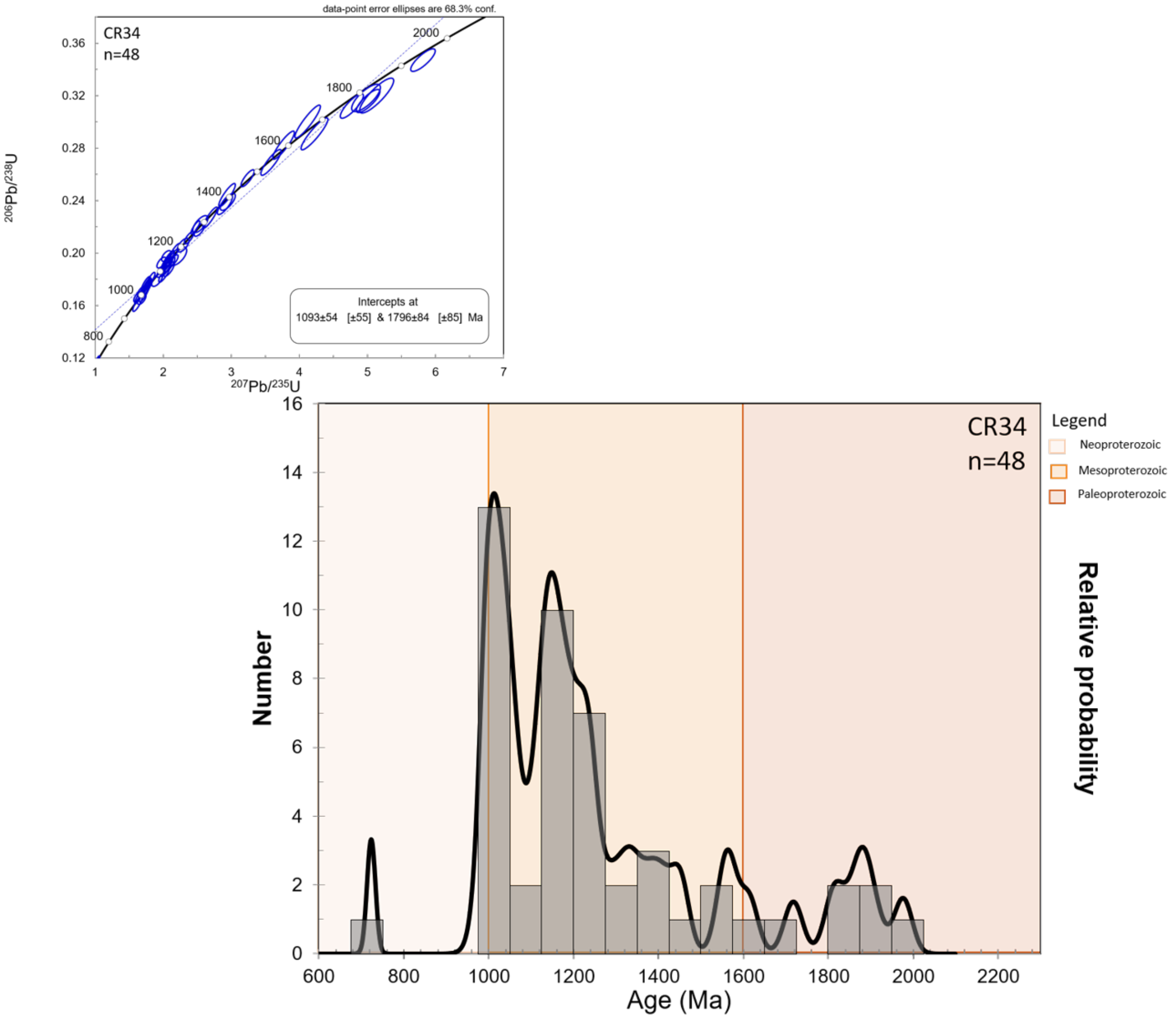

Figure 5-34 Concordia diagram (uppermost photo to the left) and probability density plot of sample CR34.

6 Discussion

6.1 Determination of emplacement ages and maximum depositional ages for successions of the Marmora Terrane

A summary of newly established emplacement ages and maximum depositional ages of the metasedimentary rocks was presented in Table 5-1 of chapter 5.4 of this thesis. Frimmel et al. (2010) reviewed the palaeotectonic evolution of southwestern Gondwana and bracketed the geological history of the Marmora Terrane within the following events:

1. Rifting of different oceanic basins during the Early Neoproterozoic
2. Amalgamation of oceanic crust to the westerly defined arc terrane (Arachania) at around 575 Ma
3. Final collision at 545 Ma to close the oceanic basins

The events coincide for the successions of the Marmora Terrane emplacement ages around 630-580 Ma. The authors interpret the diamictite of the Chameis Gate Member as part of the “snowball earth hypothesis” and it is therefore correlated as an equivalent of the Numees diamictite of the Numees Formation in the Porth Nolloth Zone (in that time interpreted as being of Marinoan age, around 630 Ma).

The maximum depositional ages calculated after Dickinson and Gehrels (2009) for the Oranjemund Group matches more or less the data from literature with ages around 625 Ma (Table 6.1-1). The single youngest zircon has been dated at 592 ± 15 Ma (1σ error), which does not assist in interpreting a significantly younger age, even when a single grain age would be accepted.

The units of the Schakalsberge Subterrane are definitely younger than proposed. Based on Dickinson and Gehrels (2009) a Cambrian emplacement age can be interpreted, even with the method providing the most conservative measure of youngest grain ages, the YC2σ age. The dated metamorphism at around 545 Ma (Frimmel and Frank, 1998) would lie within error, although at the margins (Table 6.1-1). Two single grains, not possible to merge as a cluster for YC1σ age determination as they do not overlap in 1σ error, are even of Middle Ordovician and Late Cambrian age. Those age constraints are novel and need further studies, especially how to fit those into the current paleogeographic models.

Slightly different is the case for the Chameis Subterrane. The rocks of the Dernburg Formation define a maximum depositional age around 670 Ma (after Dickinson and Gehrels, 2009). The associated Chameis Gate Member defines a maximum depositional age of 557 Ma (Table 6.1.-1) based on the strongly volcaniclastic felsic rock (CR13) associated with the diamictite (CR34). This rock could only collect mainly the Mesoproterozoic basement similar to nearly all diamictites deposited in southern Africa (e.g., Zimmermann et al., 2011; Hofmann et al., 2014; Naidoo et al., 2017; Andersen et al., 2018). If the felsic rock is in conformable contact with the diamictite, and a fault or unconformity could not be observed during fieldwork, then this is the first age constraint for one of those diamictites interpreted to be glacial and arguably related to the “snowball earth hypothesis” in southern Africa. If so then the age would be Gaskier (c. 580 Ma), or the rock is not of glacial origin but a debris flow event (e.g., Zimmermann et al., 2011). However, single detrital zircons point to a younger age at around 500 Ma. This would collide with the interpretation of the final metamorphic event at around 545 Ma. The overlying Bogenfels Formation has a slightly similar maximum depositional age with 568 Ma (Table 6.1-1). Intrusion of the gabbros took place during Latest Neoproterozoic times or Early Cambrian or later as these are the ages of the youngest zircon populations (Table 6-1).

Compiling, this means that the Chameis Subterrane successions have been deposited not earlier than 550-570 Ma including the Chameis Gate Member diamictite, wherefore the correlation with global or nearly global "snowball earth related glaciations" is compromised. The successions have been intruded by gabbros with an extensional geochemical signature containing continental crustal material at the end of the Precambrian.

The Oranjemund Subterrane rocks are older at this stage of knowledge with an Uppermost Cryogenian maximum depositional age.

On the other hand, the rocks of the Schakalsberge Subterrane are of Uppermost Ediacaran or Early Cambrian age.

Hence, if the maximum depositional ages of the Chameis Subterrane successions are final then the rocks cannot be correlated with the ones of the Schakalsberge Subterrane, which would also be valid for the carbonate successions.

The next step would be to define the mafic rocks more detailed in terms of their origin and to determine possible tectonic setting characteristics for the metasedimentary successions, if possible.

Table 6-1 Summary of the youngest concordant ages (in Ma) for each geological unit of the Marmora Terrane obtained by four different methods as describes by Dickinson and Gehrels (2009) and in chapter 4, section 4.4.2 of this thesis.

Geological unit	Sample	YSG	YPP	YC1σ (2+)	YC2σ (3+)
Schakalsberge Subterrane	CR04	1048 ± 30	1215	1192 ± 29 (3)	1204 ± 28 (5)
Schakalsberge Subterrane	CR03	504 ± 11	580	523 ± 22 (2)	516 ± 18 (3)
Oranjemund Subterrane	CR02	592 ± 15	630	625 ± 10 (3)	629 ± 10 (5)
Chameis Subterrane Bogenfels Formation	CR11	523 ± 22	550	568 ± 14 (2)	573 ± 19 (4)
Chameis Subterrane Dernburg Formation	CR12	593 ± 12	600	673 ± 12 (2)	667 ± 13 (3)
Chameis Subterrane Bakers Bay Suite	CR06	628 ± 9	1940	n/a	n/a
Chameis Subterrane Bakers Bay Suite	CR07	543 ± 7	545	540 ± 9 (2)	544 ± 10 (3)
Chameis Subterrane Chameis Gate Member	CR13	499 ± 10	500	557 ± 10 (2)	1076 ± 43 (6)
Chameis Subterrane Chameis Gate Member	CR34	724 ± 10	1130	999±20 (4)	1004 ± 21 (6)

6.2 Zircon ages and their implications

To evaluate the zircon ages, they were plotted all together in a probability density histogram as the Marmora Terrane, as well as with respect to their subterrane. Most of the successions of the Marmora Terrane have a Late Ediacaran age and a Middle to Late Mesoproterozoic age (Figure 6-1). All mafic rocks contain zircons; hence the involvement of continental crust or enriched mantle sources are evident. Models arguing with solely involved oceanic crust must be abandoned.

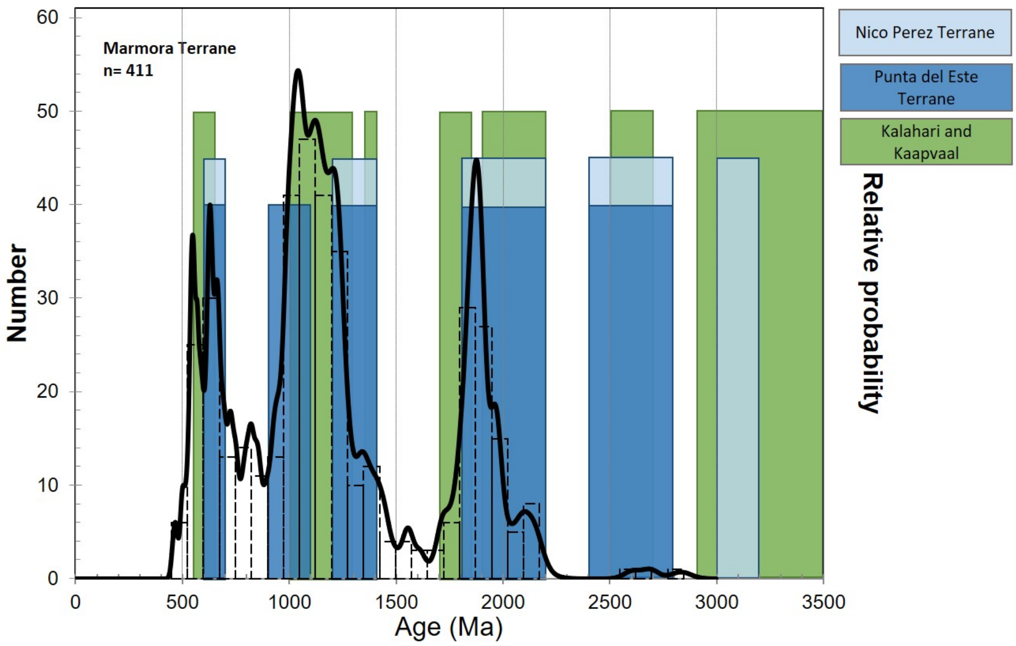

Figure 6-1 All new concordant zircon ages from the geological units of the Marmora Terrane compiled, with the main events from the south American and African side indicated in the background.

All rock successions contain zircons which are inherited from their source rocks or from the host rocks of the magmatic units. This may give some hints about the origin of the entire area or sets some pre-conditions. However, it must be stressed that the following data set are lacking and are necessary for more sound speculations:

- Provenance data of the clastic successions including quantification of the heavy minerals and seeking further minerals for age determinations such as rutile, apatite, monazite and garnet.
- Trace element and Lu-Hf data on dated zircons from all units.

Both data sets are in the process but impossible to add to this project because of the COVID-19 situation.

The lack of Paleoproterozoic ages in the middle unit, the Oranjemund Subterrane, contrasts with the clear trend of Paleoproterozoic age populations found in the Schakalsberge and Chameis subterranes. The main contribution of this age population comes from the basalt within the Schakalsberge Subterrane, and from the gabbros, metatuff and metaclastic rocks of the Dernburg Formation within the Chameis Subterrane. The gabbros may be explained as having intruded into already emplaced continental derived rock successions but the lavas either inherited the material when magma was rising, or they flew over those successions. The latter would only account for sparse occurring zircons, while the analytical work of this thesis demonstrated that even 1 kg of material yielded several zircons. The former alternative is thus more feasible at this stage of knowledge. In all cases, continental crust or enriched mantle were already representing the basement during the Late Ediacaran. Nevertheless, the existing major source of Late Mesoproterozoic successions is not available in the Nico Perez Terrane. Maybe this allows in speculating, as Basei et al. (2005) proposed, that the eastern part of south America has been related to the western area of the Kalahari craton (see also Frimmel et al., 2010). The scare occurrence of zircons older than Neoarchean also fits into this interpretation, knowing that the core of the Kaapvaal craton only rarely distributed to marginal cratonic area detritus (e.g., Naidoo et al., 2017; Andersen et al., 2018). Currently, only a major Late Neoproterozoic event has been identified in eastern South America (Dom Feliciano *Belt sensu lato*), while the Pan-African orogeny is not represented by large magma volumes south of the Damara Belt or west of Durban in southern Africa. Similarly, Late Mesoproterozoic sources are characterizing the Kalahari craton (Namaqua Natal Metamorphic Belt) but there are no such events in eastern South America in the Rio de la Plata region. A mixed possible provenance opens the question about the paleogeography. This is however outside of the scope of this thesis.

The data obtained from the Oranjemund Subterrane (Figure 6-2) corresponds well with the data published by Andersen et al. (2018) showing Late Mesoproterozoic to Early Neoproterozoic (1100-950 Ma) and Neoproterozoic (700-600 Ma) age fractions (Figure 6-3). The age cluster corresponds well with the Pan-Brazilian Orogeny around 600-700 Ma and the Punta del Este Terrane at the age cluster around 1100-900 Ma. At this stage either provenance cannot be excluded. Remarkable is the gap of ages between 1200 and 1800 Ga.

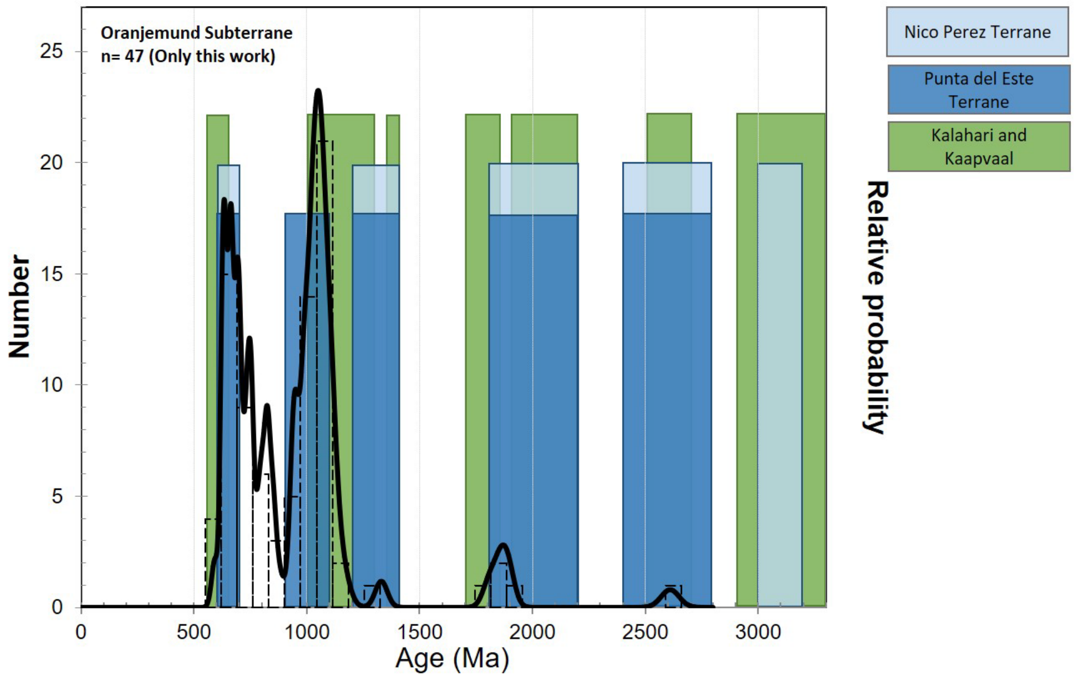

Figure 6-2 The zircon ages obtained by this work for the Oranjemund Group, with the main events from the south American and African side indicated in the background.

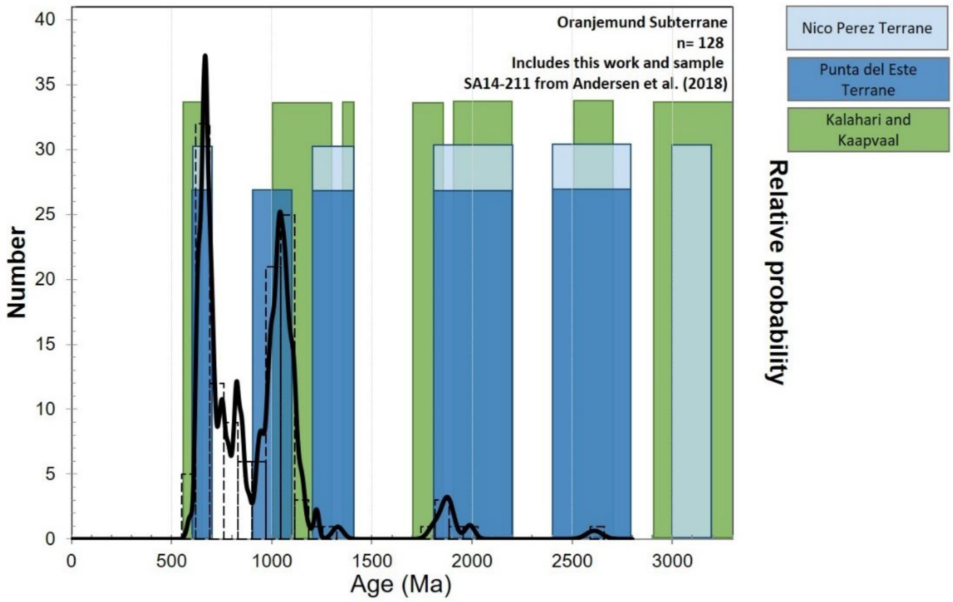

Figure 6-3 The zircon ages obtained for the Oranjemund Group by this work merged with the ages obtained for the Oranjemund Group by Andersen et al. (2018) for sample SA-211.

The rocks of the Schakalsberge Subterrane seem to match rather the African craton than the South American one (Figure 6-4). The few Cambrian to Early Ordovician ages, if reliable, are sparse and in both areas those ages had been found (e.g., Fourie et al., 2011; Van Staden et al., 2010). Again, it matches the Punta del Este Terrane and the Kalahari craton quite well. However, some of the younger ages, besides the geologically insignificant ones younger than Ordovician, rather match the Cape Granite event than rocks of the Dom Feliciano Belt. Here, Hf and trace element geochemistry would be ideal tools to determine a provenance.

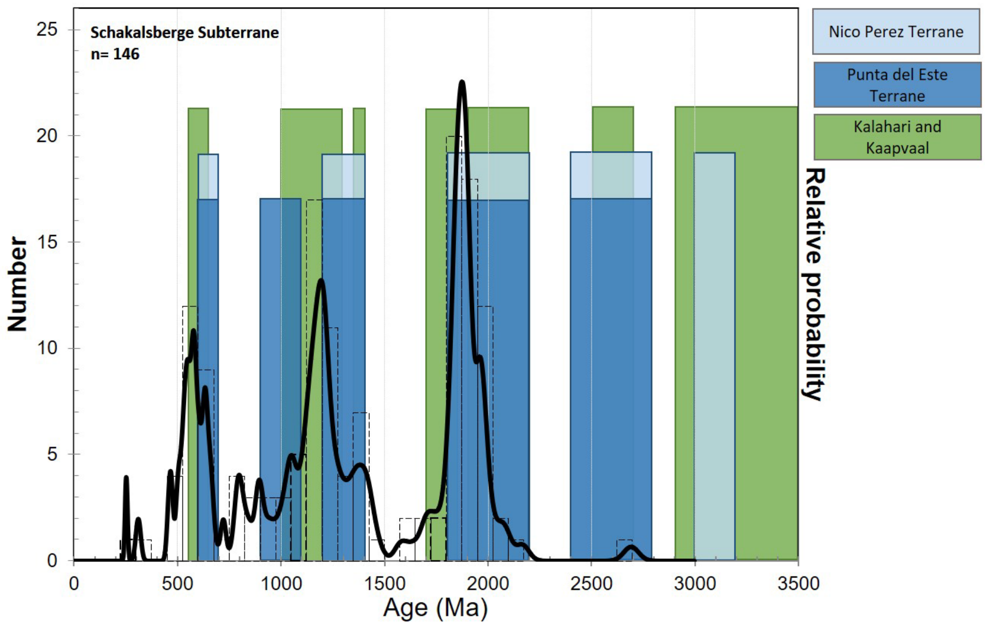

Figure 6-4 Zircon ages obtained for the Schakalsberge Subterrane, with the main events from the south American and African side indicated in the background.

The Chameis Subterrane is quite similar in its trends to the Schakalsberge Subterrane, but shows occurrence of Early Mesoproterozoic zircons, absent in South America and only sparse in few areas in southern Africa (Oriolo and Becker, 2018). The few pre-Ediacaran ages are as well extremely rare in South America but are abundant within the Port Nolloth Group and stratigraphically below these successions (Richtersfeld Igneous Complex; Frimmel et al., 2001) on the western Kalahari craton. It seems that the Chameis Subterrane could be well explained with a sole provenance from the Kalahari craton when trying to match the occurrence of the zircons dated here graphically (Figure 6-5).

However, to define similarities or dissimilarities, statistical approaches are necessary. Again, this is outside of the scope of the thesis, as the age determination (see above) where the major objective.

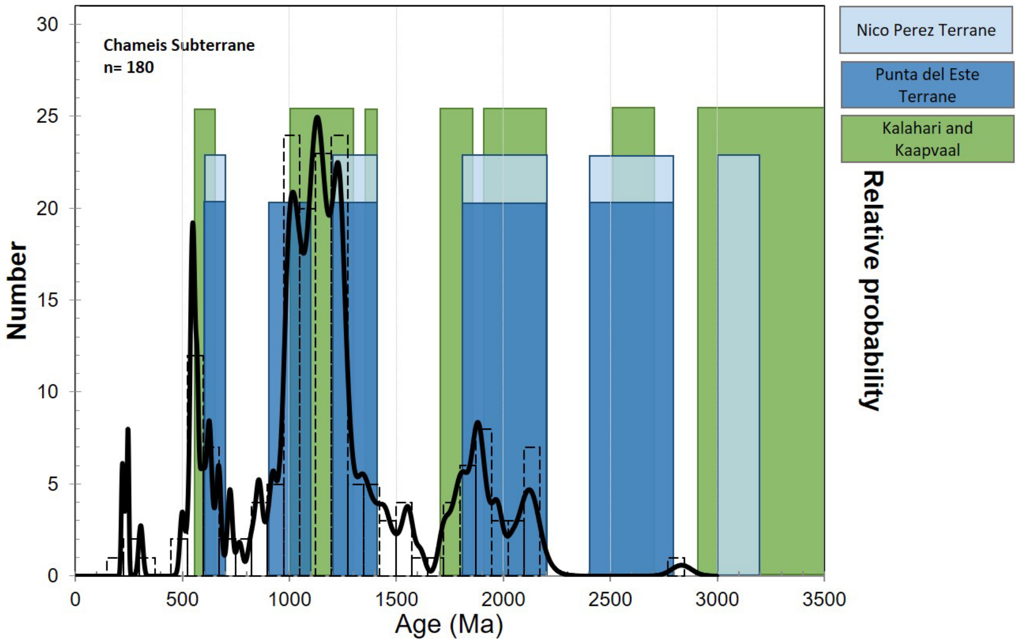

Figure 6-5 Zircon ages obtained for the Chameis Subterrane, with the main events from the south American and African side indicated in the background.

6.3 Potential source areas

The complex tectono-metamorphic history of the Marmora Terrane implies a wide variety of possible source areas for the detrital material and complicates defining an unambiguous petrogenesis for the igneous rocks as well. Besides defining the ages of certain rock successions, most other attempts of new interpretations will still be highly speculative.

Correlations are made more feasible than ever with respect to surrounding rocks, however the dataset of those surrounding rocks should also be evaluated with greatest care. As this thesis does not allow for re-evaluation of such datasets within its scope, such correlation will not be attempted.

The Marmora Terrane successions with the data so far match for both large cratonic areas the events at 550-700 Ma (Pan-African/Brasiliano orogeny), 1000-1300 Ma (the Namaqua orogeny) and at 1800-2200 Ma the Nico Perez Terrane and/or at 1900-2200 Ma the Mangondi orogeny, Limpopo event II and Bushveld.

Obvious is the lack of Late Mesoproterozoic events in the Nico Perez Terrane as the source area for the South American side. The further east located Punta del Este Terrane contains detritus of such a source to be found on the Kalahari craton, supporting the interpretation that the eastern part of South America (in this region here discussed) had been a part of Africa prior to the Atlantic rift. If this material has been transferred from the Namaqua Orogen during Early Neoproterozoic or after a possible collision in the Late Neoproterozoic awaits more substantial data but would be a viable criterion.

Both the South America and the Kalahari cratons can supply Late Neoproterozoic to even lowermost Cambrian aged detritus. However, the western margin of the Kalahari craton lacks a Pan-African event while the eastern margin of South America contains the so-called Pan-Brazilian event of a more or less similar age. The Kalahari craton, on the other side, counts with extensional magmatic rocks formed between 560 and 520 Ma in its southwestern area, the Cape Granites. Only Hf isotopes and trace element geochemistry may be able to separate the different possible sources.

The occurrence of Archean zircons, or not, is also enigmatic for successions deposited on the southern and western margin of the Kalahari craton (Fourie et al., 2011; Naidoo et al., 2013; Andersen et al., 2018, etc.). Whatever the reason was, the explanations are controversial and not of relevance here. Fact seems to be that very scarce, if any, Archean detritus from the core of the Kalahari craton (represented by the Kaapvaal craton) reached the western and southern margins, so in this case here. Archean aged zircons may also be transported from the North into the area (e.g., Zimmermann et al., 2011; Hofmann et al., 2014), but again, to define the possible origin of those aged zircons Hf isotopes and trace element data are paramount.

Intrusion and extrusion of igneous rocks on the Marmora Terrane took place at latest during Late Ediacaran prior or at the time of metamorphism and the possible collision of continental blocks. The igneous rocks shall then represent compressional magmatism, so far interpreted as extensional. Alternatively, an extensional event took place at that time, contradicting all abundant models. Hence, more data are necessary to evaluate the origin of the Marmora Terrane and to interpret more definite paleotectonic and paleogeographic models.

The data presented in this thesis show that even now it is still only speculation when defining certain positions and interactions between the cratonic blocks. More data, and especially isotopic provenance data combined with quantification of detrital material, are paramount to go ahead.

7 Conclusion

This thesis provides a novel dataset of U-Pb crystallisation ages for key rock successions of the Marmora Terrane, a suspect area either related to eastern south America or western southern Africa (Kalahari craton). Although numerous attempts of paleogeographic and palaeotectonic models have been developed, age data are paramount for such exercises and were lacking.

The presented dataset allows the interpretation of depositional ages, giving a new insight into the terrane and its possible origin.

The Oranjemund Group, representing the Oranjemund subterrane, has a maximum depositional age of Uppermost Cryogenian, around 625 Ma. The age obtained by this dataset matches more or less with the ages found in previous studies (e.g., Andersen et al., 2018). The newly obtained data does not allow the exclusion of potential sources represented by eastern south America (Punta del Este Terrane) or the western Kalahari craton. The Oranjemund Subterrane demonstrate a remarkable absence of zircons with ages between 1800 and 1200 Ma.

The Schakalsberge Subterrane is younger than previously assumed, with a Cambrian maximum depositional age, even when using the most conservative method of age determination by Dickinson and Gehrels (2009). Two grains show younger ages, and the subterrane should be further studied to see if this novel Lower Paleozoic age constrain provide basis for new palaeographic models as it post-dated the regional metamorphism at 545 Ma (Frimmel and Frank, 1998). The ages populations of the zircons coincide with events of the Punta del Este Terrane and the Kalahari craton. Moreover, the occurrence of numerous zircons points to a continental basement and not to an oceanic crust block.

The Chameis Subterrane successions have been deposited not earlier than 570-550 Ma, compromising the correlation with global or near global “snowball earth” related glaciations. A maximum depositional age for the Dernburg Formation is interpreted to be around 670 Ma, with the Chameis Gate Member having a depositional age of 557 Ma defined by an associated volcaniclastic, felsic rock. The overlying Bogenfels Formation has a younger depositional age than the Dernburg Formation, at around 568 Ma. If these are the final age determination then the diamictite of the Chameis Gate Member, if interpreted as a glacial deposit related to near-global ice ages, can only be correlated with the Gaskier ice age. The rock succession of this subterrane would be older than the Schakalsberge Subterrane making correlation obsolete, especially within the carbonate successions. In the end of the Ediacaran the Dernburg Formation has been intruded by gabbros which carry zircon. This points clearly to continental basement below the Marmora Terrane. The few but existing zircons are of Late Mesoproterozoic and Paleoproterozoic age (1,8-2,1 Ga), besides the Upper Ediacaran grains, which may be equivalent of the Schakalsberge Subterrane volcanic event. However, this is already speculation.

The dataset provided by this thesis show that U-Pb ages alone are most likely insufficient in resolving the question of source areas during deposition. However, they are very useful in determining maximum depositional ages and absolute ages for the igneous rocks within the terrane. Lu-Hf data combined with trace element distribution in zircons are ideal to understand the history of the zircons analysed. This would allow then to identify easier a possible provenance or affinity and would be a better basis for correlation than the existing data.

8 References

Andersen, T., M. A. Elburg, and J. Lehmann, 2020, Enigmatic provenance signature of sandstone from the Okwa Group, Botswana: South African Journal of Geology, v. 123, no. 3, p. 331–342, doi:10.25131/sajg.123.0022.

Andersen, T., M. A. Elburg, and B. N. Magwaza, 2019, Sources of bias in detrital zircon geochronology: Discordance, concealed lead loss and common lead correction: Earth-Science Reviews, v. 197, p. 102899, doi:10.1016/j.earscirev.2019.102899.

Andersen, T., M. A. Elburg, H. S. van Niekerk, and H. Ueckermann, 2018, Successive sedimentary recycling regimes in southwestern Gondwana: Evidence from detrital zircons in Neoproterozoic to Cambrian sedimentary rocks in southern Africa: Earth-Science Reviews, v. 181, p. 43–60, doi:10.1016/j.earscirev.2018.04.001.

Basei, M. A. S., H. E. Frimmel, M. da C. Campos Neto, C. E. G. de Araujo, N. A. de Castro, and C. R. Passarelli, 2018, The Tectonic History of the Southern Adamastor Ocean Based on a Correlation of the Kaoko and Dom Feliciano Belts, *in* S. Siegesmund, Miguel A. S. Basei, P. Oyhantçabal, and S. Oriolo, eds., Geology of Southwest Gondwana: Cham, Springer International Publishing, Regional Geology Reviews, p. 63–85, doi:10.1007/978-3-319-68920-3_3.

Basei, M. A. S., H. E. Frimmel, A. P. Nutman, F. Preciozzi, and J. Jacob, 2005, A connection between the Neoproterozoic Dom Feliciano (Brazil/Uruguay) and Gariep (Namibia/South Africa) orogenic belts – evidence from a reconnaissance provenance study: Precambrian Research, v. 139, no. 3, p. 195–221, doi:10.1016/j.precamres.2005.06.005.

Belousova, E. A., W. L. Griffin, and S. Y. O'Reilly, 2006, Zircon Crystal Morphology, Trace Element Signatures and Hf Isotope Composition as a Tool for Petrogenetic Modelling: Examples From Eastern Australian Granitoids: Journal of Petrology, v. 47, no. 2, p. 329–353, doi:10.1093/petrology/egi077.

Corfu, F., J. M. Hanchar, P. W. O. Hoskin, and P. Kinny, 2003, Atlas of Zircon Textures: Reviews in Mineralogy and Geochemistry, v. 53, no. 1, p. 469–500, doi:10.2113/0530469.

Davis, D. W., I. S. Williams, and T. E. Krogh, 2003, Historical Development of Zircon Geochronology, *in* Zircon: Mineralogical Society of America, Reviews in Mineralogy and Geochemistry, p. 145–181.

Deer, W. A., R. A. Howie, and J. Zussman, 2013, An introduction to the rock-forming minerals: London, The Minerological Society, 498 p.

Dickinson, W. R., and G. E. Gehrels, 2009, Use of U–Pb ages of detrital zircons to infer maximum depositional ages of strata: A test against a Colorado Plateau Mesozoic database: Earth and Planetary Science Letters, v. 288, no. 1–2, p. 115–125, doi:10.1016/j.epsl.2009.09.013.

Fourie, P. H., U. Zimmermann, N. J. Beukes, T. Naidoo, K. Kobayashi, J. Kosler, E. Nakamura, J. Tait, and J. N. Theron, 2011, Provenance and reconnaissance study of detrital zircons of the Palaeozoic Cape Supergroup in South Africa: revealing the interaction of the Kalahari and Río de la Plata cratons: International Journal of Earth Sciences, v. 100, no. 2–3, p. 527–541, doi:10.1007/s00531-010-0619-x.

Frimmel, H. E., 2011, Chapter 17 The Kaigas and Numees formations, Port Nolloth Group, in South Africa and Namibia: Geological Society, London, Memoirs, v. 36, no. 1, p. 223–231, doi:10.1144/M36.17.

Frimmel, H. E., 2018, The Gariep Belt, *in* S. Siegesmund, M. A. S. Basei, P. Oyhantçabal, and S. Oriolo, eds., Geology of Southwest Gondwana: Cham, Springer International Publishing, Regional Geology Reviews, p. 353–386, doi:10.1007/978-3-319-68920-3_13.

Frimmel, H. E., 2000, The stratigraphy of the Chameis Sub-terrane in the Gariep Belt in southwestern Namibia: Communications of the geological survey of Namibia, v. 12, p. 197–209.

Frimmel, H. E., M. S. Basei, and C. Gaucher, 2010, Neoproterozoic geodynamic evolution of SW-Gondwana: a southern African perspective: International Journal of Earth Sciences, v. 100, no. 2–3, p. 323–354, doi:10.1007/s00531-010-0571-9.

Frimmel, H. E., and P. G. Fölling, 2004, Late Vendian Closure of the Adamastor Ocean: Timing of Tectonic Inversion and Syn-orogenic Sedimentation in the Gariep Basin: Gondwana Research, v. 7, no. 3, p. 685–699, doi:10.1016/S1342-937X(05)71056-X.

Frimmel, H., and W. Frank, 1998, Neoproterozoic tectono-thermal evolution of the Gariep Belt and its basement, Namibia and South Africa: Precambrian Research, v. 90, no. 1–2, p. 1–28, doi:10.1016/S0301-9268(98)00029-1.

Frimmel, H. E., C. J. H. Hartnady, and F. Koller, 1996, Geochemistry and tectonic setting of magmatic units in the Pan-African Gariep Belt, Namibia: Chemical Geology, v. 130, no. 1–2, p. 101–121, doi:10.1016/0009-2541(95)00188-3.

Frimmel, H. E., and S.-Y. Jiang, 2001, Marine evaporites from an oceanic island in the Neoproterozoic Adamastor ocean: Precambrian Research, v. 105, no. 1, p. 57–71, doi:10.1016/S0301-9268(00)00104-2.

Frimmel, H. E., R. E. Zartman, and A. Späth, 2001, The Richtersveld Igneous Complex, South Africa: U-Pb Zircon and Geochemical Evidence for the Beginning of Neoproterozoic Continental Breakup: The Journal of Geology, v. 109, no. 4, p. 493–508, doi:10.1086/320795.

Gaucher, C., H. E. Frimmel, and G. J. B. Germs, 2005, Organic-walled microfossils and biostratigraphy of the upper Port Nolloth Group (Namibia): implications for latest Neoproterozoic glaciations: Geological Magazine, v. 142, no. 5, p. 539–559, doi:10.1017/S0016756805001123.

Gilberg, I. N., 2020, Connecting the late Neoproterozoic flysch sedimentation in the Gariep Belt (Namibia) with its potential source region in southern Dom Feliciano Belt (Uruguay) – a U-Pb detrital and protolith zircon study., Master thesis in geology: UiT The Arctic University of Narway.

Goldstein, J. I., D. E. Newbury, P. Echlin, D. C. Joy, C. E. Lyman, E. Lifshin, L. Sawyer, and J. R. Michael, 2003, Scanning Electron Microscopy and X-ray Microanalysis: Boston, MA, Springer US, doi:10.1007/978-1-4615-0215-9.

Hartnady, C., P. Joubert, and C. Stowe, 1985, Proterozoic Crustal Evolution in Southwestern Africa: Episodes, v. 8, no. 4, p. 236–244, doi:10.18814/epiiugs/1985/v8i4/003.

Hoffman, P. F., and D. P. Schrag, 2002, The snowball Earth hypothesis: testing the limits of global change: Terra Nova, v. 14, no. 3, p. 129–155, doi:10.1046/j.1365-3121.2002.00408.x.

Hofmann, M., U. Linnemann, K.-H. Hoffmann, G. Germs, A. Gerdes, L. Marko, K. Eckelmann, A. Gärtner, and R. Krause, 2014, The four Neoproterozoic glaciations of southern Namibia and their detrital zircon record: The fingerprints of four crustal growth events during two supercontinent cycles: Precambrian Research, v. 259, p. 176–188, doi:10.1016/j.precamres.2014.07.021.

Huhma, H. et al., 2012, The age of the Archaean greenstone belts in Finland: Special Paper - Geological Survey of Finland, v. 54, p. 73–174.

Ludwig, K. R., 2012, User's manual for isoplot/excel 3.75. a geochronological toolkit for microsoft excel.: Berkeley Geochronology Center, v. 5, p. 75.

Martin, H., H. Porada, and O. H. Walliser, 1985, Mixtite deposits of the Damara sequence, Namibia, problems of interpretation: Palaeogeography, Palaeoclimatology, Palaeoecology, v. 51, no. 1–4, p. 159–196, doi:10.1016/0031-0182(85)90084-7.

Naidoo, T., U. Zimmermann, and F. Chemale Junior, 2013, The evolution of Gondwana: U-Pb, Sm-Nd, Pb-Pb and geochemical data from Neoproterozoic to Early Palaeozoic successions of the Kango Inlier (Saldania Belt, South Africa): Sedimentary Geology, v. 294, p. 164–178, doi:10.1016/j.sedgeo.2013.05.014.

Naidoo, T., U. Zimmermann, J. Vervoort, and J. Tait, 2017, The elusive snowball earth: U-Pb zircon ages from the upper diamictite of the Gifberg Group, South Africa: Journal of African Earth Sciences, v. 129, p. 307–317, doi:10.1016/j.jafrearsci.2017.01.015.

Oriolo, S., and T. Becker, 2018, The Kalahari Craton, Southern Africa: From Archean Crustal Evolution to Gondwana Amalgamation, *in* S. Siegesmund, M. A. S. Basei, P. Oyhantçabal, and Sebastian Oriolo, eds., Geology of Southwest Gondwana: Cham, Springer International Publishing, Regional Geology Reviews, p. 133–159, doi:10.1007/978-3-319-68920-3_6.

Oyhantçabal, P., S. Oriolo, K. Wemmer, M. A. S. Basei, D. Frei, and S. Siegesmund, 2021, Provenance of metasedimentary rocks of the western Dom Feliciano Belt in Uruguay: Insights from U–Pb detrital zircon geochronology, Hf and Nd model ages, and geochemical data: Journal of South American Earth Sciences, v. 108, p. 103139, doi:10.1016/j.jsames.2020.103139.

Puetz, S. J., C. J. Spencer, and C. E. Ganade, 2021, Analyses from a validated global U–Pb detrital zircon database: Enhanced methods for filtering discordant U–Pb zircon analyses and optimizing crystallization age estimates: Earth-Science Reviews, v. 220, doi:10.1016/j.earscirev.2021.103745.

Schaltegger, U., A. K. Schmitt, and M. S. A. Horstwood, 2015, U–Th–Pb zircon geochronology by ID-TIMS, SIMS, and laser ablation ICP-MS: Recipes, interpretations, and opportunities: Chemical Geology, v. 402, p. 89–110, doi:10.1016/j.chemgeo.2015.02.028.

Schoene, B., 2014, U–Th–Pb Geochronology, *in* Treatise on Geochemistry: Elsevier, p. 341–378, doi:10.1016/B978-0-08-095975-7.00310-7.

Staden, A. V., T. Naidoo, U. Zimmermann, and G. J. B. Germs, 2006, Provenance analysis of selected clastic rocks in Neoproterozoic to lower Paleozoic successions of southern Africa from the Gariep Belt and the Kango Inlier: South African Journal of Geology, v. 109, no. 1–2, p. 215–232, doi:10.2113/gssajg.109.1-2.215.

Staden, A. V., U. Zimmermann, F. Chemale, J. Gutzmer, and G. J. B. Germs, 2010, Correlation of Ordovician diamictites from Argentina and South Africa using detrital zircon dating: Journal of the Geological Society, v. 167, no. 1, p. 217–220, doi:10.1144/0016-76492009-023.

Stern, R. A., S. Bodorkos, S. L. Kamo, A. H. Hickman, and F. Corfu, 2009, Measurement of SIMS Instrumental Mass Fractionation of Pb Isotopes During Zircon Dating: Geostandards and Geoanalytical Research, v. 33, no. 2, p. 145–168, doi:10.1111/j.1751-908X.2009.00023.x.

Wiedenbeck, M., P. Allé, F. Corfu, W. L. Griffin, M. Meier, F. Oberli, A. V. Quadt, J. C. Roddick, and W. Spiegel, 1995, Three natural zircon standards for U-Pb, Lu-Hf, trace elements and REE analyses: Geostandards and Geoanalytical Research, v. 19, no. 1, p. 1–23, doi:10.1111/j.1751-908X.1995.tb00147.x.

Zimmermann, U., 2018, The Provenance of Selected Neoproterozoic to Lower Paleozoic Basin Successions of Southwest Gondwana: A Review and Proposal for Further Research: Geology of Southwest Gondwana, p. 561–591, doi:10.1007/978-3-319-68920-3_21.

Zimmermann, U., T. Andersen, M. V. Madland, and I. S. Larsen, 2015, The role of U-Pb ages of detrital zircons in sedimentology—An alarming case study for the impact of sampling for provenance interpretation: Sedimentary Geology, v. 320, p. 38–50, doi:10.1016/j.sedgeo.2015.02.006.

Zimmermann, U., E. S. Kristoffersen, P. D. Fredriksen, S. A. R. Bertolino, S. Andò, and D. Bersani, 2016, Provenance and composition of unusually chrome and nickel-rich bucket-shaped pottery from Rogaland (southwestern Norway): Sedimentary Geology, v. 336, p. 183–196, doi:10.1016/j.sedgeo.2015.09.001.

Zimmermann, U., J. Tait, Q. G. Crowley, V. Pashley, and G. Straathof, 2011, The Witputs diamictite in southern Namibia and associated rocks: constraints for a global glaciation? International Journal of Earth Sciences, v. 100, no. 2–3, p. 511–526, doi:10.1007/s00531-010-0621-3.

Appendices

Appendix A: Tables of U-Pb data

Table 9-1 Raw data of concordant and discordant U-Pb analysis of all ablations of sample CR04

Sample	***ppm***					***Ratios***							***U-Pb discordance***		***Ages (Ma)***					
Name	**U**	**Th**	**^{206}Pb**	**$^{206}Pb_c$(%)**	**206/204**	**$^{207}Pb/^{206}Pb^*$**	**1SE**	**$^{207}Pb/^{235}U^*$**	**1SE**	**$^{206}Pb/^{238}U^*$**	**1SE**	**Rho**	**Central (%)**	**Minimum rim (%)**	**207/206**	**1s**	**207/235**	**1s**	**206/238**	**1s**
Discordance < 10 %																				
CR04_66-	96	13.5	10.5	.	1479	0.07426	0.00111	1.85481	0.04062	0.18116	0.00289	0.729	2.58	.	1048	30	1065	14	1073	16
CR04_24-	61	9.2	9	.		0.0767	0.00158	1.82518	0.0567	0.17259	0.00401	0.747	-8.45	.	1113	41	1055	20	1026	22
CR04_69-	44	11.7	5.8	.	567	0.07925	0.00142	2.32609	0.05434	0.21286	0.0032	0.644	6.12	.	1179	34	1220	17	1244	17
CR04_46-	81	12.2	9.5	.		0.07987	0.00118	2.23717	0.04422	0.20315	0.00266	0.664	-0.15	.	1194	28	1193	14	1192	14
CR04_44-	169	12.5	19.3	.		0.08026	0.00109	2.19127	0.03982	0.19801	0.0024	0.666	-3.52	.	1203	25	1178	13	1165	13
CR04_71-	342	88.6	45.1	.	6060	0.08074	0.00083	2.37449	0.04026	0.21329	0.00287	0.794	2.82	.	1215	20	1235	12	1246	15
CR04_57-	34	6.4	4.3	.	463	0.08126	0.00148	2.34231	0.0591	0.20905	0.00364	0.691	-0.37	.	1228	35	1225	18	1224	19
CR04_02-	88	21.3	15.5	.	1916	0.08251	0.00123	2.23707	0.06603	0.19665	0.00501	0.863	-8.71	.	1258	29	1193	21	1157	27
CR04_14-	35	3.2	6.4	.		0.08298	0.00147	2.35848	0.07171	0.20614	0.00509	0.812	-5.23	.	1269	35	1230	22	1208	27
CR04_51-	98	17	11.5	.	1291	0.08373	0.00201	2.30702	0.06382	0.19982	0.00276	0.5	-9.52	.	1286	46	1214	20	1174	15
CR04_42-	61	11.9	7.7	.		0.08471	0.00136	2.54556	0.05577	0.21795	0.00325	0.681	-3.18	.	1309	31	1285	16	1271	17
CR04_63-	47	5.9	6.6	.	912	0.0873	0.00122	2.80387	0.0565	0.23293	0.00339	0.721	-1.41	.	1367	27	1357	15	1350	18
CR04_25-	34	1.5	8	.	709	0.10103	0.00182	3.83763	0.12318	0.27551	0.00733	0.829	-5.1	.	1643	33	1601	26	1569	37
CR04_13-	112	12.6	28.8	.	3544	0.10419	0.00157	4.21263	0.12667	0.29325	0.00763	0.866	-2.82	.	1700	27	1676	25	1658	38
CR04_37-	33	7.4	8.4	.		0.10666	0.00188	4.34575	0.13695	0.29551	0.00772	0.828	-4.82	.	1743	32	1702	26	1669	38
CR04_30-	108	21.5	27.9	.	2820	0.10764	0.00162	4.54874	0.14136	0.30649	0.00833	0.874	-2.36	.	1760	26	1740	26	1723	41
CR04_21-	49	12.9	13.6	.		0.11044	0.00174	4.89137	0.15591	0.32121	0.0089	0.87	-0.7	.	1807	27	1801	27	1796	43
CR04_41-	56	10.1	10	.		0.1108	0.00153	4.71522	0.09585	0.30866	0.00461	0.734	-4.93	.	1813	24	1770	17	1734	23
CR04_70-	62	14.6	11.2	.	1056	0.11094	0.00167	4.5332	0.10667	0.29637	0.00536	0.768	-8.85	.	1815	27	1737	20	1673	27
CR04_26-	35	6.8	9.2	.	737	0.11111	0.00198	4.73003	0.14914	0.30876	0.00804	0.826	-5.21	.	1818	30	1773	26	1735	40
CR04_36-	200	13.2	51.9	.	2434	0.11188	0.00165	4.74679	0.1464	0.3077	0.00833	0.878	-6.28	.	1830	26	1776	26	1729	41
CR04_78-	186	14.3	37.7	.		0.11257	0.00131	5.2018	0.10666	0.33513	0.00565	0.822	1.36	.	1841	20	1853	17	1863	27
CR04_04-	115	18.8	34.1	.		0.11272	0.00162	5.10567	0.15688	0.32852	0.00893	0.884	-0.77	.	1844	25	1837	26	1831	43
CR04_07-	73	10.5	21.5	.	1879	0.11296	0.00166	5.13982	0.16497	0.33	0.00941	0.889	-0.57	.	1848	25	1843	27	1838	46
CR04_06-	114	54.4	31.8	.	2919	0.11305	0.00154	4.9185	0.1456	0.31554	0.0083	0.888	-5.02	.	1849	23	1805	25	1768	41

Appendix A: Tables of U-Pb data

Sample			ppm							Ratios			U-Pb discordance		Ages (Ma)					
Name	**U**	**Th**	**^{206}Pb**	**^{206}Pb$_c$(%)**	**206/204**	**^{207}Pb/^{206}Pb***	**1SE**	**^{207}Pb/^{235}U***	**1SE**	**^{206}Pb/^{238}U***	**1SE**	**Rho**	**Central (%)**	**Minimum rim (%)**	**207/206**	**1s**	**207/235**	**1s**	**206/238**	**1s**
CR04_22-	108	10.6	30.1	.		0.11322	0.00167	5.05179	0.15738	0.32361	0.00888	0.881	-2.75	.	1852	26	1828	26	1807	43
CR04_75-	174	14.6	34.5	.	4137	0.11332	0.00142	5.08933	0.10023	0.32574	0.00494	0.77	-2.2	.	1853	22	1834	17	1818	24
CR04_20-	78	34.9	22.7	.		0.11375	0.00184	5.26326	0.17627	0.33557	0.00984	0.875	0.31	.	1860	28	1863	29	1865	47
CR04_05-	66	9.8	19.4	.		0.1138	0.00182	5.12961	0.16337	0.32691	0.009	0.864	-2.32	.	1861	28	1841	27	1823	44
CR04_08-	166	36.4	47.4	.		0.11382	0.00157	5.05355	0.15068	0.32202	0.00851	0.886	-3.79	.	1861	24	1828	25	1800	41
CR04_19-	90	19.4	25.2	.		0.1138	0.00177	5.07254	0.15956	0.32329	0.00884	0.869	-3.39	.	1861	27	1832	27	1806	43
CR04_68-	76	22	15.9	.		0.11379	0.00163	5.34606	0.11789	0.34076	0.00571	0.759	1.83	.	1861	26	1876	19	1890	27
CR04_10-	99	20.9	28.9	.	2974	0.11387	0.00167	5.19857	0.16138	0.33113	0.00907	0.882	-1.12	.	1862	25	1852	26	1844	44
CR04_77-	94	12.4	18.2	.	1799	0.11432	0.00147	5.10299	0.12838	0.32374	0.007	0.859	-3.75	.	1869	23	1837	21	1808	34
CR04_35-	130	24.2	35.6	.	3974	0.11452	0.00237	5.22091	0.19686	0.33066	0.01041	0.835	-1.89	.	1872	36	1856	32	1842	50
CR04_09-	179	29.8	53.3	.		0.11454	0.00165	5.34821	0.17287	0.33865	0.0098	0.895	0.46	.	1873	26	1877	28	1880	47
CR04_11-	43	4.5	12.7	.		0.11469	0.00197	5.26852	0.17549	0.33317	0.00951	0.857	-1.3	.	1875	31	1864	28	1854	46
CR04_76-	274	103.6	54.2	.	6111	0.11479	0.00136	5.14026	0.10027	0.32476	0.00504	0.796	-3.89	.	1877	21	1843	17	1813	25
CR04_18-	60	9.8	16.6	.		0.1151	0.00182	5.03302	0.15628	0.31714	0.00848	0.861	-6.42	.	1881	28	1825	26	1776	42
CR04_03-	273	52.1	73.4	.	3085	0.11538	0.00249	4.90062	0.20438	0.30804	0.01099	0.855	-9.36	.	1886	37	1802	35	1731	54
CR04_15-	113	20.2	32.8	.		0.1155	0.00165	5.25685	0.16424	0.3301	0.00917	0.889	-2.97	.	1888	26	1862	27	1839	44
CR04_45-	100	18.8	19.3	.		0.11555	0.00147	5.29069	0.1072	0.33207	0.00524	0.778	-2.44	.	1889	21	1867	17	1848	25
CR04_49-	257	33	50.8	.		0.1156	0.00129	5.3313	0.0955	0.33448	0.00469	0.783	-1.78	.	1889	20	1874	15	1860	23
CR04_34-	58	14.7	16.1	.		0.11566	0.00182	5.19463	0.16157	0.32575	0.00874	0.863	-4.39	.	1890	27	1852	26	1818	42
CR04_58-	69	10.4	14	.		0.11573	0.00169	5.39629	0.11871	0.33818	0.00557	0.748	-0.82	.	1891	25	1884	19	1878	27
CR04_55-	92	17.1	18.5	.		0.11603	0.00146	5.38169	0.10446	0.33638	0.00498	0.763	-1.63	.	1896	21	1882	17	1869	24
CR04_01-	78	15.6	23.5	.	2247	0.11631	0.00192	5.3794	0.1833	0.33545	0.00999	0.874	-2.15	.	1900	28	1882	29	1865	48
CR04_40-	140	15.8	26.4	.		0.11655	0.00133	5.2301	0.09684	0.32545	0.00475	0.788	-5.29	.	1904	20	1858	16	1816	23
CR04_43-	207	18.7	39.7	.		0.11673	0.00138	5.32979	0.10385	0.33115	0.00513	0.794	-3.79	.	1907	21	1874	17	1844	25
CR04_48-	190	20.9	36.8	.		0.11696	0.00132	5.35812	0.09965	0.33224	0.00491	0.795	-3.68	.	1910	20	1878	16	1849	24
CR04_73-	107	18.3	22.7	.	1606	0.11698	0.00167	5.6753	0.14189	0.35186	0.00722	0.821	1.99	.	1911	24	1928	22	1943	34
CR04_27-	328	43.5	92.6	.	8381	0.11877	0.00165	5.4083	0.17143	0.33027	0.0094	0.898	-5.82	.	1938	24	1886	27	1840	46

Appendix A: Tables of U-Pb data

Sample		ppm				Ratios							U-Pb discordance		Ages (Ma)					
Name	**U**	**Th**	**^{206}Pb**	**^{206}Pb$_c$(%)**	**206/204**	**^{207}Pb/^{206}Pb***	**1SE**	**^{207}Pb/^{235}U***	**1SE**	**^{206}Pb/^{238}U***	**1SE**	**Rho**	**Central (%)**	**Minimum rim (%)**	**207/206**	**1s**	**207/235**	**1s**	**206/238**	**1s**
CR04_64-2-	24	4.7	5.1	.		0.11983	0.00215	5.79036	0.1545	0.35046	0.00691	0.739	-1	.	1954	30	1945	23	1937	33
CR04_28-	185	37.1	54.8	.	5385	0.1199	0.00177	5.72246	0.18212	0.34614	0.00977	0.887	-2.28	.	1955	25	1935	28	1916	47
CR04_50-	81	15.2	16	.	2002	0.12043	0.00139	5.60273	0.1049	0.33741	0.00497	0.786	-5.19	.	1963	20	1917	16	1874	24
CR04_31-	190	33.8	56.4	.	6529	0.12054	0.00183	5.85634	0.19235	0.35237	0.01027	0.887	-1.08	.	1964	26	1955	28	1946	49
CR04_59-	322	34.3	65.1	.	5775	0.12054	0.00138	5.60511	0.1285	0.33726	0.0067	0.867	-5.32	.	1964	20	1917	20	1873	32
CR04_80-	122	16.8	25.9	.	1190	0.12053	0.00306	5.8086	0.18626	0.34952	0.00686	0.612	-1.87	.	1964	46	1948	28	1932	33
CR04_39-	175	30.7	50.6	.	2242	0.12124	0.0021	5.81564	0.2019	0.34791	0.01047	0.867	-2.92	.	1974	30	1949	30	1925	50
CR04_16-	407	110.9	116.5	.	7601	0.12151	0.00173	5.48028	0.16599	0.3271	0.00874	0.882	-8.95	.	1979	25	1898	26	1824	42
CR04_62-	309	44.5	68.4	.		0.12229	0.00143	6.24686	0.12727	0.37047	0.00618	0.818	2.44	.	1990	21	2011	18	2032	29
CR04_29-	304	79.6	88.6	.	2212	0.12435	0.00223	5.87359	0.19436	0.34257	0.00952	0.84	-6.89	.	2020	30	1957	29	1899	46
Rims and doubles																				
CR04_02r-	190	26.5	33.6	.		0.08007	0.00107	2.17157	0.05862	0.1967	0.00461	0.868	-3.74	.	1199	25	1172	19	1158	25
CR04_67r-	169	15.3	20.4	.		0.08227	0.00151	2.26581	0.05335	0.19974	0.00294	0.626	-6.82	.	1252	37	1202	17	1174	16
CR04_07r-	87	9.8	23.3	.	2567	0.11055	0.00164	4.59132	0.15098	0.30122	0.00884	0.893	-6.99	.	1808	27	1748	27	1697	44
CR04_36r-	409	16.4	104.5	.	10597	0.11117	0.00182	4.55574	0.13136	0.29722	0.00705	0.823	-8.81	.	1819	29	1741	24	1677	35
CR04_22r-	426	9.1	109.6	.	7300	0.11208	0.00239	4.81472	0.20848	0.31155	0.01174	0.87	-5.3	.	1833	38	1787	36	1748	58
CR04_35-2-	100	29.7	28.1	.		0.11347	0.00202	5.24372	0.18253	0.33516	0.01002	0.859	0.47	.	1856	31	1860	30	1863	48
CR04_15r-	149	23.8	43	.	4154	0.11444	0.00158	5.20017	0.15884	0.32957	0.00898	0.892	-2.13	.	1871	24	1853	26	1836	44
CR04_43r-	269	17.9	49.1	.	4632	0.11459	0.00131	5.00343	0.12015	0.31669	0.00668	0.879	-6.09	.	1873	20	1820	20	1774	33
CR04_50r-	73	11.1	14.6	.		0.11528	0.00158	5.38523	0.11538	0.33879	0.00559	0.77	-0.21	.	1884	24	1883	18	1881	27
CR04_38r-	165	25.7	45.2	.	3609	0.11536	0.00165	5.21005	0.16248	0.32756	0.00908	0.889	-3.59	.	1885	24	1854	27	1827	44
CR04_53r-	293	52.4	57.5	.		0.11621	0.00131	5.31493	0.09797	0.3317	0.00484	0.792	-3.16	.	1899	19	1871	16	1847	23
CR04_52r-	49	5.5	9.4	.		0.11801	0.00178	5.32944	0.11961	0.32755	0.00544	0.74	-5.95	.	1926	25	1874	19	1826	26
CR04_48r-	217	26.3	44.7	.	3683	0.11904	0.00266	5.58012	0.16447	0.33998	0.00654	0.653	-3.28	.	1942	40	1913	25	1887	31
CR04_54r-	169	24	35.9	.	3956	0.12365	0.0015	6.06303	0.12185	0.35563	0.00569	0.797	-2.77	.	2010	20	1985	18	1961	27
CR04_59r-	234	19.6	47.4	.	1494	0.12437	0.00201	5.75034	0.12787	0.33534	0.00512	0.686	-8.86	-1.51	2020	28	1939	19	1864	25

Appendix A: Tables of U-Pb data

Sample			***ppm***								***Ratios***			***U-Pb discordance***		***Ages (Ma)***				
Name	**U**	**Th**	**^{206}Pb**	**^{206}Pb$_c$(%)**	**206/204**	**^{207}Pb/^{206}Pb***	**1SE**	**^{207}Pb/^{235}U***	**1SE**	**^{206}Pb/^{238}U***	**1SE**	**Rho**	**Central (%)**	**Minimum rim (%)**	**207/206**	**1s**	**207/235**	**1s**	**206/238**	**1s**
Discordance **> 10 %**																				
CR04_56-	45	12.2	4.7	.	668	0.07938	0.00225	1.91397	0.05955	0.17488	0.00227	0.416	-13.07	.	1182	53	1086	21	1039	12
CR04_65-	410	63.4	47.6	.	3831	0.08092	0.00089	2.13514	0.03527	0.19136	0.00235	0.744	-8.11	.	1220	20	1160	11	1129	13
CR04_23-	169	31.7	24.8	.	1590	0.08387	0.00132	2.00262	0.06888	0.17319	0.0053	0.889	-21.79	-3.56	1289	29	1116	23	1030	29
CR04_17-	38	8.9	6.6	.		0.08493	0.00159	2.31467	0.07046	0.19768	0.00474	0.788	-12.56	.	1314	35	1217	22	1163	26
CR04_57r-	110	14.9	12.7	.	1748	0.08555	0.00099	2.27045	0.04292	0.19249	0.00287	0.788	-15.86	-6.87	1328	22	1203	13	1135	16
CR04_61-	95	9.5	11.8	.	1420	0.08632	0.00134	2.48084	0.06244	0.20844	0.00413	0.788	-10.19	.	1345	29	1266	18	1220	22
CR04_67-	32	7.1	3.5	.		0.09215	0.00412	2.2718	0.10782	0.17879	0.00286	0.337	-30.22	-14.57	1471	83	1204	33	1060	16
CR04_32-	38	8.6	6.4	.	292	0.09346	0.00449	2.54928	0.13815	0.19783	0.00494	0.461	-24.34	-3.32	1497	88	1286	40	1164	27
CR04_33-	485	75.7	67.2	.	703	0.09756	0.00172	2.17627	0.06325	0.16178	0.00374	0.795	-41.67	-33.11	1578	31	1173	20	967	21
CR04_01r-	261	63	37.2	.	1882	0.09964	0.00175	2.1655	0.06592	0.15762	0.00392	0.817	-44.73	-36.23	1617	31	1170	21	944	22
CR04_30r-	116	11.4	24.1	.	3197	0.10328	0.00163	3.52518	0.13303	0.24756	0.00848	0.908	-17.06	-0.21	1684	28	1533	30	1426	44
CR04_38-	114	14.7	23.3	.	1551	0.10921	0.00255	4.26533	0.27368	0.28327	0.01693	0.931	-11.28	.	1786	41	1687	53	1608	85
CR04_03r-	326	19.8	86	.	4712	0.1118	0.00157	4.51208	0.15003	0.29272	0.00883	0.907	-10.76	.	1829	24	1733	28	1655	44
CR04_06r-	153	38.4	38.9	.	2913	0.11257	0.00166	4.45209	0.14019	0.28685	0.00798	0.883	-13.23	-0.17	1841	26	1722	26	1626	40
CR04_64-	37	7.6	6.5	.	838	0.11535	0.00182	4.71572	0.11717	0.2965	0.00569	0.772	-12.73	-3.67	1885	28	1770	21	1674	28
CR04_74-	51	6.4	9.1	.	1263	0.11609	0.00253	4.92693	0.16338	0.3078	0.00769	0.753	-10.04	.	1897	39	1807	28	1730	38
CR04_40-2-	107	18.2	18.4	.		0.11619	0.00141	4.75334	0.08613	0.2967	0.004	0.744	-13.36	-7.11	1898	21	1777	15	1675	20
CR04_47-	256	40.5	31.8	.	1038	0.1162	0.00158	3.43875	0.08001	0.21462	0.00405	0.812	-37.33	-31.08	1899	23	1513	18	1253	22
CR04_27r-	241	19.9	59.9	.	4356	0.11683	0.00233	4.86542	0.19667	0.30204	0.01063	0.87	-12.33	.	1908	36	1796	34	1701	53
CR04_60-	181	107.8	21	.	1085	0.11742	0.00419	3.21505	0.14755	0.19859	0.00574	0.63	-42.67	-32.16	1917	62	1461	36	1168	31
CR04_79-	113	14.3	21.1	.	807	0.1189	0.00627	4.99268	0.2869	0.30453	0.00698	0.399	-13.26	.	1940	89	1818	49	1714	34
CR04_72-	400	43.6	76.9	.	2828	0.12224	0.00149	5.36335	0.11493	0.31821	0.00561	0.823	-11.97	-4.14	1989	21	1879	18	1781	27
CR04_12-	314	36.5	78.4	.	1218	0.12498	0.00192	4.90248	0.1622	0.2845	0.00834	0.886	-23.07	-11.75	2028	25	1803	28	1614	42
CR04_52-	148	26.8	27.8	.	1107	0.12727	0.00195	5.62949	0.14487	0.32081	0.00664	0.804	-14.82	-6.03	2061	25	1921	22	1794	32
CR04_54-	207	30.1	28.6	.	738	0.13046	0.00285	4.16227	0.11673	0.2314	0.00407	0.627	-40.05	-34.37	2104	36	1667	23	1342	21

Appendix A: Tables of U-Pb data

Sample			ppm					Ratios					U-Pb discordance		Ages (Ma)					
Name	**U**	**Th**	**^{206}Pb**	**^{206}Pb$_c$(%)**	**206/204**	**^{207}Pb/^{206}Pb***	**1SE**	**^{207}Pb/^{235}U***	**1SE**	**^{206}Pb/^{238}U***	**1SE**	**Rho**	**Central (%)**	**Minimum rim (%)**	**207/206**	**1s**	**207/235**	**1s**	**206/238**	**1s**
CR04_53-	203	18.5	38.4	.	729	0.13071	0.00359	5.77816	0.18472	0.32061	0.00526	0.513	-17.09	-8.57	2108	49	1943	28	1793	26
CR04_09r-	276	42.9	80.4	.	503	0.13726	0.00402	6.29542	0.27348	0.33263	0.01068	0.739	-17.91	-4.55	2193	49	2018	38	1851	52

*Table 9-**Feil! Det er ingen tekst med den angitte stilen i dokumentet.**1 Raw data of concordant and discordant U-Pb analysis of all ablations of sample CR03*

Sample	***ppm***					***Ratios***							***U-Pb discordance***		***Ages (Ma)***					
Name	**U**	**Th**	**^{206}Pb**	**^{206}Pb$_c$(%)**	**206/204**	**^{207}Pb/^{206}Pb***	**1SE**	**^{207}Pb/^{235}U***	**1SE**	**^{206}Pb/^{238}U***	**1SE**	**Rho**	**Central (%)**	**Minimum rim (%)**	**207/206**	**1s**	**207/235**	**1s**	**206/238**	**1s**
Discordance < 10 %																				
CR03_65-	331	45	12	.	881	0.05165	0.00114	0.2864	0.00901	0.04022	0.0009	0.713	-5.88	.	270	50	256	7	254	6
CR03_91-	542	50.9	23.7	.		0.05294	0.00079	0.36176	0.01562	0.04956	0.00201	0.939	-4.55	.	326	33	314	12	312	12
CR03_47-	181	21.3	11.8	.		0.05531	0.00112	0.56448	0.01681	0.07401	0.00161	0.731	8.62	.	425	43	454	11	460	10
CR03_40-	226	35.1	15.2	.		0.05582	0.00088	0.58508	0.01503	0.07602	0.00154	0.79	6.31	.	445	33	468	10	472	9
CR03_16-	81	13.2	5.6	.		0.05785	0.00141	0.64829	0.02132	0.08127	0.00179	0.669	-4.08	.	524	53	507	13	504	11
CR03_77-	249	35.2	19.2	.		0.05917	0.0019	0.6844	0.03872	0.08389	0.00391	0.823	-9.8	.	573	71	529	23	519	23
CR03_89-	220	9.7	16.7	.		0.05682	0.00108	0.66654	0.02985	0.08508	0.00345	0.906	9.01	.	484	40	519	18	526	20
CR03_102-	148	7.2	11.5	.		0.05736	0.00138	0.68714	0.02673	0.08688	0.00266	0.786	6.48	.	506	51	531	16	537	16
CR03_105-	143	9.7	11.2	.		0.05861	0.00108	0.70681	0.02441	0.08747	0.00256	0.847	-2.28	.	553	39	543	15	541	15
CR03_120-	100	15.1	7.8	.		0.05719	0.00146	0.69501	0.0262	0.08814	0.00245	0.738	9.54	.	499	55	536	16	545	15
CR03_84-	139	17.3	11	.	703	0.0584	0.00116	0.70972	0.03202	0.08814	0.00357	0.898	-0.03	.	545	41	545	19	545	21
CR03_42-	319	19.9	25.2	.	2824	0.05853	0.00089	0.7272	0.01857	0.0901	0.00185	0.803	1.2	.	550	32	555	11	556	11
CR03_71-	246	72.7	21.1	.		0.05861	0.00087	0.74863	0.02993	0.09263	0.00344	0.928	3.46	.	553	32	567	17	571	20
CR03_34-	509	52	41.5	.	2488	0.05874	0.00081	0.75658	0.01855	0.09342	0.00189	0.827	3.42	.	557	28	572	11	576	11
CR03_92-	165	51.8	13.7	.		0.06093	0.00203	0.78511	0.05017	0.09345	0.00509	0.853	-9.99	.	637	70	588	29	576	30
CR03_64-	265	10	22.4	.		0.05823	0.00099	0.75214	0.02148	0.09369	0.00215	0.805	7.57	.	538	37	569	12	577	13
CR03_19-	159	31.1	12.8	.	1266	0.0582	0.00096	0.75549	0.01923	0.09415	0.00182	0.759	8.3	.	537	37	571	11	580	11
CR03_02-	130	22.2	10.4	.		0.06087	0.00136	0.80617	0.0244	0.09605	0.00197	0.676	-7.17	.	635	48	600	14	591	12
CR03_52-	207	23	18.2	.		0.06001	0.00094	0.81654	0.02252	0.09868	0.00224	0.825	0.45	.	604	32	606	13	607	13
CR03_117-	360	42.8	32.7	.		0.06023	0.00097	0.83121	0.03021	0.10009	0.00326	0.897	0.5	.	612	33	614	17	615	19
CR03_82-	69	17.4	6.2	.		0.06091	0.00141	0.84294	0.04112	0.10037	0.00431	0.88	-3.23	.	636	48	621	23	617	25
CR03_85-	75	12.5	6.9	.	596	0.06138	0.00116	0.85735	0.03977	0.1013	0.00429	0.914	-4.93	.	653	39	629	22	622	25
CR03_10-	622	71	54.5	.		0.06016	0.00081	0.85404	0.019	0.10296	0.00183	0.798	3.85	.	609	28	627	10	632	11
CR03_04-	164	17.6	14.5	.	1107	0.05947	0.00102	0.85299	0.02156	0.10403	0.00193	0.733	9.66	.	584	37	626	12	638	11
CR03_31-	310	29	29.2	.		0.06342	0.00092	0.93695	0.02773	0.10715	0.00277	0.872	-9.62	.	722	30	671	15	656	16

Appendix A: Tables of U-Pb data

Sample	*ppm*					*Ratios*							*U-Pb discordance*		*Ages (Ma)*					
Name	**U**	**Th**	**^{206}Pb**	**^{206}Pb$_c$(%)**	**206/204**	**^{207}Pb/^{206}Pb***	**1SE**	**^{207}Pb/^{235}U***	**1SE**	**^{206}Pb/^{238}U***	**1SE**	**Rho**	**Central (%)**	**Minimum rim (%)**	**207/206**	**1s**	**207/235**	**1s**	**206/238**	**1s**
CR03_36-	75	17.4	7.1	.	718	0.06157	0.00116	0.91732	0.02637	0.10806	0.00235	0.756	0.37	.	659	39	661	14	661	14
CR03_83-	58	27.8	5.7	.		0.06147	0.00162	0.9182	0.04489	0.10834	0.00446	0.842	1.21	.	656	54	661	24	663	26
CR03_05-	249	25.8	25.2	.	2831	0.06222	0.0009	1.01752	0.02424	0.1186	0.00225	0.795	6.32	.	682	29	713	12	723	13
CR03_30-	76	9.7	8.6	.	723	0.06432	0.00135	1.15734	0.03606	0.1305	0.00301	0.74	5.44	.	752	43	781	17	791	17
CR03_101-	227	20.8	27.2	.	2253	0.06648	0.00128	1.21655	0.04707	0.13273	0.00445	0.867	-2.33	.	821	40	808	22	803	25
CR03_51-	27	6.7	3.1	.		0.06606	0.00207	1.21061	0.0483	0.13292	0.00328	0.619	-0.48	.	808	62	805	22	805	19
CR03_78-	36	4.4	4.4	.		0.06832	0.00248	1.25585	0.07781	0.13333	0.00669	0.81	-8.64	.	878	75	826	35	807	38
CR03_49-	15	5.2	1.9	.		0.07007	0.0026	1.35733	0.06073	0.14048	0.00352	0.559	-9.53	.	931	72	871	26	847	20
CR03_27-	68	8.6	8.8	.	649	0.06822	0.00138	1.39695	0.04085	0.1485	0.00313	0.721	2.1	.	875	40	888	17	893	18
CR03_29-	69	11.2	9	.	1021	0.07096	0.00158	1.45672	0.04433	0.14889	0.00308	0.68	-6.9	.	956	43	913	18	895	17
CR03_122-	45	4.8	6.3	.		0.07111	0.00144	1.50979	0.06347	0.154	0.00567	0.876	-4.15	.	960	40	934	26	923	32
CR03_81-	89	21.9	12.5	.		0.07083	0.00123	1.52089	0.06966	0.15573	0.0066	0.926	-2.21	.	953	35	939	28	933	37
CR03_114-	15	2.3	2.1	.		0.07148	0.00278	1.58294	0.08621	0.1606	0.00613	0.701	-1.24	.	971	80	964	34	960	34
CR03_26-	62	9.2	9.5	.		0.07245	0.00127	1.77144	0.04942	0.17733	0.00385	0.779	5.83	.	999	34	1035	18	1052	21
CR03_39-	55	6.6	8.1	.		0.07288	0.00133	1.674	0.04927	0.16658	0.00386	0.786	-1.86	.	1011	34	999	19	993	21
CR03_54-	119	8.9	19.2	.		0.0732	0.00113	1.80335	0.05189	0.17868	0.00434	0.843	4.28	.	1019	30	1047	19	1060	24
CR03_96-	379	39.6	58.5	.		0.07437	0.00117	1.77626	0.08755	0.17324	0.00809	0.948	-2.21	.	1051	31	1037	32	1030	44
CR03_09-	102	9.8	15.5	.	1787	0.07479	0.00167	1.81795	0.05528	0.17628	0.00364	0.679	-1.66	.	1063	44	1052	20	1047	20
CR03_100-	58	10.8	9.3	.		0.07528	0.00151	1.87877	0.09956	0.181	0.00888	0.925	-0.37	.	1076	40	1074	35	1072	48
CR03_33-	93	17.4	14.9	.	1643	0.07717	0.00157	1.9287	0.05838	0.18127	0.00406	0.74	-4.97	.	1125	39	1091	20	1074	22
CR03_113-	486	24.3	83	.		0.07734	0.00118	1.98752	0.07933	0.18638	0.00688	0.924	-2.71	.	1130	28	1111	27	1102	37
CR03_13-	524	39.1	82.7	.	8674	0.07754	0.00107	1.95745	0.04784	0.18309	0.00369	0.824	-4.91	.	1135	27	1101	16	1084	20
CR03_14-	191	7.6	32.5	.		0.07754	0.00121	2.10676	0.05794	0.19704	0.00446	0.822	2.33	.	1135	30	1151	19	1159	24
CR03_32-	33	4.3	5.5	.		0.07769	0.00172	2.01878	0.06535	0.18847	0.00445	0.73	-2.46	.	1139	44	1122	22	1113	24
CR03_116-	57	10.9	10.4	.		0.07783	0.0018	2.11678	0.09783	0.19727	0.0079	0.866	1.74	.	1142	45	1154	32	1161	43
CR03_97-	185	8	32.6	.	1550	0.07852	0.00128	2.12876	0.1074	0.19662	0.00938	0.946	-0.28	.	1160	31	1158	35	1157	51
CR03_55-	105	6.1	18.8	.		0.07863	0.00123	2.15626	0.06365	0.1989	0.00498	0.848	0.63	.	1163	29	1167	20	1169	27

Appendix A: Tables of U-Pb data

Sample	ppm					Ratios							U-Pb discordance		Ages (Ma)					
Name	U	Th	^{206}Pb	$^{206}Pb_c$(%)	206/204	$^{207}Pb/^{206}Pb^*$	1SE	$^{207}Pb/^{235}U^*$	1SE	$^{206}Pb/^{238}U^*$	1SE	Rho	Central (%)	Minimum rim (%)	207/206	1s	207/235	1s	206/238	1s
CR03_03-	89	11	15.6	.		0.07867	0.00146	2.21276	0.06183	0.204	0.00426	0.748	3.11	.	1164	35	1185	20	1197	23
CR03_66-	205	12.1	37.6	.		0.07914	0.00122	2.18687	0.06602	0.2004	0.0052	0.859	0.16	.	1176	29	1177	21	1177	28
CR03_53-	94	7.7	16.5	.		0.07962	0.00131	2.13077	0.06295	0.1941	0.00476	0.83	-4.04	.	1187	31	1159	20	1144	26
CR03_74-	35	4	6.9	.		0.07976	0.00166	2.32	0.11075	0.21096	0.00906	0.9	3.95	.	1191	39	1218	34	1234	48
CR03_62-	170	10.7	30.6	.		0.07979	0.00122	2.17617	0.06618	0.1978	0.0052	0.864	-2.6	.	1192	30	1173	21	1164	28
CR03_61-	102	41.7	19.2	.	1913	0.07997	0.00139	2.25225	0.07021	0.20425	0.00528	0.829	0.16	.	1196	33	1197	22	1198	28
CR03_93-	84	10	15.6	.	837	0.08008	0.00147	2.28383	0.11751	0.20683	0.00994	0.934	1.17	.	1199	34	1207	36	1212	53
CR03_76-	197	14.1	39.1	.		0.08017	0.00111	2.35571	0.10627	0.21312	0.00915	0.952	4.06	.	1201	27	1229	32	1245	49
CR03_15-	65	6.9	11.6	.	1002	0.08029	0.00136	2.29034	0.06366	0.20689	0.00456	0.792	0.73	.	1204	32	1209	20	1212	24
CR03_70-	35	6.3	7.5	.	467	0.08069	0.00148	2.50974	0.11964	0.22559	0.00992	0.922	8.88	.	1214	36	1275	35	1311	52
CR03_86-	32	15.4	5.9	.	587	0.08146	0.00177	2.27366	0.11424	0.20242	0.00917	0.902	-3.94	.	1233	41	1204	35	1188	49
CR03_98-	58	5.7	10.7	.	1173	0.08173	0.00169	2.3326	0.12414	0.207	0.01015	0.922	-2.32	.	1239	39	1222	38	1213	54
CR03_88-	94	12.6	17.2	.		0.08317	0.00259	2.32962	0.14482	0.20316	0.01093	0.866	-6.96	.	1273	60	1221	44	1192	59
CR03_22-	47	14.1	9.5	.	1026	0.0848	0.00158	2.71738	0.08057	0.23241	0.00535	0.777	3.05	.	1311	34	1333	22	1347	28
CR03_72-	233	15.8	50.2	.	3637	0.08643	0.00132	2.7286	0.12747	0.22897	0.01011	0.945	-1.53	.	1348	29	1336	35	1329	53
CR03_60-	58	5.7	12.4	.		0.0872	0.00155	2.79819	0.08911	0.23272	0.00615	0.829	-1.32	.	1365	33	1355	24	1349	32
CR03_63-	17	3.2	3.4	.		0.08858	0.00262	2.74315	0.10959	0.2246	0.00603	0.673	-7.04	.	1395	56	1340	30	1306	32
CR03_104-	89	4.5	19.5	.	1188	0.08864	0.00169	2.87347	0.13426	0.2351	0.01003	0.913	-2.8	.	1396	36	1375	35	1361	52
CR03_08-	210	37.8	44	.	3311	0.08899	0.00134	2.97074	0.08045	0.24212	0.00544	0.83	-0.49	.	1404	29	1400	21	1398	28
CR03_18-	52	4.4	11.5	.		0.08937	0.00171	3.10631	0.09679	0.25208	0.0062	0.789	2.93	.	1412	34	1434	24	1449	32
CR03_24-	248	35.9	55.5	.	4802	0.08978	0.00132	3.14577	0.08695	0.25414	0.00594	0.846	3.07	.	1421	27	1444	21	1460	31
CR03_11-	49	6	11.1	.	656	0.0915	0.00164	3.29557	0.09581	0.26122	0.00598	0.788	3.01	.	1457	32	1480	23	1496	31
CR03_57-	257	18.5	63.1	.		0.09764	0.00168	3.6114	0.11888	0.26824	0.00753	0.853	-3.39	.	1580	30	1552	26	1532	38
CR03_46-	110	13	28.4	.	1977	0.10487	0.00173	4.1525	0.1377	0.28719	0.00826	0.867	-5.59	.	1712	30	1665	27	1627	41
CR03_121-	184	36.9	54.5	.		0.11478	0.00225	4.99485	0.27959	0.31561	0.01654	0.936	-6.59	.	1876	34	1818	47	1768	81
CR03_17-	90	29	27.5	.		0.11544	0.00191	5.50063	0.17463	0.34558	0.00936	0.853	1.63	.	1887	29	1901	27	1913	45
CR03_06-	86	11.6	26.5	.	1252	0.12137	0.00269	5.96788	0.21212	0.35662	0.00991	0.782	-0.61	.	1976	38	1971	31	1966	47

Appendix A: Tables of U-Pb data

Sample	*ppm*					*Ratios*							*U-Pb discordance*		*Ages (Ma)*					
Name	**U**	**Th**	**^{206}Pb**	**^{206}Pb$_c$(%)**	**206/204**	**^{207}Pb/^{206}Pb***	**1SE**	**^{207}Pb/^{235}U***	**1SE**	**^{206}Pb/^{238}U***	**1SE**	**Rho**	**Central (%)**	**Minimum rim (%)**	**207/206**	**1s**	**207/235**	**1s**	**206/238**	**1s**
CR03_118-	70	8.8	21.8	.	1163	0.12198	0.00425	5.51985	0.31302	0.32819	0.01469	0.789	-9.01	.	1985	59	1904	49	1830	71
CR03_58-	38	10.1	13.1	.		0.12838	0.00252	6.58128	0.2514	0.3718	0.01218	0.857	-2.14	.	2076	33	2057	34	2038	57
CR03_23-	51	4.5	17.8	.	2070	0.12882	0.00236	6.95629	0.2466	0.39164	0.01188	0.856	2.74	.	2082	31	2106	31	2130	55
CR03_43-	616	60.7	211.3	.	22316	0.1353	0.00253	6.99113	0.25618	0.37476	0.01181	0.86	-6.25	.	2168	32	2110	33	2052	55
CR03_38-	36	8.5	16.5	.	1866	0.18438	0.00411	12.75069	0.56407	0.50155	0.01916	0.864	-3.26	.	2693	36	2661	42	2620	82
Rims and doubles																				
CR03_77r-	331	69.6	25.3	.		0.05746	0.00146	0.66538	0.03425	0.08398	0.00376	0.87	2.16	.	509	54	518	21	520	22
CR03_67r-	67	5.1	11.3	.	469	0.07385	0.00486	1.83024	0.16866	0.17974	0.01159	0.7	2.95	.	1037	129	1056	61	1066	63
CR03_35r-	93	8.1	13.9	.	863	0.07646	0.00163	1.78572	0.05432	0.1694	0.00367	0.713	-9.58	.	1107	42	1040	20	1009	20
CR03_68r-	157	14.2	38.8	.		0.09153	0.00143	3.30625	0.16546	0.26197	0.01246	0.95	3.25	.	1458	29	1483	39	1500	64
Discordance > 10 %																				
CR03_112-	166	29	3.3	.		0.05285	0.00214	0.16227	0.00813	0.02227	0.00066	0.588	-56.59	.	322	90	153	7	142	4
CR03_69-	246	37.7	5.6	.		0.05013	0.00129	0.17143	0.0076	0.0248	0.00089	0.814	-21.74	.	201	58	161	7	158	6
CR03_109-	373	52.8	14.2	.	926	0.05092	0.00091	0.30007	0.01009	0.04274	0.00122	0.847	14.01	.	237	40	266	8	270	8
CR03_01-	192	15.4	7	.		0.05427	0.00162	0.32161	0.01121	0.04298	0.00077	0.514	-29.61	.	382	63	283	9	271	5
CR03_103-	83	12.6	3.2	.	254	0.05034	0.0025	0.30058	0.01761	0.0433	0.00134	0.528	30.26	.	211	107	267	14	273	8
CR03_95-	183	18.7	13.8	.	676	0.06999	0.00169	0.82979	0.04165	0.08598	0.00378	0.877	-44.47	-11.4	928	48	613	23	532	22
CR03_37-	73	11	5.6	.	705	0.06428	0.00164	0.77679	0.02609	0.08764	0.00191	0.649	-29.07	-0.62	751	53	584	15	542	11
CR03_78r-	150	1.1	12.2	.		0.06149	0.00178	0.75878	0.0409	0.0895	0.00407	0.843	-16.51	.	656	58	573	24	553	24
CR03_90-	60	9	4.8	.		0.06332	0.00135	0.78326	0.03621	0.08971	0.00368	0.888	-23.99	.	719	43	587	21	554	22
CR03_28-	26	5	2.1	.		0.06265	0.002	0.80211	0.03106	0.09286	0.00203	0.565	-18.6	.	696	66	598	17	572	12
CR03_21-	106	12.2	8.8	.	821	0.06364	0.00122	0.85072	0.02423	0.09694	0.00204	0.738	-19.13	.	730	40	625	13	596	12
CR03_45-	80	5.2	7	.		0.05865	0.00108	0.80216	0.02333	0.0992	0.00224	0.776	10.51	.	554	39	598	13	610	13
CR03_119-	75	3.3	6.4	.	597	0.06602	0.0026	0.90271	0.05245	0.09917	0.00424	0.735	-25.64	.	807	79	653	28	610	25
CR03_107-	323	22	29.6	.	1463	0.06509	0.00236	0.91032	0.04312	0.10143	0.00309	0.643	-20.84	.	777	76	657	23	623	18

Appendix A: Tables of U-Pb data

Sample	***ppm***					***Ratios***							***U-Pb discordance***		***Ages (Ma)***					
Name	**U**	**Th**	**^{206}Pb**	**^{206}Pb$_c$(%)**	**206/204**	**^{207}Pb/^{206}Pb***	**1SE**	**^{207}Pb/^{235}U***	**1SE**	**^{206}Pb/^{238}U***	**1SE**	**Rho**	**Central (%)**	**Minimum rim (%)**	**207/206**	**1s**	**207/235**	**1s**	**206/238**	**1s**
CR03_20-	150	24.1	13.2	.		0.05854	0.00099	0.82026	0.02087	0.10163	0.00193	0.747	14.1	.	550	36	608	12	624	11
CR03_50-	82	8.8	7.6	.	570	0.06385	0.00194	0.90956	0.0373	0.10332	0.00284	0.671	-14.63	.	737	63	657	20	634	17
CR03_73-	91	11.4	8.8	.		0.05848	0.00107	0.84062	0.03622	0.10425	0.00407	0.906	17.51	.	548	39	619	20	639	24
CR03_48-	126	20.6	12	.	523	0.06485	0.0012	0.96072	0.02898	0.10744	0.00256	0.791	-15.26	.	770	37	684	15	658	15
CR03_12-	90	18.6	10.3	.	1178	0.0704	0.00151	1.2906	0.03787	0.13296	0.00266	0.683	-15.32	.	940	42	842	17	805	15
CR03_108-	9	1.3	1.1	.	115	0.06203	0.00431	1.19039	0.09389	0.13918	0.00518	0.472	26.05	.	675	143	796	44	840	29
CR03_44-	119	19.1	6.8	.	464	0.0765	0.00672	0.68506	0.06195	0.06495	0.00141	0.24	-65.37	-35.09	1108	176	530	37	406	9
CR03_35-	188	22.3	26.5	.	1110	0.08264	0.00169	1.84354	0.05835	0.16179	0.00392	0.765	-25.11	-10	1261	39	1061	21	967	22
CR03_72r-	343	64.6	71.3	.	1519	0.0922	0.00186	2.8197	0.14395	0.22181	0.0104	0.919	-13.49	.	1471	37	1361	38	1291	55
CR03_79-	329	42	54.8	.	1021	0.09331	0.00281	2.33823	0.12579	0.18174	0.00811	0.829	-30.33	-7.39	1494	55	1224	38	1076	44
CR03_110-	431	78	56.7	0.42	2414	0.10314	0.00201	2.05829	0.09125	0.14474	0.00577	0.899	-51.43	-39.62	1681	35	1135	30	871	32
CR03_07-	192	24.5	27	.	387	0.1042	0.0051	2.36755	0.12545	0.16478	0.00336	0.385	-45.4	-33.33	1700	87	1233	38	983	19
CR03_99-	169	19	28.7	.	2312	0.10489	0.00448	2.78872	0.21998	0.19284	0.01278	0.84	-36.62	-6.74	1712	78	1353	59	1137	69
CR03_87-	258	22.5	34.3	.	1312	0.10617	0.00291	2.16243	0.12519	0.14771	0.00753	0.881	-52.16	-36.91	1735	48	1169	40	888	42
CR03_41-	311	20.2	34.6	.	1237	0.10897	0.00267	1.88403	0.06293	0.12539	0.00285	0.68	-60.63	-55.09	1782	45	1075	22	762	16
CR03_94-	171	27	12.3	.	287	0.1095	0.03417	1.22989	0.38725	0.08146	0.00344	0.134	-74.57	.	1791	638	814	176	505	20
CR03_124-	265	33.7	73.7	.		0.11425	0.00222	4.65195	0.25278	0.29531	0.01498	0.934	-12.15	.	1868	33	1759	45	1668	75
CR03_87r-	196	17.8	46.1	.	2964	0.11943	0.00238	4.30235	0.23847	0.26127	0.01352	0.933	-25.93	-5	1948	34	1694	46	1496	69
CR03_115-	191	20.4	55.3	.	5038	0.12087	0.00339	5.18346	0.31887	0.31103	0.01703	0.89	-12.94	.	1969	49	1850	52	1746	84
CR03_25-	200	25.9	54.6	.	3909	0.12642	0.00219	5.54768	0.25015	0.31828	0.01325	0.923	-14.92	.	2049	29	1908	39	1781	65
CR03_68-	38	16.1	10.4	.	118	0.17118	0.02634	6.56691	1.09382	0.27822	0.01774	0.383	-43.18	-4.15	2569	271	2055	147	1582	89
CR03_56-	44	4	17.5	.		0.17452	0.0039	10.36055	0.43594	0.43057	0.01535	0.847	-13.39	-0.17	2601	34	2468	39	2308	69
CR03_80-	409	46	155.5	.	16891	0.18485	0.0068	10.31429	0.7935	0.40468	0.02735	0.878	-22.1	.	2697	59	2463	71	2191	126
CR03_106-	125	5.5	11.2	.	90	0.219	0.01204	3.03985	0.19393	0.10067	0.00326	0.508	-82.82	-80.08	2973	85	1418	49	618	19
CR03_123-	85	6.4	43.1	.		0.22026	0.00701	15.74527	1.38658	0.51845	0.04257	0.932	-11.88	.	2983	49	2861	84	2693	181

Appendix A: Tables of U-Pb data

Table 9-2 Raw data of concordant and discordant U-Pb analysis of all ablations of sample CR02

Sample	*ppm*					*Ratios*							*U-Pb discordance*		*Ages (Ma)*					
Name	**U**	**Th**	**^{206}Pb**	**^{206}Pb$_c$(%)**	**206/204**	**^{207}Pb/^{206}Pb***	**1SE**	**^{207}Pb/^{235}U***	**1SE**	**^{206}Pb/^{238}U***	**1SE**	**Rho**	**Central (%)**	**Minimum rim (%)**	**207/206**	**1s**	**207/235**	**1s**	**206/238**	**1s**
Discordance < 10 %																				
CR02_74-	281	27.5	22.5	.	1207	0.0607	0.00097	0.80547	0.02443	0.09625	0.00248	0.849	-6.02	.	629	34	600	14	592	15
CR02-04-	546	23.2	44.7	.	4559	0.06204	0.00085	0.8633	0.01792	0.10092	0.00157	0.75	-8.66	.	676	29	632	10	620	9
CR02_43-	167	9.3	13.2	.	975	0.06045	0.00104	0.85094	0.02041	0.10209	0.0017	0.695	1.16	.	620	34	625	11	627	10
CR02_30-	235	11.8	18.9	.	2099	0.06091	0.00106	0.85943	0.02089	0.10233	0.00173	0.696	-1.33	.	636	36	630	11	628	10
CR02-07-	161	4.8	13.5	.		0.0617	0.00118	0.88099	0.02246	0.10355	0.00175	0.663	-4.52	.	664	39	642	12	635	10
CR02_47-	65	9.2	5.2	.	685	0.06022	0.00171	0.86134	0.02952	0.10374	0.00198	0.557	4.27	.	611	60	631	16	636	12
CR02_48-	159	14.5	12.8	.	1250	0.0627	0.00159	0.9031	0.02792	0.10446	0.00184	0.57	-8.67	.	698	52	653	15	641	11
CR02_75-	78	11	6.8	.	635	0.06195	0.00187	0.89939	0.03837	0.10529	0.00318	0.708	-4.26	.	673	64	651	21	645	19
CR02_79-	311	35.9	27.3	.	1261	0.06221	0.00124	0.92015	0.02989	0.10728	0.00275	0.79	-3.75	.	681	42	662	16	657	16
CR02_86-	94	8.8	8.8	.	1166	0.06352	0.00218	0.93958	0.04377	0.10728	0.00338	0.677	-9.97	.	726	71	673	23	657	20
CR02_56-	224	29.7	22.8	.	1636	0.06095	0.001	0.90703	0.03158	0.10793	0.00331	0.881	3.83	.	637	34	655	17	661	19
CR02_44-	712	97.6	59.5	0.15	5005	0.06336	0.00089	0.94311	0.02019	0.10796	0.00174	0.753	-8.69	.	720	28	675	11	661	10
CR02_113-	212	45.8	20.5	.		0.06033	0.00078	0.89966	0.01787	0.10815	0.00164	0.762	7.95	.	615	27	652	10	662	10
CR02_120-	414	16.3	39.9	.		0.06023	0.00075	0.90676	0.01782	0.10918	0.00165	0.771	9.63	.	612	25	655	9	668	10
CR02_55-	439	20.9	45.1	.	3697	0.06366	0.00104	0.96187	0.03363	0.10959	0.00339	0.885	-8.64	.	730	34	684	17	670	20
CR02_106-2-	443	37.9	45	.	1456	0.06112	0.00093	0.94562	0.02135	0.11221	0.00187	0.739	6.92	.	643	31	676	11	686	11
CR02_34-	250	34.7	21.7	.	1537	0.06353	0.00095	0.9913	0.02309	0.11317	0.00202	0.765	-5.05	.	726	30	699	12	691	12
CR02_51-	817	4.5	71.8	.	8267	0.06453	0.00104	1.00753	0.0271	0.11324	0.00243	0.799	-9.39	.	759	33	708	14	692	14
CR02_26-	93	9.8	8.3	.		0.06309	0.00116	0.98722	0.02463	0.11348	0.00192	0.679	-2.73	.	711	39	697	13	693	11
CR02-01-	84	1.8	7.9	.		0.06196	0.00141	0.98523	0.02895	0.11533	0.00213	0.63	4.86	.	673	48	696	15	704	12
CR02_25-	214	10.7	19.5	.		0.06406	0.00112	1.02288	0.02474	0.1158	0.00193	0.691	-5.3	.	744	34	715	12	706	11
CR02-23-	310	10.2	29.3	0.5	2004	0.0653	0.00125	1.08011	0.02922	0.11996	0.0023	0.708	-7.26	.	784	38	744	14	730	13
CR02_96-	177	13.8	19	.	2543	0.0627	0.00121	1.03905	0.03891	0.12018	0.00386	0.858	5.06	.	698	40	723	19	732	22
CR02-17-	92	6.1	8.9	.	853	0.06476	0.00119	1.08047	0.02713	0.121	0.00207	0.683	-4.2	.	767	37	744	13	736	12
CR02_60-	178	9.6	20.4	.	1805	0.06514	0.00127	1.0902	0.04097	0.12139	0.0039	0.854	-5.46	.	779	39	749	20	739	22
CR02_104-	437	49	49.8	0.44	2391	0.06306	0.00089	1.07503	0.02309	0.12364	0.00199	0.751	6.16	.	710	30	741	11	751	11
CR02_54-	209	3.9	19.8	.	2839	0.06373	0.00102	1.08871	0.0253	0.12389	0.00209	0.724	2.91	.	733	33	748	12	753	12
CR02_89-	72	4.9	7.8	.	747	0.06433	0.00135	1.10277	0.0427	0.12432	0.00405	0.841	0.39	.	753	42	755	21	755	23
CR02_66-	667	48.8	82.4	.		0.06667	0.00108	1.18991	0.04622	0.12945	0.00457	0.908	-5.47	.	827	32	796	21	785	26

Appendix A: Tables of U-Pb data

Sample	***ppm***					***Ratios***							***U-Pb discordance***		***Ages (Ma)***					
Name	**U**	**Th**	**^{206}Pb**	**^{206}Pb$_c$(%)**	**206/204**	**^{207}Pb/^{206}Pb***	**1SE**	**^{207}Pb/^{235}U***	**1SE**	**^{206}Pb/^{238}U***	**1SE**	**Rho**	**Central (%)**	**Minimum rim (%)**	**207/206**	**1s**	**207/235**	**1s**	**206/238**	**1s**
CR02-22-	117	4.9	12.2	.		0.06686	0.00102	1.19786	0.02949	0.12994	0.00251	0.786	-5.84	.	833	30	800	14	788	14
CR02-02-	462	17.6	50	.		0.06616	0.00089	1.21255	0.02587	0.13292	0.0022	0.777	-0.93	.	812	28	806	12	804	13
CR02-10-	75	5.3	8.2	.	708	0.06478	0.00123	1.21465	0.03247	0.13599	0.00256	0.705	7.61	.	767	39	807	15	822	15
CR02_102-	596	109.8	74.4	.	8252	0.06629	0.0007	1.24678	0.02256	0.13641	0.002	0.811	1.16	.	815	21	822	10	824	11
CR02_90-	331	12.1	40.7	.	4393	0.0667	0.00118	1.25886	0.05003	0.13689	0.00487	0.896	-0.15	.	828	37	827	22	827	28
CR02_84-	267	27.1	32.3	.		0.06511	0.00099	1.25618	0.04121	0.13992	0.00407	0.886	9.08	.	778	31	826	19	844	23
CR02-18-	42	2.4	4.7	.		0.06789	0.00133	1.31388	0.0348	0.14036	0.0025	0.672	-2.28	.	865	40	852	15	847	14
CR02_63-	171	29	23.5	.		0.06751	0.00114	1.35491	0.05239	0.14557	0.00506	0.899	2.84	.	853	35	870	23	876	28
CR02_36-	69	5.3	8.4	.		0.0707	0.00125	1.51813	0.03777	0.15574	0.00272	0.702	-1.77	.	949	37	938	15	933	15
CR02_42-	134	12.3	16.2	.	1587	0.07037	0.00128	1.51912	0.03843	0.15657	0.00274	0.692	-0.16	.	939	36	938	15	938	15
CR02_37-	140	11	17.4	.		0.07139	0.00112	1.56283	0.03769	0.15877	0.00292	0.762	-2.08	.	969	30	956	15	950	16
CR02_28-	336	43.9	42.1	.		0.07242	0.00167	1.5899	0.04576	0.15921	0.00275	0.601	-4.9	.	998	45	966	18	952	15
CR02_67-	579	23.4	88.3	.	7105	0.06984	0.00106	1.53859	0.05939	0.15978	0.00567	0.92	3.72	.	924	30	946	24	956	32
CR02_29-	169	10.7	21.8	.	1976	0.07212	0.00113	1.635	0.03981	0.16443	0.00306	0.764	-0.86	.	989	31	984	15	981	17
CR02_103-	67	12.3	10.2	.	792	0.07203	0.00119	1.64553	0.03795	0.1657	0.00267	0.698	0.18	.	987	33	988	15	988	15
CR02_94-	263	61.6	39.2	.	2778	0.07156	0.0012	1.65389	0.06344	0.16762	0.00579	0.9	2.82	.	974	33	991	24	999	32
CR02-03-	227	22.8	31.8	.		0.07206	0.00096	1.71419	0.03826	0.17253	0.00309	0.803	4.2	.	988	25	1014	14	1026	17
CR02_117-	58	11	9.4	.		0.07238	0.00112	1.777	0.04101	0.17806	0.00305	0.743	6.5	.	997	30	1037	15	1056	17
CR02_85-	128	4.7	19.9	.	1806	0.0726	0.00133	1.824	0.0636	0.18222	0.00541	0.851	8.26	.	1003	37	1054	23	1079	29
CR02_99-	335	16.9	46	.	6020	0.07263	0.00138	1.52715	0.06162	0.15249	0.00543	0.883	-9.49	.	1004	36	941	25	915	30
CR02_33-	300	5.5	39.1	.	3330	0.0727	0.00105	1.67301	0.03847	0.16691	0.00298	0.777	-1.12	.	1006	29	998	15	995	16
CR02_83-	236	43	33.5	.	3368	0.07286	0.00126	1.6467	0.05857	0.16392	0.00509	0.874	-3.36	.	1010	34	988	22	979	28
CR02_119-	188	10.1	30.8	.	3264	0.07313	0.00095	1.83714	0.03732	0.18221	0.00284	0.766	6.57	.	1017	26	1059	13	1079	15
CR02_62-	53	1.6	8.3	.		0.07339	0.00134	1.73426	0.06968	0.17138	0.00613	0.89	-0.54	.	1025	36	1021	26	1020	34
CR02_95-	129	19.6	20.3	.	1450	0.07346	0.00127	1.78099	0.0675	0.17584	0.00593	0.89	1.85	.	1027	34	1039	25	1044	33
CR02_101-	170	15.1	28.7	.		0.07347	0.00096	1.8591	0.03681	0.18352	0.00274	0.754	6.26	.	1027	25	1067	13	1086	15
CR02-09-	104	5	14.5	.	1662	0.07359	0.00122	1.74763	0.04082	0.17225	0.00283	0.703	-0.6	.	1030	33	1026	15	1024	16
CR02_100-	426	15.2	65.2	.	5801	0.07366	0.00108	1.72114	0.06257	0.16947	0.00564	0.915	-2.41	.	1032	29	1016	23	1009	31
CR02_88-	262	13.2	44.8	.	2927	0.07432	0.00107	1.96992	0.07399	0.19224	0.00667	0.924	8.66	.	1050	28	1105	25	1134	36
CR02_41-	57	5.7	7.3	.		0.07436	0.00155	1.6934	0.04694	0.16517	0.00303	0.661	-6.74	.	1051	39	1006	18	985	17
CR02_97-	89	14.8	15	.	1978	0.07436	0.00138	1.92244	0.07618	0.18751	0.00656	0.883	5.87	.	1051	36	1089	26	1108	36
CR02_71-	136	7.4	23.2	.	1383	0.07442	0.0014	1.82575	0.07718	0.17793	0.00673	0.895	0.29	.	1053	36	1055	28	1056	37

Appendix A: Tables of U-Pb data

Sample	***ppm***					***Ratios***							***U-Pb discordance***		***Ages (Ma)***					
Name	**U**	**Th**	**^{206}Pb**	**^{206}Pb$_c$(%)**	**206/204**	**^{207}Pb/^{206}Pb***	**1SE**	**^{207}Pb/^{235}U***	**1SE**	**^{206}Pb/^{238}U***	**1SE**	**Rho**	**Central (%)**	**Minimum rim (%)**	**207/206**	**1s**	**207/235**	**1s**	**206/238**	**1s**
CR02_87-	160	14.6	24.8	.		0.07442	0.00106	1.80149	0.06393	0.17557	0.00571	0.916	-1.04	.	1053	28	1046	23	1043	31
CR02-12-	410	19.1	55.6	.	6452	0.07447	0.00107	1.73281	0.03776	0.16875	0.00277	0.753	-5.03	.	1054	28	1021	14	1005	15
CR02_109-	452	50.6	70.9	.	4131	0.07449	0.00085	1.77026	0.03403	0.17235	0.00267	0.807	-3.05	.	1055	23	1035	12	1025	15
CR02_59-	30	1.2	4.7	.		0.07466	0.0015	1.71699	0.06827	0.16679	0.00572	0.863	-6.62	.	1059	39	1015	26	994	32
CR02_111-	261	19	43.8	.		0.07466	0.00096	1.90019	0.03887	0.1846	0.00294	0.78	3.36	.	1059	25	1081	14	1092	16
CR02_78-	211	35.6	31.6	.	2143	0.07497	0.0011	1.83136	0.05849	0.17716	0.00502	0.888	-1.66	.	1068	29	1057	21	1051	28
CR02_50-	143	15	18.9	.	2575	0.07507	0.0014	1.78242	0.0458	0.17219	0.00306	0.691	-4.68	.	1071	37	1039	17	1024	17
CR02_92-	126	18.9	20.1	.	1809	0.07511	0.00137	1.8832	0.07115	0.18183	0.00602	0.876	0.55	.	1072	37	1075	25	1077	33
CR02-15-	131	5.2	18.9	.		0.07518	0.0011	1.87347	0.04491	0.18074	0.00343	0.791	-0.23	.	1073	29	1072	16	1071	19
CR02_73-	375	62.7	53.4	.	3624	0.07595	0.00142	1.78885	0.06509	0.17083	0.00533	0.858	-7.6	.	1094	34	1041	24	1017	29
CR02_31-	185	9.8	26.1	.	2807	0.07599	0.00122	1.87766	0.04509	0.1792	0.00319	0.742	-3.2	.	1095	32	1073	16	1063	17
CR02_68-	346	30.8	55.5	.	3176	0.07616	0.00125	1.76171	0.07054	0.16777	0.00613	0.912	-9.77	.	1099	29	1031	26	1000	34
CR02_116-	294	22.5	47	.	2760	0.07613	0.00119	1.84443	0.04326	0.17571	0.00308	0.747	-5.43	.	1099	31	1061	15	1043	17
CR02_77-	292	24.7	46.3	.	5104	0.07622	0.00092	1.98481	0.06156	0.18887	0.0054	0.922	1.42	.	1101	24	1110	21	1115	29
CR02_76-	262	15.1	40.2	.		0.07638	0.00098	1.92965	0.05971	0.18322	0.00516	0.91	-2.03	.	1105	25	1091	21	1085	28
CR02_27-	60	8.6	8.4	.		0.07641	0.00198	1.85058	0.05981	0.17566	0.00338	0.596	-6.12	.	1106	51	1064	21	1043	19
CR02_118-	43	2.8	7.2	.		0.07702	0.00138	1.97315	0.0473	0.1858	0.00295	0.662	-2.24	.	1122	34	1106	16	1099	16
CR02-13-	266	18.7	38.4	.	5145	0.07855	0.00128	1.95273	0.04656	0.18031	0.00314	0.732	-8.61	.	1161	31	1099	16	1069	17
CR02_107-	72	12.5	15.9	.		0.08561	0.00124	2.84674	0.06622	0.24116	0.00439	0.782	5.29	.	1329	27	1368	17	1393	23
CR02-05-	102	20.9	26.4	.		0.11047	0.00176	4.84306	0.13157	0.31797	0.007	0.811	-1.73	.	1807	29	1792	23	1780	34
CR02_82-	140	49.1	40.1	.	5468	0.11325	0.00193	5.18022	0.20879	0.33176	0.01212	0.906	-0.33	.	1852	29	1849	34	1847	59
CR02_35-	43	3.4	11.2	.		0.11462	0.00217	5.27383	0.14819	0.3337	0.00693	0.739	-1.08	.	1874	32	1865	24	1856	33
CR02-06-	116	5.7	32	.	2999	0.11576	0.00194	5.44094	0.14643	0.34089	0.00717	0.781	-0.05	.	1892	29	1891	23	1891	34
CR02_64-	26	12.5	12.2	.		0.17528	0.00442	11.8924	0.76902	0.49209	0.0293	0.921	-1.35	.	2609	40	2596	61	2580	127
Rims and doubles																				
CR02_107r-	402	35.3	40.3	1.47	959	0.06309	0.00158	0.97525	0.03615	0.11212	0.00307	0.738	-3.88	.	711	51	691	19	685	18
CR02-01-2-	77	1.8	7.2	.		0.06094	0.00124	0.95324	0.02562	0.11345	0.002	0.656	9.22	.	637	42	680	13	693	12
CR02_60-2-	65	6.9	7.4	.		0.06354	0.00138	1.05088	0.04129	0.11996	0.00393	0.833	0.59	.	726	45	729	20	730	23
CR02-22-2-	226	14	22.7	.	1906	0.06402	0.00093	1.12829	0.02571	0.12783	0.00224	0.77	4.75	.	742	30	767	12	775	13
CR02_37-2-	235	19.4	28.9	.		0.07228	0.0011	1.561	0.03656	0.15663	0.00278	0.759	-6.03	.	994	28	955	14	938	16
CR02_85r-	368	10	57.9	.		0.07289	0.00101	1.8137	0.06116	0.18046	0.00555	0.912	6.29	.	1011	28	1050	22	1069	30

Appendix A: Tables of U-Pb data

Sample	***ppm***					***Ratios***							***U-Pb discordance***		***Ages (Ma)***					
Name	**U**	**Th**	**^{206}Pb**	**^{206}Pb$_c$(%)**	**206/204**	**^{207}Pb/^{206}Pb***	**1SE**	**^{207}Pb/^{235}U***	**1SE**	**^{206}Pb/^{238}U***	**1SE**	**Rho**	**Central (%)**	**Minimum rim (%)**	**207/206**	**1s**	**207/235**	**1s**	**206/238**	**1s**
CR02_59-2-	181	6	29.1	.		0.07404	0.00124	1.7342	0.0657	0.16988	0.00577	0.897	-3.21	.	1042	32	1021	24	1011	32
CR02_117r-	224	30.8	35.7	.	2301	0.07402	0.00087	1.80936	0.03678	0.1773	0.00294	0.817	1.07	.	1042	23	1049	13	1052	16
CR02_65r-	339	47	59.8	.		0.07491	0.0012	1.86049	0.08121	0.18013	0.00731	0.93	0.16	.	1066	31	1067	29	1068	40
CR02_118r-	181	10.7	30.1	.	2300	0.07514	0.00123	1.90922	0.04807	0.18428	0.00353	0.76	1.82	.	1072	31	1084	17	1090	19
CR02_50-2-	321	25.7	43.5	.		0.07555	0.0012	1.83594	0.04395	0.17625	0.00316	0.749	-3.67	.	1083	30	1058	16	1046	17
CR02_97r-	234	19	39.1	.	4042	0.07562	0.00099	1.94192	0.07025	0.18626	0.00628	0.932	1.62	.	1085	24	1096	24	1101	34
CR02_116r-	44	3.2	7.3	.		0.07779	0.00183	1.94406	0.05937	0.18125	0.00352	0.636	-6.45	.	1142	46	1096	20	1074	19
CR02-06-2-	39	3.9	10.9	.		0.11672	0.00225	5.5319	0.16197	0.34375	0.00758	0.753	-0.11	.	1907	33	1906	25	1905	36
Discordance > 10 %																				
CR02_40-2-	1149	52.9	60	5.74	304	0.06764	0.0015	0.58913	0.01779	0.06317	0.0013	0.681	-55.6	-42.51	857	44	470	11	395	8
CR02_53r-	1215	48.4	63.8	1.73	938	0.06265	0.00115	0.5884	0.01768	0.06812	0.00162	0.792	-40.27	-16	696	37	470	11	425	10
CR02_38-	659	144.9	38.9	7.87	220	0.07009	0.00503	0.6677	0.05113	0.06909	0.00185	0.35	-55.54	-13.44	931	140	519	31	431	11
CR02_40-3-	252	20.3	13.9	2.07	594	0.07173	0.00192	0.70523	0.03247	0.07131	0.00267	0.813	-56.48	-36.1	978	51	542	19	444	16
CR02_104r-	398	39.8	30.6	2.76	551	0.06058	0.0013	0.68323	0.01822	0.08179	0.0013	0.595	-19.58	.	624	45	529	11	507	8
CR02_46-	504	54.9	34	6.57	258	0.02571	0.00117	0.29161	0.01448	0.08227	0.00163	0.399	-20.84	-15.28	-479	50	260	11	510	10
CR02-08-	293	18.1	16.6	.	857	0.06726	0.00147	0.77068	0.05293	0.08311	0.00541	0.948	-40.71	.	846	44	580	30	515	32
CR02_32r-	402	15.8	27.6	3.78	420	0.06025	0.00207	0.69689	0.02746	0.08388	0.00163	0.492	-15.87	.	613	71	537	16	519	10
CR02_45-	1059	61.2	74	4.17	411	0.06224	0.00127	0.74566	0.01974	0.08688	0.00146	0.634	-22.21	.	683	44	566	11	537	9
CR02_38r-	778	95	54.6	2.31	703	0.06393	0.00115	0.77255	0.01859	0.08765	0.0014	0.661	-27.87	-8.86	739	37	581	11	542	8
CR02_105-	442	154.8	39	4.06	401	0.06159	0.00165	0.7941	0.02529	0.09351	0.0016	0.539	-13.25	.	660	56	593	14	576	9
CR02_43r-	160	6.8	12.1	0.08	1676	0.06248	0.0011	0.84681	0.02161	0.0983	0.00182	0.726	-13.06	.	691	37	623	12	604	11
CR02-16-	704	43.7	56.7	1.16	1276	0.06334	0.00106	0.86428	0.01897	0.09897	0.00141	0.65	-16.19	.	720	34	632	10	608	8
CR02_49-	178	16.9	13.7	.		0.06708	0.00241	0.92722	0.03754	0.10025	0.00186	0.458	-28	.	840	74	666	20	616	11
CR02_58-	622	64.7	58.1	.	3090	0.06327	0.00104	0.88294	0.03252	0.10121	0.00334	0.895	-14.03	.	717	33	643	18	621	20
CR02_79r-	229	39.9	19.7	.	1074	0.07081	0.00122	0.99527	0.03256	0.10195	0.00284	0.85	-35.93	-16.22	952	34	701	17	626	17
CR02_45-2-	463	6.2	37.7	0.06	4386	0.06374	0.0012	0.92137	0.02202	0.10484	0.00155	0.618	-12.93	.	733	38	663	12	643	9
CR02_32-	834	99.8	71.4	2.95	564	0.0652	0.00105	0.94894	0.02132	0.10556	0.00165	0.696	-18.01	.	781	33	678	11	647	10
CR02_110-	94	14.2	9.2	.	503	0.05932	0.00134	0.89019	0.02441	0.10883	0.00169	0.566	15.81	0.84	579	47	646	13	666	10
CR02_53-	191	11.2	16.2	2.06	620	0.06811	0.00663	1.02167	0.10155	0.10878	0.00218	0.202	-24.9	.	872	197	715	51	666	13
CR02_70-2-	407	25	43.1	.	1089	0.07224	0.00134	1.10309	0.04401	0.11075	0.00391	0.884	-33.47	-7.83	993	38	755	21	677	23
CR02-11r-	245	25.7	22.1	.	2087	0.06992	0.0015	1.07595	0.03066	0.11161	0.0021	0.66	-27.74	-9.97	926	43	742	15	682	12

Appendix A: Tables of U-Pb data

Sample	***ppm***					***Ratios***							***U-Pb discordance***		***Ages (Ma)***					
Name	**U**	**Th**	**^{206}Pb**	**^{206}Pb$_c$(%)**	**206/204**	**^{207}Pb/^{206}Pb***	**1SE**	**^{207}Pb/^{235}U***	**1SE**	**^{206}Pb/^{238}U***	**1SE**	**Rho**	**Central (%)**	**Minimum rim (%)**	**207/206**	**1s**	**207/235**	**1s**	**206/238**	**1s**
CR02_106-	173	12.6	17.8	.	1859	0.05982	0.0011	0.93156	0.02177	0.11295	0.00164	0.621	16.39	2.47	597	39	668	11	690	10
CR02_108-	860	32.8	97.2	.		0.06178	0.00093	1.05778	0.02198	0.12418	0.00178	0.688	14.03	1.53	666	32	733	11	755	10
CR02_114-2-	398	27.5	45.1	.		0.06254	0.00079	1.08802	0.02129	0.12617	0.00188	0.763	11.22	.	693	25	748	10	766	11
CR02_28r-	406	55.8	41.6	1.47	993	0.07141	0.00112	1.26493	0.03042	0.12848	0.00235	0.759	-20.79	-5.19	969	31	830	14	779	13
CR02_66r-	16	0.8	1.9	.		0.06172	0.0029	1.09986	0.06681	0.12924	0.00498	0.634	19.01	.	665	98	753	32	784	28
CR02_69-	75	9.2	12.2	.		0.07022	0.00125	1.66432	0.06867	0.17189	0.0064	0.902	10.14	.	935	32	995	26	1023	35
CR02_57-	490	34.1	70.5	2.35	646	0.07454	0.00136	1.53384	0.0572	0.14924	0.00486	0.873	-16.16	.	1056	35	944	23	897	27
CR02-19-	76	9.3	6.3	.		0.07467	0.00207	1.07565	0.04213	0.10448	0.00289	0.707	-41.52	-22.87	1060	54	742	21	641	17
CR02_24-	775	66.7	58	.	1204	0.07484	0.00173	0.97865	0.02863	0.09484	0.00169	0.61	-47.17	-36.1	1064	46	693	15	584	10
CR02_24r-	835	44.1	57.8	.	1065	0.07525	0.0012	0.90913	0.02061	0.08763	0.00141	0.71	-51.72	-44.01	1075	30	657	11	541	8
CR02_40-	71	5.8	7.5	.	570	0.07543	0.00174	1.43617	0.04284	0.13808	0.00262	0.636	-24.3	-8.17	1080	45	904	18	834	15
CR02_39-	150	4.8	18.7	.		0.07555	0.00151	1.69722	0.04705	0.16293	0.00314	0.694	-10.95	.	1083	37	1007	18	973	17
CR02_72-	390	42.7	56	.	1604	0.07645	0.00138	1.51724	0.06836	0.14395	0.00594	0.916	-23.15	.	1107	34	937	28	867	33
CR02_61-	289	32.4	36.4	.	1633	0.0765	0.00133	1.43138	0.05412	0.13571	0.00455	0.887	-27.64	-5.18	1108	34	902	23	820	26
CR02_70-	882	94.3	81.7	.	1095	0.07697	0.00137	1.02623	0.04004	0.0967	0.00336	0.89	-49.05	-32.76	1120	35	717	20	595	20
CR02-21-	201	14.8	22.5	.	2997	0.07735	0.00138	1.48338	0.03717	0.1391	0.00244	0.7	-27.41	-15.16	1130	35	924	15	840	14
CR02_93-	466	72.9	38.8	.	985	0.07736	0.00196	0.98768	0.04024	0.0926	0.00296	0.784	-51.7	-36.25	1131	50	698	21	571	17
CR02_114-	447	38.6	62.2	.	1909	0.07742	0.00175	1.6705	0.05174	0.1565	0.00331	0.682	-18.47	-0.93	1132	43	997	20	937	18
CR02_98-	110	25.8	14.8	.	709	0.07839	0.00136	1.63435	0.06556	0.15121	0.00547	0.902	-23.07	.	1157	32	984	25	908	31
CR02-11-	322	41	26.3	.	986	0.07859	0.00194	1.1083	0.03391	0.10228	0.00184	0.588	-48.2	-37.99	1162	49	757	16	628	11
CR02-14-	887	46.5	74.2	.	760	0.08243	0.00147	1.18948	0.0279	0.10466	0.0016	0.65	-51.33	-44.72	1256	35	796	13	642	9
CR02_115-	88	19.8	11.1	3.07	400	0.08284	0.00638	1.55449	0.12364	0.13609	0.00269	0.248	-37.26	-2.85	1266	142	952	49	823	15
CR02_80-	413	43.9	60.2	.	1681	0.08894	0.00158	2.10831	0.07457	0.17193	0.00526	0.865	-29.28	-13.94	1403	33	1152	24	1023	29
CR02_39-2-	28	2	3.1	.	282	0.09183	0.00583	1.74944	0.1344	0.13816	0.00598	0.563	-45.81	-18.96	1464	113	1027	50	834	34
CR02_81-	201	62.3	22.8	.	478	0.09501	0.00167	1.74157	0.05732	0.13294	0.0037	0.846	-50.31	-41.3	1528	31	1024	21	805	21
CR02_81-2-	28	4.4	1.7	.	179	0.0951	0.00413	0.99885	0.06478	0.07618	0.00367	0.743	-71.56	-60.24	1530	78	703	33	473	22
CR02_82-2-	680	101.9	116.2	.	1168	0.0955	0.00164	2.66078	0.10652	0.20208	0.00731	0.903	-25	-7.3	1538	31	1318	30	1186	39
CR02_93r-	756	229.4	52.6	.	384	0.10372	0.00244	1.12205	0.04432	0.07846	0.00249	0.803	-73.86	-68.74	1692	42	764	21	487	15
CR02_112-	955	205.6	73.1	.	290	0.11146	0.00211	1.29759	0.03225	0.08443	0.00136	0.647	-74.17	-71.67	1823	35	845	14	523	8
CR02_52-	147	18.9	34.8	.		0.11816	0.00202	5.03369	0.13733	0.30898	0.00657	0.779	-11.4	-1.36	1929	31	1825	23	1736	32
CR02_91-	303	24.5	31.2	.	155	0.14372	0.01899	2.31408	0.32597	0.11678	0.00571	0.347	-72.37	-55.66	2272	228	1217	100	712	33
CR02_65-	279	134.4	20.5	.	163	0.16266	0.00557	1.67908	0.09016	0.07487	0.0031	0.771	-84.07	-81	2484	56	1001	34	465	19

Table 9-3 Raw data of concordant and discordant U-Pb analysis of all ablations of sample CR11

Sample	***ppm***					***Ratios***							***U-Pb discordance***		***Ages (Ma)***					
Name	**U**	**Th**	**^{206}Pb**	**^{206}Pb$_c$(%)**	**206/204**	**^{207}Pb/^{206}Pb***	**1SE**	**^{207}Pb/^{235}U***	**1SE**	**^{206}Pb/^{238}U***	**1SE**	**Rho**	**Central (%)**	**Minimum rim (%)**	**207/206**	**1s**	**207/235**	**1s**	**206/238**	**1s**
Discordance < 10 %																				
CR11_03-	256	41.1	11.3	.		0.05241	0.00097	0.3511	0.01377	0.04859	0.00168	0.881	0.81	.	303	40	306	10	306	10
CR11_15-2-	75	7.7	5.8	.		0.05838	0.00175	0.67984	0.036	0.08446	0.00369	0.824	-4.07	.	544	65	527	22	523	22
CR11_20-	130	12.6	9.3	.	974	0.05852	0.00113	0.7104	0.01664	0.08804	0.00116	0.565	-1.04	.	549	40	545	10	544	7
CR11_26-	271	48.6	20.1	.		0.05976	0.00102	0.73982	0.01542	0.08979	0.00107	0.574	-7.09	.	595	37	562	9	554	6
CR11_10-2-	296	22.6	24.9	.		0.05793	0.00112	0.73156	0.0325	0.09159	0.00366	0.9	7.48	.	527	42	557	19	565	22
CR11_24-	975	80.7	74.4	.	6928	0.05863	0.00068	0.74801	0.0121	0.09253	0.00103	0.691	3.2	.	554	24	567	7	570	6
CR11_14-	61	7.5	5.3	.	528	0.05956	0.00204	0.769	0.04134	0.09364	0.00388	0.77	-1.9	.	588	76	579	24	577	23
CR11_11-	202	19.7	17.4	.		0.05945	0.00113	0.76849	0.03485	0.09376	0.00386	0.908	-1.04	.	584	39	579	20	578	23
CR11_21-	243	29.5	28.7	0.11	2585	0.06998	0.00099	1.37729	0.02955	0.14274	0.00231	0.753	-7.79	.	928	29	879	13	860	13
CR11_13-	29	1.6	4.3	.		0.07228	0.0025	1.63278	0.09623	0.16384	0.00782	0.81	-1.69	.	994	64	983	37	978	43
CR11_23-	109	19.2	15.1	.		0.07287	0.00107	1.68225	0.03347	0.16743	0.00224	0.672	-1.32	.	1010	30	1002	13	998	12
CR11_05-	39	7.7	6.2	.	420	0.07576	0.00192	1.83326	0.09462	0.17551	0.00789	0.871	-4.61	.	1089	48	1057	34	1042	43
CR11_17-2-	502	7.6	83.1	.	4585	0.07647	0.00136	1.89139	0.09834	0.17939	0.00876	0.94	-4.29	.	1107	35	1078	35	1064	48
CR11_06-	91	32.2	15.3	.		0.07797	0.00143	1.94891	0.09041	0.1813	0.00773	0.919	-6.81	.	1146	34	1098	31	1074	42
CR11_07-	151	9.9	28.2	.		0.07862	0.00187	2.17127	0.10974	0.2003	0.00894	0.883	1.36	.	1163	46	1172	35	1177	48
CR11_19-	241	34.9	38.3	.		0.08112	0.00113	2.17307	0.04699	0.1943	0.00321	0.765	-7.1	.	1224	26	1172	15	1145	17
CR11_25-	282	18.3	46.3	.		0.08148	0.00109	2.22522	0.04556	0.19806	0.00307	0.756	-6.05	.	1233	26	1189	14	1165	16
CR11_08-	142	30.8	27.9	.	2573	0.08173	0.00154	2.36778	0.11632	0.21012	0.00953	0.924	-0.85	.	1239	36	1233	35	1229	51
CR11_22-	247	59.6	46.3	.		0.08317	0.00104	2.58465	0.04757	0.22539	0.00303	0.732	3.22	.	1273	24	1296	13	1310	16
CR11_27-	229	68.8	41.3	.		0.08338	0.00116	2.46493	0.04708	0.21441	0.00281	0.687	-2.22	.	1278	26	1262	14	1252	15
CR11_12-2-	107	26.2	23.7	.	1606	0.08909	0.00172	2.894	0.15708	0.23559	0.01195	0.935	-3.34	.	1406	35	1380	41	1364	62
CR11_18-	195	51.2	55.2	.		0.1061	0.00218	4.32399	0.27287	0.29557	0.01764	0.945	-4.2	.	1733	35	1698	52	1669	88
CR11_28-	131	32.2	32.1	.		0.10696	0.0016	4.28392	0.09734	0.29048	0.00496	0.752	-6.76	.	1748	28	1690	19	1644	25

Appendix A: Tables of U-Pb data

Sample	*ppm*					*Ratios*							*U-Pb discordance*		*Ages (Ma)*					
Name	**U**	**Th**	**^{206}Pb**	**$^{206}Pb_c$(%)**	**206/204**	**$^{207}Pb/^{206}Pb^*$**	**1SE**	**$^{207}Pb/^{235}U^*$**	**1SE**	**$^{206}Pb/^{238}U^*$**	**1SE**	**Rho**	**Central (%)**	**Minimum rim (%)**	**207/206**	**1s**	**207/235**	**1s**	**206/238**	**1s**
CR11_29-	82	31.5	20.9	.		0.11024	0.00185	4.59529	0.132	0.30234	0.00706	0.813	-6.33	.	1803	29	1748	24	1703	35
CR11_16-	83	6.9	29.6	.		0.1304	0.00347	6.59587	0.48926	0.36686	0.0254	0.934	-4.91	.	2103	44	2059	65	2015	120
CR11_04-	48	7.5	18	.	1689	0.13122	0.00274	6.9651	0.47094	0.38497	0.02476	0.951	-0.83	.	2114	35	2107	60	2099	115
CR11_30-	94	17.8	30.4	.	1609	0.13334	0.00218	6.94356	0.16888	0.37767	0.00679	0.739	-4.2	.	2142	28	2104	22	2065	32
CR11_01-	60	6.7	20.7	.		0.13393	0.00316	6.65273	0.43815	0.36025	0.02215	0.934	-9.01	.	2150	39	2066	58	1983	105
CR11_02-	812	27.3	401	.	29171	0.20094	0.00595	13.87877	1.20842	0.50094	0.04102	0.94	-9.26	.	2834	47	2741	82	2618	176
Rims and doubles																				
CR11_09r-	1031	99.1	34.9	.		0.05042	0.00076	0.25815	0.01015	0.03713	0.00135	0.923	9.73	.	215	34	233	8	235	8
CR11_20-2-	102	10.8	7.1	.		0.05867	0.00125	0.69092	0.01728	0.0854	0.00113	0.527	-5.03	.	555	44	533	10	528	7
CR11_20-3-	213	39.9	15.2	.		0.0583	0.00089	0.70357	0.01394	0.08753	0.0011	0.637	-0.02	.	541	32	541	8	541	7
CR11_26r-	229	50.1	17	.		0.06015	0.00089	0.74491	0.01422	0.08982	0.00109	0.635	-9.34	.	609	32	565	8	554	6
CR11_24-2-	1039	78.2	78.4	.		0.05843	0.00066	0.73759	0.01173	0.09155	0.00102	0.703	3.59	.	546	24	561	7	565	6
CR11_26-2-	491	27.8	38.8	.		0.06049	0.00078	0.7964	0.01419	0.09548	0.00118	0.691	-5.64	.	621	27	595	8	588	7
CR11_14r-	290	5.9	26.6	.	2390	0.05893	0.00178	0.79945	0.04216	0.09839	0.00425	0.82	7.5	.	565	61	597	24	605	25
CR11_23-2-	171	33.9	24.3	.	1850	0.07332	0.00093	1.73174	0.03118	0.17129	0.0022	0.712	-0.39	.	1023	25	1020	12	1019	12
CR11_17-	369	6.3	66.1	.		0.07472	0.00132	1.97759	0.1027	0.19196	0.00937	0.94	7.31	.	1061	35	1108	35	1132	51
CR11_06c-	413	27.6	65.8	.	4137	0.07598	0.00116	1.85155	0.08727	0.17674	0.00788	0.946	-4.5	.	1095	31	1064	31	1049	43
CR11_22r-	350	110.5	64.3	.	3989	0.08401	0.00112	2.55517	0.04812	0.22058	0.00293	0.705	-0.68	.	1293	26	1288	14	1285	15
CR11_12-	93	21.9	22.2	.	2231	0.08938	0.00171	3.13899	0.1743	0.2547	0.01328	0.939	3.98	.	1412	35	1442	43	1463	68
Discordance >10%																				
CR11_09-	874	98.4	29.1	.		0.05157	0.00091	0.26201	0.00965	0.03685	0.00119	0.878	-12.67	.	266	38	236	8	233	7
CR11_15-	63	5.8	4.9	.		0.06087	0.00193	0.70612	0.03652	0.08413	0.00343	0.789	-18.7	.	635	68	542	22	521	20
CR11_10-	274	12.3	22.4	.	1419	0.05717	0.00139	0.7066	0.03369	0.08964	0.00368	0.861	11.55	.	498	52	543	20	553	22
CR11_16r-	127	13.2	10.8	.	838	0.05611	0.00202	0.70254	0.04083	0.09081	0.00415	0.786	23.67	.	457	81	540	24	560	25
CR11_21r-	235	19.8	26	.		0.06975	0.00097	1.29222	0.02283	0.13437	0.00146	0.616	-12.49	-0.48	921	28	842	10	813	8

Appendix A: Tables of U-Pb data

Sample	*ppm*					*Ratios*							*U-Pb discordance*		*Ages (Ma)*					
Name	**U**	**Th**	**^{206}Pb**	**^{206}Pb$_c$(%)**	**206/204**	**^{207}Pb/^{206}Pb***	**1SE**	**^{207}Pb/^{235}U***	**1SE**	**^{206}Pb/^{238}U***	**1SE**	**Rho**	**Central (%)**	**Minimum rim (%)**	**207/206**	**1s**	**207/235**	**1s**	**206/238**	**1s**
CR11_31-	132	12	32.3	.	1271	0.13163	0.00285	5.25313	0.1615	0.28945	0.00631	0.71	-25.66	-17.34	2120	37	1861	26	1639	32

Table 9-4 Raw data of concordant and discordant U-Pb analysis of all ablations of sample CR12

Sample	***ppm***					***Ratios***							***U-Pb discordance***		***Ages (Ma)***					
Name	**U**	**Th**	**^{206}Pb**	**^{206}Pb$_c$(%)**	**206/204**	**^{207}Pb/^{206}Pb***	**1SE**	**^{207}Pb/^{235}U***	**1SE**	**^{206}Pb/^{238}U***	**1SE**	**Rho**	**Central (%)**	**Minimum rim (%)**	**207/206**	**1s**	**207/235**	**1s**	**206/238**	**1s**
Discordance < 10 %																				
CR12_58-	117	25.4	3.8	.	498	0.05047	0.0014	0.24166	0.00854	0.03473	0.00076	0.622	1.57	.	217	62	220	7	220	5
CR12_54-	134	24.8	12.1	.		0.06069	0.00093	0.80586	0.02137	0.09631	0.00208	0.816	-5.91	.	628	30	600	12	593	12
CR12_55-3-	59	9.1	5.8	.	587	0.06006	0.00115	0.88714	0.02598	0.10713	0.00237	0.755	8.74	.	606	41	645	14	656	14
CR12_19-	159	17.1	14.9	.		0.06273	0.00092	0.95	0.01914	0.10984	0.00152	0.688	-4.11	.	699	31	678	10	672	9
CR12_59-	60	4.6	6.1	.	744	0.06196	0.00115	0.94084	0.02785	0.11013	0.00253	0.777	0.11	.	673	38	673	15	673	15
CR12_17-	158	36.5	20.6	0.87	1044	0.06921	0.00117	1.44943	0.04022	0.15188	0.00334	0.792	0.76	.	905	34	910	17	912	19
CR12_24-2-	277	27	37.1	.	3842	0.07147	0.00094	1.5209	0.03026	0.15434	0.0023	0.749	-5.05	.	971	25	939	12	925	13
CR12_57-	165	20	24	.		0.07197	0.00133	1.58258	0.0603	0.15949	0.00532	0.875	-3.39	.	985	37	963	24	954	30
CR12_60-	116	6.7	17.6	.	2338	0.07213	0.00103	1.64083	0.04539	0.16499	0.00391	0.856	-0.56	.	990	27	986	17	984	22
CR12_47c-	116	13.1	18.7	.		0.07237	0.00106	1.71779	0.04679	0.17215	0.00396	0.844	2.99	.	996	29	1015	17	1024	22
CR12_14-	64	15.4	9.4	.	730	0.07308	0.00116	1.72514	0.03778	0.17122	0.00259	0.692	0.29	.	1016	30	1018	14	1019	14
CR12_16-	144	14.3	21.7	.		0.07337	0.00105	1.77697	0.03689	0.17567	0.00263	0.721	2.03	.	1024	27	1037	13	1043	14
CR12_07-	194	26.6	29.4	.	2166	0.07399	0.00104	1.83147	0.03646	0.17953	0.00254	0.71	2.43	.	1041	28	1057	13	1064	14
CR12_34-	137	18.9	21.5	.		0.07525	0.00116	1.84389	0.0399	0.17771	0.00269	0.7	-2.1	.	1075	30	1061	14	1054	15
CR12_08-	191	30.9	27.1	.	2228	0.07528	0.00117	1.79939	0.05791	0.17337	0.00489	0.877	-4.55	.	1076	29	1045	21	1031	27
CR12_18-	224	19.7	34.7	.	3270	0.07546	0.00109	1.89668	0.04119	0.18228	0.00295	0.745	-0.15	.	1081	30	1080	14	1079	16
CR12_56-	19	1.7	3.1	.		0.07554	0.00192	1.84773	0.06471	0.17741	0.00428	0.689	-3.01	.	1083	50	1063	23	1053	23
CR12_29-	89	28.2	15	.		0.07582	0.00138	2.0023	0.05041	0.19152	0.00334	0.693	3.91	.	1090	35	1116	17	1130	18
CR12_39-	205	91.8	33.4	.		0.07611	0.00103	1.93492	0.0488	0.18439	0.00392	0.844	-0.69	.	1098	26	1093	17	1091	21
CR12_02-	173	28.6	28.9	.		0.07642	0.00101	2.09044	0.0428	0.19839	0.00309	0.761	5.98	.	1106	25	1146	14	1167	17
CR12_13-	271	55.1	42.7	.	3595	0.07643	0.00104	1.93581	0.03849	0.18369	0.00266	0.728	-1.9	.	1106	26	1094	13	1087	14
CR12_52-	63	14.9	11.5	.		0.07656	0.00109	2.08624	0.05982	0.19764	0.00491	0.867	5.21	.	1110	28	1144	20	1163	26
CR12_23-	182	19.5	29.3	.	1703	0.07661	0.0011	1.97965	0.04335	0.18742	0.00309	0.753	-0.35	.	1111	27	1109	15	1107	17
CR12_11-	168	20.5	27.2	.	1884	0.07698	0.00099	2.03203	0.04078	0.19145	0.00295	0.769	0.84	.	1121	26	1126	14	1129	16
CR12_04-	252	24.7	41.9	.		0.0771	0.00101	2.10047	0.0422	0.19758	0.00301	0.759	3.74	.	1124	26	1149	14	1162	16

Appendix A: Tables of U-Pb data

Sample	*ppm*					*Ratios*							*U-Pb discordance*		*Ages (Ma)*					
Name	**U**	**Th**	**^{206}Pb**	**^{206}Pb$_c$(%)**	**206/204**	**^{207}Pb/^{206}Pb***	**1SE**	**^{207}Pb/^{235}U***	**1SE**	**^{206}Pb/^{238}U***	**1SE**	**Rho**	**Central (%)**	**Minimum rim (%)**	**207/206**	**1s**	**207/235**	**1s**	**206/238**	**1s**
CR12_12-	238	42.9	41	.		0.07749	0.00103	2.15878	0.04329	0.20204	0.00304	0.751	5.06	.	1134	25	1168	14	1186	16
CR12_45-	248	39	42.2	.		0.07771	0.0011	2.05222	0.04275	0.19154	0.00293	0.735	-0.92	.	1139	28	1133	14	1130	16
CR12_41-	432	19.1	75.4	.		0.07814	0.00098	2.10084	0.04212	0.195	0.00305	0.781	-0.18	.	1150	24	1149	14	1148	16
CR12_06-	237	7.7	36	.		0.07824	0.00166	1.96069	0.05271	0.18176	0.00301	0.616	-7.19	.	1153	41	1102	18	1077	16
CR12_05-	210	20.9	37.1	.		0.07853	0.00098	2.25117	0.04285	0.20792	0.00298	0.754	5.44	.	1160	24	1197	13	1218	16
CR12_31-	368	26.7	66.8	.		0.07954	0.00097	2.24636	0.04502	0.20484	0.00326	0.795	1.46	.	1185	23	1196	14	1201	17
CR12_51-	61	6.7	12.5	.		0.07973	0.00134	2.41194	0.07148	0.2194	0.00535	0.823	8.19	.	1190	32	1246	21	1279	28
CR12_48-	34	13.8	7.1	.		0.0801	0.0016	2.41704	0.07842	0.21886	0.0056	0.789	7.03	.	1199	38	1248	23	1276	30
CR12_09-	131	10.9	23.5	.	1111	0.08045	0.00116	2.34738	0.04804	0.21162	0.00307	0.709	2.67	.	1208	27	1227	15	1237	16
CR12_03-	98	3.3	17.7	.	1789	0.08074	0.0011	2.40029	0.05055	0.2156	0.00346	0.762	3.93	.	1215	26	1243	15	1259	18
CR12_21-	153	23.4	27.4	.	2942	0.08112	0.00126	2.30943	0.04878	0.20648	0.00295	0.677	-1.28	.	1224	30	1215	15	1210	16
CR12_44-	277	33.8	51.2	.	3535	0.08146	0.00114	2.32633	0.0495	0.20712	0.00331	0.752	-1.7	.	1233	27	1220	15	1213	18
CR12_38-	248	18.8	46.8	.		0.08154	0.00109	2.37514	0.04844	0.21125	0.00326	0.757	0.08	.	1235	24	1235	15	1235	17
CR12_33-	81	28	14.6	.		0.08174	0.00125	2.3057	0.04949	0.20458	0.00309	0.704	-3.48	.	1239	29	1214	15	1200	17
CR12_30-	96	10.5	17.9	.	1433	0.08193	0.00126	2.39179	0.05157	0.21174	0.0032	0.701	-0.51	.	1244	28	1240	15	1238	17
CR12_40-	288	116.7	54.8	.	4996	0.08197	0.00121	2.39028	0.05131	0.21149	0.0033	0.728	-0.72	.	1245	28	1240	15	1237	18
CR12_20-	113	20	20.6	.		0.08213	0.00111	2.40396	0.05005	0.21229	0.00336	0.76	-0.67	.	1249	25	1244	15	1241	18
CR12_22-	213	36.2	42.5	.	3873	0.08707	0.00119	2.76844	0.0579	0.23061	0.00365	0.757	-1.98	.	1362	26	1347	16	1338	19
CR12_01-	90	9.5	19.8	.	2218	0.09047	0.00127	3.21826	0.06983	0.25801	0.00427	0.764	3.45	.	1435	26	1462	17	1480	22
CR12_35c-	389	47.3	82.9	.		0.09297	0.00118	3.05908	0.0597	0.23864	0.00355	0.762	-8.04	.	1487	23	1423	15	1380	18
CR12_49-	181	9.5	48.5	.	4944	0.09448	0.00146	3.772	0.12814	0.28957	0.00876	0.89	9.09	.	1518	28	1587	27	1639	44
CR12_32-	375	64.8	84.2	.	6822	0.0957	0.00123	3.31335	0.07554	0.25111	0.00473	0.826	-7.07	.	1542	23	1484	18	1444	24
CR12_26-	125	30.7	37.9	.		0.11332	0.00184	5.32805	0.12974	0.341	0.00617	0.744	2.38	.	1853	28	1873	21	1891	30
CR12_10-	123	27.2	35	.	1900	0.11475	0.00155	5.30384	0.13639	0.33523	0.00734	0.851	-0.75	.	1876	24	1869	22	1864	35
CR12_15-	142	59.3	40	.		0.11486	0.00185	5.13942	0.13306	0.32451	0.00657	0.782	-4.03	.	1878	28	1843	22	1812	32
CR12_37-	80	20.7	24.4	.		0.11532	0.0017	5.37433	0.12545	0.33799	0.00611	0.775	-0.49	.	1885	25	1881	20	1877	29
CR12_42-	131	41.2	40.4	.		0.11645	0.00177	5.41747	0.13322	0.33742	0.00653	0.787	-1.7	.	1902	26	1888	21	1874	31

Appendix A: Tables of U-Pb data

Sample	*ppm*					*Ratios*							*U-Pb discordance*		*Ages (Ma)*					
Name	**U**	**Th**	**^{206}Pb**	**^{206}Pb$_c$(%)**	**206/204**	**^{207}Pb/^{206}Pb***	**1SE**	**^{207}Pb/^{235}U***	**1SE**	**^{206}Pb/^{238}U***	**1SE**	**Rho**	**Central (%)**	**Minimum rim (%)**	**207/206**	**1s**	**207/235**	**1s**	**206/238**	**1s**
CR12_28-	53	9.2	16.6	.		0.1259	0.00225	6.23333	0.22579	0.35909	0.01131	0.87	-3.61	.	2041	30	2009	32	1978	54
CR12_61-	46	10.1	16.7	.		0.13007	0.00207	7.05245	0.25001	0.39323	0.01245	0.893	2.18	.	2099	27	2118	32	2138	58
Rims and doubles																				
CR12_19-2-	164	19.7	15.1	.	1235	0.06005	0.00107	0.88653	0.02066	0.10708	0.0016	0.641	8.78	.	605	38	645	11	656	9
CR12_47r-	118	1.4	12.5	.	1582	0.06348	0.00123	0.99731	0.03554	0.11395	0.00341	0.84	-4.19	.	724	40	702	18	696	20
CR12_18-2-	144	9.8	21.9	.		0.07464	0.00124	1.82799	0.04132	0.17762	0.00273	0.68	-0.5	.	1059	33	1056	15	1054	15
CR12_34-4-	253	27.8	41.3	.		0.07463	0.00098	1.89974	0.03831	0.18462	0.00283	0.76	3.46	.	1059	25	1081	13	1092	15
CR12_34-3-	160	17.1	25.7	.		0.07491	0.00109	1.87405	0.03919	0.18143	0.00272	0.716	0.87	.	1066	29	1072	14	1075	15
CR12_23-2-	155	10.2	24.6	.	2096	0.07588	0.00113	1.93535	0.04057	0.18498	0.00272	0.703	0.23	.	1092	28	1093	14	1094	15
CR12_48r-	52	18.6	10.8	.	1066	0.08041	0.00132	2.44776	0.0729	0.22077	0.00548	0.833	7.21	.	1207	31	1257	21	1286	29
CR12_32r-	209	18	45.2	.	4037	0.09312	0.00121	3.13234	0.06907	0.24396	0.00435	0.808	-6.21	.	1490	23	1441	17	1407	23
CR12_49-2-	198	9.3	50.6	.		0.09325	0.00115	3.55463	0.11321	0.27647	0.00812	0.922	6.08	.	1493	21	1539	25	1574	41
CR12_28-2-	54	14.9	17.9	.		0.12853	0.00218	6.63167	0.17123	0.37422	0.00728	0.754	-1.61	.	2078	29	2064	23	2049	34
Discordance > 10 %																				
CR12_53-	190	24.3	6.2	.	374	0.06817	0.00392	0.33019	0.0206	0.03513	0.00085	0.386	-75.79	-57.98	874	111	290	16	223	5
CR12_43-2-	176	44.5	6.4	.	650	0.05542	0.00126	0.32069	0.00879	0.04197	0.00065	0.561	-39.03	.	429	49	282	7	265	4
CR12_43-	160	47	6.1	.		0.05322	0.00126	0.31823	0.00895	0.04337	0.00066	0.541	-19.44	.	338	50	281	7	274	4
CR12_25-	175	22.9	6.6	.		0.05329	0.00106	0.31988	0.00776	0.04353	0.0006	0.567	-19.93	.	341	43	282	6	275	4
CR12_55-	37	9.2	3.7	.		0.05963	0.00155	0.88582	0.03123	0.10774	0.00257	0.677	12.39	.	590	54	644	17	660	15
CR12_55-2-	36	8.1	3.6	.	476	0.06596	0.00425	0.9835	0.06868	0.10815	0.00291	0.386	-18.7	.	805	133	695	35	662	17
CR12_24-	313	19.6	35.6	.		0.06858	0.00086	1.24486	0.02735	0.13164	0.00237	0.82	-10.67	.	886	25	821	12	797	14
CR12_50-	89	6	17.4	.	1502	0.07642	0.00108	2.20241	0.06272	0.20901	0.00517	0.869	11.65	.	1106	28	1182	20	1224	28
CR12_27-	757	70.3	100.6	.	5500	0.07649	0.00092	1.59851	0.02905	0.15157	0.00207	0.752	-19.16	-9.31	1108	23	970	11	910	12
CR12_46-	63	27	10.8	.	930	0.08562	0.00324	2.23415	0.09173	0.18925	0.00301	0.388	-17.39	.	1330	69	1192	29	1117	16
CR12_35-	429	45.3	82.7	.		0.09024	0.00117	2.69421	0.05575	0.21653	0.00349	0.778	-12.86	-3.36	1431	24	1327	15	1263	18

Appendix A: Tables of U-Pb data

Table 9-5 Raw data of concordant and discordant U-Pb analysis of all ablations of sample CR06

Sample	***ppm***					***Ratios***							***U-Pb discordance***		***Ages (Ma)***					
Name	**U**	**Th**	**^{206}Pb**	**^{206}Pb$_c$(%)**	**206/204**	**^{207}Pb/^{206}Pb***	**1SE**	**^{207}Pb/^{235}U***	**1SE**	**^{206}Pb/^{238}U***	**1SE**	**Rho**	**Central (%)**	**Minimum rim (%)**	**207/206**	**1s**	**207/235**	**1s**	**206/238**	**1s**
Discordance < 10 %																				
CR06-01-3-	261	9.7	8.4	.		0.05155	0.00101	0.27775	0.00722	0.03908	0.00067	0.66	-7.08	.	266	45	249	6	247	4
CR06-08-	314	8.1	26.3	.		0.06104	0.00085	0.86071	0.01796	0.10227	0.00159	0.747	-2.11	.	641	27	631	10	628	9
CR06-05-	190	13.2	38	.		0.08614	0.00121	2.88331	0.0663	0.24276	0.00443	0.793	4.95	.	1341	26	1378	17	1401	23
CR06-03-	118	13.8	30.6	.	2059	0.10849	0.00233	4.65504	0.1506	0.31119	0.00754	0.749	-1.78	.	1774	37	1759	27	1747	37
CR06-07-	126	13.4	37	.		0.11754	0.00181	5.73906	0.15609	0.35411	0.00795	0.825	2.11	.	1919	27	1937	24	1954	38
CR06-04-	218	18	66.6	.		0.12019	0.002	6.06745	0.16551	0.36612	0.00791	0.792	3.09	.	1959	29	1986	24	2011	37
Rims and doubles																				
CR06-04r	100	5.3	24.3	.		0.06323	0.00127	0.92235	0.02765	0.1058	0.00236	0.744	-9.91	.	716	41	664	15	648	14
CR06-08-2-	111	3.1	9.4	.		0.10674	0.00179	4.36679	0.13113	0.29672	0.0074	0.83	-4.52	.	1744	31	1706	25	1675	37
Discordance > 10 %																				
CR06-01-4-	381	12.5	12	.	916	0.05249	0.00112	0.2787	0.00769	0.03851	0.00067	0.63	-21	.	307	47	250	6	244	4
CR06-01-	415	15.7	13.3	.	1764	0.05239	0.00098	0.28097	0.00684	0.0389	0.00061	0.642	-18.99	.	302	43	251	5	246	4
CR06-01-2-	275	9.9	9.4	.	1086	0.06149	0.00164	0.35578	0.01233	0.04196	0.00093	0.64	-60.85	-40.88	656	56	309	9	265	6
CR06-10-	206	20.8	14.5	.	1390	0.06407	0.0023	0.78274	0.03194	0.0886	0.00171	0.473	-27.57	.	744	74	587	18	547	10
CR06-06-	316	7.2	26.7	.	1115	0.06559	0.00102	0.93609	0.02143	0.10351	0.00175	0.736	-20.95	-2.46	793	33	671	11	635	10
CR06-02-	148	20.3	37.2	.	3062	0.12472	0.00237	5.24524	0.18659	0.30503	0.00917	0.845	-17.34	-4.63	2025	32	1860	30	1716	45
CR06-02-2-	133	20.8	44.2	.	392	0.16117	0.00952	8.86192	0.5743	0.3988	0.01062	0.411	-14.5	.	2468	97	2324	59	2163	49
CR06-09-	57	3.7	4.8	.	45	0.30495	0.01359	4.48298	0.21677	0.10662	0.002	0.389	-85.19	-83.83	3496	71	1728	40	653	12

Appendix A: Tables of U-Pb data

Table 9-6 Raw data of concordant and discordant U-Pb analysis of all ablations of sample CR07

Sample	***ppm***					***Ratios***							***U-Pb discordance***		***Ages (Ma)***					
Name	**U**	**Th**	**^{206}Pb**	**^{206}Pb$_c$(%)**	**206/204**	**^{207}Pb/^{206}Pb***	**1SE**	**^{207}Pb/^{235}U***	**1SE**	**^{206}Pb/^{238}U***	**1SE**	**Rho**	**Central (%)**	**Minimum rim (%)**	**207/206**	**1s**	**207/235**	**1s**	**206/238**	**1s**
Discordance < 10 %																				
CR07_09-2-	105	29.2	6.6	.		0.0583	0.00122	0.69769	0.02084	0.08679	0.00184	0.711	-0.9	.	541	45	537	12	537	11
CR07_17	208	90.7	15.3	.		0.05848	0.00085	0.70866	0.01402	0.08789	0.00118	0.679	-0.93	.	548	30	544	8	543	7
CR07_08-2-	189	29.4	12.5	.		0.05945	0.00108	0.73403	0.02051	0.08954	0.00191	0.762	-5.53	.	584	39	559	12	553	11
CR07_07-2-	12	5.5	0.9	.		0.06199	0.00345	0.86051	0.05518	0.10067	0.00321	0.497	-8.63	.	674	120	630	30	618	19
CR07_03-	107	16.5	8	.		0.06029	0.00102	0.83837	0.02533	0.10086	0.00253	0.829	0.96	.	614	34	618	14	619	15
CR07_06-2-	207	11.3	19.4	.		0.06586	0.00107	1.14705	0.03061	0.12632	0.00268	0.795	-4.64	.	802	33	776	14	767	15
CR07_02-	83	11.1	10	.	1152	0.07084	0.0014	1.55955	0.05246	0.15967	0.00435	0.81	0.25	.	953	40	954	21	955	24
CR07_16-	121	12.9	16.2	.		0.07336	0.00109	1.60812	0.03604	0.15898	0.00267	0.749	-7.65	.	1024	29	973	14	951	15
CR07_14-	99	15.5	18.1	.		0.08158	0.00117	2.38994	0.05049	0.21248	0.0033	0.734	0.59	.	1235	27	1240	15	1242	18
CR07_04-	38	8	6.7	.		0.08571	0.0017	2.74723	0.09331	0.23248	0.00641	0.812	1.32	.	1332	36	1341	25	1347	34
CR07_15-	236	88.7	59.1	.	4265	0.10918	0.00142	4.37824	0.09048	0.29084	0.00467	0.777	-8.88	-0.71	1786	23	1708	17	1646	23
CR07_13-	29	11.2	7.7	.		0.1118	0.00217	4.748	0.12262	0.30802	0.00524	0.659	-6.1	.	1829	34	1776	22	1731	26
CR07_01-	122	11.6	32.9	.		0.12065	0.00179	5.84765	0.19051	0.35152	0.01019	0.89	-1.41	.	1966	24	1954	28	1942	49
Rims and doubles																				
CR07_06r	122	5.3	9.6	.		0.06247	0.00128	0.91765	0.0281	0.10655	0.00242	0.742	-5.7	.	690	43	661	15	653	14
CR07_04-2-	65	9.9	10.5	.	1039	0.08329	0.0016	2.45173	0.08737	0.21348	0.00641	0.843	-2.48	.	1276	36	1258	26	1247	34
CR07_14-2-	193	37.7	34.8	.	3656	0.08331	0.00097	2.41029	0.04562	0.20983	0.00312	0.786	-4.18	.	1277	22	1246	14	1228	17
CR07_13-2-	41	18.5	10.8	.		0.11349	0.00194	4.84196	0.11868	0.30942	0.00544	0.717	-7.26	.	1856	30	1792	21	1738	27
Discordance > 10 %																				
CR07_10-	68	23.5	2.3	.	197	0.05729	0.00254	0.32455	0.01517	0.04109	0.00061	0.32	-49.33	.	503	96	285	12	260	4
CR07_11-2-	19	6.5	1.2	.	104	0.0626	0.00324	0.67419	0.0377	0.07811	0.00166	0.38	-31.35	.	695	109	523	23	485	10
CR07_11-	27	11.2	1.8	.		0.06168	0.00195	0.67885	0.02433	0.07983	0.00136	0.474	-26.29	.	663	67	526	15	495	8
CR07_07-	20	3.7	1.3	.		0.06209	0.00202	0.77602	0.03042	0.09065	0.00199	0.56	-18.15	.	677	67	583	17	559	12

Appendix A: Tables of U-Pb data

Sample	*ppm*					*Ratios*							*U-Pb discordance*		*Ages (Ma)*					
Name	**U**	**Th**	**^{206}Pb**	**$^{206}Pb_c$(%)**	**206/204**	**$^{207}Pb/^{206}Pb^*$**	**1SE**	**$^{207}Pb/^{235}U^*$**	**1SE**	**$^{206}Pb/^{238}U^*$**	**1SE**	**Rho**	**Central (%)**	**Minimum rim (%)**	**207/206**	**1s**	**207/235**	**1s**	**206/238**	**1s**
CR07_09-	40	6	2.7	.		0.05521	0.00214	0.69891	0.04452	0.09182	0.00465	0.794	36.2	.	421	86	538	27	566	27
CR07_08-	162	29.2	10.9	.		0.06191	0.00104	0.7837	0.02121	0.09181	0.00194	0.782	-16.31	.	671	35	588	12	566	11
CR07_06-	353	9.1	28.1	.		0.06357	0.00096	0.94118	0.02417	0.10738	0.00223	0.808	-10.09	.	727	31	673	13	658	13
CR07_12-2-	543	22.8	71.3	.		0.07538	0.00082	1.65322	0.03744	0.15907	0.00316	0.878	-12.66	.	1079	21	991	14	952	18
CR07_12-	99	23.2	14.9	.		0.07909	0.00139	1.96127	0.04505	0.17984	0.00266	0.643	-10.01	.	1174	34	1102	15	1066	15
CR07_05-	196	38.5	34.3	.	3851	0.10837	0.00169	3.48414	0.10494	0.23317	0.00601	0.856	-26.31	-15.64	1772	27	1524	24	1351	31
CR07_05-2-	227	49.8	46	.	4334	0.10842	0.00143	3.52507	0.07828	0.2358	0.00421	0.804	-25.52	-18.09	1773	24	1533	18	1365	22

Table 9-7 Raw data of concordant and discordant U-Pb analysis of all ablations of sample CR13

Sample	***ppm***					***Ratios***							***U-Pb discordance***		***Ages (Ma)***					
Name	**U**	**Th**	**^{206}Pb**	**^{206}Pb$_c$(%)**	**206/204**	**^{207}Pb/^{206}Pb***	**1SE**	**^{207}Pb/^{235}U***	**1SE**	**^{206}Pb/^{238}U***	**1SE**	**Rho**	**Central (%)**	**Minimum rim (%)**	**207/206**	**1s**	**207/235**	**1s**	**206/238**	**1s**
Discordance < 10 %																				
CR13_33-	619	212.9	39.4	.	2117	0.05708	0.00145	0.63301	0.02075	0.08043	0.00166	0.631	0.82	.	495	53	498	13	499	10
CR13_24-	178	26.8	12.7	.	709	0.05932	0.00185	0.73085	0.02696	0.08935	0.00177	0.537	-4.93	.	579	67	557	16	552	10
CR13_11-	484	37.1	35.7	.	1636	0.05931	0.00117	0.74453	0.0204	0.09105	0.00173	0.692	-2.99	.	578	42	565	12	562	10
CR13_30-	283	40.9	22.8	.	1320	0.06107	0.00146	0.85891	0.02842	0.102	0.00233	0.691	-2.55	.	642	50	630	16	626	14
CR13_39-	282	45.6	26.2	.	1771	0.06306	0.00178	1.02823	0.03602	0.11827	0.00244	0.589	1.56	.	710	58	718	18	721	14
CR13_32-	47	4.2	5	.		0.06747	0.00192	1.26403	0.0449	0.13588	0.0029	0.6	-3.87	.	852	56	830	20	821	16
CR13_07-	129	23.6	15	.		0.0687	0.00161	1.33065	0.04107	0.14048	0.00281	0.649	-5.08	.	890	46	859	18	847	16
CR13_02-	227	23.2	26.8	.	1105	0.06927	0.00126	1.36936	0.04003	0.14337	0.00328	0.782	-5.09	.	907	38	876	17	864	18
CR13_34-	176	22.1	20.5	.	1250	0.07135	0.00168	1.47193	0.05048	0.14963	0.00374	0.728	-7.58	.	967	47	919	21	899	21
CR13_44-	45	16.5	7	.		0.07242	0.0024	1.62824	0.07903	0.16307	0.00579	0.732	-2.58	.	998	64	981	31	974	32
CR13_40-	392	12.5	50.9	.	3429	0.07136	0.00167	1.62861	0.0521	0.16553	0.0036	0.68	2.2	.	968	45	981	20	987	20
CR13_19-	119	14	17.2	.	565	0.07364	0.00182	1.83326	0.06646	0.18055	0.00478	0.731	4.03	.	1032	48	1057	24	1070	26
CR13_35-	313	26.8	42.3	.	2607	0.07376	0.00157	1.7626	0.05371	0.17332	0.00378	0.716	-0.47	.	1035	41	1032	20	1030	21
CR13_22-	784	134.9	106.1	.		0.07544	0.00149	1.74416	0.05464	0.16768	0.00408	0.777	-8.09	.	1080	39	1025	20	999	23
CR13_37-	95	8.9	14.1	.		0.07613	0.00189	1.96187	0.06838	0.1869	0.00458	0.704	0.6	.	1098	48	1103	23	1105	25
CR13_17-	126	20.7	19.1	.	1048	0.07623	0.00155	1.94899	0.05789	0.18544	0.00401	0.727	-0.43	.	1101	39	1098	20	1097	22
CR13_20-	217	31.2	31.3	.	1603	0.07653	0.00162	1.93983	0.07452	0.18384	0.0059	0.835	-2.06	.	1109	41	1095	26	1088	32
CR13_46-	286	49.8	51.1	.		0.07784	0.00173	1.96701	0.0784	0.18328	0.00607	0.831	-5.5	.	1143	42	1104	27	1085	33
CR13_48-	106	17.1	20.4	.		0.07852	0.00167	2.15814	0.09009	0.19935	0.00716	0.86	1.11	.	1160	41	1168	29	1172	38
CR13_47-	123	52.7	24.7	.		0.07996	0.00207	2.25218	0.09721	0.20428	0.00705	0.799	0.21	.	1196	52	1197	30	1198	38
CR13_15-	183	39.9	32.2	.		0.08034	0.00168	2.40306	0.0755	0.21693	0.00509	0.747	5.5	.	1205	40	1244	23	1266	27
CR13_13-	350	31.4	56.7	.	4173	0.08155	0.00162	2.24542	0.0667	0.1997	0.00442	0.744	-5.4	.	1235	37	1195	21	1174	24
CR13_31-	111	25.6	19.3	.	1016	0.08298	0.0022	2.51989	0.08926	0.22025	0.00516	0.662	1.26	.	1269	52	1278	26	1283	27
CR13_12-	190	5.1	51.7	.	3663	0.11105	0.00237	5.22369	0.20307	0.34115	0.01109	0.836	4.8	.	1817	38	1856	33	1892	53
CR13_28-	214	54.3	59.8	.	1572	0.11774	0.00347	5.61775	0.25416	0.34605	0.01187	0.758	-0.39	.	1922	51	1919	39	1916	57

Appendix A: Tables of U-Pb data

Sample	***ppm***					***Ratios***							***U-Pb discordance***		***Ages (Ma)***					
Name	**U**	**Th**	**^{206}Pb**	**^{206}Pb$_c$(%)**	**206/204**	**^{207}Pb/^{206}Pb***	**1SE**	**^{207}Pb/^{235}U***	**1SE**	**^{206}Pb/^{238}U***	**1SE**	**Rho**	**Central (%)**	**Minimum rim (%)**	**207/206**	**1s**	**207/235**	**1s**	**206/238**	**1s**
CR13_01-	223	38.8	70.3	.		0.12502	0.0028	6.23307	0.21648	0.3616	0.00959	0.764	-2.25	.	2029	37	2009	30	1990	45
CR13_05-	205	42.8	63.3	.	1448	0.13035	0.00353	6.43453	0.25314	0.35802	0.01021	0.725	-7.17	.	2103	46	2037	35	1973	48
CR13_21-	232	38.3	71.6	.	3309	0.13458	0.00349	6.80907	0.25559	0.36696	0.00996	0.723	-7.73	.	2159	45	2087	33	2015	47
CR13_16-	100	28.3	32.4	.	638	0.13566	0.00512	7.00245	0.32789	0.37435	0.01037	0.592	-6.59	.	2173	64	2112	42	2050	49
Rims and doubles																				
CR13_02-2-	314	21.8	32.4	.		0.06615	0.0013	1.23722	0.05081	0.13565	0.00489	0.877	1.17	.	811	40	818	23	820	28
CR13_32-2-	52	4.8	5.9	.		0.06769	0.00229	1.33476	0.05495	0.14301	0.00335	0.57	0.32	.	859	66	861	24	862	19
CR13_31r-	739	59.2	112.4	.	4935	0.08126	0.00174	2.15542	0.06604	0.19237	0.0042	0.713	-8.31	.	1228	42	1167	21	1134	23
Discordance > 10 %																				
CR13_10-	598	81.4	19.9	.	1074	0.0559	0.00151	0.32553	0.01169	0.04223	0.001	0.662	-41.39	.	449	57	286	9	267	6
CR13_42-	325	50.9	11.1	.		0.05421	0.00155	0.33225	0.01199	0.04445	0.00098	0.611	-26.79	.	380	62	291	9	280	6
CR13_42-2-	364	46	12.3	.		0.05759	0.00171	0.35706	0.01303	0.04497	0.00095	0.578	-45.83	-2.12	514	62	310	10	284	6
CR13_23-	275	16.2	10.7	.	528	0.05879	0.00157	0.40023	0.01605	0.04937	0.00148	0.748	-45.53	.	559	58	342	12	311	9
CR13_45-	750	84.9	48.9	.		0.05687	0.00142	0.53505	0.02089	0.06824	0.00205	0.769	-12.96	.	487	54	435	14	426	12
CR13_03-	805	93.3	68.2	.	2164	0.06564	0.00176	0.92349	0.03784	0.10204	0.00317	0.757	-22.24	.	795	54	664	20	626	19
CR13_36-	104	15.4	8.7	.	327	0.05834	0.00147	0.8518	0.02936	0.10589	0.0025	0.685	20.59	.	543	52	626	16	649	15
CR13_27-	540	41.1	50.6	0.33	2138	0.06708	0.00141	1.11814	0.04188	0.12089	0.00375	0.829	-13.18	.	840	42	762	20	736	22
CR13_07-3-	90	9.5	9.5	.		0.06767	0.00201	1.18253	0.04304	0.12673	0.00265	0.575	-11.05	.	859	61	792	20	769	15
CR13_43-	97	17.2	11.5	.	675	0.07639	0.00217	1.67101	0.07103	0.15864	0.00502	0.744	-15.19	.	1105	57	998	27	949	28
CR13_14-	1285	148	166.5	.		0.07772	0.00153	1.7082	0.04915	0.15941	0.00335	0.73	-17.57	-1.14	1140	39	1012	18	953	19
CR13_49-	576	168.7	86.7	.	2688	0.07872	0.0016	1.67396	0.06702	0.15424	0.00532	0.862	-22.13	.	1165	39	999	25	925	30
CR13_38-	295	97.4	8.8	.	400	0.07904	0.00306	0.42662	0.01928	0.03915	0.00091	0.514	-80.39	-74.33	1173	77	361	14	248	6
CR13_18-	389	16.6	39.3	.	1919	0.07913	0.00173	1.37483	0.04663	0.12601	0.00327	0.765	-37	-21.96	1175	42	878	20	765	19
CR13_38-2-	327	105	10.1	.	247	0.07941	0.00403	0.44618	0.02487	0.04075	0.00094	0.413	-79.76	-71.91	1182	95	375	17	257	6
CR13_41-	181	17.9	32.8	.	2185	0.09713	0.00233	3.14237	0.11916	0.23464	0.00689	0.774	-14.9	.	1570	44	1443	29	1359	36

Appendix A: Tables of U-Pb data

Sample	***ppm***					***Ratios***							***U-Pb discordance***		***Ages (Ma)***					
Name	**U**	**Th**	**^{206}Pb**	**^{206}Pb$_c$(%)**	**206/204**	**^{207}Pb/^{206}Pb***	**1SE**	**^{207}Pb/^{235}U***	**1SE**	**^{206}Pb/^{238}U***	**1SE**	**Rho**	**Central (%)**	**Minimum rim (%)**	**207/206**	**1s**	**207/235**	**1s**	**206/238**	**1s**
CR13_09-	583	82.7	90	.		0.11404	0.00327	2.89823	0.13038	0.18432	0.00638	0.77	-45.05	-34.01	1865	50	1381	34	1091	35
CR13_08-	228	12.7	39.7	.	2164	0.11415	0.00373	3.37802	0.16046	0.21462	0.00741	0.726	-36.09	-22.93	1867	62	1499	37	1253	39
CR13_35r-	188	12.6	6.8	.	197	0.12274	0.00806	0.91019	0.08986	0.05378	0.00396	0.746	-85.18	-77.55	1996	113	657	48	338	24
CR13_29-	389	19.6	96.9	.	1540	0.12913	0.00467	5.34227	0.23297	0.30005	0.00731	0.559	-21.48	-9.59	2086	61	1876	37	1692	36
CR13_25-	380	158.2	90	.	866	0.12972	0.01032	5.19558	0.43847	0.29049	0.00817	0.333	-24.32	-1.34	2094	140	1852	72	1644	41
CR13_26-	100	22.1	7.4	.	218	0.13083	0.00526	1.72645	0.08032	0.0957	0.00225	0.504	-75.27	-71.38	2109	69	1018	30	589	13
CR13_04-	198	49.4	46.9	.	1391	0.13776	0.00357	6.03056	0.32934	0.31749	0.01526	0.88	-21.91	-3.3	2199	44	1980	48	1777	75
CR13_06-	78	12.6	24.5	.	617	0.14258	0.004	7.16572	0.28335	0.3645	0.01017	0.706	-13.14	-1.08	2259	48	2132	35	2003	48
CR13_07-2-	99	14.8	22.9	.	34	0.46589	0.03631	17.37789	1.57361	0.27053	0.01247	0.509	-69.93	-64.58	4137	117	2956	87	1543	63

Appendix A: Tables of U-Pb data

*Table 9-**Feil! Det er ingen tekst med den angitte stilen i dokumentet.**8 Raw data of concordant and discordant U-Pb analysis of all ablations of sample CR34*

Sample	***ppm***					***Ratios***							***U-Pb discordance***		***Ages (Ma)***					
Name	**U**	**Th**	**^{206}Pb**	**^{206}Pb$_c$(%)**	**206/204**	**^{207}Pb/^{206}Pb***	**1SE**	**^{207}Pb/^{235}U***	**1SE**	**^{206}Pb/^{238}U***	**1SE**	**Rho**	**Central (%)**	**Minimum rim (%)**	**207/206**	**1s**	**207/235**	**1s**	**206/238**	**1s**
Discordance < 10 %																				
CR34_23-	513	48.5	39.6	.	3661	0.06355	0.00076	1.0408	0.01941	0.11878	0.0017	0.768	-0.48	.	727	24	724	10	724	10
CR34_07-	93	6.9	9.8	.		0.0707	0.00116	1.62323	0.03688	0.16653	0.00261	0.691	5.04	.	949	33	979	14	993	14
CR34_43-	170	15	21.2	.		0.07157	0.0008	1.64595	0.04184	0.16679	0.00381	0.898	2.29	.	974	22	988	16	994	21
CR34-71-	73	3.8	6.8	.		0.07215	0.00169	1.69798	0.04888	0.17068	0.00287	0.584	2.79	.	990	48	1008	18	1016	16
CR34_33-	157	27	21.3	.		0.07164	0.00098	1.74217	0.04391	0.17638	0.00373	0.838	7.94	.	976	27	1024	16	1047	20
CR34_40-	385	25.2	50.5	.	6188	0.07257	0.00077	1.73349	0.04172	0.17325	0.00374	0.897	3.03	.	1002	21	1021	15	1030	21
CR34_14-	256	17.6	28.8	.	2773	0.07269	0.00087	1.76692	0.03815	0.17629	0.00317	0.833	4.45	.	1005	24	1033	14	1047	17
CR34_22-	54	5.8	5.6	.	671	0.07288	0.00115	1.6212	0.04704	0.16132	0.00393	0.839	-4.96	.	1011	32	978	18	964	22
CR34_36-	156	16.5	21.3	.		0.07329	0.00096	1.81029	0.04698	0.17915	0.00401	0.862	4.29	.	1022	26	1049	17	1062	22
CR34_48-	94	7.7	12.3	.		0.07342	0.00117	1.76251	0.05065	0.17409	0.00416	0.831	0.94	.	1026	32	1032	19	1035	23
CR34_49-	155	36.5	20	.	1454	0.07368	0.00102	1.75619	0.04976	0.17288	0.00428	0.873	-0.49	.	1033	28	1029	18	1028	24
CR34_42-	144	19.4	18	.		0.07392	0.00101	1.72621	0.05139	0.16937	0.00448	0.889	-3.18	.	1039	25	1018	19	1009	25
CR34-52-	139	4.2	12.8	.		0.07412	0.00137	1.68321	0.04098	0.16469	0.0026	0.648	-6.4	.	1045	35	1002	16	983	14
CR34-73-	126	6.4	12.5	.		0.07427	0.00122	1.97177	0.04302	0.19254	0.00276	0.657	8.96	0.23	1049	32	1106	15	1135	15
CR34-74-	121	6.7	12.6	.		0.075	0.00135	2.04488	0.04671	0.19775	0.00277	0.612	9.7	1.25	1068	34	1131	16	1163	15
CR34_26-	104	8.4	12.6	.		0.07699	0.0012	1.97739	0.04584	0.18627	0.0032	0.742	-1.93	.	1121	30	1108	16	1101	17
CR34_13-	206	18.2	25.8	.	2786	0.07737	0.00091	2.09962	0.04355	0.19682	0.00337	0.825	2.66	.	1131	23	1149	14	1158	18
CR34-60-	61	6.3	6	.	706	0.07738	0.00163	1.91258	0.05319	0.17927	0.00326	0.654	-6.52	.	1131	41	1085	19	1063	18
CR34_34-	65	8.3	9.6	.	909	0.07747	0.00132	2.06531	0.06655	0.19335	0.00529	0.849	0.6	.	1133	33	1137	22	1140	29
CR34-75-	91	6.5	9.4	.	1182	0.07752	0.00134	2.05919	0.04733	0.19266	0.00292	0.66	0.12	.	1135	34	1135	16	1136	16
CR34_04-	181	18.4	22.3	.	2138	0.07763	0.00086	2.05207	0.04222	0.19171	0.00332	0.841	-0.66	.	1138	22	1133	14	1131	18
CR34_31-	96	18.9	14.8	.		0.07823	0.00104	2.16405	0.05607	0.20062	0.00447	0.859	2.46	.	1153	25	1170	18	1179	24
CR34_45-	244	27	34.9	.		0.07846	0.00106	2.04793	0.05229	0.1893	0.0041	0.848	-3.85	.	1159	26	1132	17	1118	22
CR34_50-	123	33	17.3	.		0.07857	0.00111	2.04821	0.05723	0.18907	0.00456	0.864	-4.22	.	1161	26	1132	19	1116	25
CR34-70-	308	73.1	30.9	.	2131	0.07946	0.00115	2.01781	0.0548	0.18417	0.00423	0.845	-8.63	.	1184	27	1122	18	1090	23

Appendix A: Tables of U-Pb data

Sample	*ppm*					*Ratios*							*U-Pb discordance*		*Ages (Ma)*					
Name	**U**	**Th**	**^{206}Pb**	**^{206}Pb$_c$(%)**	**206/204**	**^{207}Pb/^{206}Pb***	**1SE**	**^{207}Pb/^{235}U***	**1SE**	**^{206}Pb/^{238}U***	**1SE**	**Rho**	**Central (%)**	**Minimum rim (%)**	**207/206**	**1s**	**207/235**	**1s**	**206/238**	**1s**
CR34_19-	79	13	9.8	.	1219	0.07951	0.00118	2.09686	0.05078	0.19128	0.00366	0.791	-5.2	.	1185	29	1148	17	1128	20
CR34-56-	392	16.9	41.7	.		0.08046	0.00101	2.15629	0.04041	0.19436	0.00271	0.743	-5.73	.	1208	24	1167	13	1145	15
CR34-64-	165	5.8	17.2	.		0.08048	0.00131	2.08277	0.0524	0.18769	0.0036	0.763	-9	.	1209	31	1143	17	1109	20
CR34-63-	89	2.2	10.1	.		0.08077	0.00155	2.29337	0.05806	0.20593	0.00339	0.65	-0.79	.	1216	37	1210	18	1207	18
CR34-61-	16	0.9	1.8	.		0.08118	0.00253	2.21134	0.08656	0.19756	0.00469	0.606	-5.68	.	1226	58	1185	27	1162	25
CR34_09-	118	14.9	15.9	.		0.08148	0.00102	2.37746	0.04643	0.21162	0.00318	0.769	0.39	.	1233	24	1236	14	1237	17
CR34_10-	465	19	65.4	.		0.08169	0.00074	2.47381	0.04399	0.21962	0.00336	0.859	3.71	.	1238	18	1264	13	1280	18
CR34-68-	112	5.5	14.3	.		0.0832	0.00172	2.54728	0.07278	0.22204	0.00437	0.689	1.61	.	1274	39	1286	21	1293	23
CR34-55-	238	19.3	28.3	.	3693	0.08436	0.00122	2.53479	0.05367	0.21792	0.00337	0.731	-2.54	.	1301	27	1282	15	1271	18
CR34_32-	87	21.1	15.3	.	1790	0.08579	0.00101	2.68515	0.0705	0.227	0.00532	0.893	-1.22	.	1334	22	1324	19	1319	28
CR34_38-2-	100	12.2	18.7	.		0.08729	0.00111	2.93862	0.07933	0.24416	0.00582	0.883	3.37	.	1367	25	1392	20	1408	30
CR34_25-	47	4.5	7.2	.	727	0.08902	0.00132	2.90524	0.07442	0.23669	0.00494	0.815	-2.78	.	1405	28	1383	19	1369	26
CR34_18-	96	11.8	14.9	.		0.08945	0.00153	2.94863	0.07316	0.23907	0.0043	0.725	-2.51	.	1414	32	1394	19	1382	22
CR34_17-	189	11.8	31.2	.		0.09135	0.00104	3.23838	0.06493	0.25711	0.00424	0.823	1.62	.	1454	20	1466	16	1475	22
CR34_30-	98	9.3	20.6	.	2242	0.09661	0.00125	3.58266	0.09819	0.26895	0.00649	0.881	-1.75	.	1560	23	1546	22	1535	33
CR34_28-	168	38.4	37.1	.	2543	0.09682	0.00116	3.76793	0.10406	0.28225	0.00703	0.901	2.81	.	1564	22	1586	22	1603	35
CR34_03-	97	15.4	18	.		0.09944	0.0012	4.11883	0.12385	0.3004	0.00828	0.916	5.61	.	1614	21	1658	25	1693	41
CR34_06-	190	19.4	32.9	.		0.10524	0.00133	4.22132	0.12866	0.29092	0.00807	0.91	-4.77	.	1718	22	1678	25	1646	40
CR34_16-	126	21.1	25.1	.	2619	0.11085	0.00143	4.76981	0.11277	0.31209	0.00618	0.838	-3.92	.	1813	22	1780	20	1751	30
CR34_08-	193	53.1	40.4	.		0.11336	0.00208	4.97541	0.14013	0.31833	0.00681	0.76	-4.47	.	1854	33	1815	24	1782	33
CR34-66-	140	15.9	24.1	.	2213	0.11498	0.00152	5.00818	0.11451	0.3159	0.0059	0.817	-6.69	.	1880	23	1821	19	1770	29
CR34_46-	74	17.9	18.2	.		0.11632	0.00194	5.13189	0.16425	0.31998	0.00875	0.854	-6.68	.	1900	29	1841	27	1790	43
CR34_01-	491	56.9	106.1	.		0.12144	0.00143	5.81268	0.11863	0.34715	0.00578	0.816	-3.3	.	1977	21	1948	18	1921	28
Rims and doubles																				
CR34_40-3-	96	20.5	10.4	.		0.07035	0.00128	1.41155	0.04549	0.14553	0.00388	0.826	-7.14	.	938	36	894	19	876	22
CR34_40-2-	113	11.7	14.5	.		0.07264	0.00092	1.70101	0.04392	0.16983	0.00382	0.87	0.77	.	1004	25	1009	17	1011	21

Appendix A: Tables of U-Pb data

Sample	*ppm*					***Ratios***							***U-Pb discordance***		***Ages (Ma)***					
Name	**U**	**Th**	**^{206}Pb**	**^{206}Pb$_c$(%)**	**206/204**	**^{207}Pb/^{206}Pb***	**1SE**	**^{207}Pb/^{235}U***	**1SE**	**^{206}Pb/^{238}U***	**1SE**	**Rho**	**Central (%)**	**Minimum rim (%)**	**207/206**	**1s**	**207/235**	**1s**	**206/238**	**1s**
CR34_17-2-	161	10.2	26.1	.		0.09104	0.00109	3.16818	0.06399	0.25238	0.00411	0.806	0.25	.	1448	22	1449	16	1451	21
CR34_03-2-	357	21.4	61.1	.	7359	0.09428	0.00096	3.49709	0.06181	0.26903	0.00389	0.818	1.65	.	1514	19	1527	14	1536	20
Discordance > 10 %																				
CR34-53-	232	22.1	14.4	.	1247	0.06489	0.0013	0.97075	0.02642	0.10849	0.002	0.677	-14.59	.	771	40	689	14	664	12
CR34-52r-	194	10.2	15	.	1777	0.07065	0.0013	1.31153	0.03224	0.13464	0.0022	0.665	-14.94	.	947	36	851	14	814	12
CR34_05-	86	1.4	5.8	.	397	0.07475	0.00207	1.06883	0.035	0.1037	0.00181	0.532	-42.09	-28.6	1062	53	738	17	636	11
CR34-65-	87	7.8	7.8	.	1082	0.07587	0.00196	1.60562	0.05049	0.15349	0.00276	0.573	-16.82	.	1092	51	972	20	920	15
CR34-69-	425	36.9	33.9	.	3301	0.0775	0.00139	1.45708	0.04382	0.13635	0.00329	0.803	-29.12	-13.65	1134	33	913	18	824	19
CR34_02-	34	5.5	3.8	.		0.07759	0.00194	1.83001	0.05396	0.17107	0.00268	0.532	-11.25	.	1136	49	1056	19	1018	15
CR34-54-	120	6.3	8.8	.	580	0.07756	0.00166	1.41657	0.05131	0.13246	0.00388	0.808	-31.25	-12.31	1136	41	896	22	802	22
CR34_44-	51	13.6	5.3	.	533	0.07762	0.00166	1.50239	0.04913	0.14038	0.00347	0.756	-27.23	-10.04	1137	41	931	20	847	20
CR34_39-	265	35.1	34.5	.		0.07828	0.00105	1.85737	0.04894	0.17208	0.00391	0.862	-12.22	.	1154	27	1066	17	1024	21
CR34-57-	99	24.5	10.3	.		0.07845	0.00174	1.90055	0.07981	0.17571	0.00627	0.85	-10.72	.	1158	42	1081	28	1044	34
CR34_15-	119	12.2	13.1	.		0.07851	0.00149	1.89676	0.04668	0.17523	0.00275	0.637	-11.1	.	1160	37	1080	16	1041	15
CR34_21-	118	10.7	13.4	.	1256	0.07854	0.00158	1.90382	0.04843	0.17581	0.00273	0.611	-10.87	.	1161	39	1082	17	1044	15
CR34_47-	90	24.4	12.1	.	1159	0.07981	0.00133	1.96509	0.05582	0.17858	0.00411	0.81	-12.1	.	1192	31	1104	19	1059	22
CR34-51-	131	7.2	12.2	.	1230	0.08088	0.00257	1.81715	0.10149	0.16294	0.00749	0.823	-21.7	.	1219	61	1052	37	973	41
CR34-72-	45	4.3	4.5	.		0.08161	0.00244	1.96359	0.0685	0.1745	0.00313	0.514	-17.45	-0.35	1236	55	1103	23	1037	17
CR34_35-2-	173	65.2	21.7	.	1335	0.08192	0.00166	1.8468	0.05751	0.16351	0.00386	0.759	-23.15	-7.75	1244	39	1062	21	976	21
CR34-76-	98	8.6	7.5	.	889	0.08204	0.00206	1.62746	0.0496	0.14387	0.0025	0.569	-32.57	-20.49	1247	48	981	19	866	14
CR34_24-	92	10.2	11.4	.	699	0.08212	0.00144	2.13664	0.05106	0.1887	0.00305	0.677	-11.69	.	1248	33	1161	17	1114	17
CR34-59-	156	3.6	13.5	.		0.08243	0.0071	1.7472	0.15502	0.15372	0.00328	0.241	-28.53	.	1256	161	1026	57	922	18
CR34_38-	132	17.8	17.5	.		0.08301	0.00106	2.04405	0.05699	0.17859	0.00443	0.889	-17.94	-2.71	1269	25	1130	19	1059	24
CR34_37-	178	22	25.4	.	3053	0.0831	0.00101	2.15848	0.05674	0.18839	0.00439	0.887	-13.6	.	1272	23	1168	18	1113	24
CR34_11-	82	6.4	10.1	.	1541	0.08449	0.002	2.29722	0.06704	0.1972	0.00336	0.583	-12.03	.	1304	44	1211	21	1160	18
CR34-62-	285	10.3	30.8	.		0.08489	0.0012	2.29361	0.04771	0.19596	0.003	0.735	-13.26	-3.1	1313	26	1210	15	1154	16

Appendix A: Tables of U-Pb data

Sample	***ppm***					***Ratios***							***U-Pb discordance***		***Ages (Ma)***					
Name	**U**	**Th**	**^{206}Pb**	**^{206}Pb$_c$(%)**	**206/204**	**^{207}Pb/^{206}Pb***	**1SE**	**^{207}Pb/^{235}U***	**1SE**	**^{206}Pb/^{238}U***	**1SE**	**Rho**	**Central (%)**	**Minimum rim (%)**	**207/206**	**1s**	**207/235**	**1s**	**206/238**	**1s**
CR34_35-	24	11	2.6	.	230	0.08564	0.00324	1.79849	0.08633	0.15231	0.00451	0.616	-33.53	-13.73	1330	73	1045	31	914	25
CR34_27-	99	24.1	15.1	.		0.09245	0.00132	2.5795	0.09056	0.20235	0.00649	0.914	-21.4	-4.68	1477	26	1295	26	1188	35
CR34-67-	9	1.4	0.5	.	54	0.10791	0.02809	1.51442	0.39949	0.10178	0.00435	0.162	-67.67	.	1764	557	936	161	625	25
CR34_41-	73	18.9	12.2	.		0.10862	0.00179	3.2543	0.10694	0.21729	0.00618	0.865	-31.51	-20.53	1776	27	1470	26	1268	33
CR34_12-	403	18.3	66.2	.		0.1097	0.00181	3.84258	0.08995	0.25405	0.00422	0.71	-20.84	-13.24	1794	29	1602	19	1459	22
CR34_20-	298	54.4	59.5	.	5637	0.12206	0.00149	5.37064	0.17557	0.31911	0.00968	0.928	-11.59	.	1987	20	1880	28	1785	47
CR34_29-	59	8	19.2	.		0.12514	0.00164	7.03207	0.23564	0.40755	0.01257	0.92	10.06	.	2031	22	2115	30	2204	58
CR34-58-	331	21.4	66.7	.	7332	0.18474	0.00437	9.07838	0.3219	0.35641	0.00942	0.745	-31.36	-23.63	2696	38	2346	32	1965	45

Appendix B: CL images of zircon grains after LA-ICP-MS. Analysed grains marked with sample name and a white circle indicating the impact crater from laser ablation.

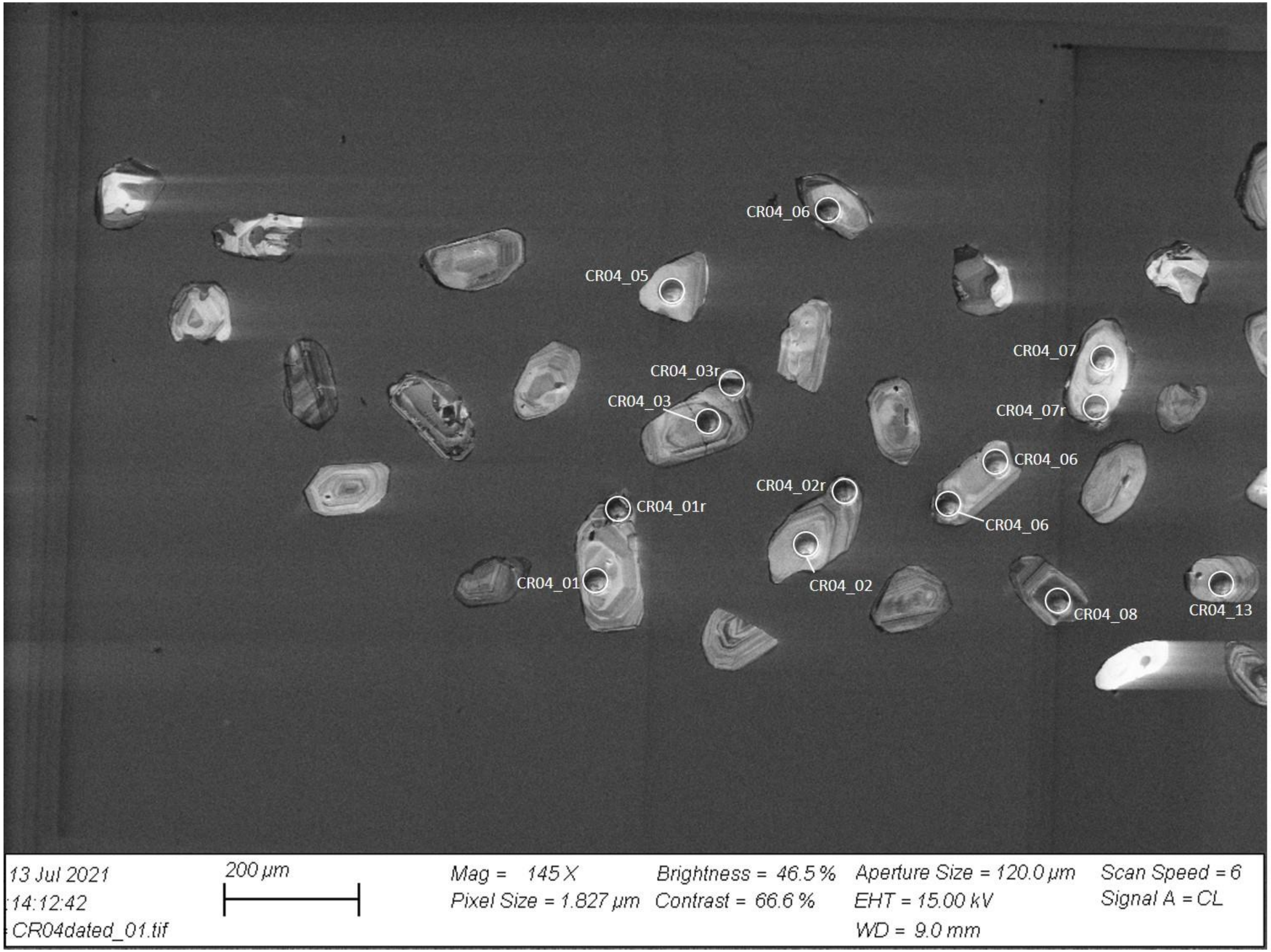

Appendix B: CL images of zircon grains after LA-ICP-MS. Analysed grains marked with sample name and a white circle indicating the impact crater from laser ablation.

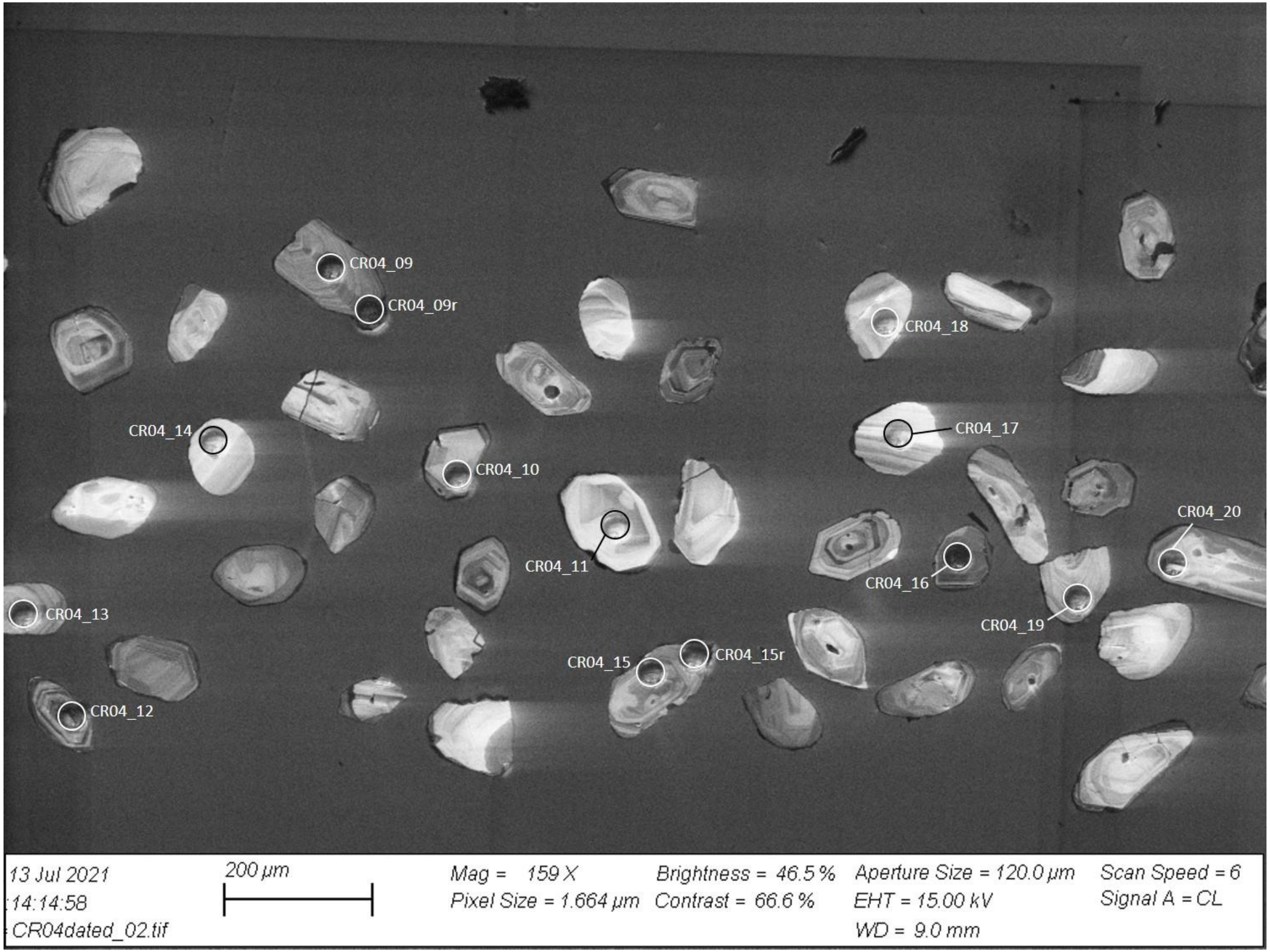

Appendix B: CL images of zircon grains after LA-ICP-MS. Analysed grains marked with sample name and a white circle indicating the impact crater from laser ablation.

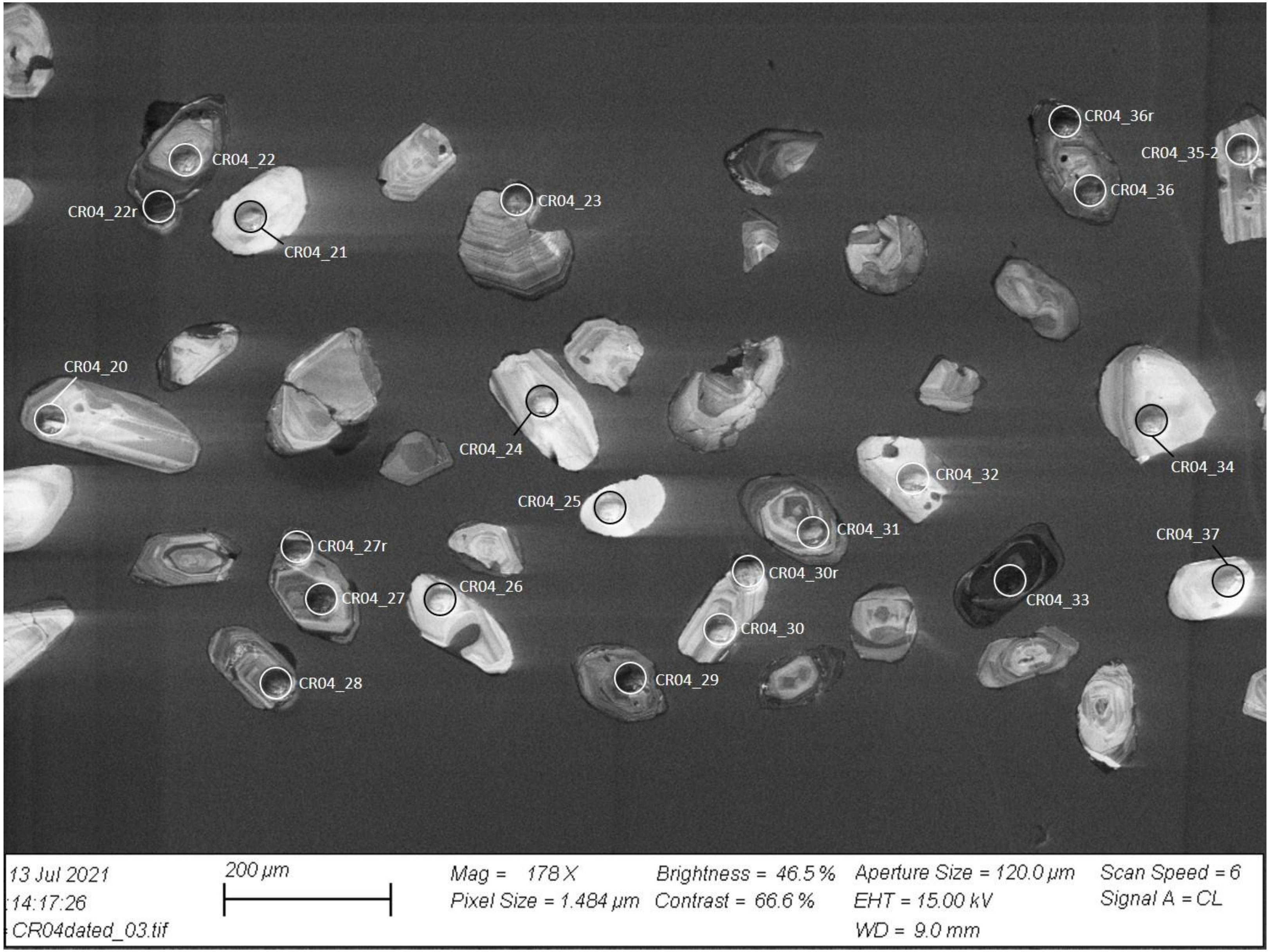

Appendix B: CL images of zircon grains after LA-ICP-MS. Analysed grains marked with sample name and a white circle indicating the impact crater from laser ablation.

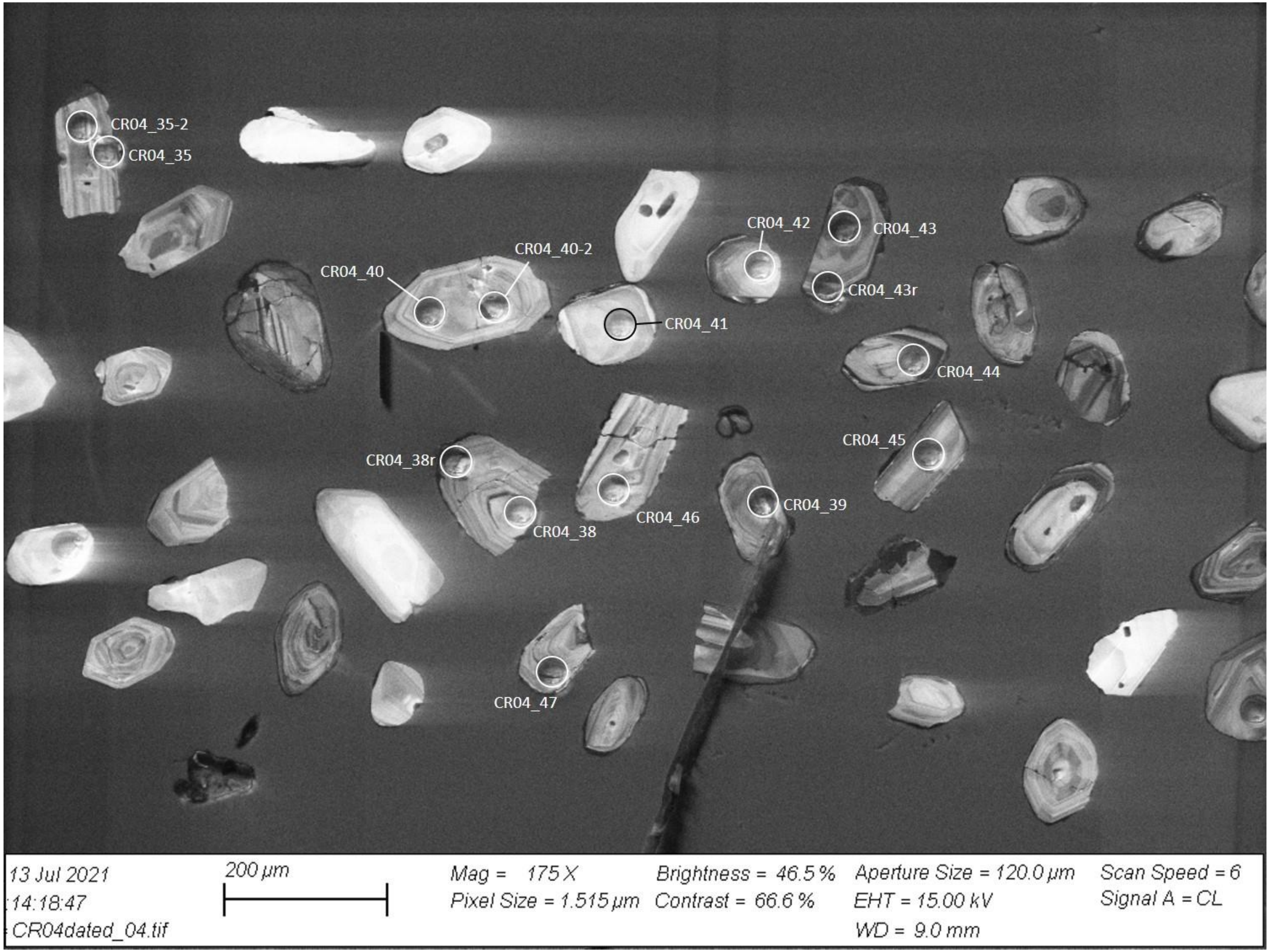

Appendix B: CL images of zircon grains after LA-ICP-MS. Analysed grains marked with sample name and a white circle indicating the impact crater from laser ablation.

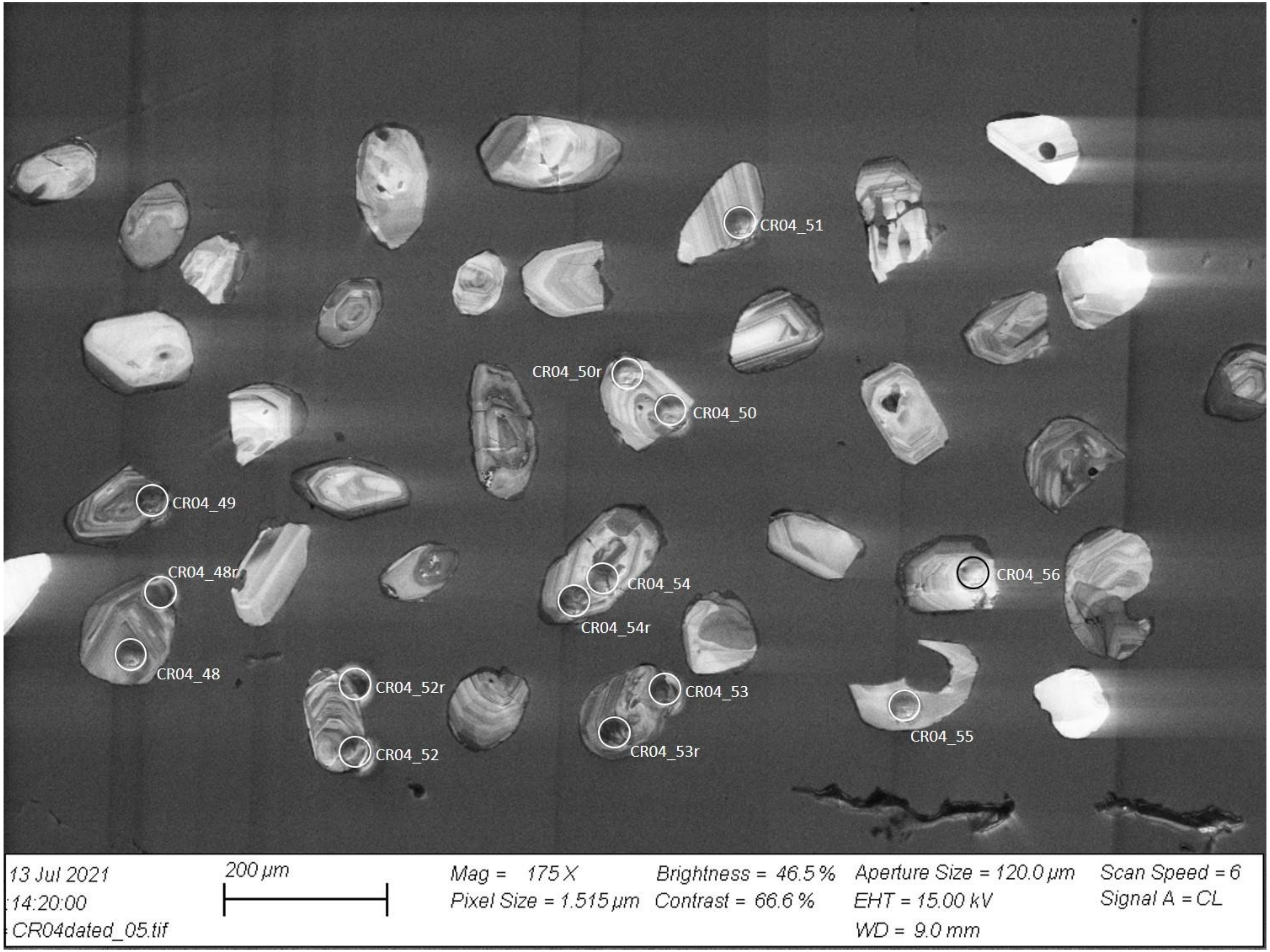

Appendix B: CL images of zircon grains after LA-ICP-MS. Analysed grains marked with sample name and a white circle indicating the impact crater from laser ablation.

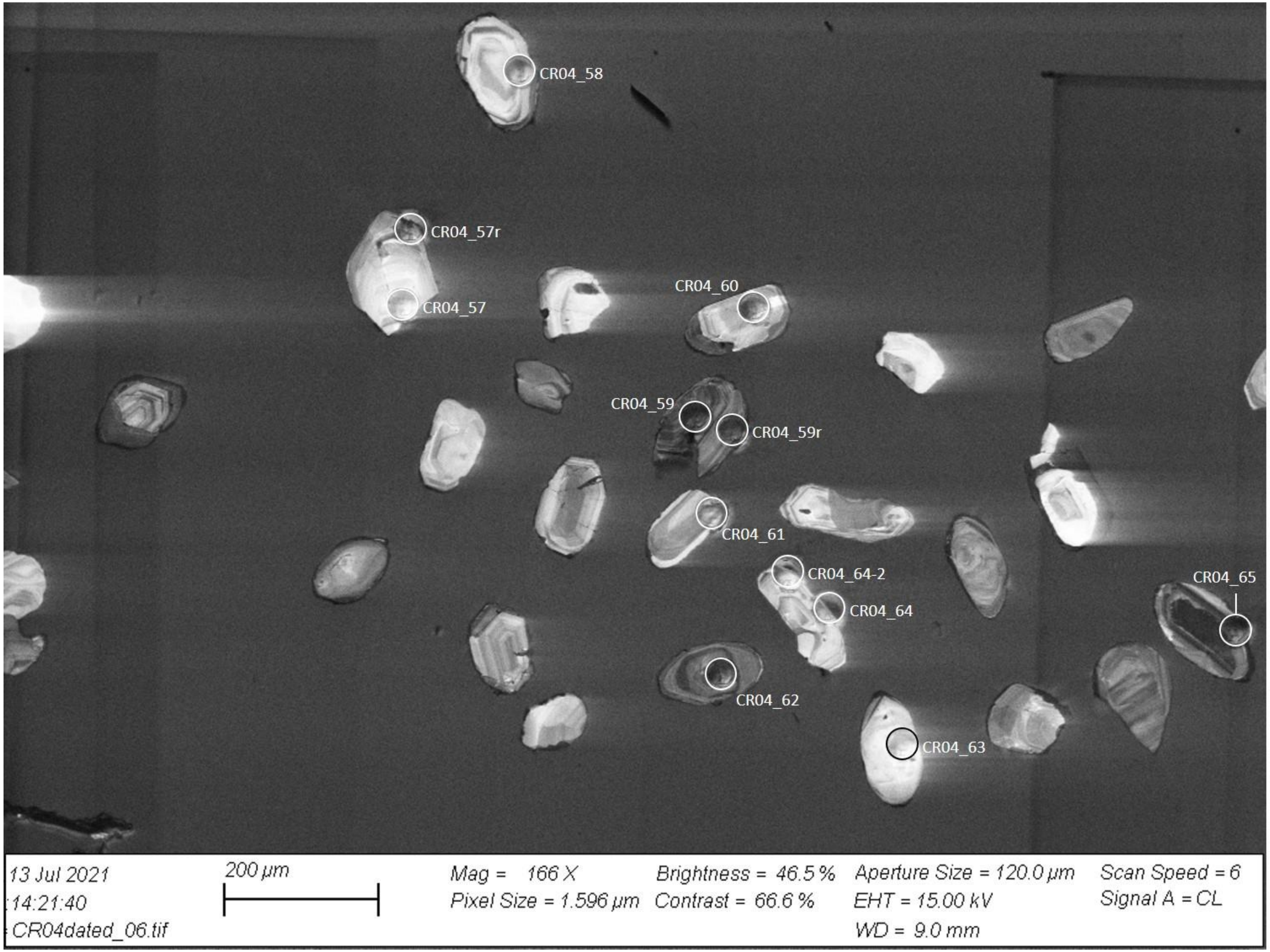

Appendix B: CL images of zircon grains after LA-ICP-MS. Analysed grains marked with sample name and a white circle indicating the impact crater from laser ablation.

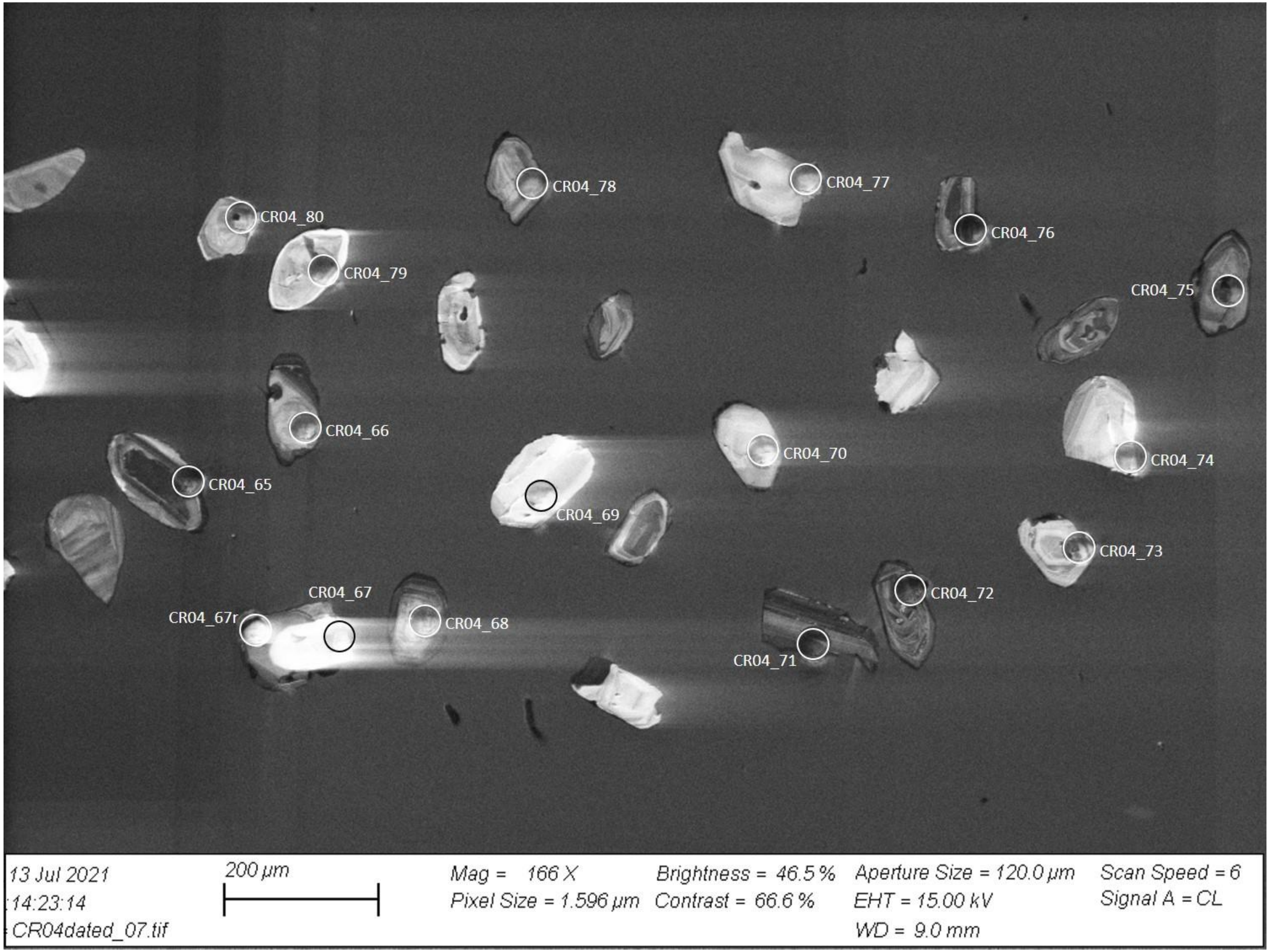

Appendix B: CL images of zircon grains after LA-ICP-MS. Analysed grains marked with sample name and a white circle indicating the impact crater from laser ablation.

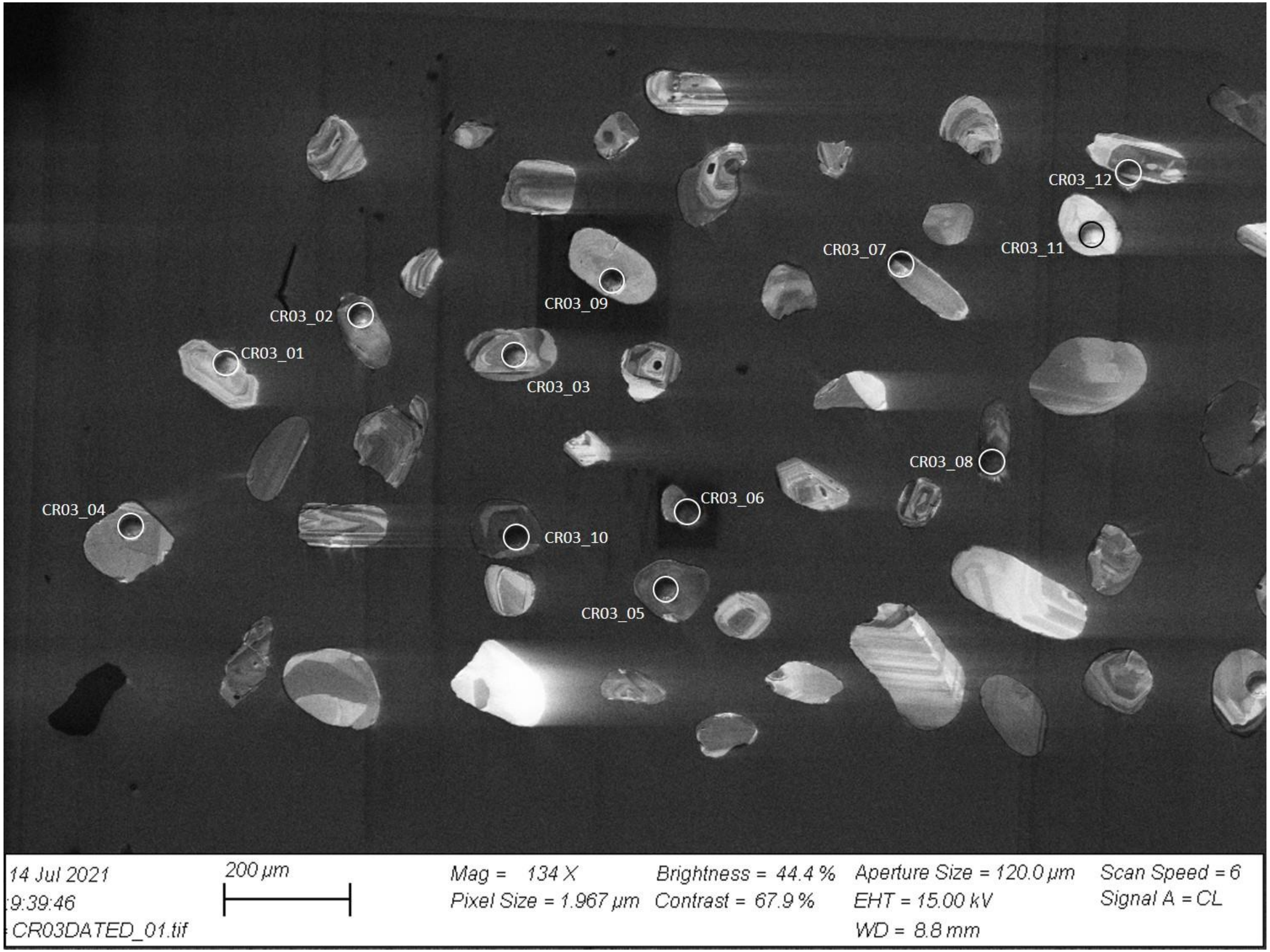

Appendix B: CL images of zircon grains after LA-ICP-MS. Analysed grains marked with sample name and a white circle indicating the impact crater from laser ablation.

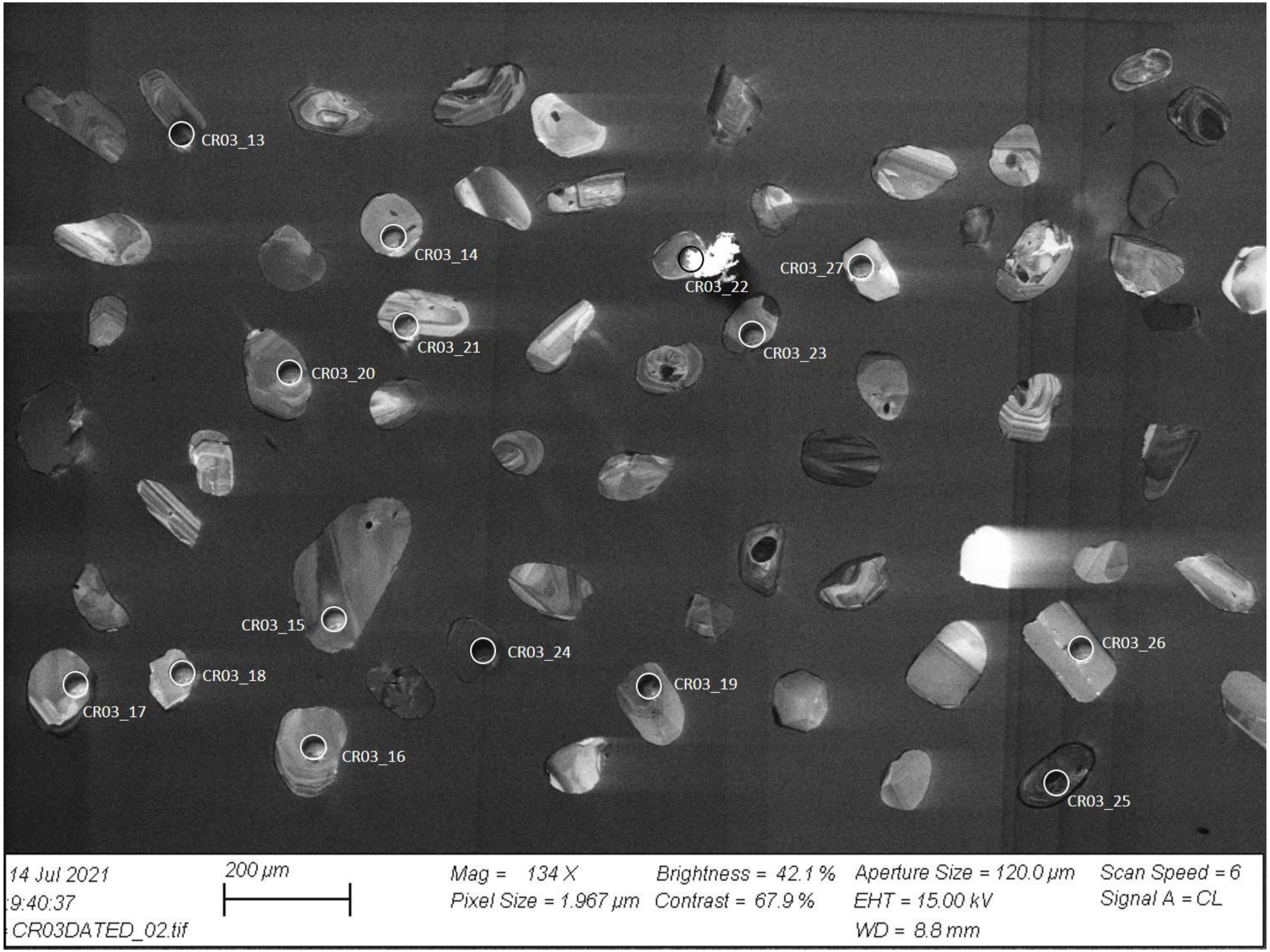

Appendix B: CL images of zircon grains after LA-ICP-MS. Analysed grains marked with sample name and a white circle indicating the impact crater from laser ablation.

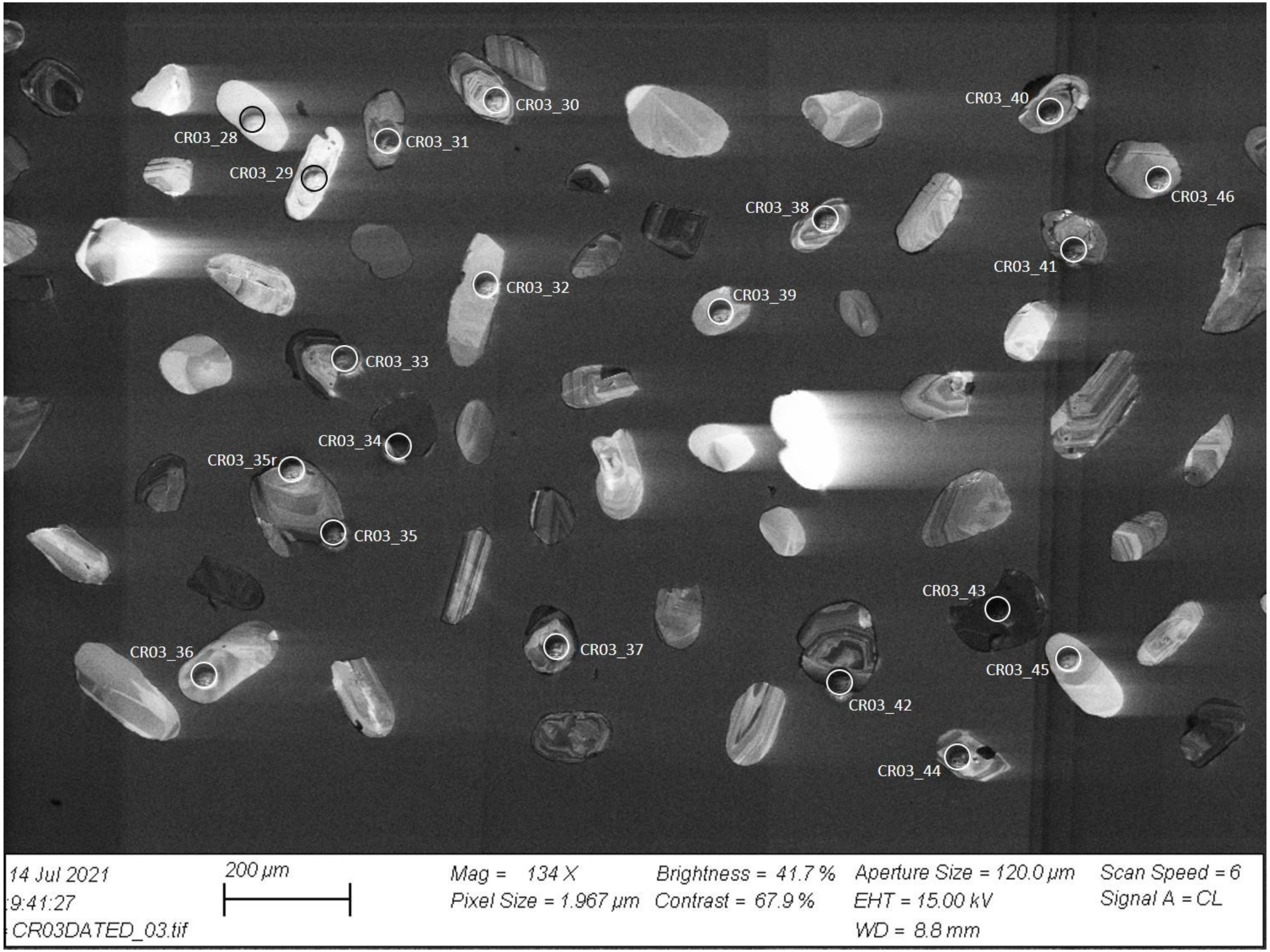

Appendix B: CL images of zircon grains after LA-ICP-MS. Analysed grains marked with sample name and a white circle indicating the impact crater from laser ablation.

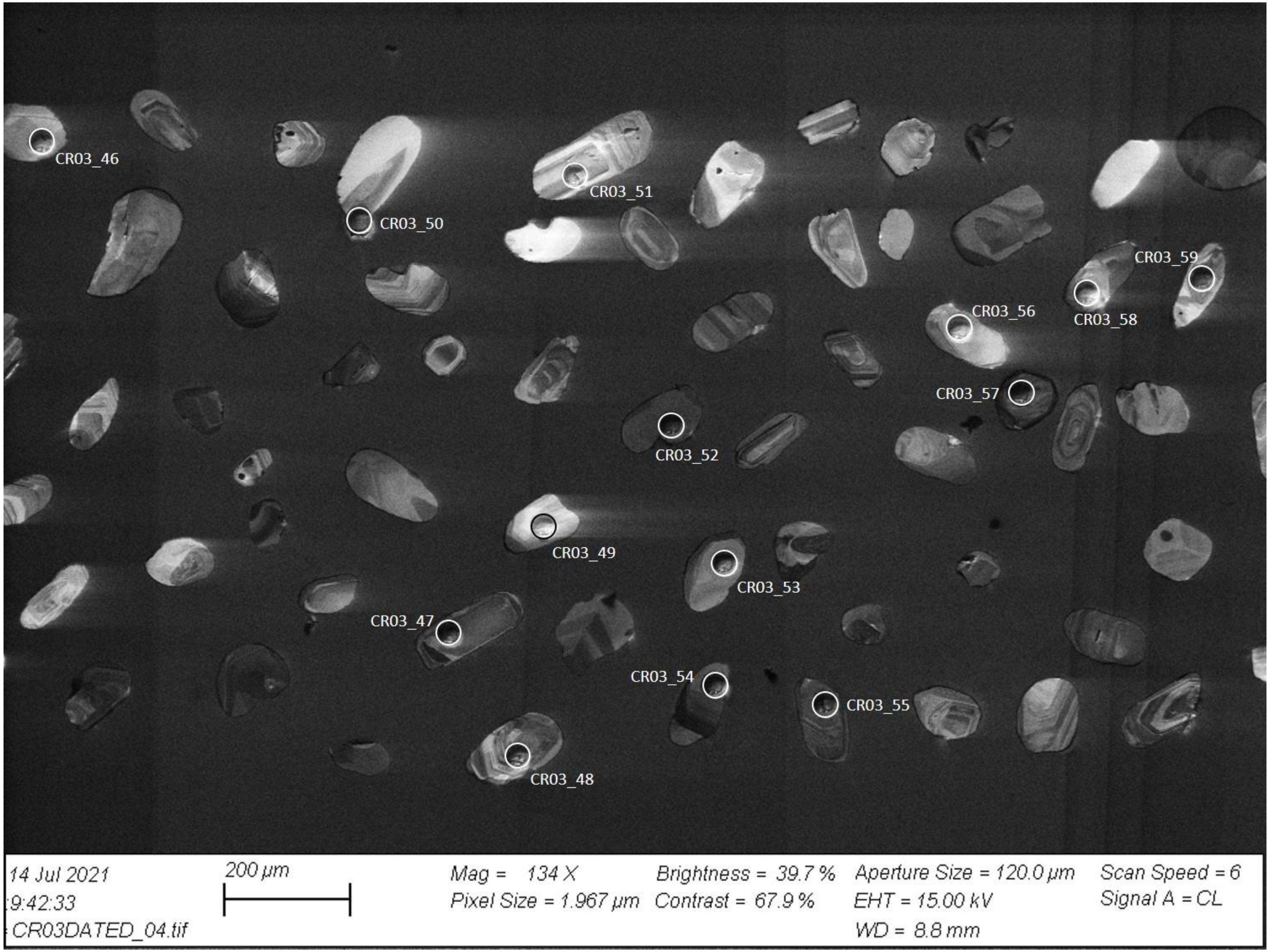

Appendix B: CL images of zircon grains after LA-ICP-MS. Analysed grains marked with sample name and a white circle indicating the impact crater from laser ablation.

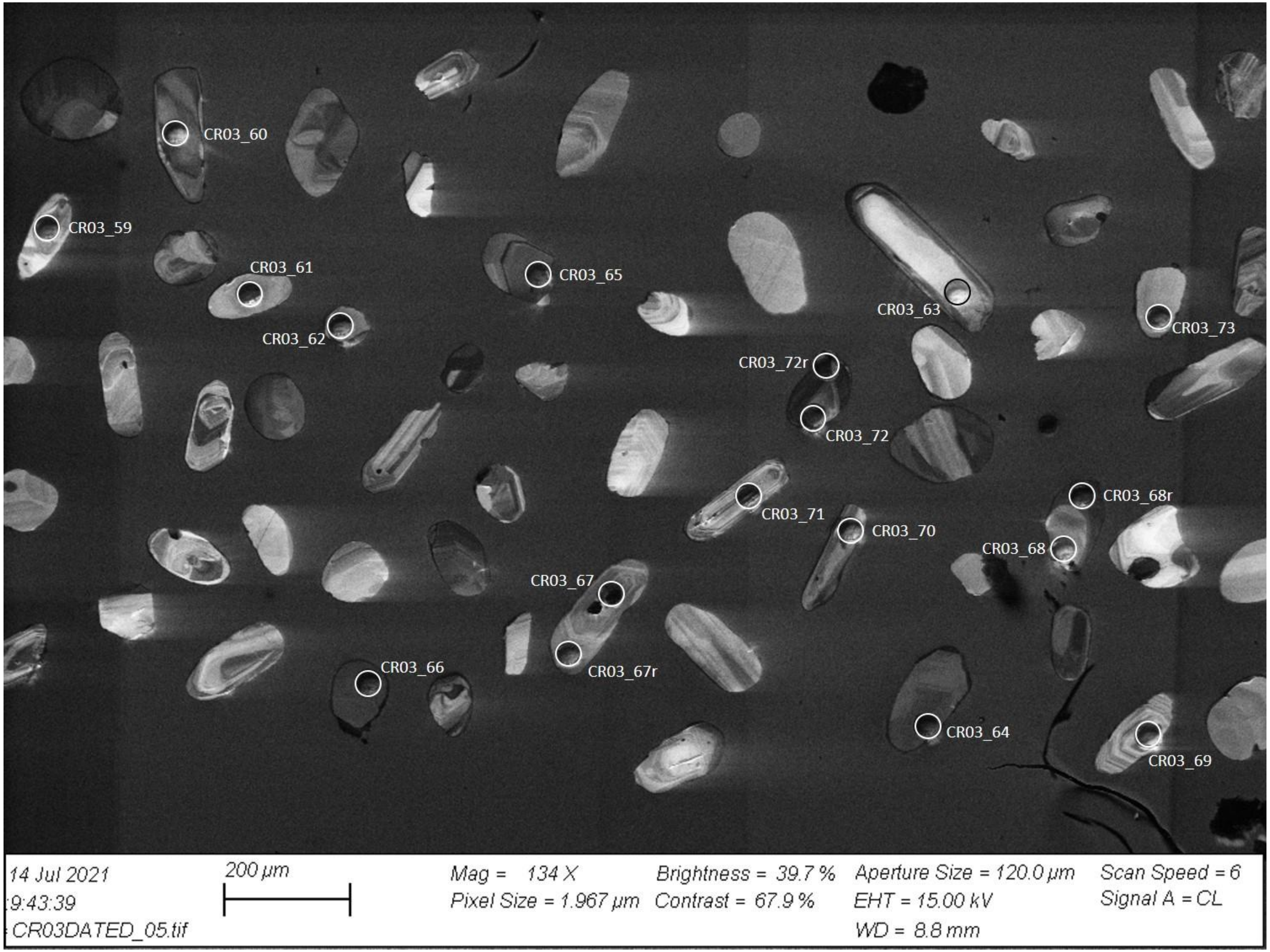

Appendix B: CL images of zircon grains after LA-ICP-MS. Analysed grains marked with sample name and a white circle indicating the impact crater from laser ablation.

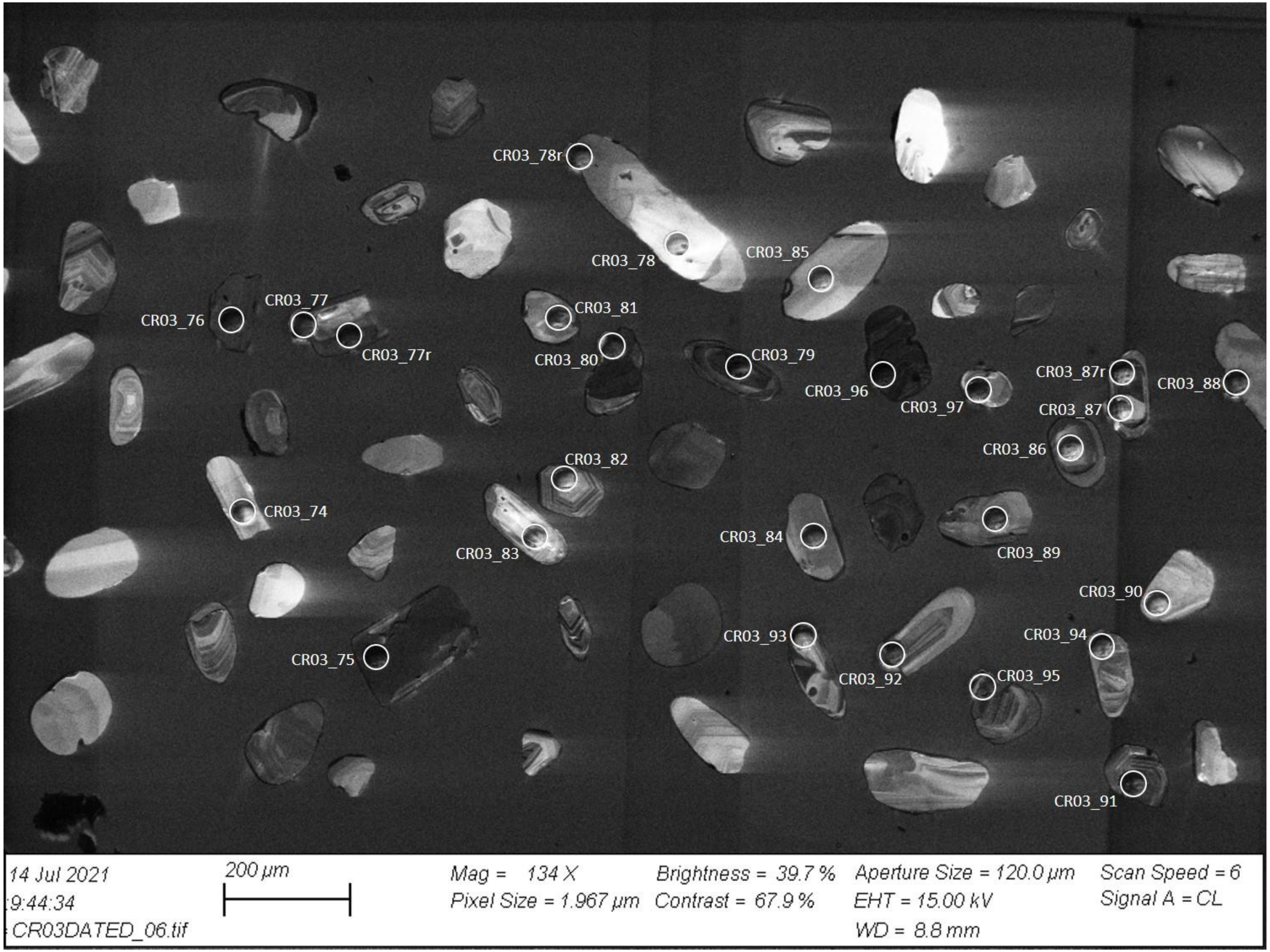

Appendix B: CL images of zircon grains after LA-ICP-MS. Analysed grains marked with sample name and a white circle indicating the impact crater from laser ablation.

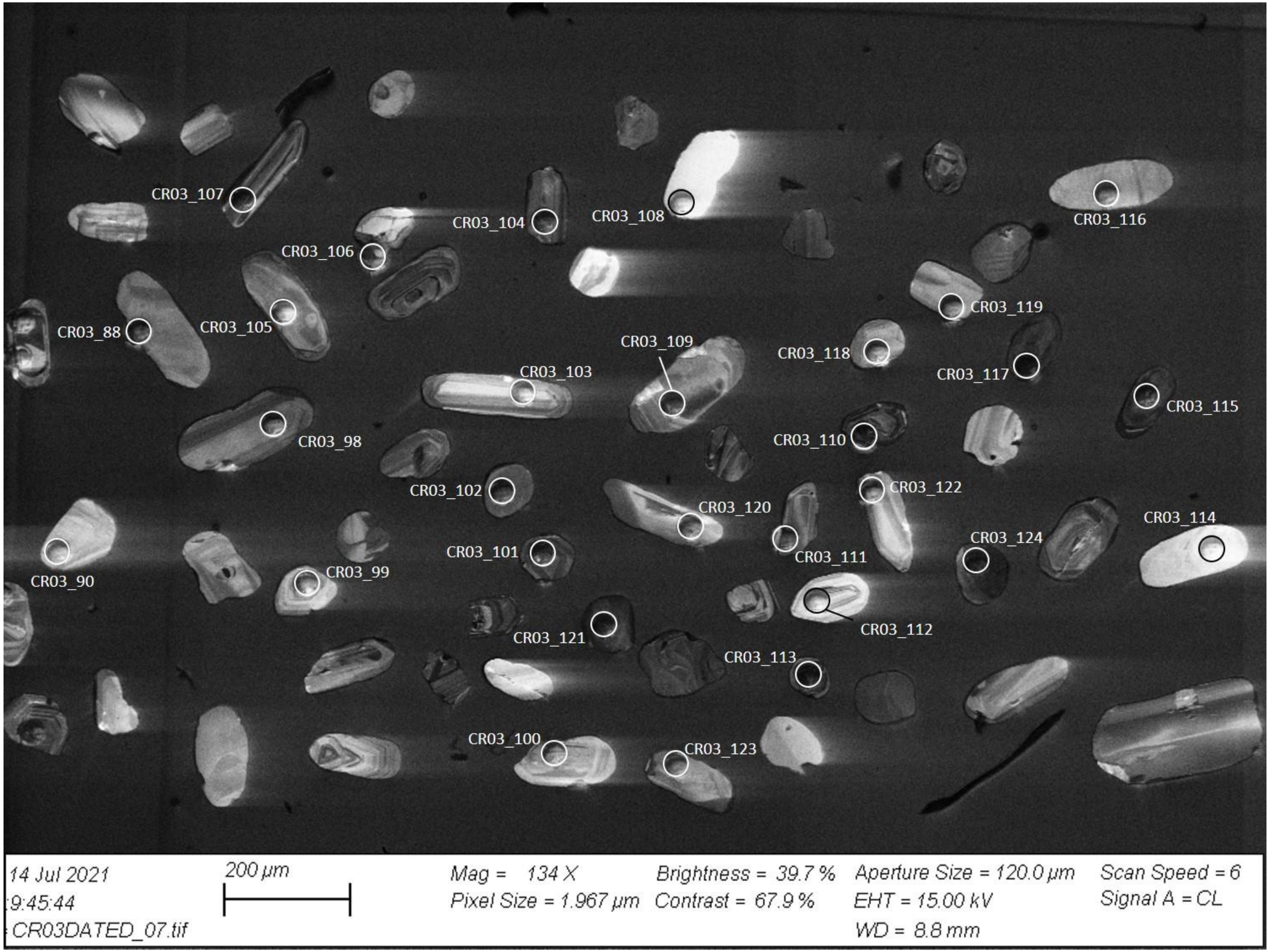

Appendix B: CL images of zircon grains after LA-ICP-MS. Analysed grains marked with sample name and a white circle indicating the impact crater from laser ablation.

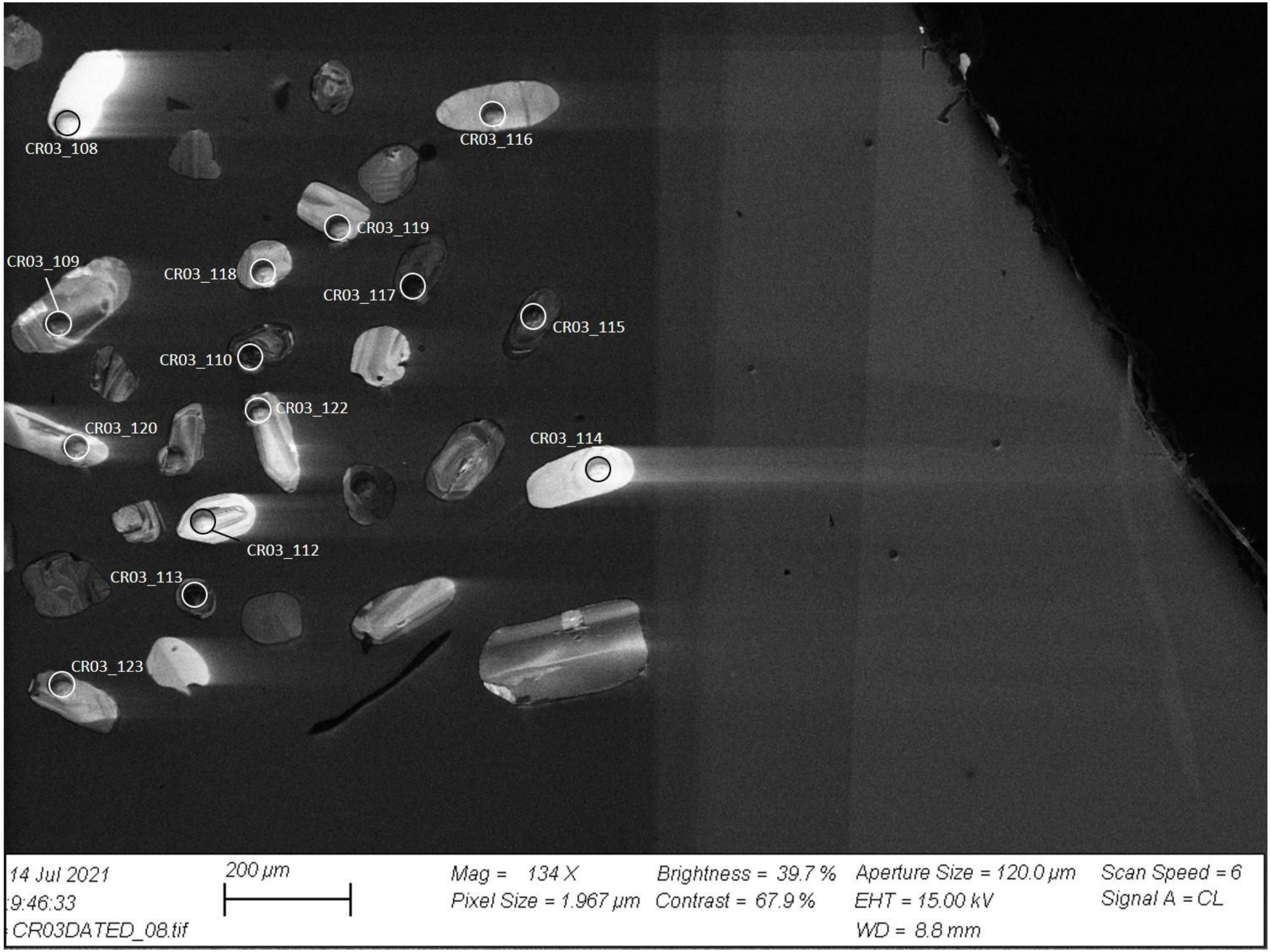

Appendix B: CL images of zircon grains after LA-ICP-MS. Analysed grains marked with sample name and a white circle indicating the impact crater from laser ablation.

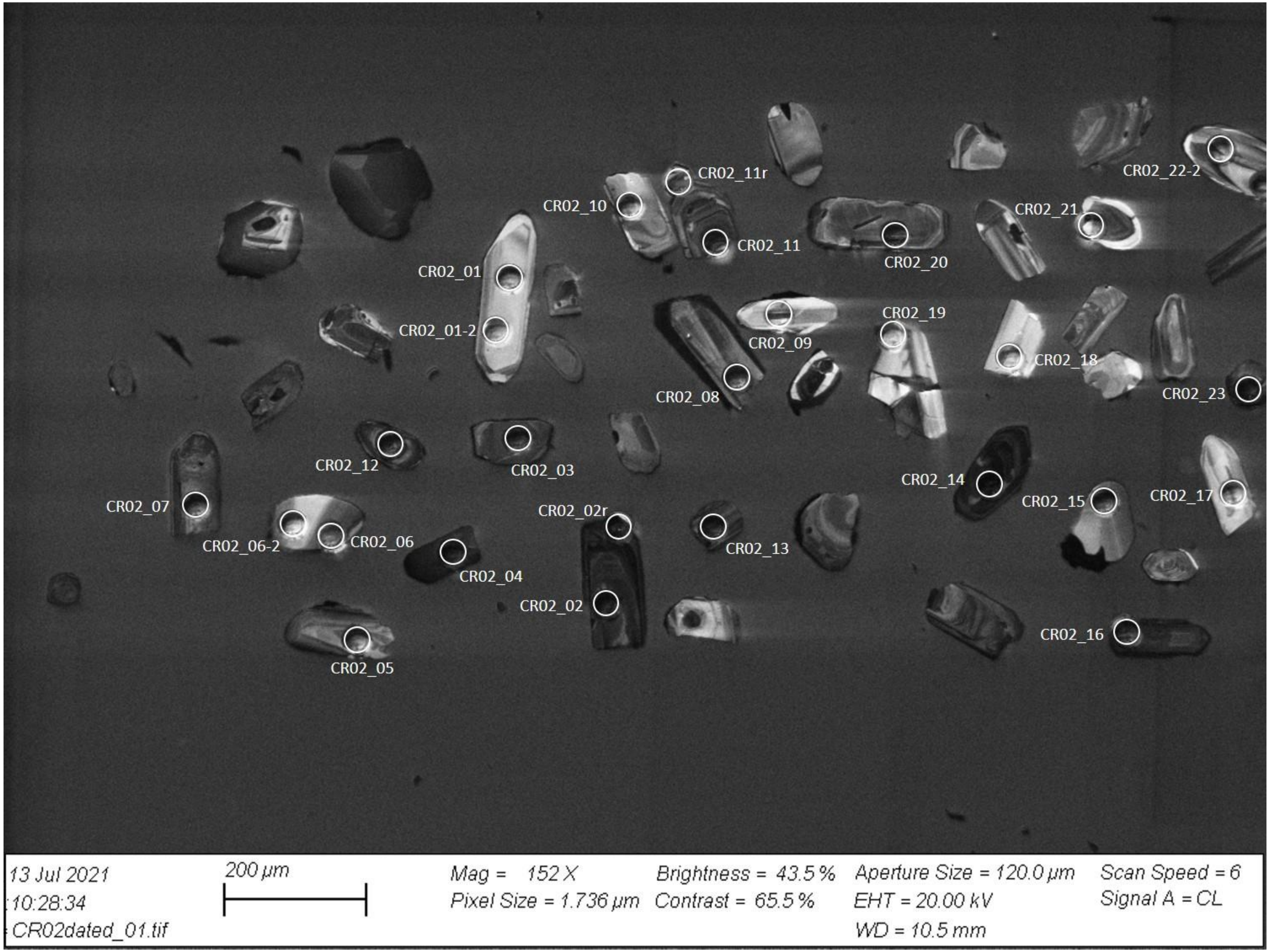

Appendix B: CL images of zircon grains after LA-ICP-MS. Analysed grains marked with sample name and a white circle indicating the impact crater from laser ablation.

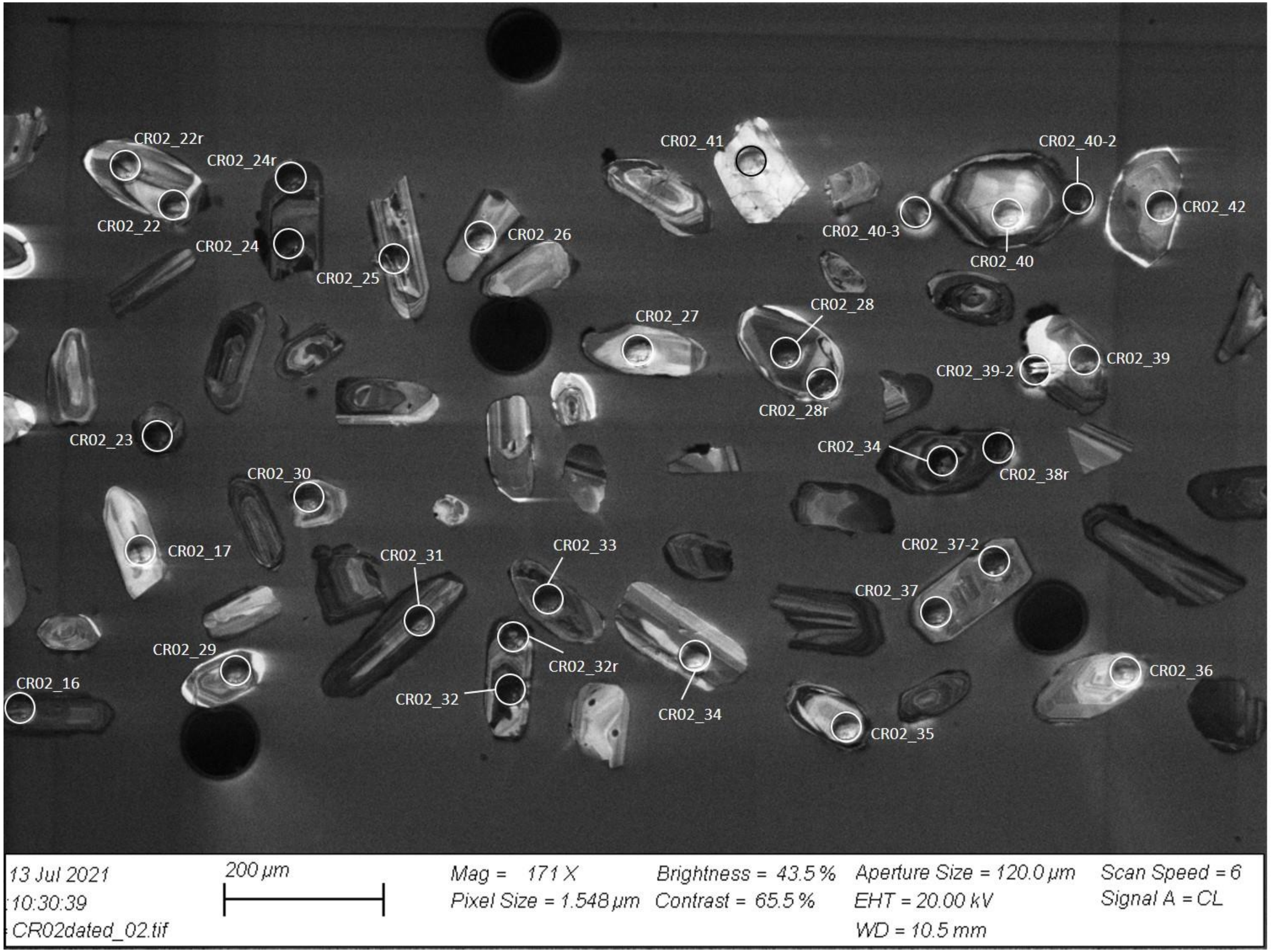

Appendix B: CL images of zircon grains after LA-ICP-MS. Analysed grains marked with sample name and a white circle indicating the impact crater from laser ablation.

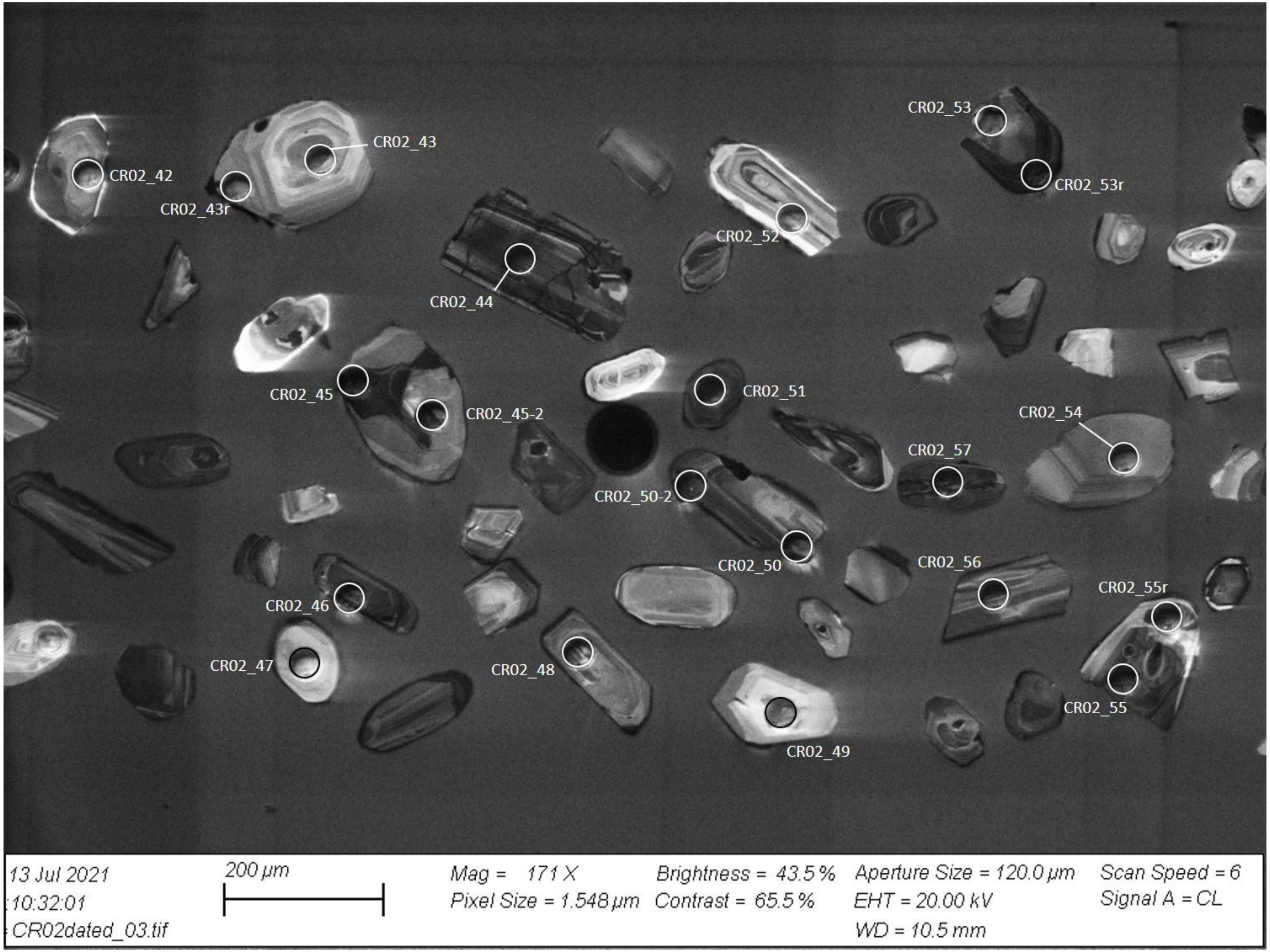

Appendix B: CL images of zircon grains after LA-ICP-MS. Analysed grains marked with sample name and a white circle indicating the impact crater from laser ablation.

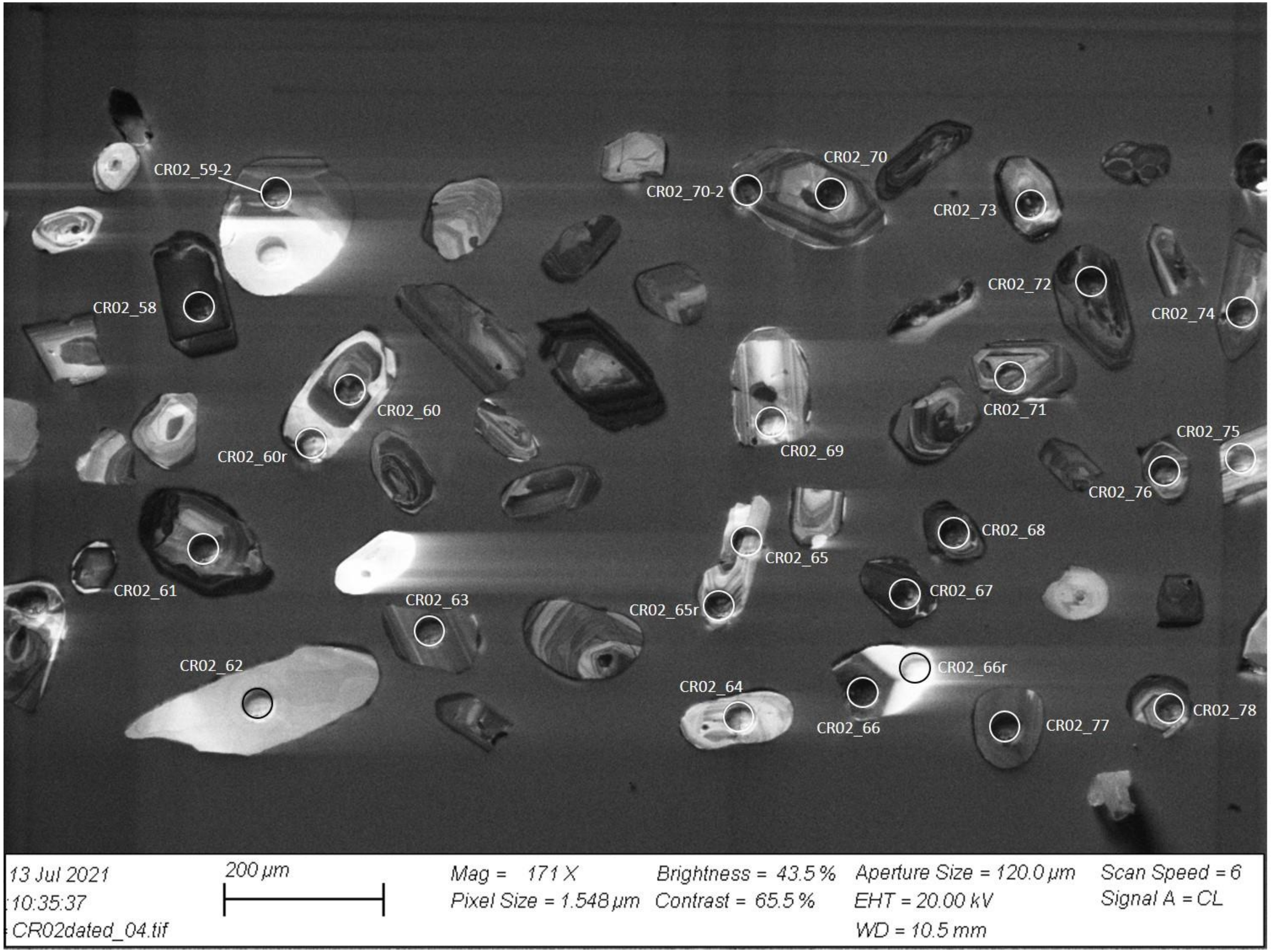

Appendix B: CL images of zircon grains after LA-ICP-MS. Analysed grains marked with sample name and a white circle indicating the impact crater from laser ablation.

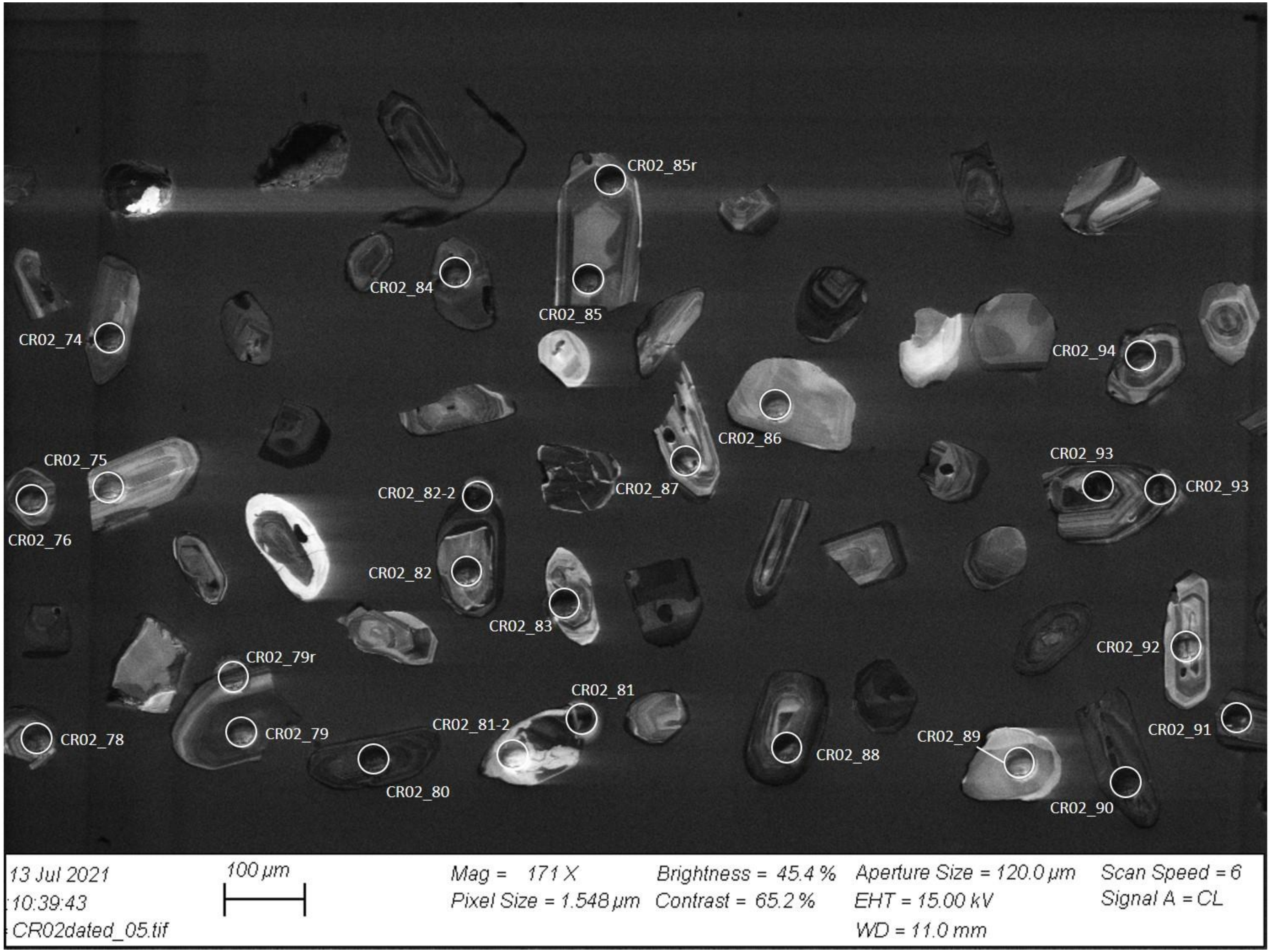

Appendix B: CL images of zircon grains after LA-ICP-MS. Analysed grains marked with sample name and a white circle indicating the impact crater from laser ablation.

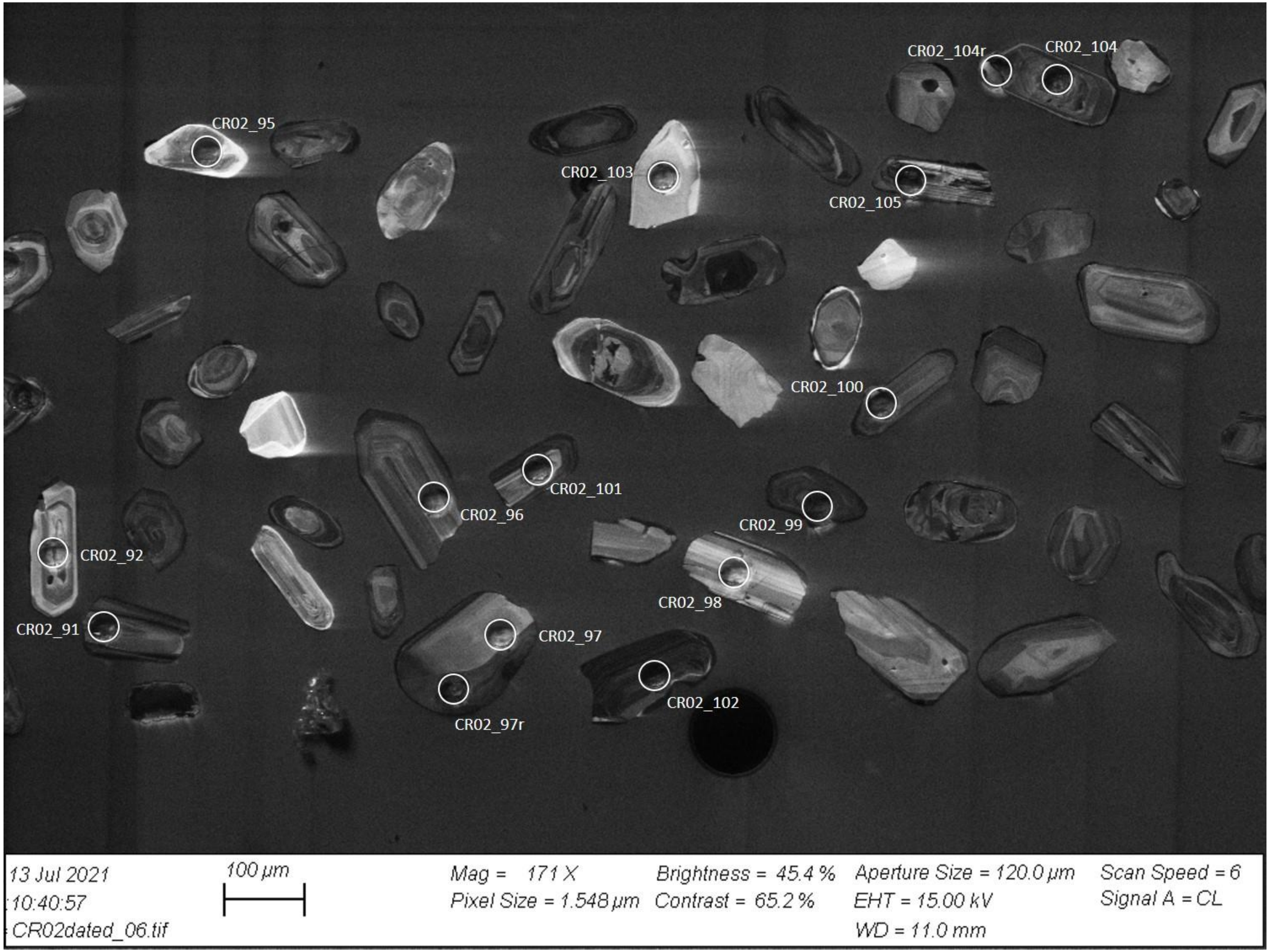

Appendix B: CL images of zircon grains after LA-ICP-MS. Analysed grains marked with sample name and a white circle indicating the impact crater from laser ablation.

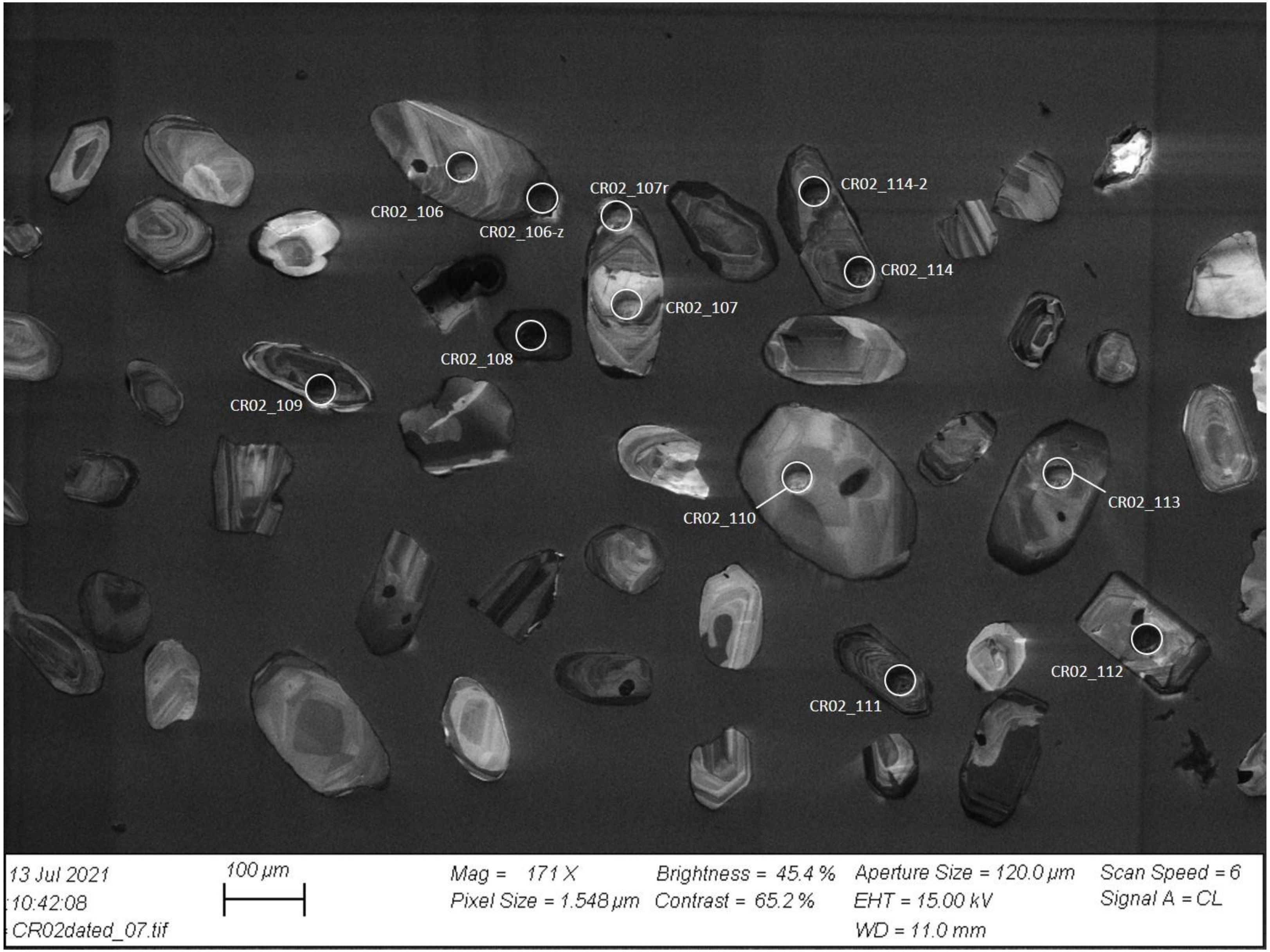

Appendix B: CL images of zircon grains after LA-ICP-MS. Analysed grains marked with sample name and a white circle indicating the impact crater from laser ablation.

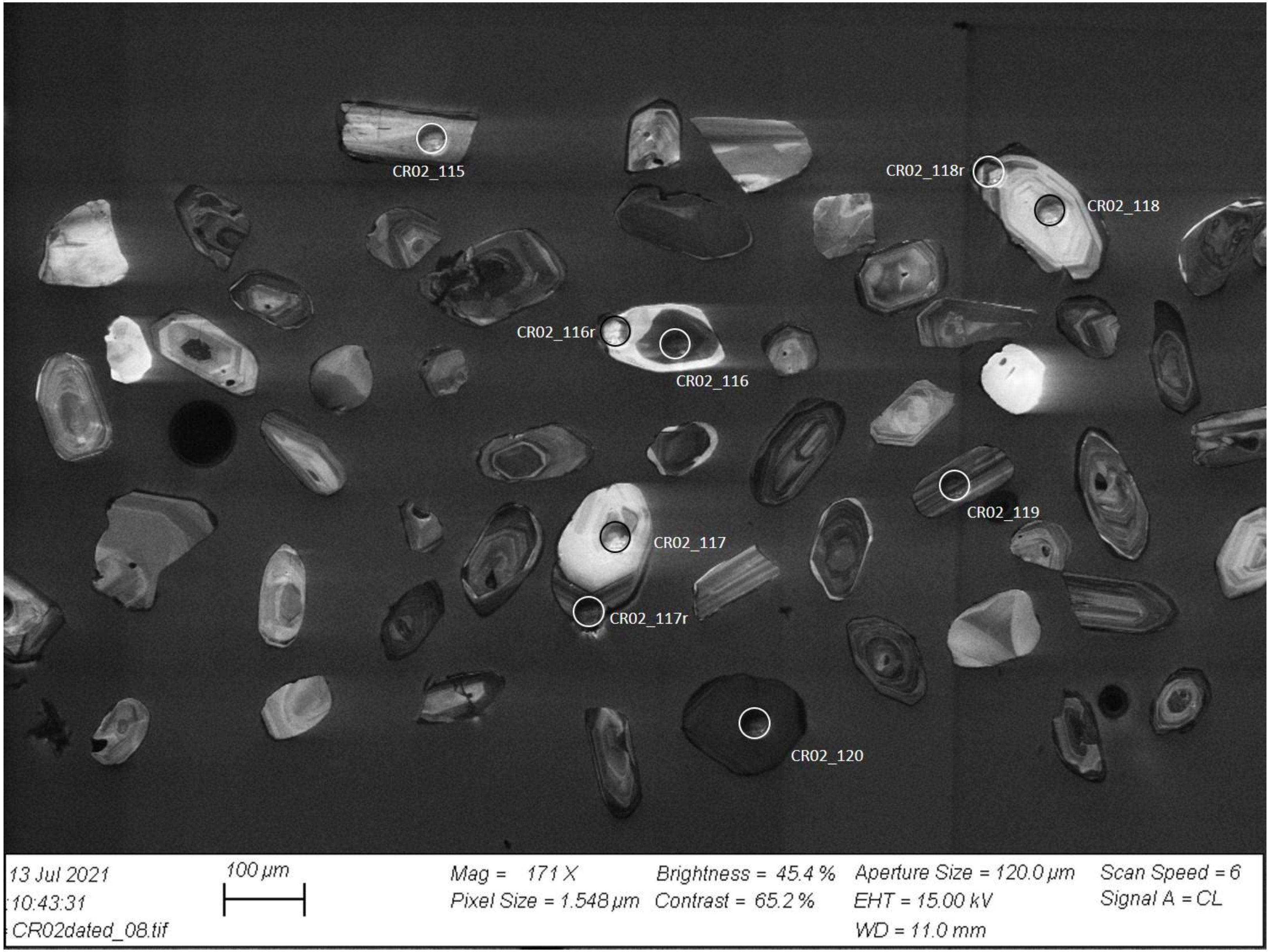

Appendix B: CL images of zircon grains after LA-ICP-MS. Analysed grains marked with sample name and a white circle indicating the impact crater from laser ablation.

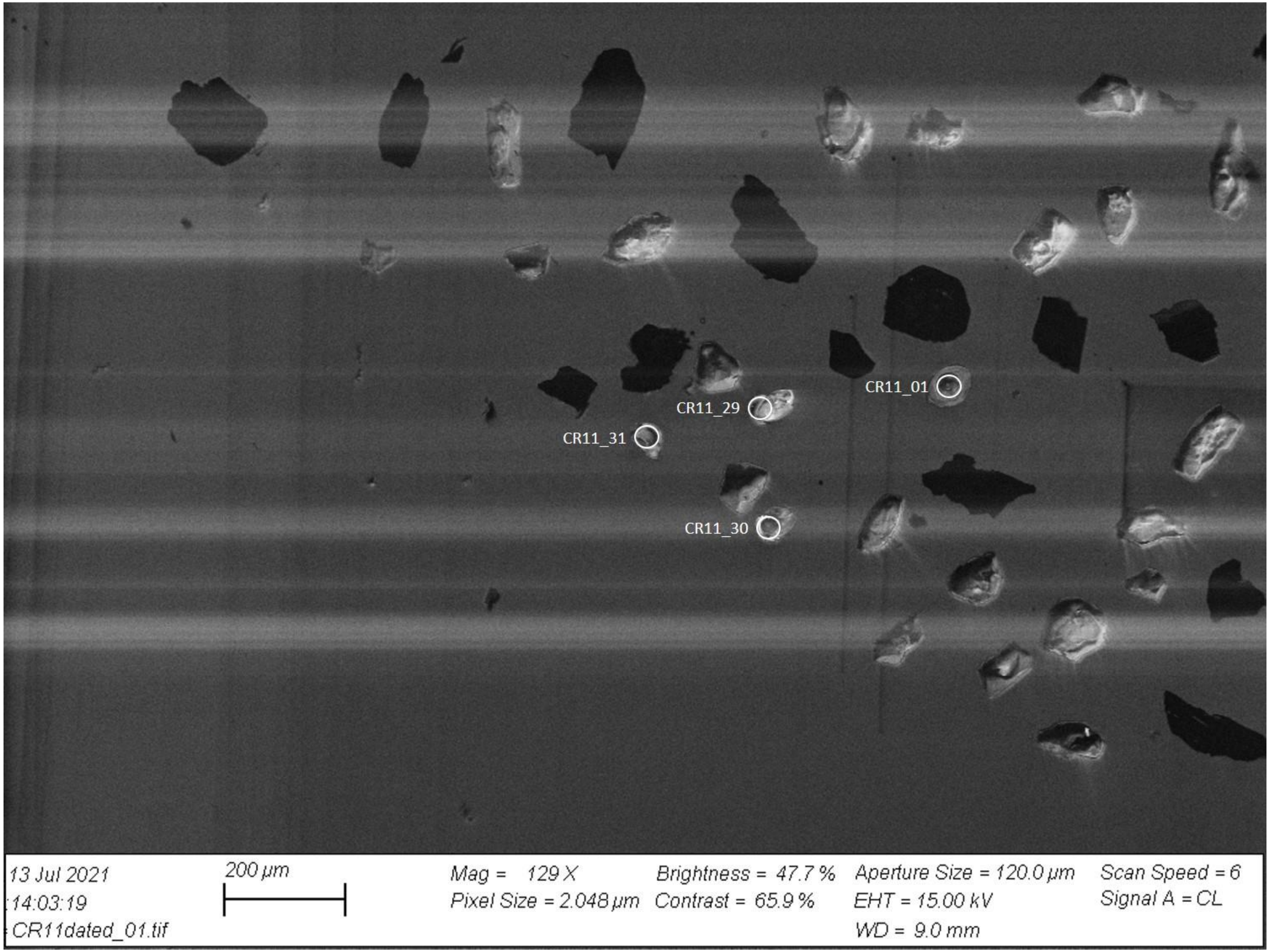

Appendix B: CL images of zircon grains after LA-ICP-MS. Analysed grains marked with sample name and a white circle indicating the impact crater from laser ablation.

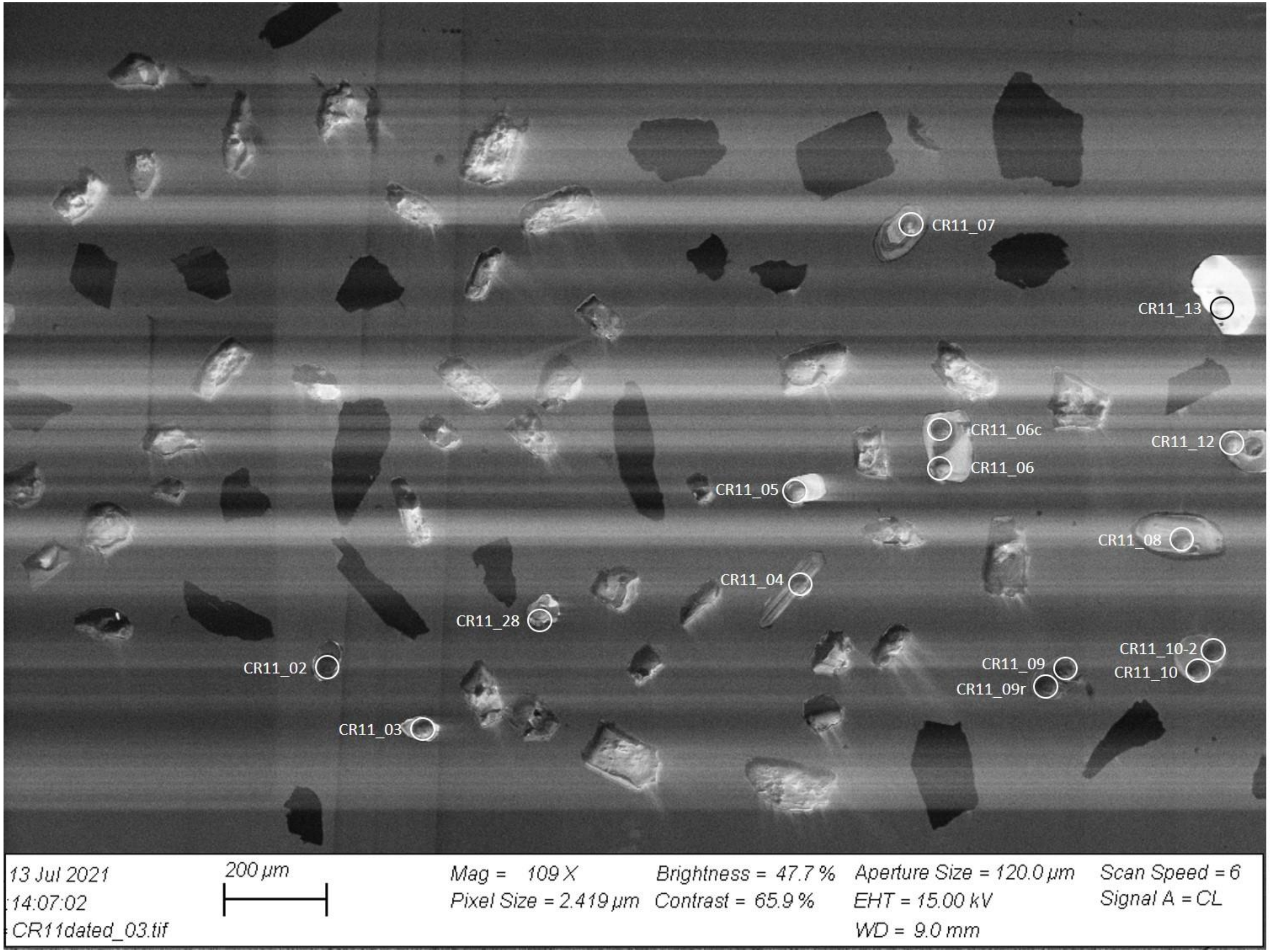

Appendix B: CL images of zircon grains after LA-ICP-MS. Analysed grains marked with sample name and a white circle indicating the impact crater from laser ablation.

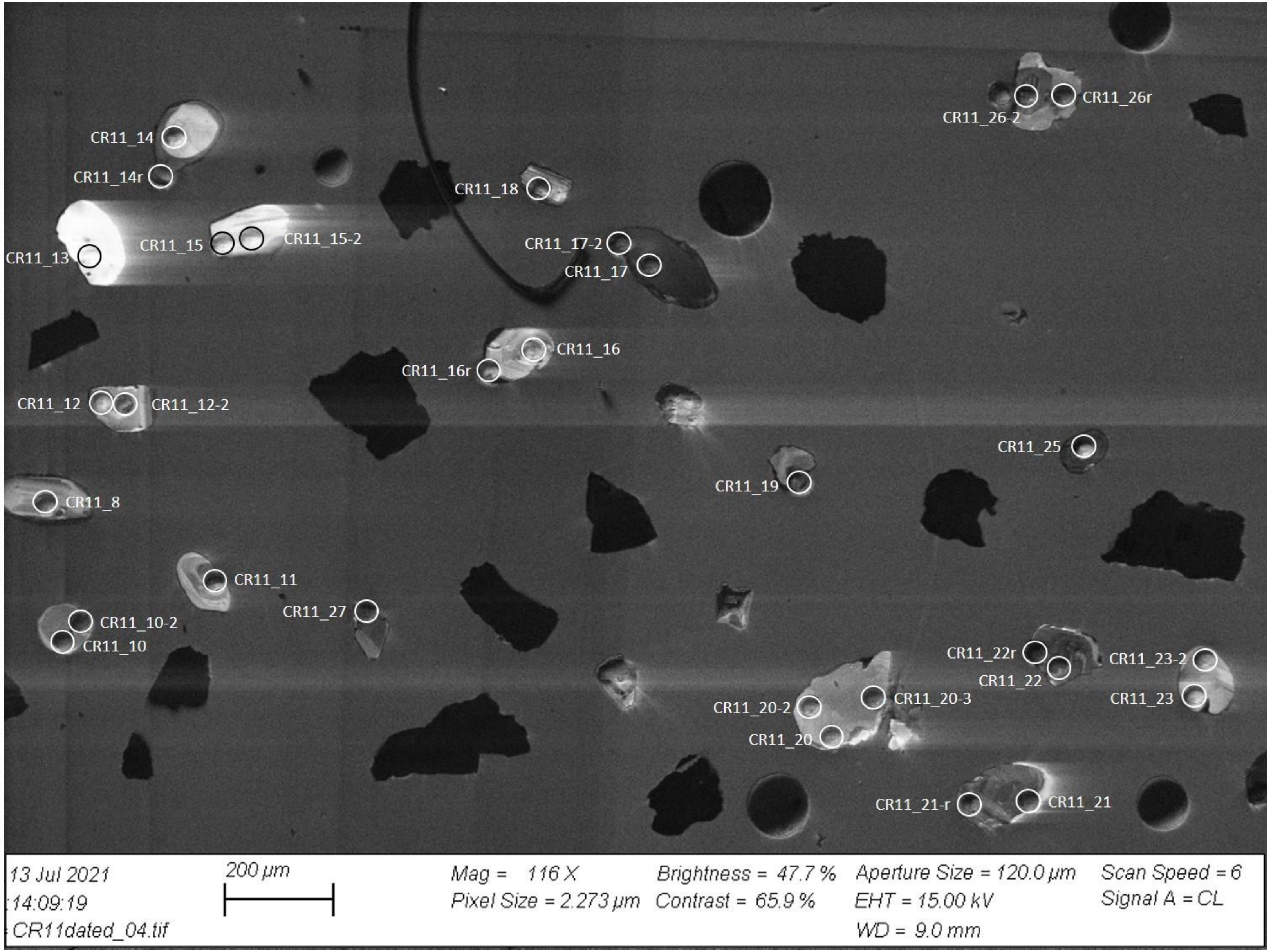

Appendix B: CL images of zircon grains after LA-ICP-MS. Analysed grains marked with sample name and a white circle indicating the impact crater from laser ablation.

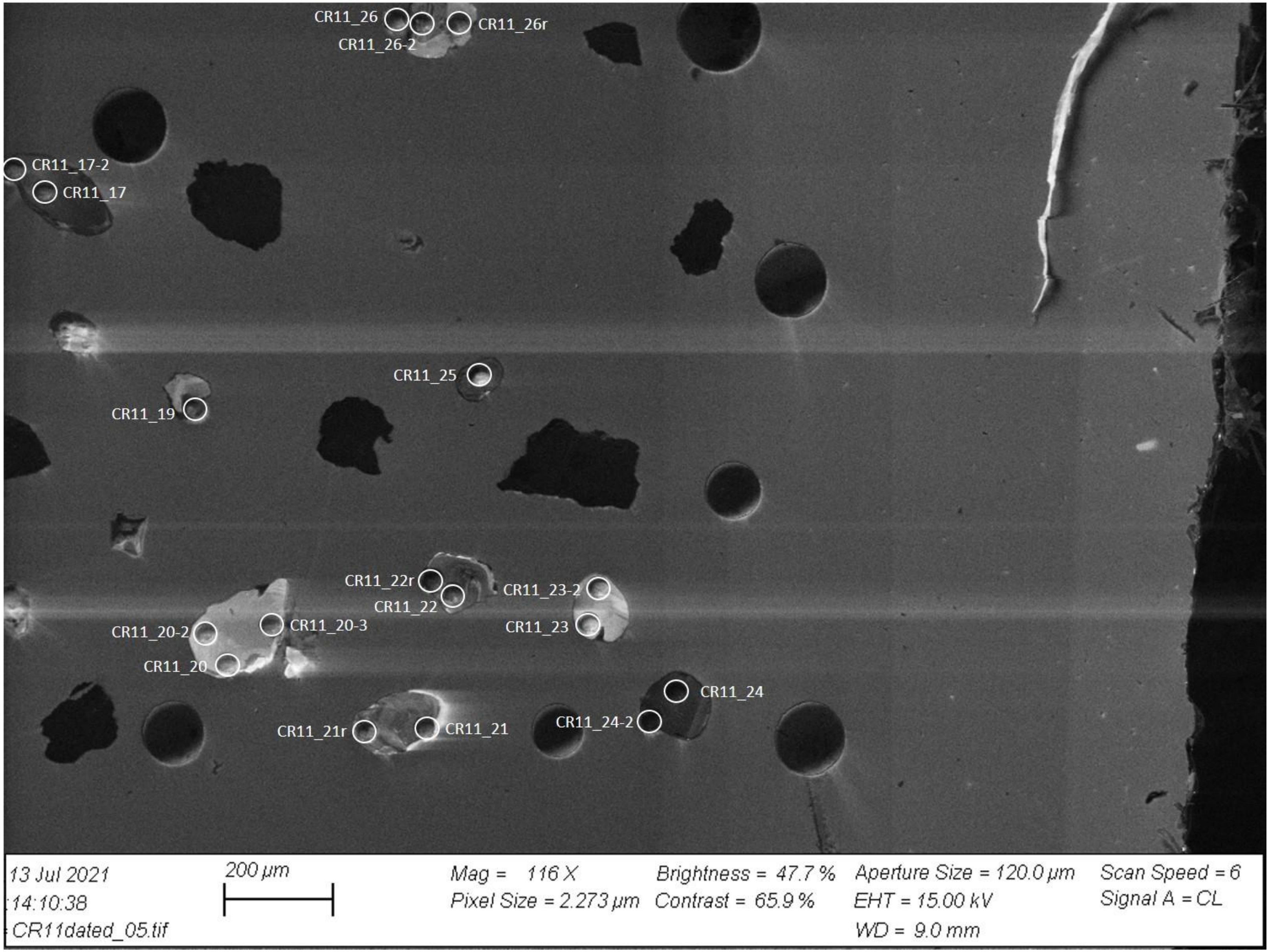

Appendix B: CL images of zircon grains after LA-ICP-MS. Analysed grains marked with sample name and a white circle indicating the impact crater from laser ablation.

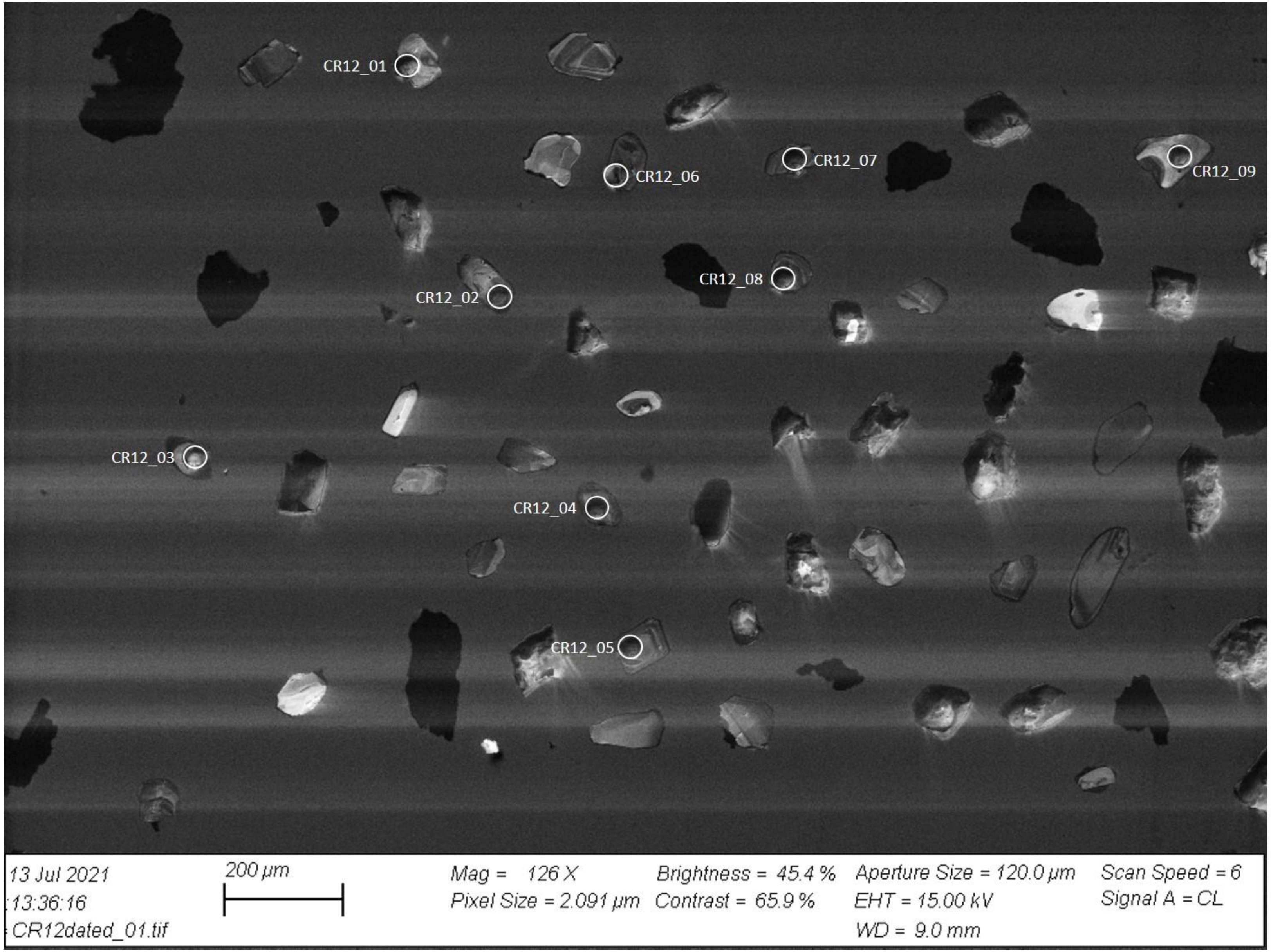

Appendix B: CL images of zircon grains after LA-ICP-MS. Analysed grains marked with sample name and a white circle indicating the impact crater from laser ablation.

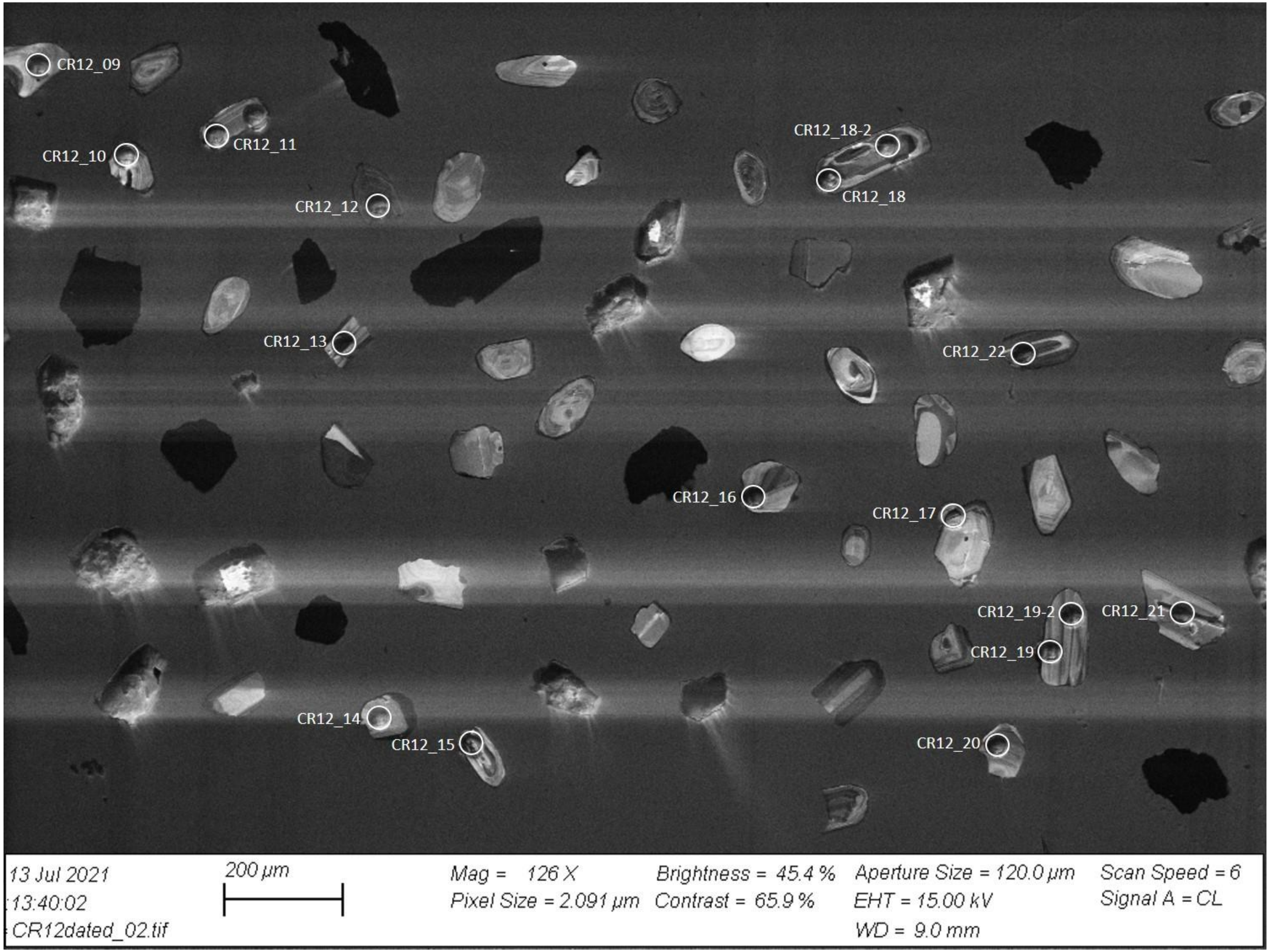

Appendix B: CL images of zircon grains after LA-ICP-MS. Analysed grains marked with sample name and a white circle indicating the impact crater from laser ablation.

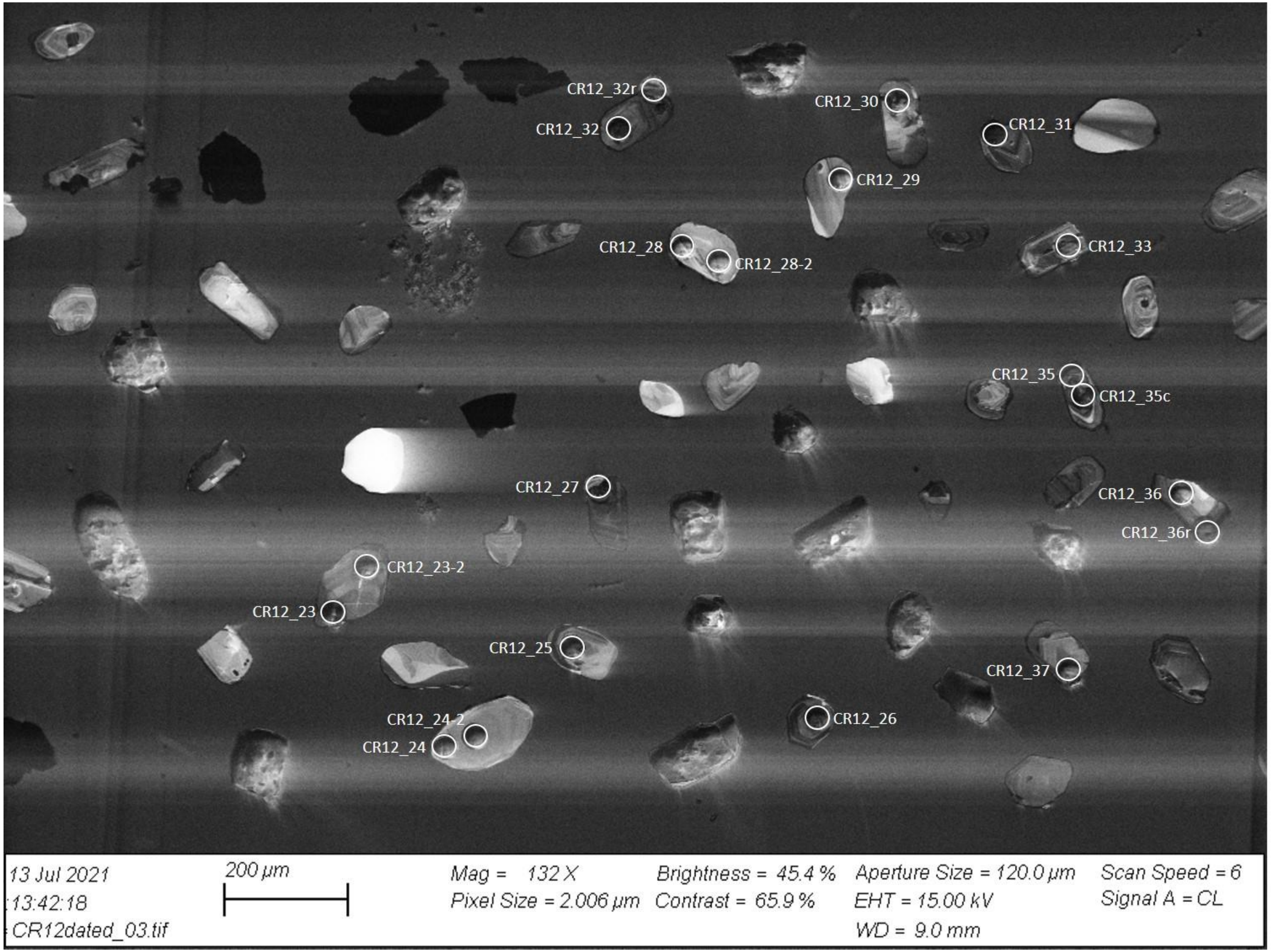

Appendix B: CL images of zircon grains after LA-ICP-MS. Analysed grains marked with sample name and a white circle indicating the impact crater from laser ablation.

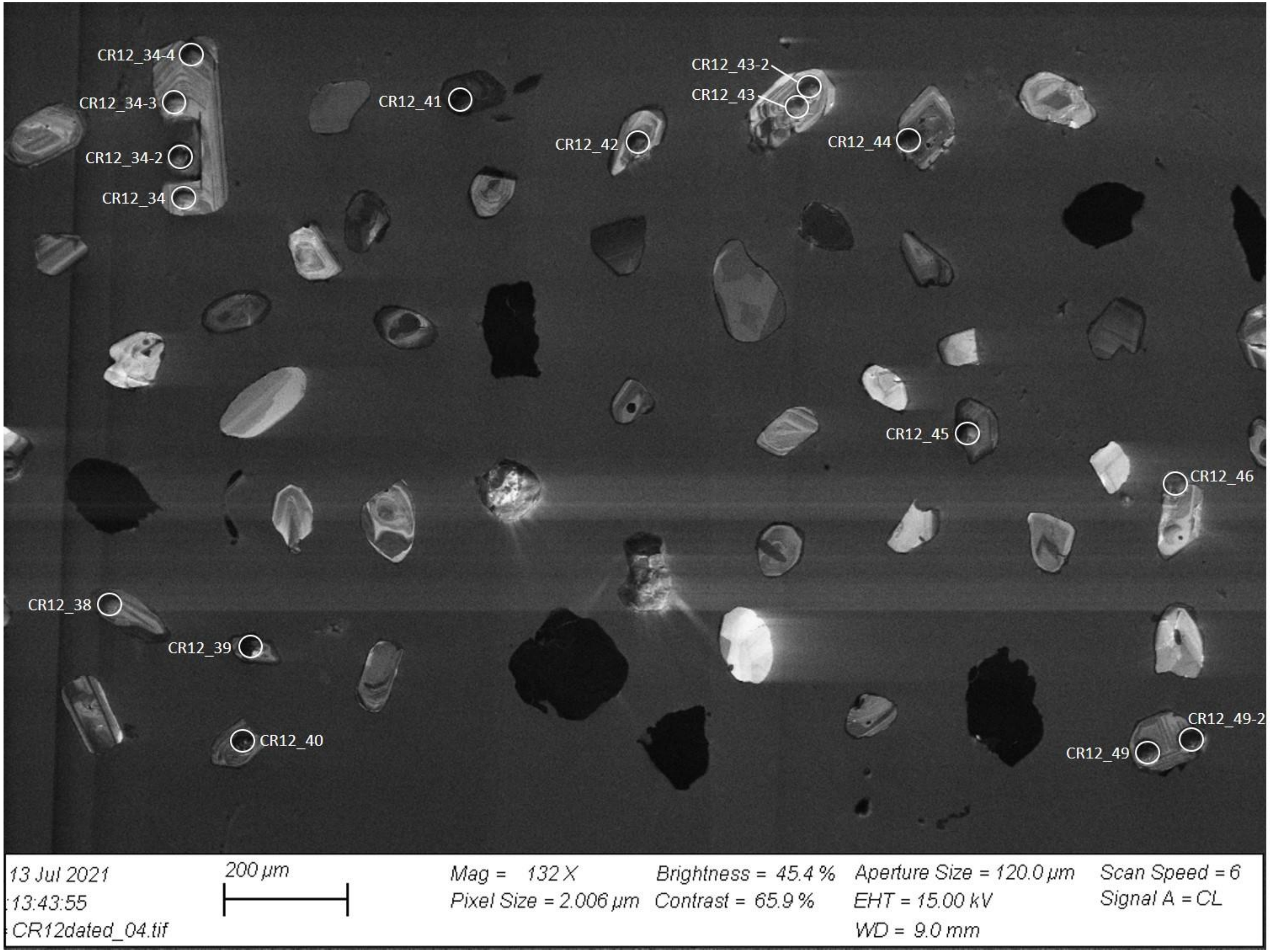

Appendix B: CL images of zircon grains after LA-ICP-MS. Analysed grains marked with sample name and a white circle indicating the impact crater from laser ablation.

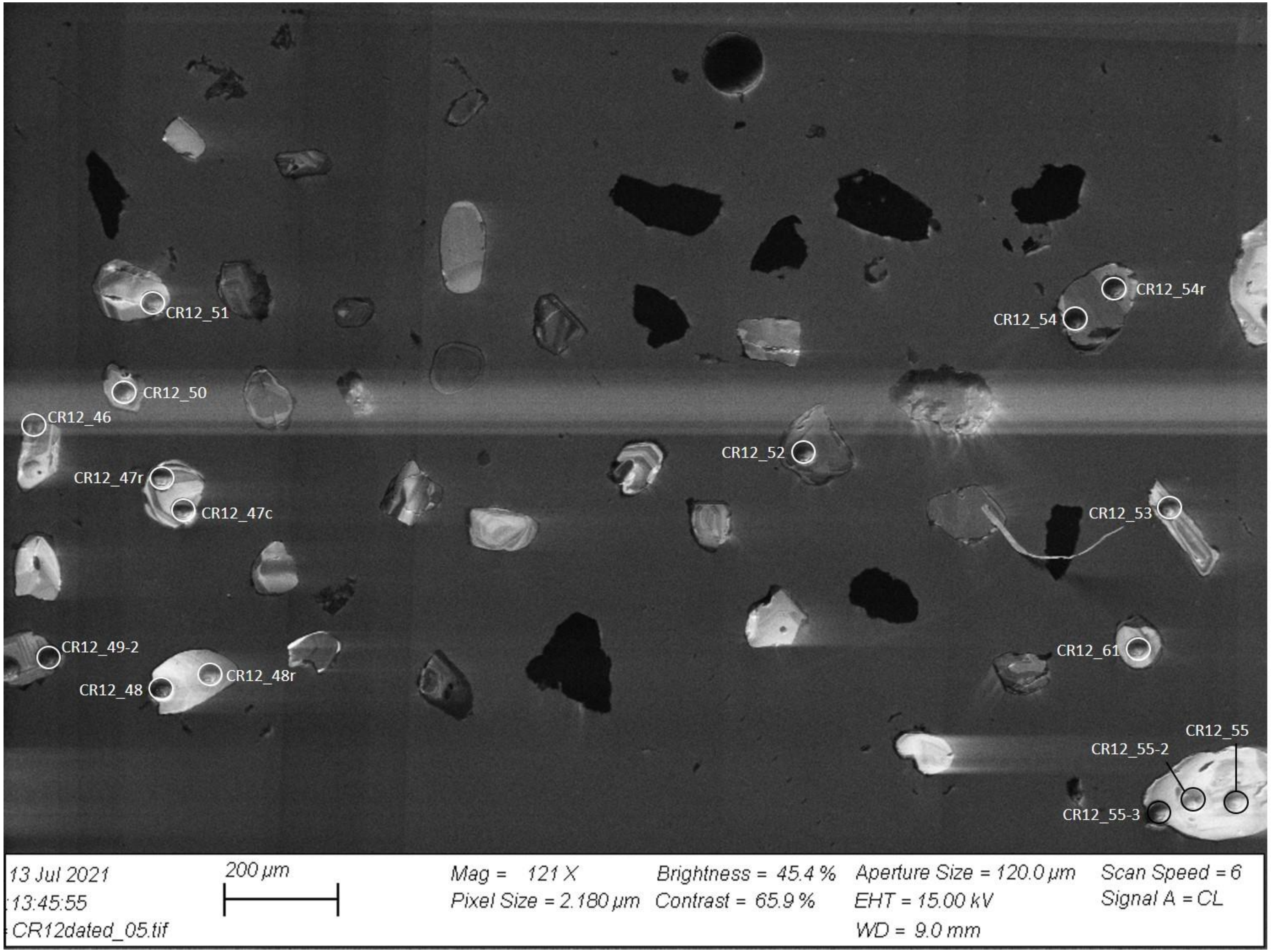

Appendix B: CL images of zircon grains after LA-ICP-MS. Analysed grains marked with sample name and a white circle indicating the impact crater from laser ablation.

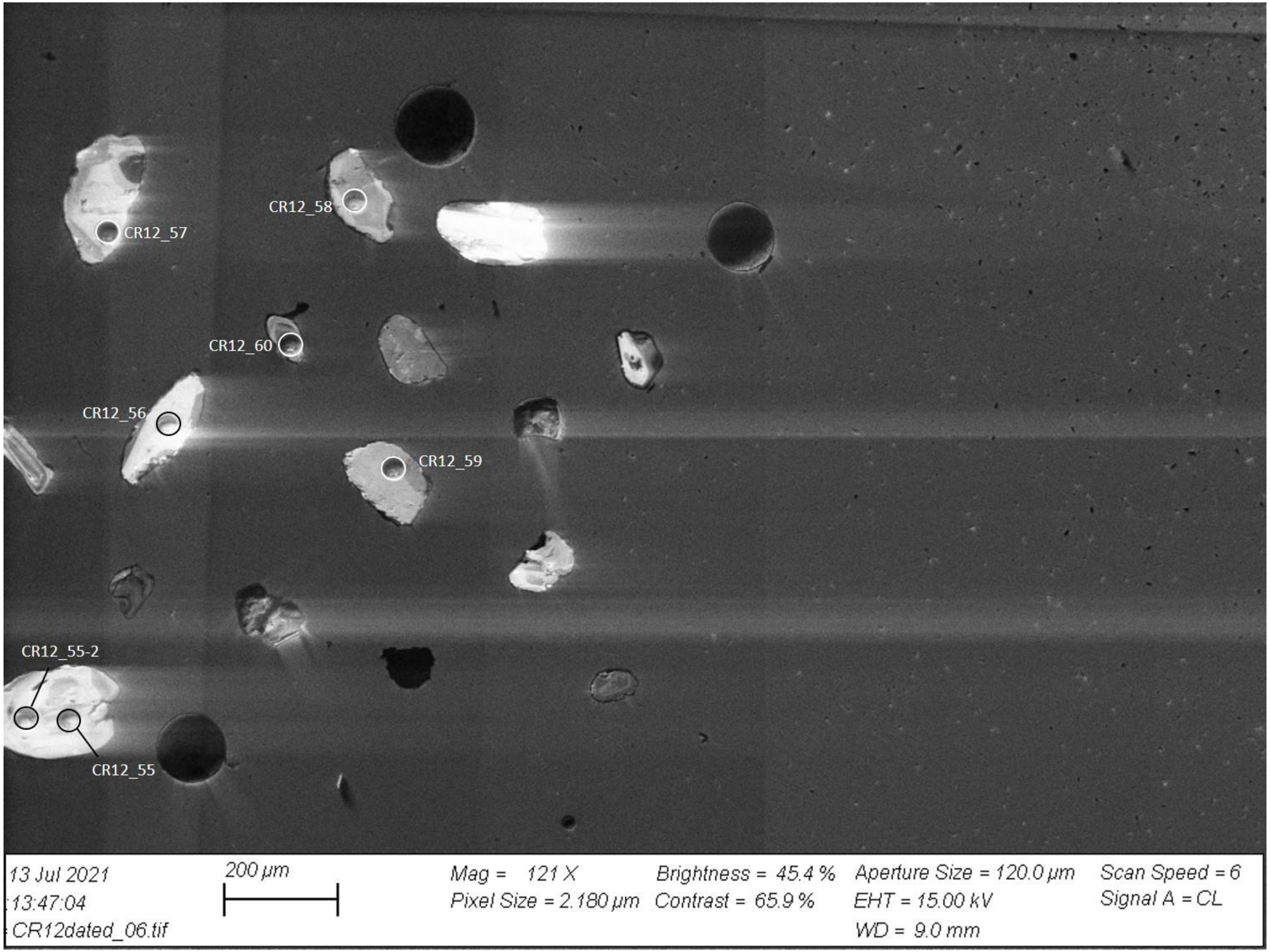

Appendix B: CL images of zircon grains after LA-ICP-MS. Analysed grains marked with sample name and a white circle indicating the impact crater from laser ablation.

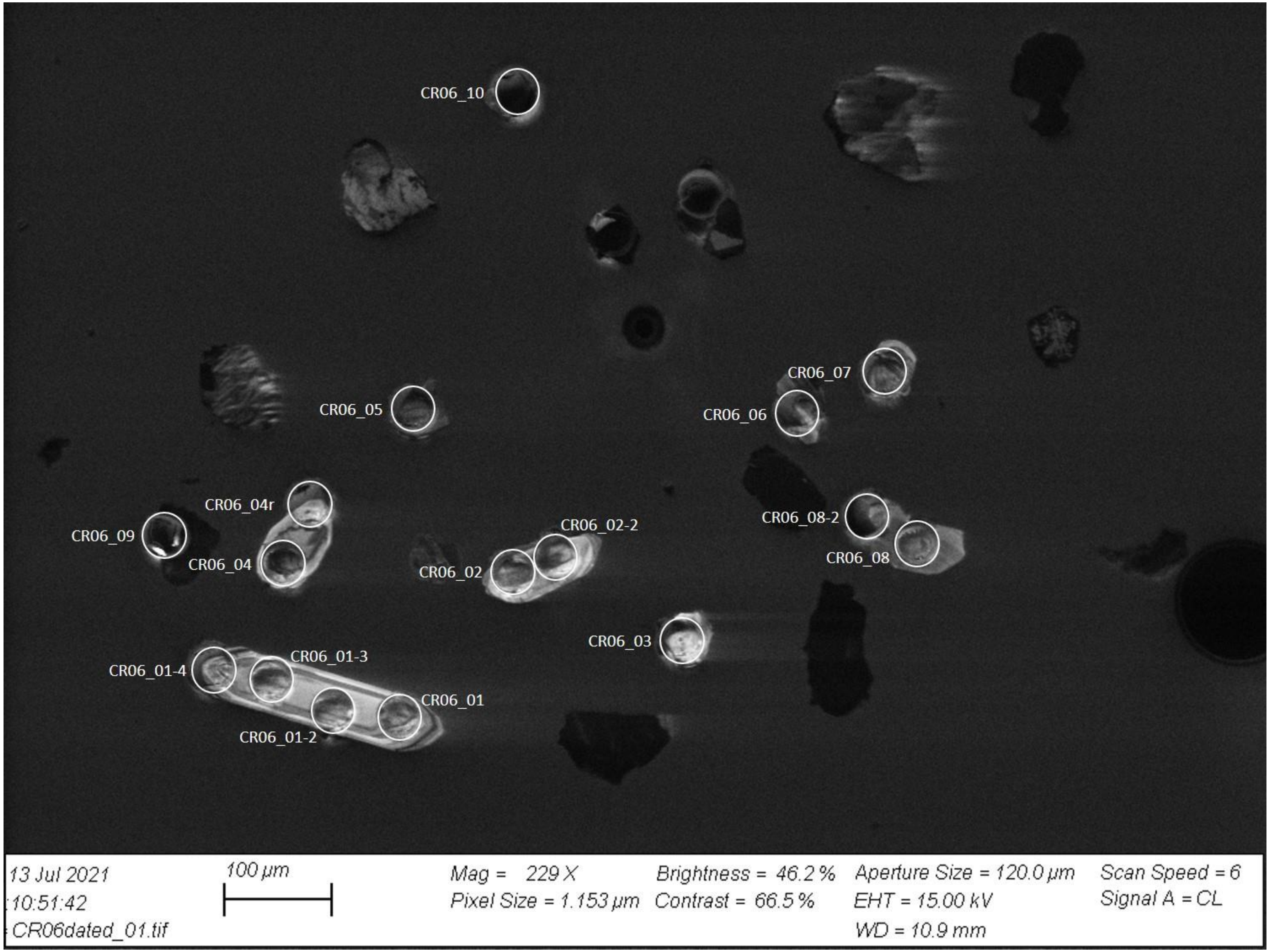

Appendix B: CL images of zircon grains after LA-ICP-MS. Analysed grains marked with sample name and a white circle indicating the impact crater from laser ablation.

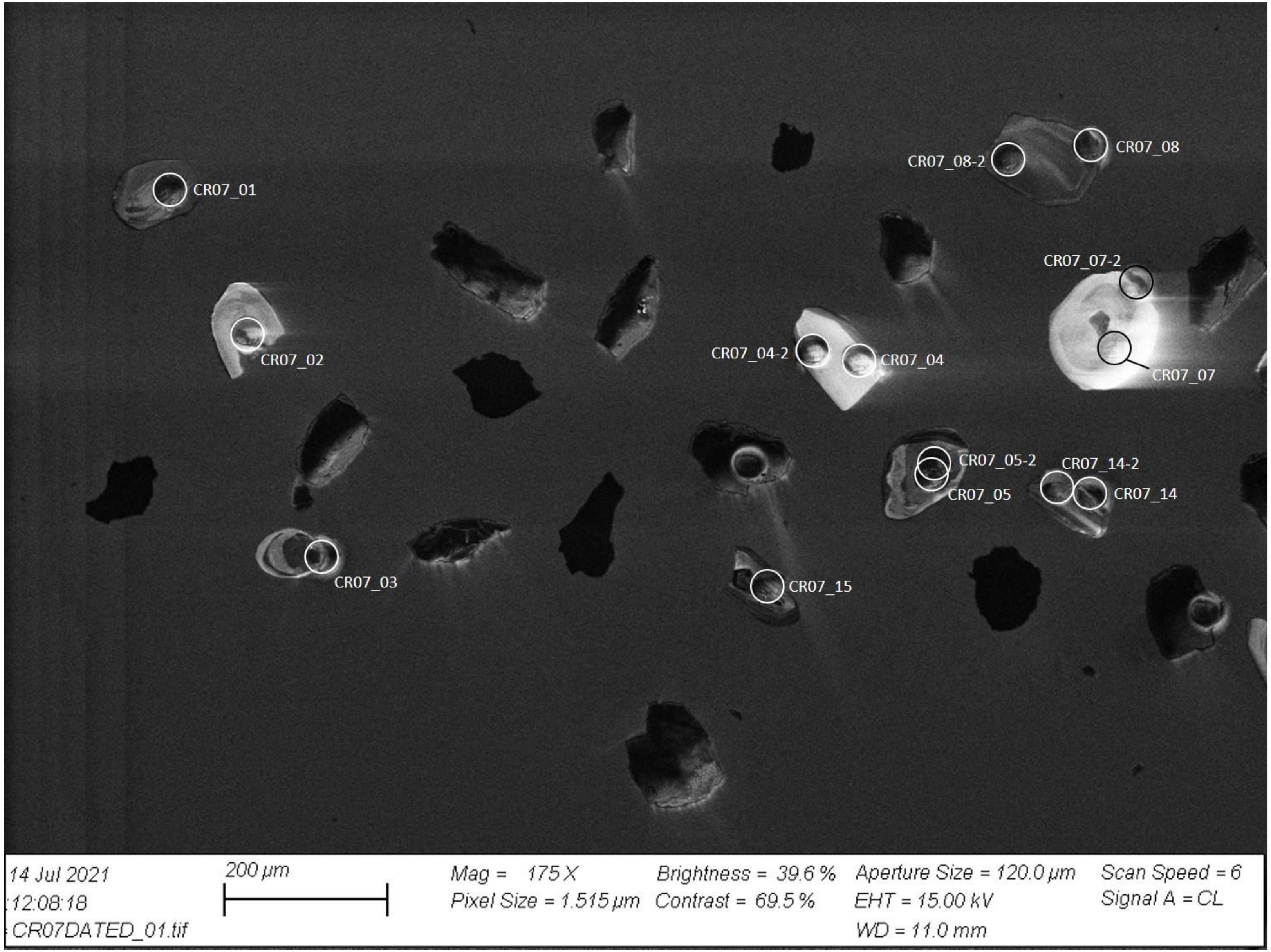

Appendix B: CL images of zircon grains after LA-ICP-MS. Analysed grains marked with sample name and a white circle indicating the impact crater from laser ablation.

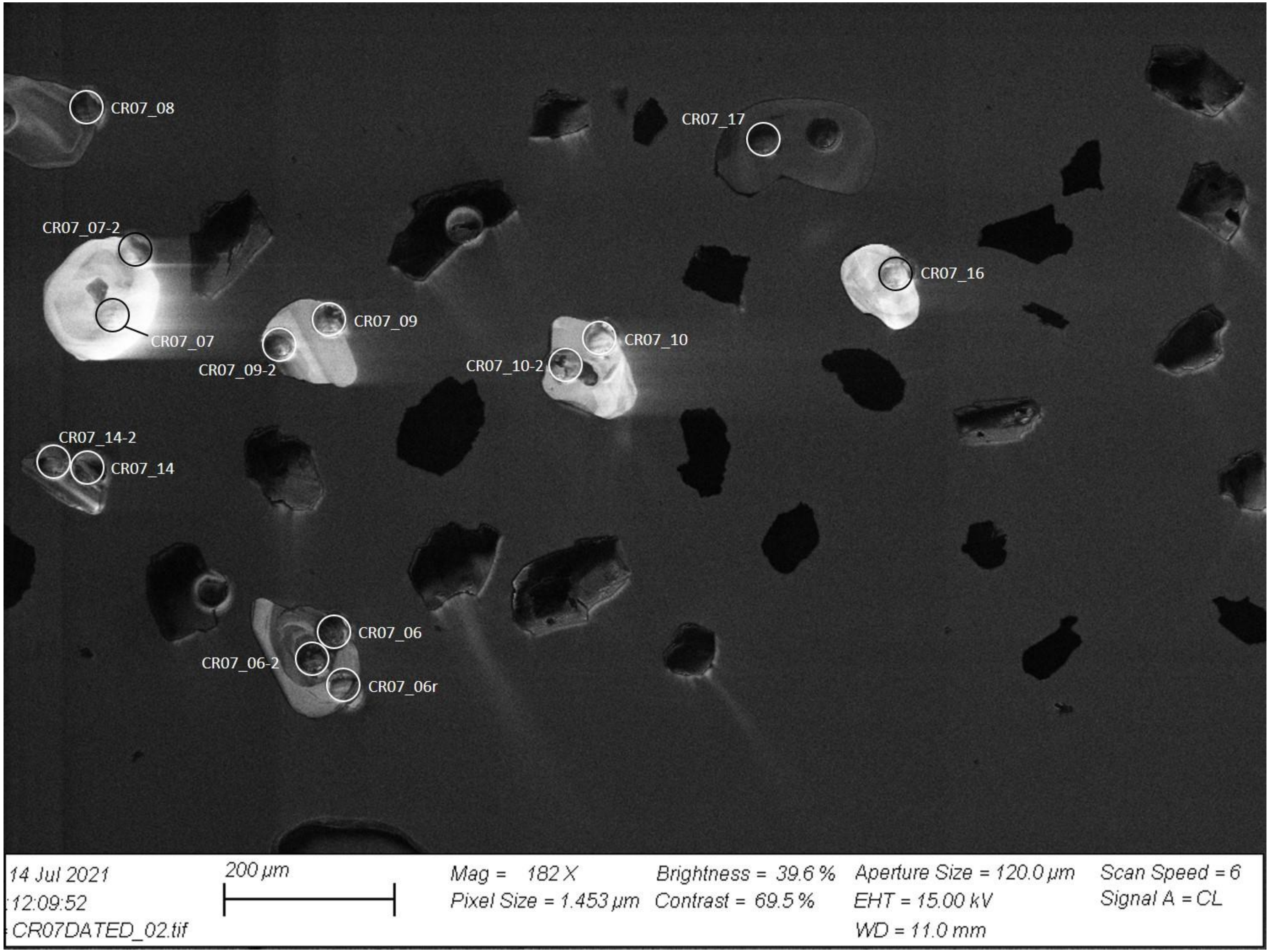

Appendix B: CL images of zircon grains after LA-ICP-MS. Analysed grains marked with sample name and a white circle indicating the impact crater from laser ablation.

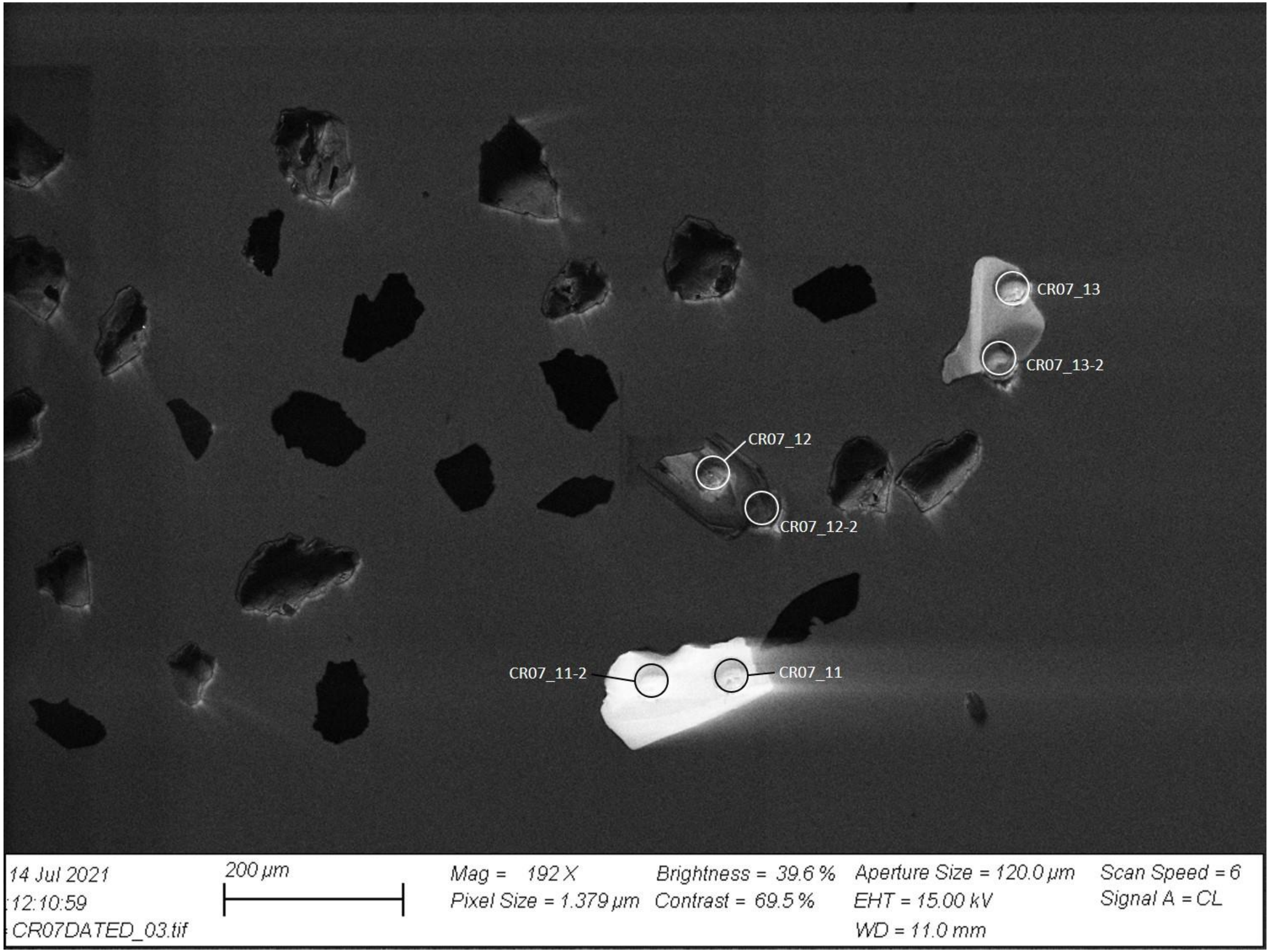

Appendix B: CL images of zircon grains after LA-ICP-MS. Analysed grains marked with sample name and a white circle indicating the impact crater from laser ablation.

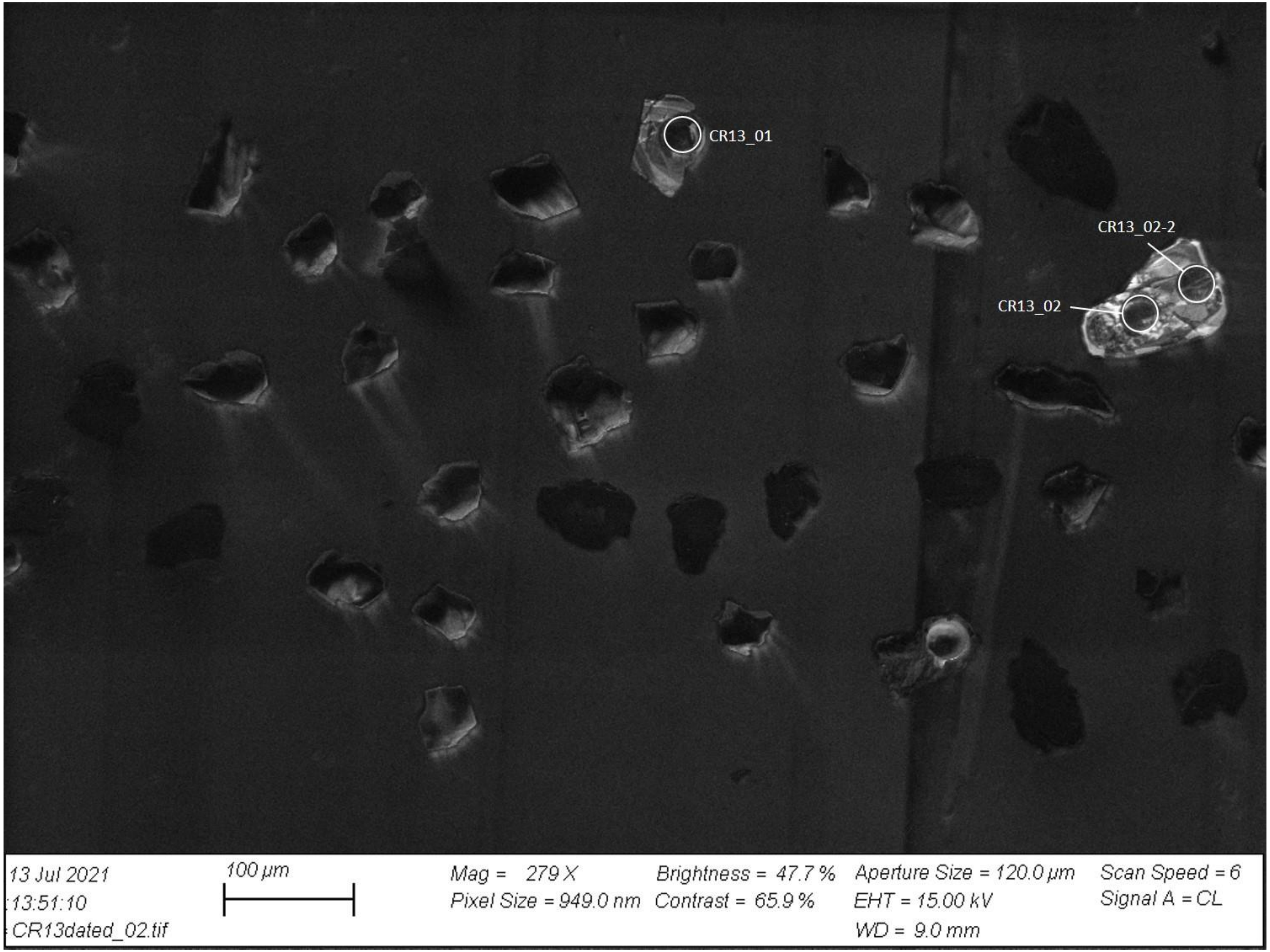

Appendix B: CL images of zircon grains after LA-ICP-MS. Analysed grains marked with sample name and a white circle indicating the impact crater from laser ablation.

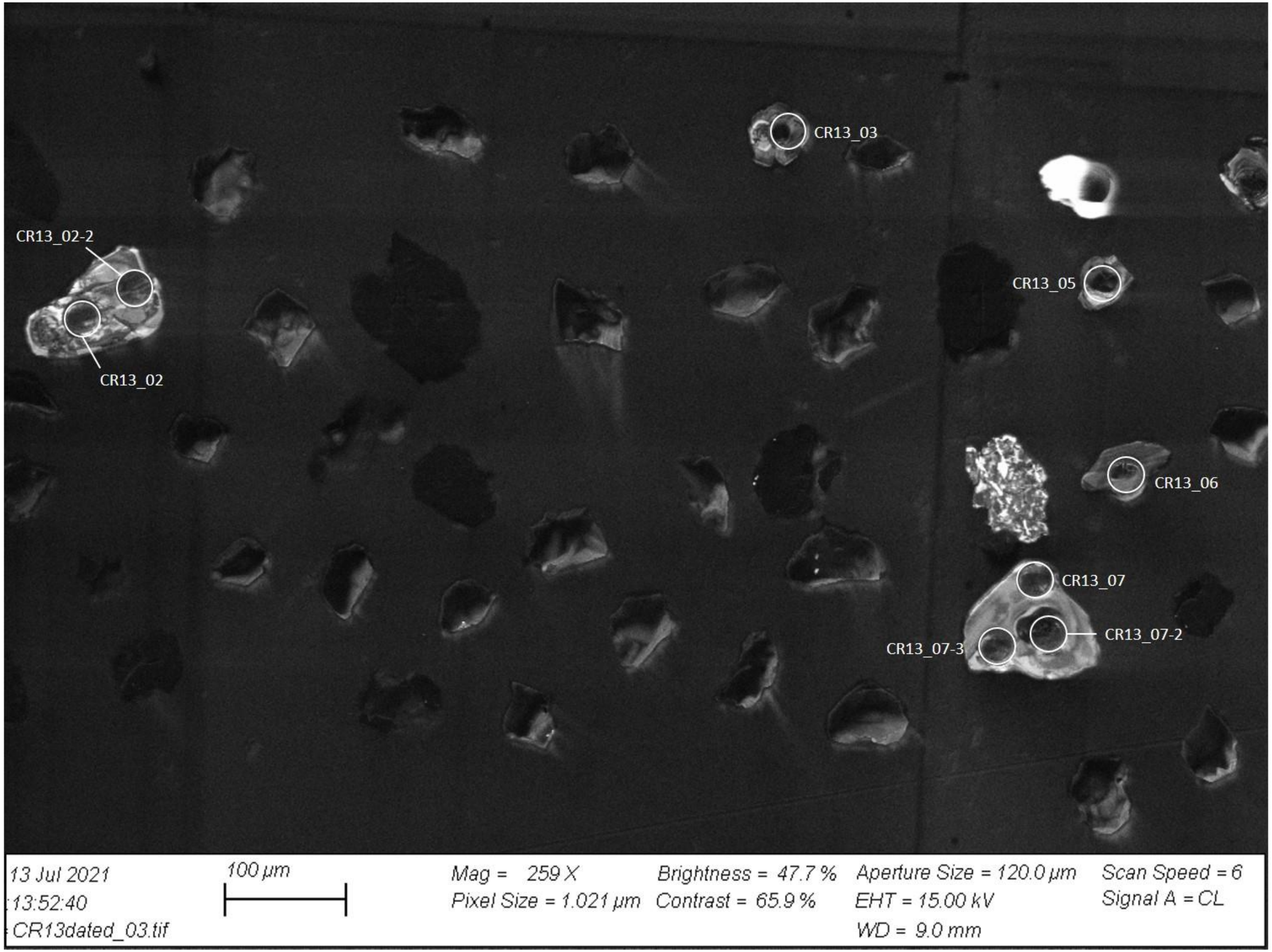

Appendix B: CL images of zircon grains after LA-ICP-MS. Analysed grains marked with sample name and a white circle indicating the impact crater from laser ablation.

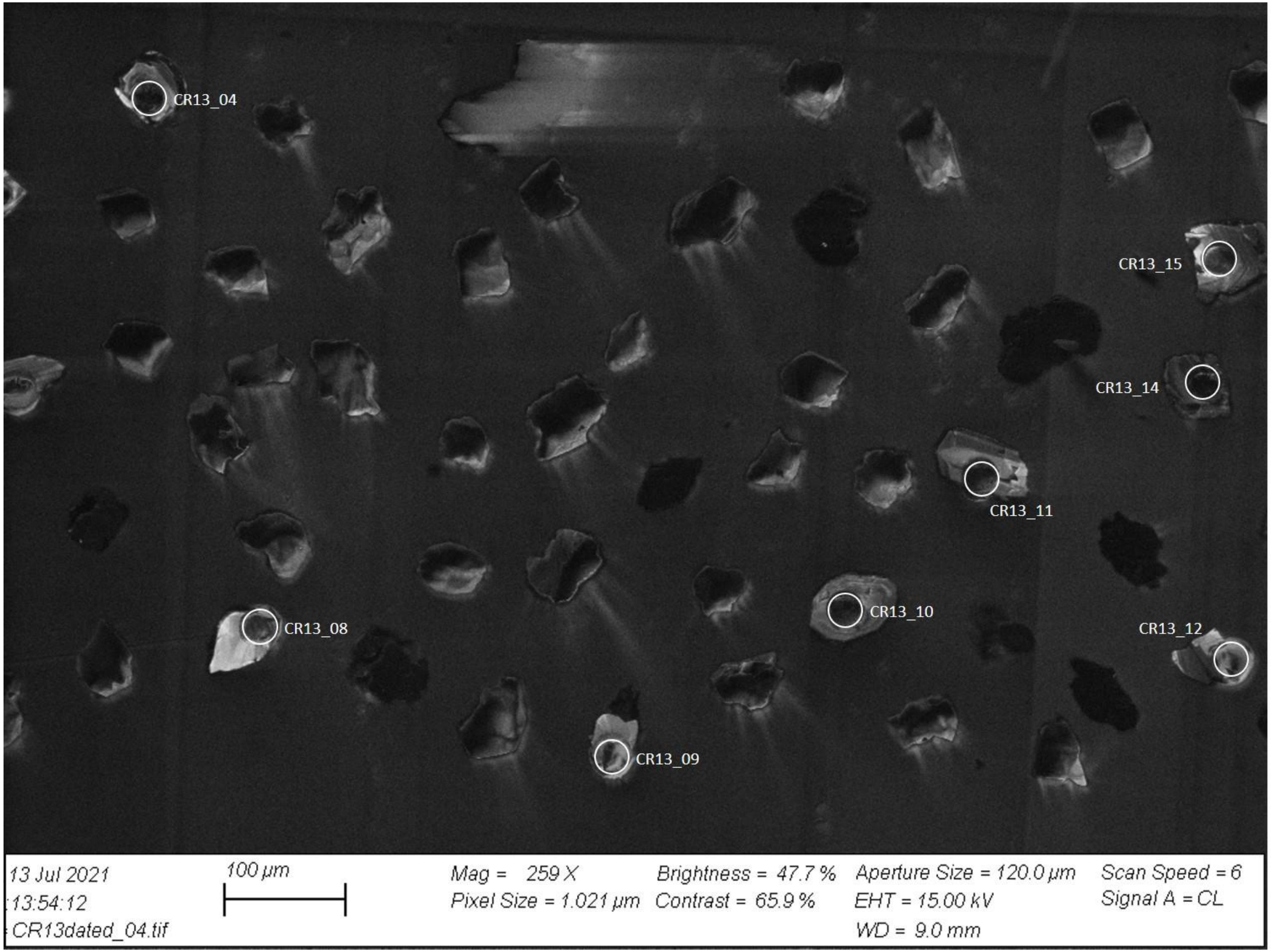

Appendix B: CL images of zircon grains after LA-ICP-MS. Analysed grains marked with sample name and a white circle indicating the impact crater from laser ablation.

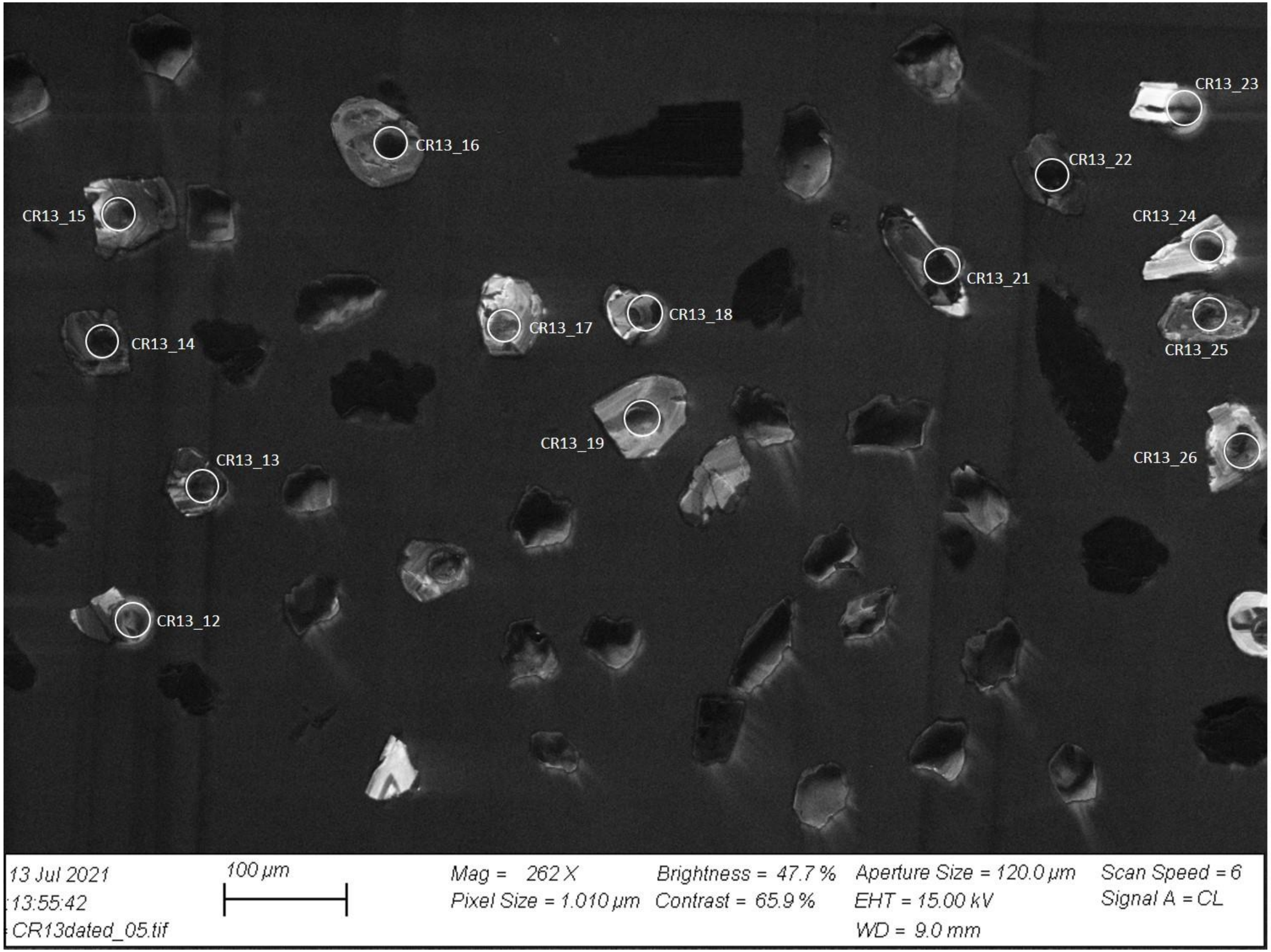

Appendix B: CL images of zircon grains after LA-ICP-MS. Analysed grains marked with sample name and a white circle indicating the impact crater from laser ablation.

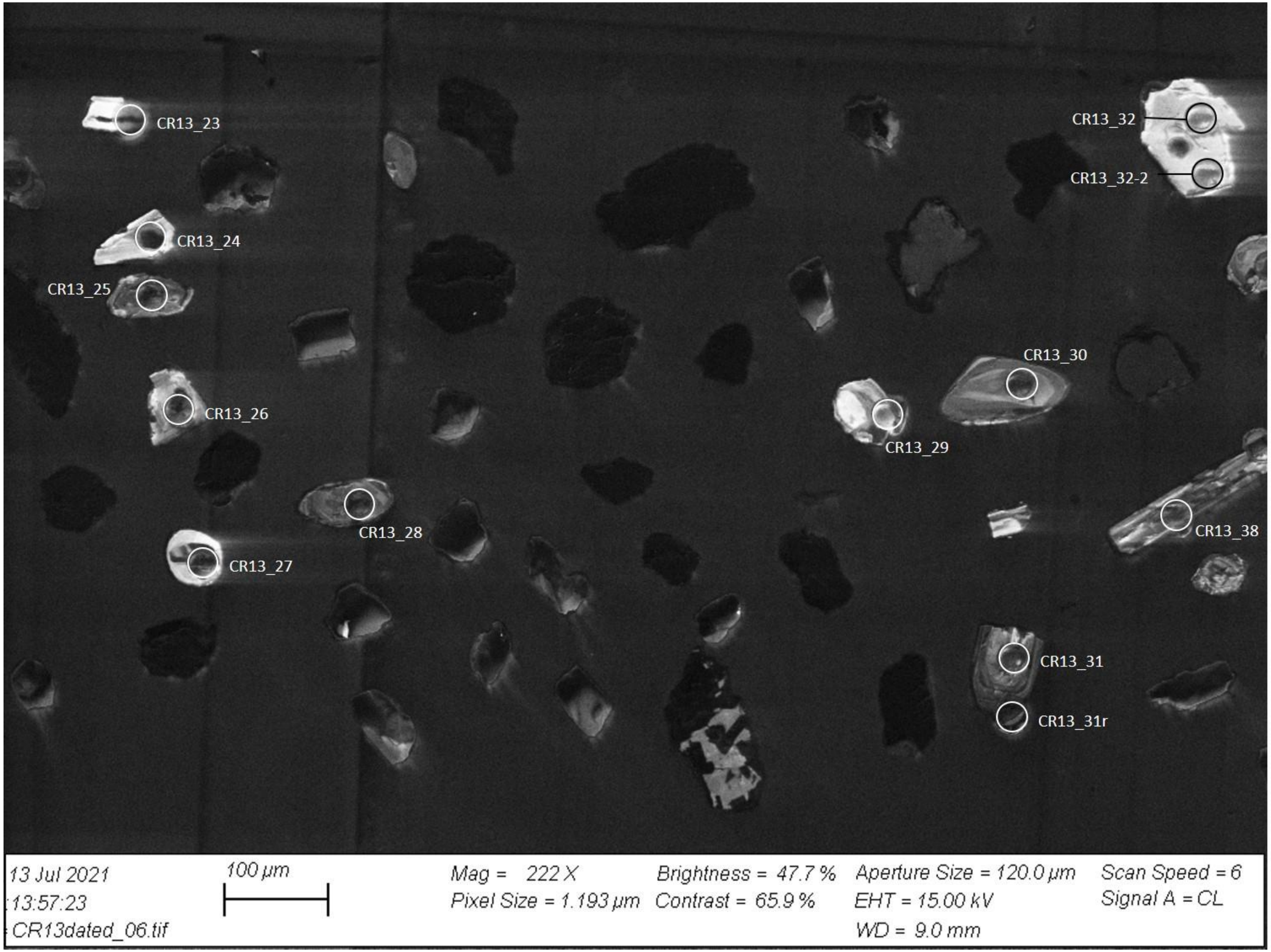

Appendix B: CL images of zircon grains after LA-ICP-MS. Analysed grains marked with sample name and a white circle indicating the impact crater from laser ablation.

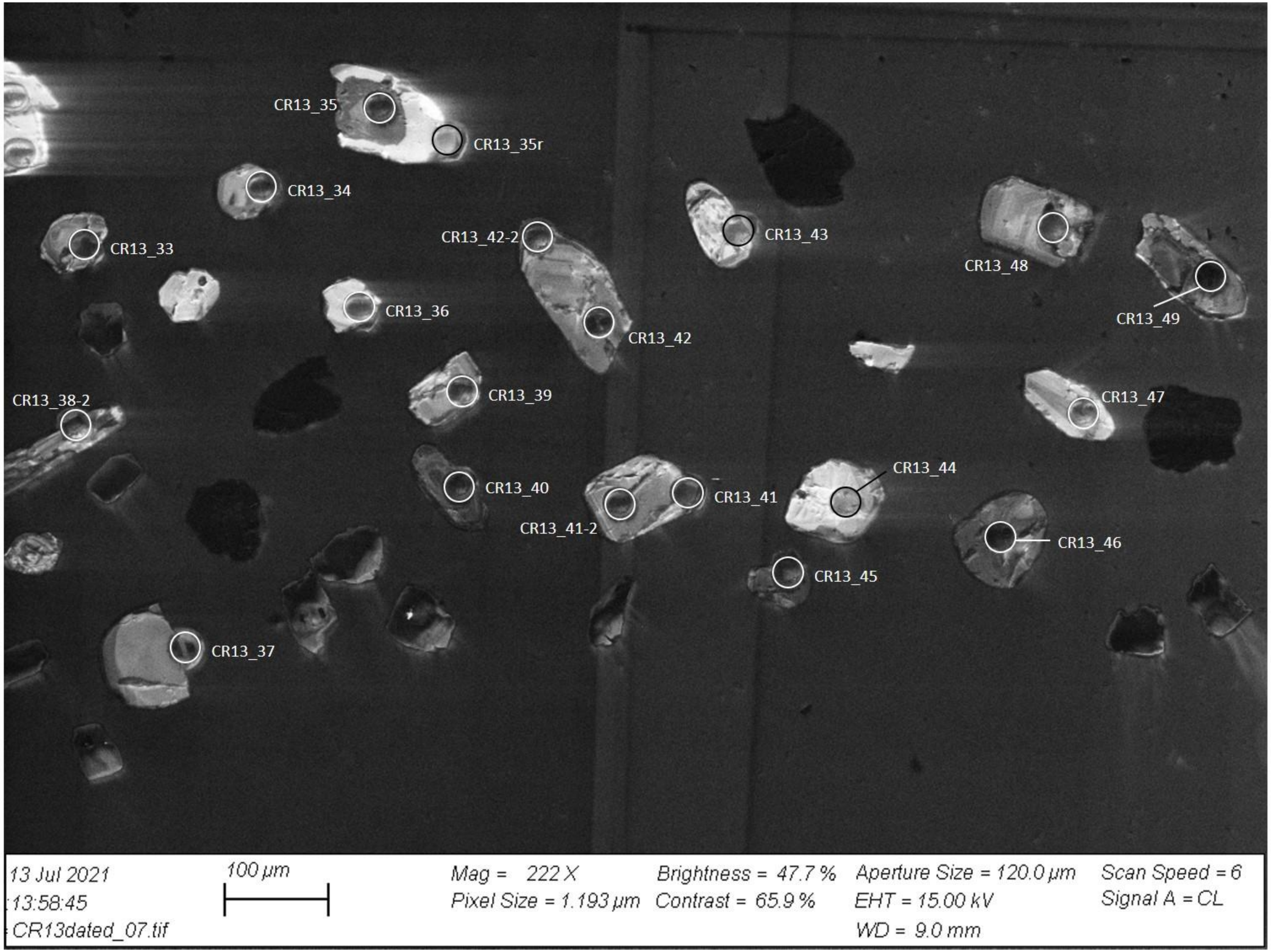

Appendix B: CL images of zircon grains after LA-ICP-MS. Analysed grains marked with sample name and a white circle indicating the impact crater from laser ablation.

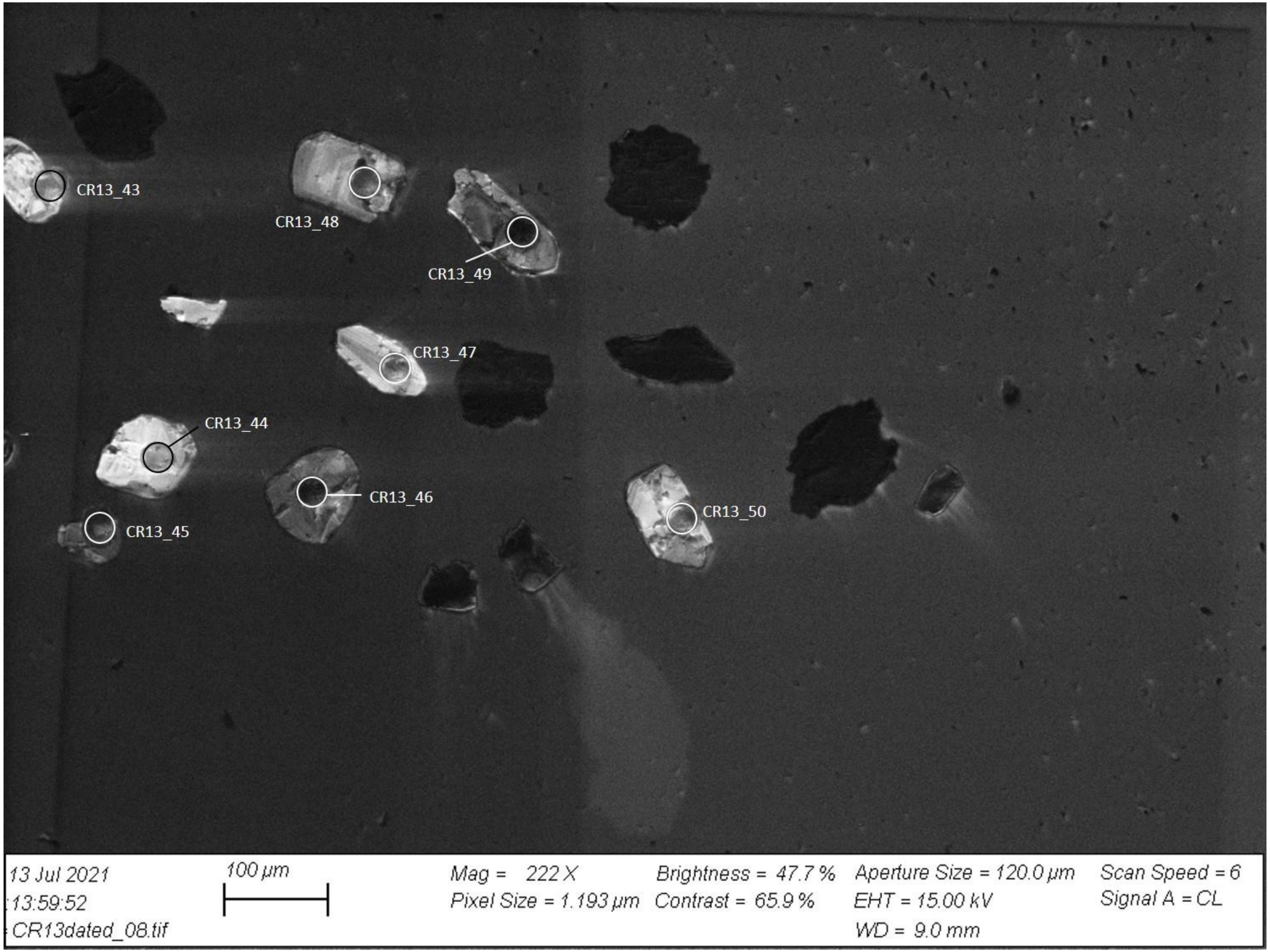

Appendix B: CL images of zircon grains after LA-ICP-MS. Analysed grains marked with sample name and a white circle indicating the impact crater from laser ablation.

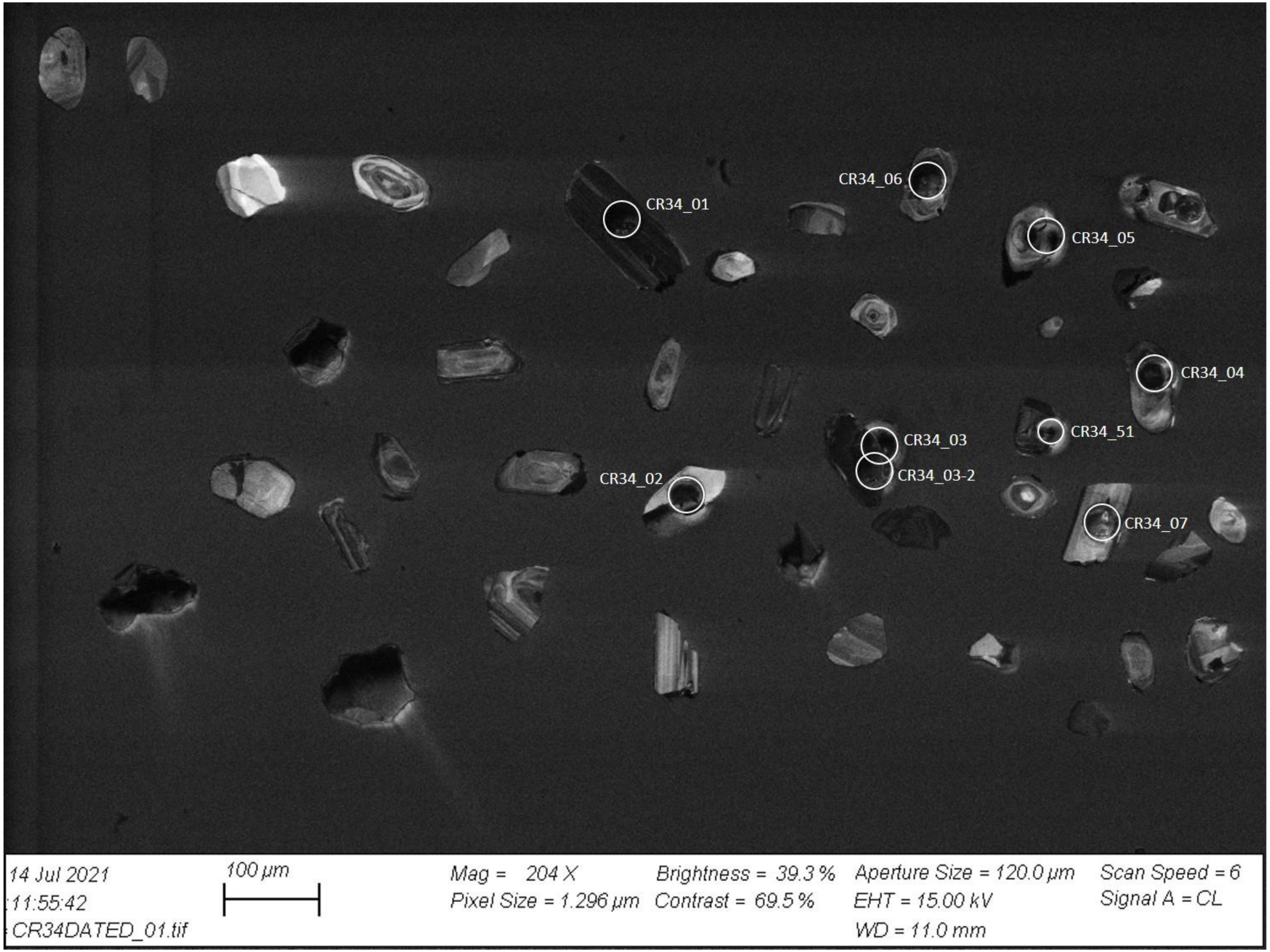

Appendix B: CL images of zircon grains after LA-ICP-MS. Analysed grains marked with sample name and a white circle indicating the impact crater from laser ablation.

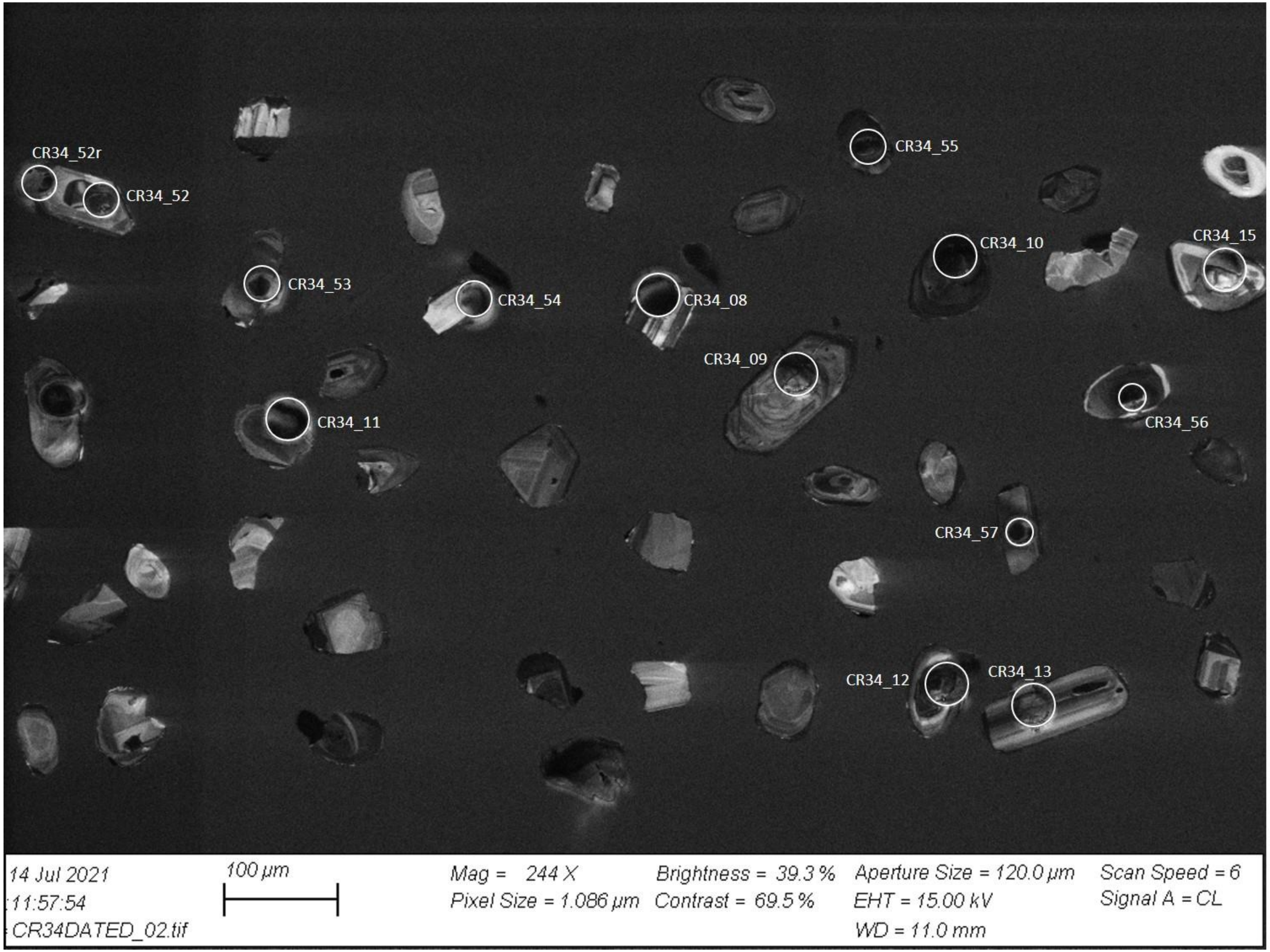

Appendix B: CL images of zircon grains after LA-ICP-MS. Analysed grains marked with sample name and a white circle indicating the impact crater from laser ablation.

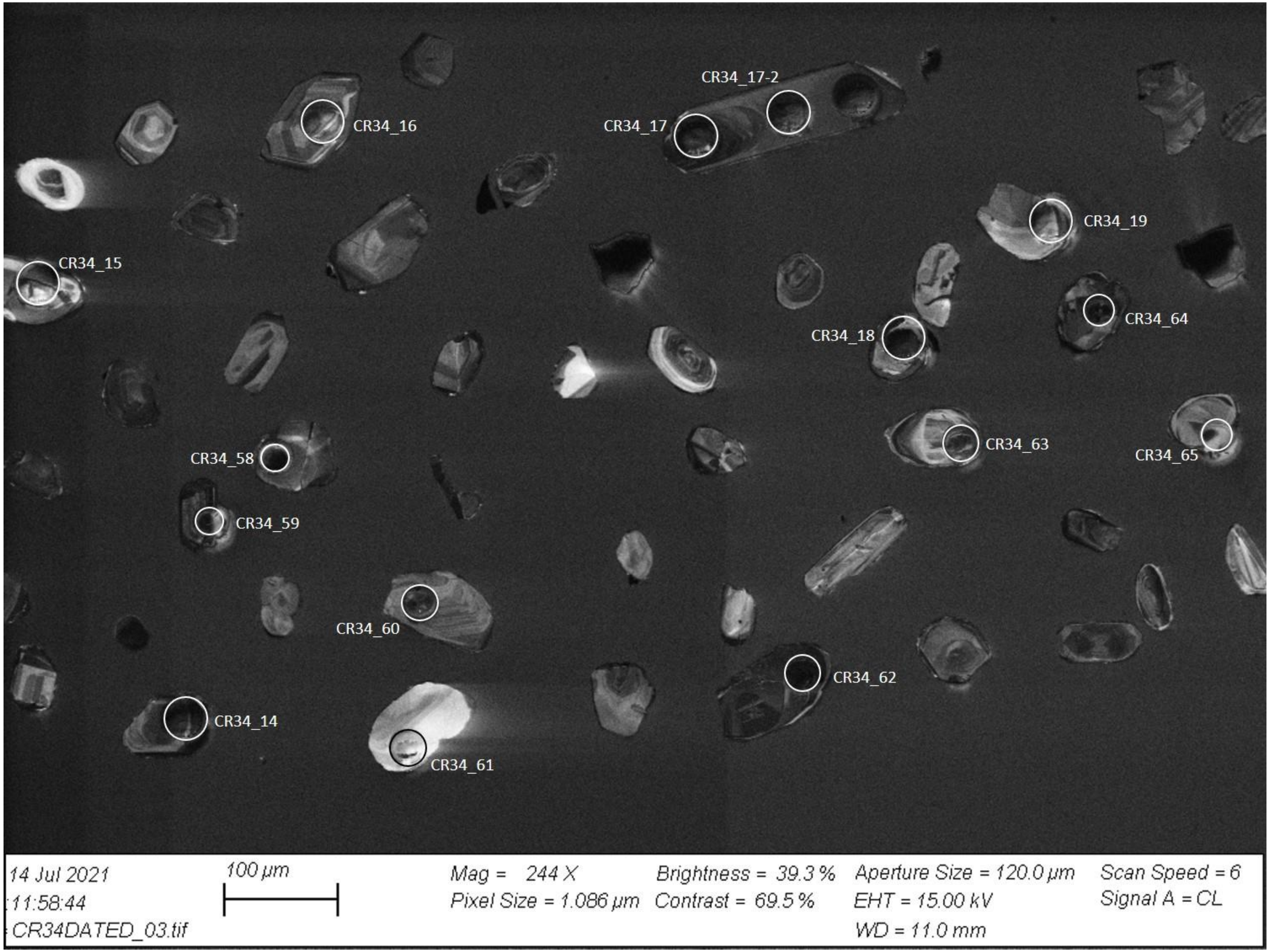

Appendix B: CL images of zircon grains after LA-ICP-MS. Analysed grains marked with sample name and a white circle indicating the impact crater from laser ablation.

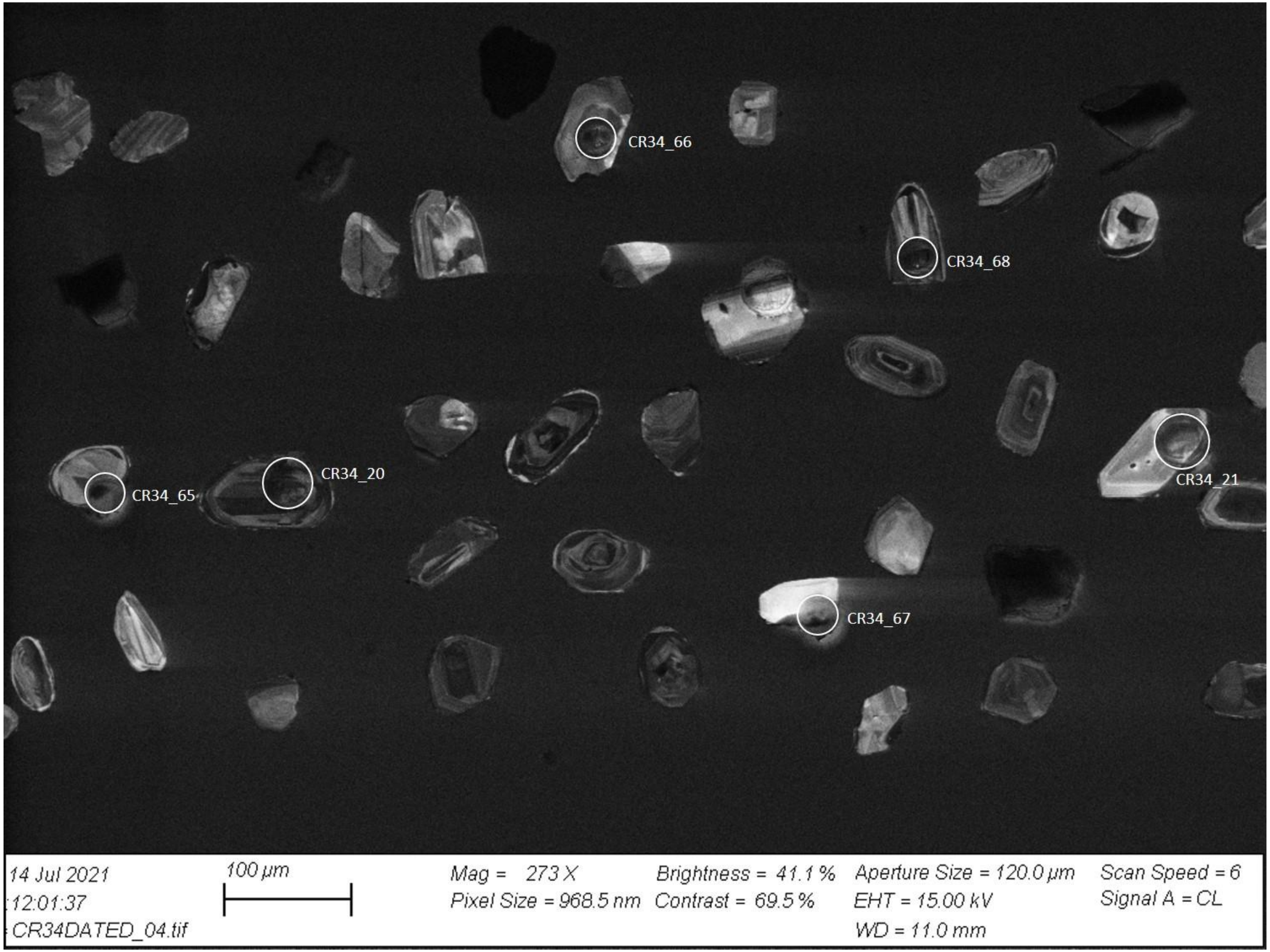

Appendix B: CL images of zircon grains after LA-ICP-MS. Analysed grains marked with sample name and a white circle indicating the impact crater from laser ablation.

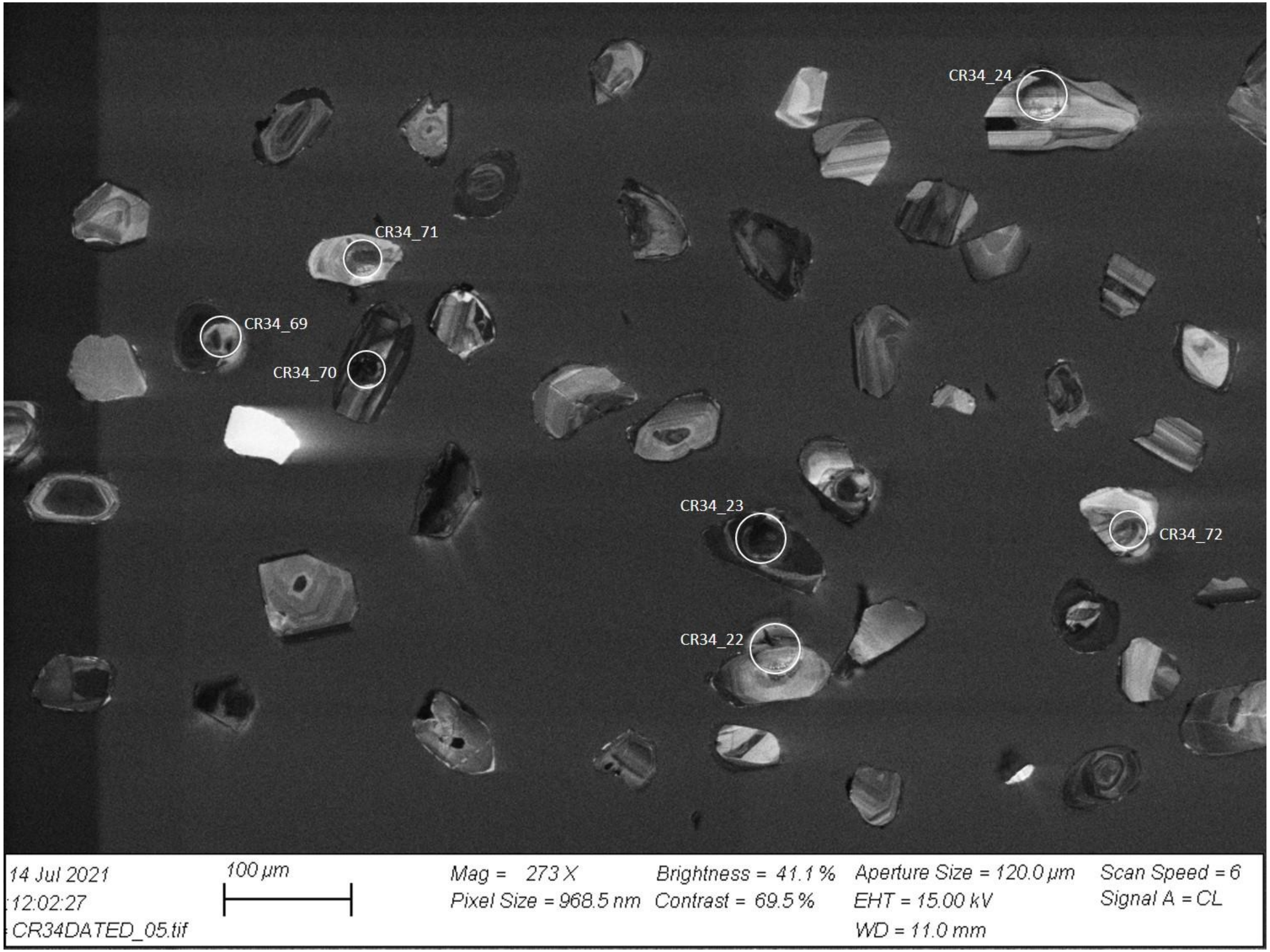

Appendix B: CL images of zircon grains after LA-ICP-MS. Analysed grains marked with sample name and a white circle indicating the impact crater from laser ablation.

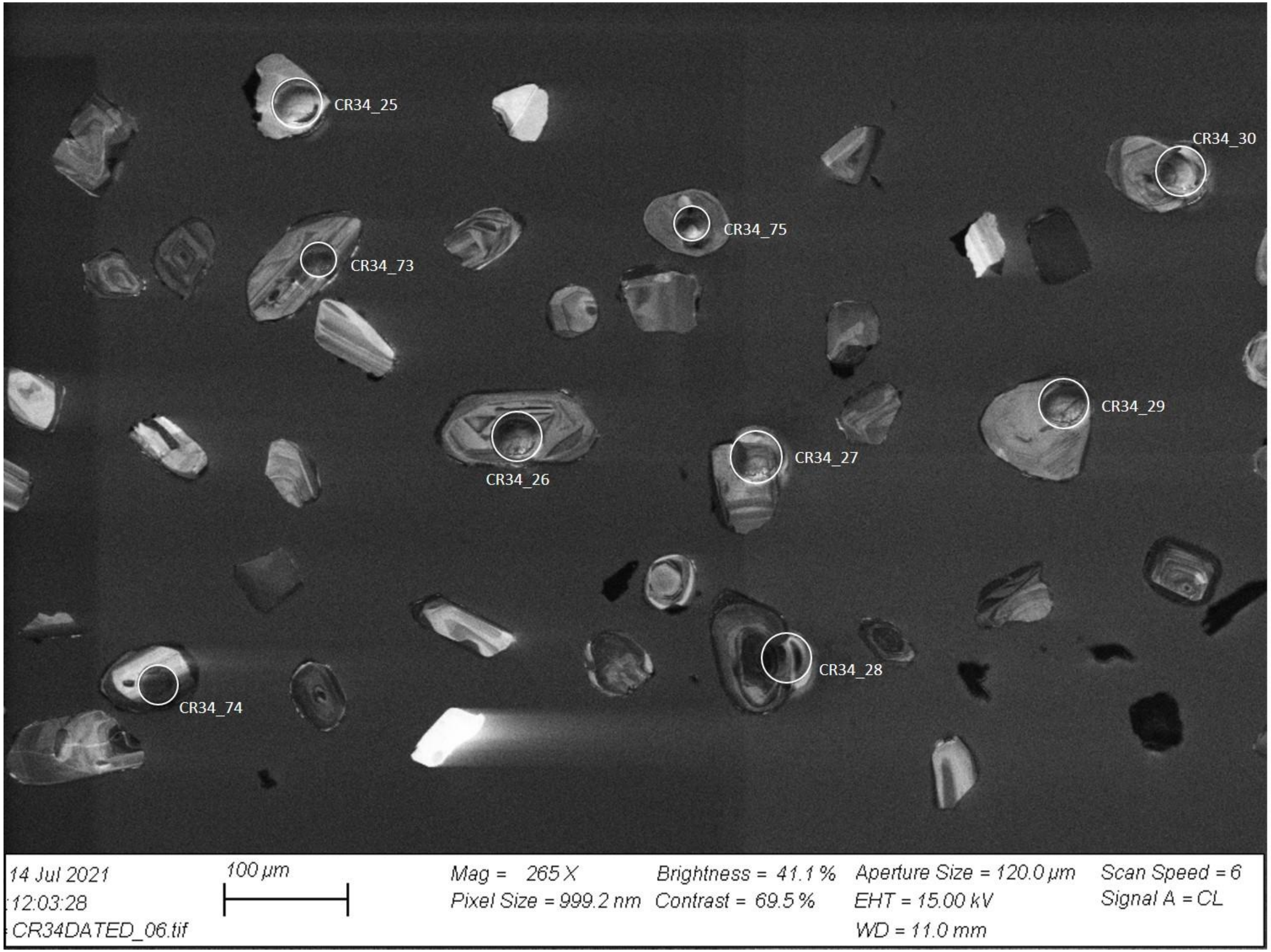

Appendix B: CL images of zircon grains after LA-ICP-MS. Analysed grains marked with sample name and a white circle indicating the impact crater from laser ablation.

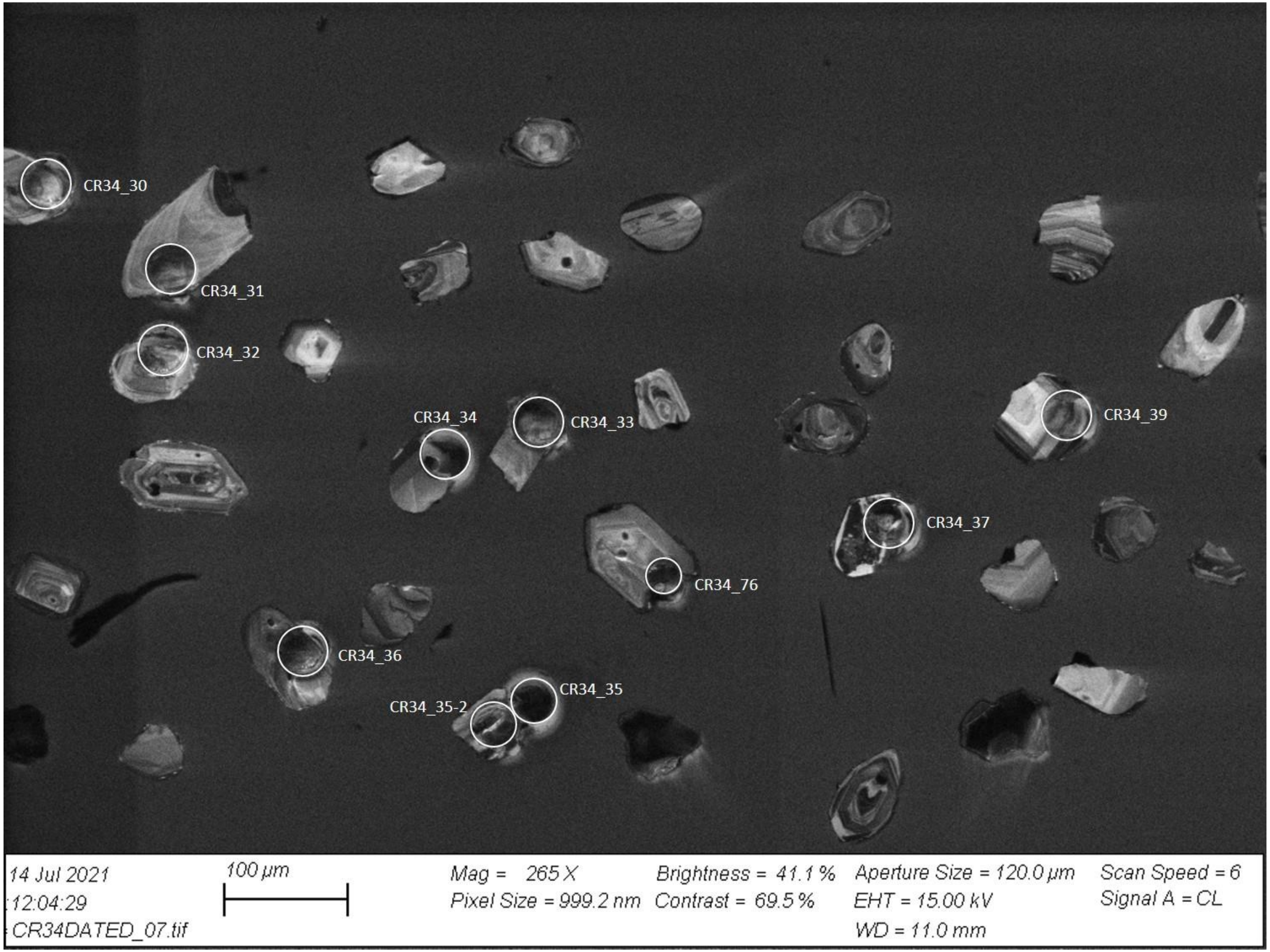

Appendix B: CL images of zircon grains after LA-ICP-MS. Analysed grains marked with sample name and a white circle indicating the impact crater from laser ablation.

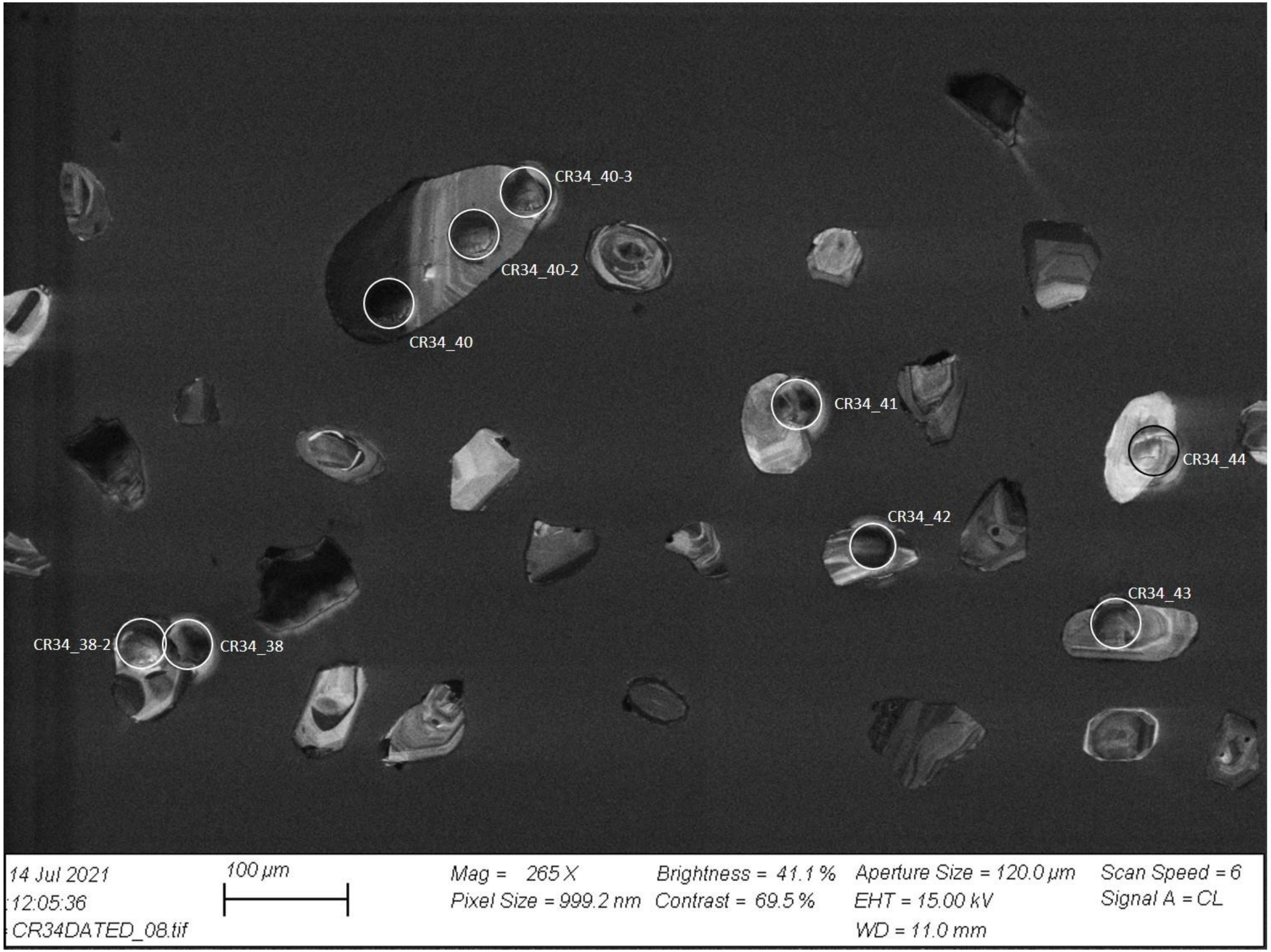

Appendix B: CL images of zircon grains after LA-ICP-MS. Analysed grains marked with sample name and a white circle indicating the impact crater from laser ablation.

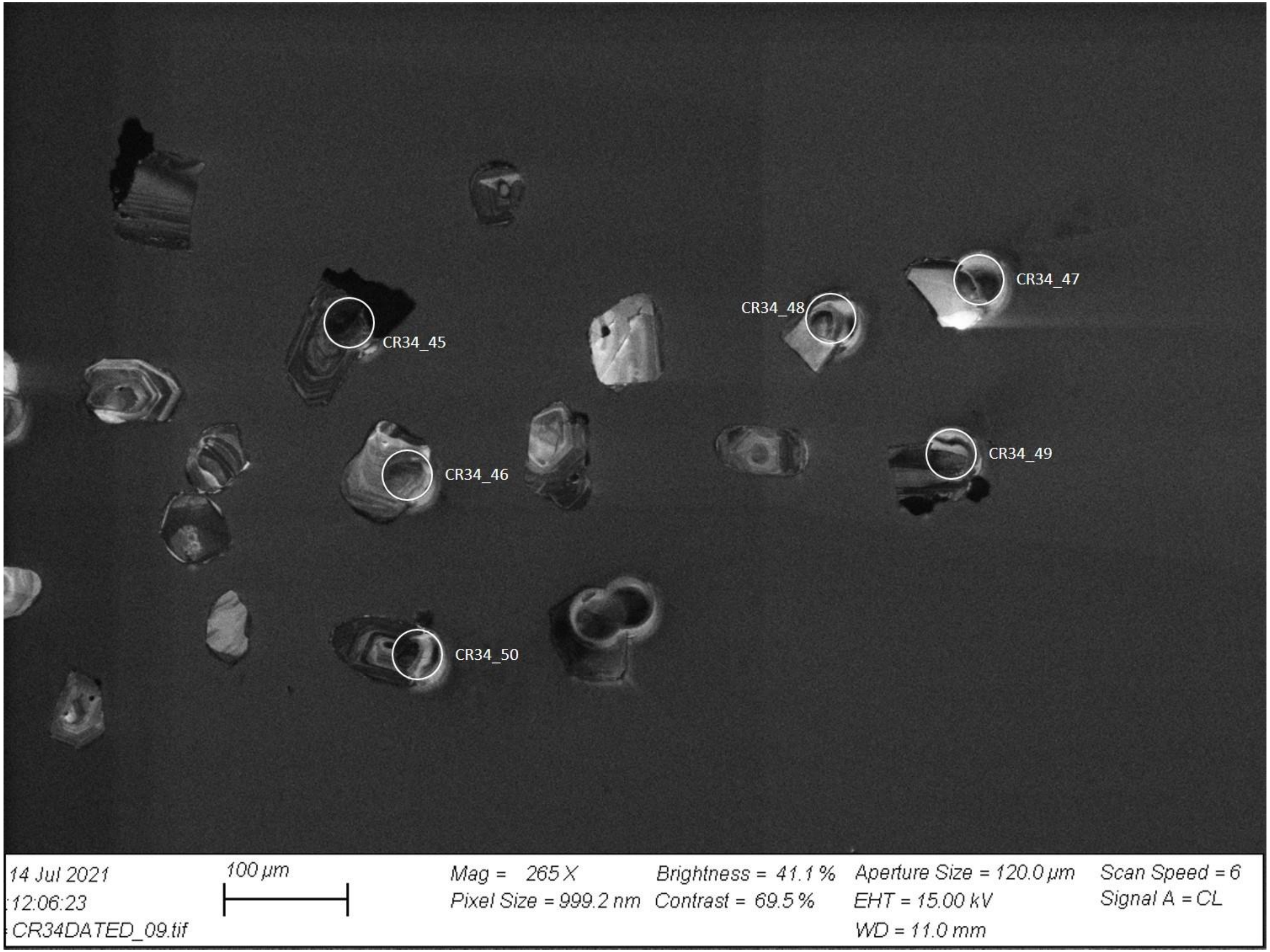

Appendix C Whole-rock geochemical data

SAMPLE	U-Pb	**SiO2**	**Al2O3**	**Fe2O3t**	**MgO**	**CaO**	**Na2O**	**K2O**	**TiO2**	**P2O5**	**MnO**	**LOI**	**sum**	**Nb**	**Ta**	**Hf**	**U**	**Pb**	**Nd**	**Sm**	**Eu**	**Yb**	**Lu**	**SREE**	**TOT/C**	**TOTS**	**La**	**Zr**	**Sc**	**Th**
	sample	%	%	%	%	%	%	%	%	%	%	%	%	PPM	PPM	PPM	PPM	PPM	PPM	PPM	PPM	PPM	PPM	**PPM**	%	%	PPM	PPM	PPM	PPM
		0.01	0.01	0.04	0.01	0.01	0.01	0.01	0.01	0.010	0.01	0.1	0.0	0.1	0.1	0.1	0.1	0.1	0.3	0.05	0.02	0.05	0.01		0.02	0.02	0.1	0.1	1	0.2
Chameis Subterrane																														
G20	CR11	56.13	16.94	7.87	4.64	0.52	0.45	5.96	0.96	0.057	0.10	5.4	99.0	19.6	1.4	5.9	3.0	2.4	36.5	7.14	1.50	4.57	0.76	50.5	0.01	bdl	38.5	192.2	22	12.9
G21	CR11	59.07	19.16	5.79	2.85	0.62	0.38	6.67	0.88	0.033	0.13	4.0	99.6	19.4	1.4	6.1	3.1	1.8	26.6	5.19	1.09	3.32	0.55	36.7	0.03	bdl	28.0	203.5	28	14.5
G22	CR11	59.42	16.90	7.12	3.80	0.53	0.61	5.99	0.81	0.067	0.09	4.7	100.0	22.5	2.1	5.7	3.2	2.2	23.2	4.54	0.95	2.91	0.48	32.1	0.04	bdl	24.5	219.4	32	14.7
G23	CR11	57.49	17.94	7.60	4.88	0.72	0.34	4.36	0.98	0.076	0.13	4.8	99.3	19.7	1.5	5.1	2.9	8.6	29.9	5.84	1.22	3.74	0.62	41.3	bdl	bdl	31.5	174.8	28	12.1
G24	CR11	65.33	15.19	6.09	2.41	0.50	0.56	4.84	0.83	0.048	0.14	3.9	99.8	19.4	1.6	5.2	2.5	15.1	17.6	3.81	0.97	3.21	0.48	26.1	bdl	0.03	18.0	193.0	22	12.5
G25A	CR12	78.85	8.16	4.08	3.34	0.19	1.16	0.22	0.25	0.047	0.07	3.1	99.5	9.8	0.8	4.2	1.3	3.4	17.1	3.57	0.83	1.98	0.28	23.8	bdl	bdl	16.2	135.3	6	8.3
G25D	CR12	80.30	8.42	3.78	3.17	0.18	1.22	0.20	0.26	0.039	0.06	2.5	100.1	10.2	0.9	3.9	0.9	3.0	22.5	4.68	1.09	2.60	0.37	31.2	bdl	bdl	21.3	135.2	5	8.6
G25E	CR12	73.57	9.72	5.64	4.66	0.20	1.51	0.22	0.38	0.058	0.07	3.7	99.7	12.3	1.0	5.1	1.5	3.3	18.2	3.79	0.88	2.11	0.30	25.3	0.02	bdl	17.3	173.0	7	9.8
G25F	CR12	65.33	11.53	2.49	3.47	4.68	2.84	0.44	0.32	0.184	0.09	9.0	100.4	11.6	1.1	7.2	1.1	3.5	16.5	3.35	0.78	1.86	0.26	22.7	1.98	bdl	15.6	239.8	8	8.0
G25G	CR12	75.98	10.30	3.81	3.29	0.24	2.05	0.15	0.31	0.038	0.09	2.9	99.1	12.1	1.1	3.9	2.5	3.4	19.3	4.01	0.94	2.23	0.32	26.8	0.04	bdl	18.3	133.2	8	12.6
G25H	CR12	74.70	8.60	5.23	4.77	0.31	1.68	0.34	0.33	0.049	0.09	3.0	99.1	11.0	0.9	4.3	2.2	3.9	20.6	4.24	0.99	2.36	0.33	28.5	0.05	bdl	19.5	151.4	6	10.4
G26	CR12	42.56	13.22	11.30	5.98	14.60	2.05	0.33	1.34	0.224	0.09	8.0	99.7	8.9	0.8	3.1	0.3	3.1	11.8	3.76	1.40	3.67	0.54	20.3	1.41	bdl	8.1	104.7	31	3.5
G27	CR12	44.86	12.97	11.77	6.02	11.26	2.08	0.35	1.40	0.199	0.09	8.8	99.8	9.8	0.9	3.2	0.4	3.3	8.5	2.62	0.98	2.55	0.38	15.0	0.71	bdl	5.9	105.7	38	3.5
G28	CR12	44.56	14.67	11.14	5.86	11.58	2.05	0.49	1.44	0.149	0.09	7.4	99.4	10.7	0.8	3.3	0.4	1.6	9.1	2.78	1.04	2.71	0.40	16.0	0.81	bdl	6.3	106.8	35	2.9
G29	CR12	41.80	15.39	11.10	6.63	12.27	3.05	0.12	1.24	0.140	0.15	8.1	100.0	12.1	0.7	2.8	0.5	1.1	11.3	3.60	1.34	3.51	0.52	20.3	1.09	bdl	7.7	100.9	35	2.7
G30	CR12	43.78	13.72	11.58	6.24	11.67	2.23	0.32	1.55	0.188	0.11	8.8	100.2	12.5	1.1	3.1	0.2	2.3	10.0	3.11	1.16	3.03	0.45	17.7	1.15	bdl	6.9	116.3	41	4.4
G31	CR12	46.39	14.02	11.17	5.87	12.50	3.09	0.60	1.17	0.180	0.12	4.6	99.7	12.2	0.7	3.3	0.2	1.5	11.1	3.12	1.21	2.78	0.46	18.7	0.79	bdl	9.0	90.5	38	3.3
G32	CR12	46.84	12.08	10.42	5.78	13.41	2.20	0.32	1.18	0.178	0.10	7.8	100.3	11.2	0.8	2.5	0.3	2.8	9.3	2.94	1.10	2.87	0.42	16.6	1.38	bdl	6.3	98.4	32	3.1
G51	CR13	71.39	13.49	2.42	1.73	0.61	6.26	1.16	0.56	0.014	0.14	1.5	99.3	13.3	1.0	6.5	1.3	2.5	23.4	4.78	0.83	2.43	0.32	31.7	0.04	bdl	28.0	190.6	7	18.3
G52	CR13	72.19	12.88	2.03	1.40	1.67	5.53	0.85	0.47	0.018	0.14	2.6	99.8	12.7	1.1	5.5	1.4	2.2	12.2	2.63	0.57	3.35	0.60	19.3	0.05	0.04	12.3	183.0	8	13.1
G53	CR13	75.20	13.07	1.93	1.36	0.53	5.25	0.90	0.47	0.017	0.12	1.0	99.8	12.9	1.1	5.9	1.6	3.5	13.5	2.88	0.62	3.67	0.66	21.3	0.05	bdl	13.8	176.7	5	16.2

Appendix C Whole-rock geochemical data

SAMPLE	U-Pb	SiO2	Al2O3	Fe2O3t	MgO	CaO	Na2O	K2O	TiO2	P2O5	MnO	LOI	sum	Nb	Ta	Hf	U	Pb	Nd	Sm	Eu	Yb	Lu	SREE	TOT/C	TOTS	La	Zr	Sc	Th
	sample	%	%	%	%	%	%	%	%	%	%	%	%	PPM	PPM	PPM	PPM	PPM	PPM	PPM	PPM	PPM	PPM	PPM	%	%	PPM	PPM	PPM	PPM
		0.01	0.01	0.04	0.01	0.01	0.01	0.01	0.01	0.010	0.01	0.1	0.0	0.1	0.1	0.1	0.1	0.1	0.3	0.05	0.02	0.05	0.01		0.02	0.02	0.1	0.1	1	0.2
G54	CR13	69.01	14.63	2.34	1.46	1.07	5.63	1.12	0.53	0.019	0.14	3.3	99.2	14.3	1.2	5.8	1.4	2.8	20.4	4.19	0.73	2.13	0.28	27.8	0.09	bdl	24.5	180.8	4	15.1
G55	CR13	67.81	13.91	3.41	2.94	1.38	5.71	1.00	0.56	0.036	0.14	2.3	99.2	14.9	1.1	6.7	1.5	2.4	22.0	4.78	0.90	3.78	0.55	32.0	0.15	bdl	22.4	219.3	5	16.4
G57	CR13	69.18	13.83	2.15	1.35	1.61	6.54	0.92	0.52	0.019	0.17	2.9	99.2	13.7	0.8	6.1	1.9	1.8	19.7	4.23	0.79	3.35	0.48	28.6	0.11	0.04	20.2	194.0	8	16.7
G58	CR13	46.76	15.39	11.76	5.42	8.13	0.88	0.15	1.21	0.194	0.10	9.5	99.5	7.5	0.3	2.1	0.1	2.9	6.2	2.64	0.93	2.52	0.41	12.7	0.05	0.03	2.1	81.1	42	2.3
G60	CR13	49.74	13.30	11.97	8.87	8.06	0.70	0.17	1.01	0.189	0.09	5.1	99.2	6.8	0.5	1.8	0.2	3.5	8.4	3.52	1.24	3.36	0.54	17.1	0.04	0.04	2.9	77.0	41	2.8
G61	CR13	48.16	16.76	11.44	5.25	9.43	0.87	0.19	1.14	0.188	0.12	5.8	99.4	6.8	0.4	1.9	0.1	2.6	7.9	3.37	1.18	3.22	0.52	16.2	bdl	bdl	2.6	82.8	46	2.4
G62	CR13	43.07	16.06	12.45	9.53	12.39	0.85	0.11	1.28	0.110	0.18	3.8	99.8	5.9	0.2	2.1	0.1	0.5	6.9	2.93	1.03	2.80	0.45	14.1	bdl	0.02	2.3	73.8	48	2.0
G63	CR13	41.80	17.64	13.18	9.98	10.18	0.72	0.15	1.10	0.192	0.11	5.1	100.1	7.0	0.1	2.9	0.2	3.5	9.2	3.81	1.34	3.64	0.59	18.6	0.11	0.09	3.3	83.0	45	3.6
G64	CR34	65.22	16.59	3.57	1.07	0.94	8.31	0.19	0.78	0.008	0.15	2.6	99.4	25.7	0.9	9.5	2.1	5.1	17.6	5.90	1.46	4.82	0.66	30.5	bdl	0.03	5.6	284.0	13	10.6
G65	CR34	53.36	14.71	16.00	0.36	3.25	8.41	0.06	0.81	0.180	0.04	2.7	99.9	17.7	1.4	6.8	2.4	1.4	10.1	3.37	0.90	3.66	0.49	18.5	0.60	0.02	4.1	248.1	12	15.8
G66	CR34	59.87	15.64	4.72	2.17	3.51	8.84	0.10	0.95	0.080	0.04	3.9	99.8	19.2	1.5	8.4	2.1	2.0	16.8	5.62	1.39	4.59	0.63	29.0	0.49	0.05	5.3	310.2	35	10.5
G67	CR34	56.17	14.74	11.15	2.21	2.51	8.00	0.09	0.96	0.120	0.05	3.9	99.9	21.7	1.7	9.4	4.1	1.9	12.6	4.16	1.09	3.75	0.51	22.1	0.31	0.05	5.1	322.0	23	14.0
G68	CR34	55.36	14.80	5.63	0.88	7.29	8.30	0.07	0.74	0.120	0.07	6.6	99.9	16.9	1.2	7.5	2.4	1.8	15.4	4.78	1.31	3.95	0.51	26.0	1.44	0.02	6.5	250.0	15	11.4
Schakalsberge Subterrane																														
R112	CR03	41.16	13.39	11.80	3.30	14.62	2.11	0.12	1.40	0.144	0.14	12.4	181.8	18.3	1.2	4.1	0.6	1.5	17.7	4.02	1.42	1.62	0.23	25.0	2.42	bdl	12.2	143.6	22	4.0
R113	CR03	45.29	14.25	12.50	8.41	6.79	2.79	0.13	1.60	0.270	0.10	7.8	205.3	20.7	1.9	4.9	0.3	1.5	18.9	4.25	1.50	1.71	0.22	26.6	1.14	bdl	13.1	161.0	28	3.2
R114	CR03	43.05	14.77	13.61	7.30	6.26	3.43	0.08	2.41	0.240	0.18	9.1	204.7	21.4	1.7	5.3	0.6	1.8	20.9	4.69	1.66	1.89	0.25	29.4	1.35	0.05	14.6	159.0	27	4.1
R115	CR03	45.68	14.16	14.64	6.21	7.71	2.88	0.14	1.90	0.250	0.12	6.6	219.9	19.8	1.8	6.1	0.5	1.1	16.9	3.80	1.34	1.53	0.26	23.8	1.34	0.04	11.9	173.0	31	4.0
R116	CR03	47.34	14.11	11.17	4.84	9.95	3.15	0.13	1.80	0.191	0.13	8.7	204.3	20.6	1.6	3.9	0.6	1.5	23.0	5.14	1.82	2.07	0.24	32.3	1.58	bdl	15.9	158.7	25	4.7

Appendix C Whole-rock geochemical data

SAMPLE	U-Pb	**SiO2**	**Al2O3**	**Fe2O3t**	**MgO**	**CaO**	**Na2O**	**K2O**	**TiO2**	**P2O5**	**MnO**	**LOI**	**sum**	**Nb**	**Ta**	**Hf**	**U**	**Pb**	**Nd**	**Sm**	**Eu**	**Yb**	**Lu**	**SREE**	**TOT/C**	**TOTS**	**La**	**Zr**	**Sc**	**Th**
	sample	%	%	%	%	%	%	%	%	%	%	%	%	PPM	PPM	PPM	PPM	PPM	PPM	PPM	PPM	PPM	PPM	**PPM**	%	%	PPM	PPM	PPM	PPM
		0.01	0.01	0.04	0.01	0.01	0.01	0.01	0.01	0.010	0.01	0.1	0.0	0.1	0.1	0.1	0.1	0.1	0.3	0.05	0.02	0.05	0.01		0.02	0.02	0.1	0.1	1	0.2
Oranjemund Subterrane																														
R138	CR02	77.14	10.19	3.78	1.56	0.34	1.95	2.00	0.71	0.160	0.05	2.0	340.0	14.7	1.1	6.9	3.1	28.0	36.8	7.10	1.20	3.18	0.49	48.8	0.06	0.03	39.8	277.4	7	15.8
R139	CR02	72.22	14.18	3.49	1.05	1.58	2.02	2.42	0.46	0.107	0.02	1.7	381.5	11.7	1.0	8.7	2.8	19.2	34.1	6.55	1.16	3.18	0.47	45.5	0.13	bdl	34.2	324.9	8	14.4
R140	CR02	72.37	12.96	3.54	0.97	1.34	2.27	2.29	0.46	0.114	0.02	2.7	318.6	11.2	0.9	7.1	3.1	16.2	29.8	5.65	1.00	2.75	0.41	39.6	0.21	bdl	30.0	270.0	8	10.6
R141	CR02	58.68	9.10	2.64	1.04	12.71	2.33	1.47	0.42	0.110	0.37	11.4	297.9	9.2	0.8	7.3	3.1	12.6	25.1	4.76	0.84	2.31	0.34	33.4	0.34	bdl	25.2	253.3	8	11.4
R142	CR02	67.59	11.52	4.56	1.32	4.81	1.78	2.78	0.43	0.111	0.09	4.1	166.1	6.5	0.5	3.4	2.4	15.8	26.9	5.06	0.89	2.46	0.37	35.7	2.68	bdl	26.7	126.1	7	6.3
R143	CR02	59.50	14.60	6.97	2.01	4.44	0.95	5.38	0.88	0.172	0.06	4.1	216.5	8.4	0.7	4.5	2.8	20.6	32.9	6.25	1.10	3.03	0.45	43.7	0.58	0.04	33.0	166.0	9	8.5
R144	CR02	68.69	13.76	5.42	1.00	3.15	1.94	2.73	0.59	0.129	0.04	2.7	256.6	13.9	0.9	5.4	4.0	15.6	35.9	6.84	1.21	3.32	0.49	47.8	0.34	0.04	36.1	189.7	17	13.8
R145	CR02	65.45	14.37	6.07	1.22	3.52	2.47	2.48	0.64	0.171	0.03	3.0	317.0	9.9	0.9	7.1	2.9	12.7	28.2	5.36	0.95	2.60	0.39	37.5	0.22	bdl	28.3	270.2	8	10.5